Dynamic Analysis of Cracked Rotor in Viscous Medium and its Crack Diagnosis using Intelligent Techniques

Adik Ramdayal Yadao

Department of Mechanical Engineering
National Institute of Technology Rourkela

Dynamic Analysis of Cracked Rotor in Viscous Medium and its Crack Diagnosis using Intelligent Techniques

Dissertation submitted to the

National Institute of Technology Rourkela

in partial fulfillment of the requirements

of the degree of

Doctor of Philosophy

in

Mechanical Engineering

by

Adik Ramdayal Yadao

(Roll Number: 512ME117)

under the supervision of

Prof. Dayal R. Parhi

Novemenber, 2016

Department of Mechanical Engineering

National Institute of Technology Rourkela

Department of Mechanical Engineering
National Institute of Technology Rourkela

November 20, 2016

Certificate of Examination

Roll Number: 512ME117

Name: Adik Ramdayal Yadao

Title of Dissertation: Dynamic Analysis of Cracked Rotor in Viscous Medium and its Crack Diagnosis using Intelligent Techniques

We the below signed, after checking the dissertation mentioned above and the official record book (s) of the student, hereby state our approval of the dissertation submitted in partial fulfillment of the requirement of the degree of Doctor of Philosophy in Mechanical Engineering at National Institute of Technology, Rourkela. We are satisfied with the volume, quality, correctness, and originality of the work.

Dayal R. Parhi
Principal Supervisor

Saurav Dutta
Member (DSC)

Pabitra Mohan Khilar
Member (DSC)

Shishir Kumar Sahu
Member (DSC)

Vinay Sharma
External Examiner

Kalipada Maity
Chairperson (DSC)

S S Mahapatra
Head of the Department

Department of Mechanical Engineering
National Institute of Technology Rourkela

Dr. Dayal R. Parhi
Professor

November 20, 2016

Supervisor Certificate

This is to certify that the work presented in this dissertation entitled *"Dynamic analysis of Cracked Rotor in Viscous Medium and its Crack Diagnosis using Intelligent Techniques"* by *"Adik Ramdayal Yadao"*, Roll Number: 512ME117, is a record of original research carried out by him under my supervision and guidance in partial fulfillment of the requirements of the degree of *Doctor of philosophy* in *Mechanical Engineering*. Neither this dissertation nor any part of it has been submitted for any degree or diploma to any institute or university in India or abroad.

Dayal R. Parhi
Professor

To my Parents,
with all my love

Declaration of Originality

I, ***Adik Yadao***, Roll Number: ***512ME117*** hereby declare that this dissertation entitled *"**Dynamic Analysis of Cracked Rotor in Viscous Medium and its Crack Diagnosis using Intelligent Techniques**"* represents my original work carried out as a doctoral student of NIT Rourkela and, to the best of my knowledge, it contains no material previously published or written by another person, nor any material presented for the award of any degree or diploma of NIT Rourkela or any other institution. Any contribution made to this research by others, with whom I have worked at NIT Rourkela or elsewhere, is explicitly acknowledged in the dissertation. Works of other authors cited in this dissertation have been duly acknowledged under the section "Bibliography". I have also submitted my original research records to the scrutiny committee for evaluation of my dissertation.

I am fully aware that in case of my non-compliance detected in the future, the Senate of NIT Rourkela may withdraw the degree awarded to me on the basis of the present dissertation.

November 20, 2016

NIT Rourkela

Adik Ramdayal Yadao

Acknowledgment

My first thank is to the Almighty God, without whose blessings, I wouldn't have been writing this “acknowledgments".

I would like to extend my heartfelt indebtedness and gratitude to Prof. Dayal R. Parhi for his kindness in providing me an opportunity to work under his supervision and guidance. During this period, without his endless efforts, immense knowledge, deep patience, invaluable guidance and answers to my numerous questions, this research would have never been possible. I am especially obliged to him for teaching me both research and writing skills, which have been proven beneficial for my current research and future career. He showed me different ways to approach a research problem and the need to be persistent to accomplish any goal. It has been a great honor and pleasure for me to do research under the supervision of Dr. Dayal R. Parhi. I am thankful to Prof. Animesh Biswas, Director of National Institute of Technology, for giving me an opportunity to be a part of this institute of national importance and to work under the supervision of Prof. Dayal R. Parhi. I am sincerely obliged to Prof. S. S. Mahapatra, Head of the Department, Department of Mechanical Engineering, for providing me all official and laboratory facilities during the research period. His incessant encouragement towards research work has inspired me a lot.

I express my gratitude to Prof. K. P. Maity, Chairman DSC and DSC members for their indebted help and valuable suggestions for the accomplishment of the dissertation. I thank all the members of the Department of Mechanical Engineering, and the Institute, who helped me in various ways towards the completion of my work.

I would like to thank all my friends and lab-mates for their encouragement and understanding. Their support and lots of lovely memories with them can never be captured in words. Finally, I thank my parents, beloved wife and the entire family members for their unlimited support and strength.

November 20, 2016 ***Adik Ramdayal Yadao***

NIT Rourkela Roll Number: 512ME117

Abstract

Fatigue cracks have high potential to cause catastrophic failures in the rotor which can lead to catastrophic failure if undetected properly and in time. This fault may interrupt smooth, effective and efficient operation and performance of the machines. Thereby the importance of identification of crack in the rotor is not only for leading safe operation but also to prevent the loss of economy and lives.The condition monitoring of the engineering systems is attracted by the researchers and scientists very much to invent the automated fault diagnosis mechanism using the change in dynamic response before and after damage. When the rotor with transverse crack immersed in the viscous fluid, analysis of cracked rotor is difficult and complex. The analysis of cracked rotor partially submerged in the viscous fluid is widely used in various engineering systems such as long spinning shaft used drilling the seabed for the extracting the oil, high-speed turbine rotors, and analysis of centrifuges in a fluid medium. Therefore, dynamic analysis of cracked rotor partially submerged in the viscous medium have been presented in the current study. The theoretical analysis has been performed to measure the vibration signatures (Natural Frequencies and Amplitude) of multiple cracked mild steel rotor partially submerged in the viscous medium. The presence of the crack in rotor generates an additional flexibility. That is evaluated by strain energy release rate given by linear fracture mechanics. The additional flexibility alters the dynamic characteristics of cracked rotor in a viscous fluid. The local stiffness matrix has been calculated by the inverse of local dimensionless compliance matrix. The finite element analysis has been carried out to measure the vibration characteristics of cracked rotor partially submerged in the viscous medium using commercially available finite element software package ANSYS. It is observed from the current analysis, the various factors such as the viscosity of fluid, depth and position of the cracks affect the performance of the rotor and effectiveness of crack detection techniques. Various Artificial Intelligent (AI) techniques such as fuzzy logic, hybrid BPNN-RBFNN neural network, MANFIS and hybrid fuzzy-rule base controller based multiple faults diagnosis systems are developed using the dynamic response of rotating cracked rotor in a viscous medium to monitor the presence of crack. Experiments have been conducted to authenticate the performance and accuracy of proposed methods. Good agreement is observed between the results.

Keywords: Rotor; Dynamic response; Viscous fluid; Dynamic response; Navier-Stokes equation; Fuzzy; Neural network.

Contents

Certificate of Examination i
Supervisor Certificate ii
Dedication iii
Declaration of Originality iv
Acknowledgement v
Abstract vi
Contents vii
List of Figures xii
List of Tables xvii
Nomenclatures xx
1 Introduction 1
1.1 Motivation of Research work 1
1.2 Aims and Objectives of the Research Work 2
1.3 Methodologies Applied for Proposed Research Work 3
1.4 Novelty of Proposed Research Work 4
1.5 Outline of the Proposed Research work 5
2 Literature Review 7
2.1 Introduction 7
2.2 Analysis of Differerent Methodologies for Crack Identification in Rotor 8
2.2.1 Classical Methods for Identification of Crack 8
2.2.2 Finite Element Method used for Identification of Crack 16
2.2.3 Wavelet Transform and Wavelet Finite Element Method used for Identification of Crack 18
2.2.4 Other Approaches are used for Identification of Crack 19
2.2.5 Artificial Intelligence Techniques used for Identification of Crack 21
2.2.5.1 Fuzzy Logic Technique 21
2.2.5.2 Artificial Neural Network Technique 23
2.2.5.3 Adaptive Neuro-Fuzzy Inference System (ANFIS) 26
2.2.5.4 Rule-Base Technique 29
2.3 Summary 30
3 Theoretical Analysis of Dynamic Response of Rotor with Multiple Transverse Crack Partially Submerged in Viscous Medium 31

3.1 Introduction 31
3.2 Theoretical Analysis of Spinning Rotor with Transverse Crack in Viscous Medium 32
3.2.1 Dynamic Analysis of Rotating Non-cracked Cantilever Rotor with Additional Mass Partially Submerged in Viscous Medium 32
3.2.1.1 Equation of Fluid Velocities 33
3.2.1.2 Analysis of Fluid Forces 36
3.2.1.3 Dynamic Response of the Spinning Rotor System 37
3.2.2 Dynamic Analysis of Rotating Multiple Cracked Cantilever Rotor Partially Submerged in the Viscous Medium 45
3.2.2.1 Determination of the Local Flexibility and Local Stiffness Matrix of a Cracked Rotor under Axial and Bending Loading 45
3.2.3 Dynamic Response of Rotating Fixed-Fixed Rotor with Additional Mass at Mid Span Submerged in the Viscous Medium 57
3.2.3.1 Analysis of Rotating Non-Cracked Fixed-Fixed Rotor 57
3.2.3.2 Analysis of Rotating Multiple Crack Fixed-Fixed Rotor 63
3.3 Evaluation and Comparison of Experimental and Theoretical Analysis Result for the Cantilever Rotor System 69
3.4 Comparison and Authentication of Theoretical and Experimental Analysis Results 76
3.5 Discussion 78
3.6 Summary 79
4 Finite Element Analysis of Multiple Cracked Cantilever Rotor Partially Submerged in Fluid Medium For Measurement of Dynamic Response 80
4.1 Introduction 80
4.2 Analysis of Finite Element Method using ANSYS 81
4.3 Finite Element Analysis of Rotor with Transverse Cracks Partially Submerged in the Viscous Fluid 82
4.3.1 Description of SOLID187 Element used for Solid Rotor 83
4.3.2 Description of FLUID30 Element used for Fluid Medium 84
4.3.3 Material Properties and Boundary Condition of Rotor and Viscous Fluid medium 85
4.4 Discussion 95
4.5 Summary 96

5 Analysis of Fuzzy System for Detecting the Multiple Crack in Cantilever Rotor 97
5.1 Introduction 97
5.2 Fuzzy Logic System 98
5.2.1 Concept of Fuzzy Membership Function 100
5.2.2 Designing the Fuzzy Logic Model using Fuzzy Rule 102
5.2.3 Modeling of Defuzzification Mechanism 103
5.3 Analysis of Mamdani Fuzzy Logic Mechanism for Identification of Multiple Crack in Rotor 103
5.3.1 Designing the Mamdani Fuzzy Logic Mechanism for Identification of Crack in Rotor 105
5.4 Analysis of Takagi-Sugeno Fuzzy Logic Mechanism for Identification of Crack in Rotor 115
5.5 Analysis of Hybrid Fuzzy Logic Mechanism for Identification of Multiple Crack in Rotor 117
5.6 Results and Discussion 118
5.7 Summary 125
6 Analysis of Hybrid BPNN-RBFNN Neural Network for Identification of Multiple Crack in Rotor Partially Submerged in the Viscous Medium 126
6.1 Introduction 126
6.2 Artificial Neural Network Technique 129
6.2.1 Learning Paradigms of Artificial Neural Network 130
6.3 Analysis of Feed Forward Back Propagation Neural Network Controller used for Multiple Crack Identification in Rotor 131
6.3.1 Learning Back Propagation Technique 131
6.3.2 Neural Controller Mechanism 132
6.4 Analysis of Radial Basis Function Neural Network used for Multiple Crack Identification in Rotor 135
6.4.1 Radial Basis Function Neural Network Mechanism 135
6.4.1.1 Finding the Centers of RBF unit 137
6.4.1.2 Finding the width of RBF unit 138
6.4.1.3 Finding the Weights 138
6.4.1.4 Selection of H and q 138
6.4.2 Radial Basis Function Neural Network for Finding the Crack Locations

and Depths in Rotor 139
6.5 Hybrid BPNN-RBFNN Neural Network Mechanism for Finding the Multiple Crack in Rotor 140
6.6 Results and Discussion 141
6.7 Summary 147
7 Analysis of Multiple Adaptive Neuro-Fuzzy Inference System for Identification of Multiple Crack in Rotor 148
7.1 Introduction 149
7.2 Analysis of Multiple Adaptive Neuro-Fuzzy Inference System for Identification of Crack 150
7.3 Results and Discussion 155
7.4 Summary 159
8 Analysis of Hybrid Fuzzy-Rule Base Technique for Multiple Crack Identification in Rotor 160
8.1 Introduction 160
8.2 Analysis of Rule-Base Technique for Identification of Multiple Crack in Rotor 161
8.2.1 Designing of Rule-Base Technique for Identification of Multiple Crack 161
8.3 Analysis of Hybrid Fuzzy-Rule Base Tecnique for Finding the Multiple Crack in Rotor 164
8.4 Results and Discussion 165
8.5 Summary 169
9 Analysis & Description of Experimental Investigation 170
9.1 Detail Specification of Apparatus used in the Experimental Analysis 170
9.2 Experimental Procedure for the Analysis of Rotor System 175
9.3 Results and Discussion 176
10 Results and Discussion 178
10.1 Introduction 178
10.2 Analysis of Results 178
10.3 Summary 184
11 Conclusions and Scope for Future Research 185
11.1 Introduction 185
11.2 Conclusions 185
11.3 Scope for Future Research 188

Appendix-A **189**
Bibliography **191**
Dissemination **202**
Vitae **204**

List of Figures

3.1 Representation of whirling position of cantilever rotor 33

3.2 Frequency Ratio (ω/ω_0) Vs Non-dimensional Amplitude Ratio (δ^*/ε^*), Mild Steel Rotor R_1=0.01m, L=1.0m, q=12, R_D= 0.055m,T_D= 0.020m, M_D = 1.0kg for finite region 39

3.3 Frequency Ratio (ω/ω_0) Vs Non-dimensional Amplitude Ratio (δ^*/ε^*), Mild Steel Rotor R_1=0.01m, L=0.8m, q =12, R_D = 0.055m,T_D= 0.020m, M_D = 1.0kg for finite region 40

3.4 Frequency Ratio (ω/ω_0) Vs Non-dimensional Amplitude Ratio (δ^*/ε^*), Mild Steel Rotor R_1=0.01m, L=0.8m, R_D = 0.055m,T_D= 0.020m, M_D = 1.0kg for finite region 40

3.5 Frequency Ratio (ω/ω_0) Vs Non-dimensional Amplitude Ratio (δ^*/ε^*), Mild Steel Rotor R_1=0.01m, L=0.8m,q=12, ν=0.541stokes & M*=0.136, M_{D1} = 1.0kg, M_{D2}=0.75kg , M_{D3}=0.50kg for finite region 41

3.6 Frequency Ratio (ω/ω_0) Vs Non-dimensional Amplitude Ratio (δ^*/ε^*), Mild Steel Rotor R_1=0.01m, L=0.8m, q =12, ν =0.0633,0.541,2.9 stokes & M*=0.127, 0.136,0.146, R_D=0.055m, T_D= 0.020m, M_D=1.0kg for finite region 42

3.7 Frequency Ratio (ω/ω_0) Vs Non-dimensional Amplitude Ratio (δ^*/ε^*), Mild Steel Rotor R_1=0.01m, L=1.0m, q=12, R_D= 0.055m,T_D= 0.020m, M_D = 1.0kg for infinite region 43

3.8 Frequency Ratio (ω/ω_0) Vs Non-dimensional Amplitude Ratio (δ^*/ε^*), Mild Steel Rotor R_1=0.01m, L=0.8m, q=12, R_D = 0.055m,T_D= 0.020m, M_D = 1.0kg, for infinite region 43

3.9 Frequency Ratio (ω/ω_0) Vs Non-dimensional Amplitude Ratio (δ^*/ε^*), Mild Steel Rotor R_1=0.01m, L=0.8m, q =12, ν=0.541stokes & M*=0.136,M_{D1}=1.0kg, M_{D2}=0.75kg, M_{D3}=0.50kg for infinite region 44

3.10 Frequency Ratio (ω/ω_0) Vs Non-dimensional Amplitude Ratio (δ^*/ε^*), Mild Steel Rotor R_1=0.01m, L=0.8m, q=12, R_D = 0.055m,T_D= 0.020m, M_D = 1.0kg, for infinite region 44

3.11(a) Geometry of a cantilever rotor with crack element 46

3.11(b) Cross section of crack element 46

3.11(c) Coupling force on the crack element 46

3.12 Frequency Ratio (ω/ω_0) Vs Non-dimensional Amplitude Ratio (δ^*/ε^*), Mild Steel Rotor R_1=0.01m, L=0.8m, q=12, L_1/L= 0.313, L_2/L=0.563, R_D = 0.055m, T_D = 0.020m, M_D = 1.0kg for 44-Direction 52

3.13 Frequency Ratio (ω/ω_0) Vs Non-dimensional Amplitude Ratio (δ^*/ε^*), Mild Steel Rotor R1=0.01m, L=0.8m, q=12, L_1/L= 0.313, L_2/L=0.563, R_D=0.055m, T_D=0.020m, M_D = 1.0kg for 55-Direction 52

3.14 Frequency Ratio (ω/ω_0) Vs Non-dimensional Amplitude Ratio (δ^*/ε^*), Mild Steel Rotor R_1=0.01m, L=0.8m, q=12, L_1/L= 0.313, L_2/L=0.563, R_D = 0.055m, T_D= 0.020m, M_D = 1.0kg 53

3.15 Frequency Ratio (ω/ω_0) Vs Non-dimensional Amplitude Ratio (δ^*/ε^*), Mild Steel Rotor R_1=0.01m, L=0.8m, a1/D= 0.125, a2/D=0.150, L1/L= 0.313, L_2/L=0.563, R_D = 0.055m,T_D= 0.020m, M_D = 1.0kg for 44-Direction 54

3.16 Frequency Ratio (ω/ω_0) Vs Non-dimensional Amplitude Ratio (δ^*/ε^*), Mild Steel Rotor R_1=0.01m, L=0.8m, q=12, a1/D= 0.125, a2/D=0.150, L_1/L= 0.313, L_2/L=0.563, ν=0.541 & M*=0.136, R_D = 0.055m, T_D= 0.020m, M_D = 1.0kg 55

3.17 Relative Crack Position Vs Natural Frequency Mild Steel Rotor R1=0.01m, L=0.8m, Relative crack depth a1/D=0.225, a2/D= 0.250, R_D = 0.055m, T_D= 0.020m, M_D = 1.0kg 56

3.18 Relative Crack Depth Vs Natural Frequency Mild Steel Rotor R_1=0.01m, L=0.8m, Relative crack depth L_1/L=0.313,L_2/L=0.563, R_D=0.055m, T_D= 0.020m, M_D=1.0kg 56

3.19 Full view of fixed-fixed rotor 57

3.20 Frequency Ratio (ω/ω_0) Vs Non-dimensional Amplitude Ratio (δ^*/ε^*), Mild Steel Rotor R_1=0.01m, L=1.0m, q=12, R_D = 0.055m,T_D= 0.020m, M_D = 1.0kg 60

3.21 Frequency Ratio (ω/ω_0) Vs Non-dimensional Amplitude Ratio (δ^*/ε^*), Mild Steel Rotor R_1=0.01m, L=0.8m, q=12, R_D = 0.055m,T_D= 0.020m, M_D = 1.0kg 60

3.22 Frequency Ratio (ω/ω_0) Vs Non-dimensional Amplitude Ratio (δ^*/ε^*), Mild Steel Rotor R_1=0.01m, L=0.8m, R_D = 0.055m,T_D= 0.020m, M_D = 1.0kg 61

3.23 Frequency Ratio (ω/ω_0) Vs Non-dimensional Amplitude Ratio (δ^*/ε^*), Mild Steel Rotor R_1=0.01m, L=0.8m, q=12, ν=0.541stokes & M*=0.136,M_{D1}=1.0kg, M_{D2}=0.75kg, M_{D3}=0.60kg M_{D4}=0.50kg 62

3.24 Frequency Ratio (ω/ω_0) Vs Non-dimensional Amplitude Ratio (δ^*/ε^*), Mild Steel Rotor R_1=0.01m, L=0.8m, q=12, ν=0.0633,0.541, 2.9 stokes&M*=0.127, 0.136,0.146, R_D=0.055m, T_D= 0.020m, M_D=1.0kg 62

3.25 Schematic representation of multiple cracked fixed-fixed rotor submerged in the viscous fluid..... 63

3.26 Frequency Ratio (ω/ω_0) Vs Non-dimensional Amplitude Ratio (δ^*/ε^*), Mild Steel Rotor R_1=0.01m, L=0.8m, q=12, L_1/L= 0.313, L_2/L=0.563, R_D = 0.055m, T_D= 0.020m, M_D = 1.0kg for 44-Direction..... 66

3.27 Frequency Ratio (ω/ω_0) Vs Non-dimensional Amplitude Ratio (δ^*/ε^*), Mild Steel Rotor R_1=0.01m, L=0.8m, q=12, L_1/L= 0.313, L_2/L=0.563, R_D = 0.055m, T_D= 0.020m, M_D = 1.0kg for 55-Direction..... 67

3.28 Frequency Ratio (ω/ω_0) Vs Non-dimensional Amplitude Ratio (δ^*/ε^*), Mild Steel Rotor R_1=0.01m, L=0.8m, q=12, L_1/L= 0.313, L_2/L=0.563, R_D = 0.055m, T_D= 0.020m, M_D = 1.0kg..... 68

3.29 Frequency Ratio ($\omega/\omega 0$) Vs Non-dimensional Amplitude Ratio (δ^*/ε^*), Mild Steel Rotor R1=0.01m, L=0.8m, q=12, a1/D=0.125, a2/D=0.150, L1/L=0.313,L2/L=0.563,ν=0.541Stokes, M*=0.136, RD=0.055m, TD= 0.020m, MD=1.0kg..... 68

3.30 Schematic block diagram representation of experimental set up..... 69

3.31 Frequency Ratio (ω/ω_0) Vs Non-dimensional Amplitude Ratio (δ^*/ε^*), Mild Steel Rotor R_1=0.01m, L=0.8m, q=12, R_D= 0.055m, T_D= 0.020m, M_D = 1.0kg for non-cracked rotor..... 70

3.32 Frequency Ratio (ω/ω_0) Vs Non-dimensional Amplitude Ratio(δ^*/ε^*), Mild Steel Rotor R_1=0.01m, L=0.8m, q=12, R_D= 0.0.55m, T_D= 0.020m, M_D = 1.0kg, for non-crack rotor..... 71

3.33 Frequency Ratio (ω/ω_0) Vs Non-dimensional Amplitude Ratio (δ^*/ε^*), Mild Steel Rotor R_1=0.01m, L=0.8m, q=12, R_D = 0.55m,T_D= 0.020m, M_D = 1.0kg for non-cracked rotor..... 71

3.34 Frequency Ratio (ω/ω_0) Vs Non-dimensional Amplitude Ratio (δ^*/ε^*), Mild Steel Rotor R_1=0.01m, L=0.8m, q=12, a1/D= 0.125, a2/D=0.150, L_1/L= 0.313, L_2/L=0.563 R_D = 0.055m,T_D= 0.020m, M_D = 1.0kg for 44-Direction..... 72

3.35 Frequency Ratio (ω/ω_0) Vs Non-dimensional Amplitude Ratio (δ^*/ε^*), Mild Steel Rotor R_1=0.01m, L=0.8m, q=12, a1/D= 0.125, a2/D=0.150, L_1/L= 0.313, L_2/L=0.563, R_D = 0.055m, T_D= 0.020m, M_D = 1.0kg 72

3.36 Frequency Ratio (ω/ω_0) Vs Non-dimensional Amplitude Ratio (δ^*/ε^*), Mild Steel Rotor R_1=0.01m, L=0.8m, q =12,a1/D=0.250, a2/D=0.225, L_1/L = 0.313, L_2/L=0.563, R_D = 0.055m, T_D= 0.020m, M_D = 1.0kg for 44- Direction 73

3.37 Frequency Ratio (ω/ω_0) Vs Non-dimensional Amplitude Ratio (δ^*/ε^*), Mild

Steel Rotor R_1=0.01m, L=0.8m, q =12,a1/D=0.225,a2/D=0.150, L_1/L = 0.313, L_2/L=0.563, R_D = 0.055m, T_D= 0.020m, M_D = 1.0kg for 44- Direction 73

3.38 Frequency Ratio (ω/ω_0) Vs Non-dimensional Amplitude Ratio (δ^*/ε^*), Mild Steel Rotor R_1=0.01m, L=0.8m, q =12,a1/D=0.150,a2/D=0.125, L_1/L = 0.313, L_2/L=0.563, R_D = 0.055m, T_D= 0.020m, M_D = 1.0kg for 44- Direction 74

3.39 Frequency Ratio (ω/ω_0) Vs Non-dimensional Amplitude Ratio (δ^*/ε^*),Mild SteelRotorR_1=0.01m,L=0.8m,q=12,a1/D=0.250,a2/D=0.225, L_1/L = 0.313, L_2/L=0.563, R_D = 0.055m, T_D= 0.020m, M_D = 1.0kg for 55- Direction 74

3.40 Frequency Ratio (ω/ω_0) Vs Non-dimensional Amplitude Ratio (δ^*/ε^*), Mild Steel Rotor R_1=0.01m, L=0.8m, q =12, a1/D=0.225, a2/D=0.150, L_1/L = 0.313, L_2/L=0.563, R_D = 0.055m, T_D= 0.020m, M_D = 1.0kg for 55- Direction 75

3.41 Frequency Ratio (ω/ω_0) Vs Non-dimensional Amplitude Ratio (δ^*/ε^*), Mild Steel rotor R_1=0.01m, L=0.8m, q =12, a1/D=0.150, a2/D=0.125, L_1/L = 0.313, L_2/L=0.563, R_D = 0.055m, T_D= 0.020m, M_D = 1.0kg for 55- Direction 75

4.1 Geometry of SOLID187 element ..... …83

4.2 Geometry of FLUID30 (3-D acoustic fluid) element ..... …….84

4.3 Frequency Ratio (ω/ω_0) Vs Non-dimensional Amplitude Ratio (δ^*/ε^*), Mild Steel Rotor R_1=0.01m, L=0.8m, q =12, R_D = 0.055m, T_D= 0.020m, M_D = 1.0kg for No crack ..... …….86

4.4 Frequency Ratio (ω/ω_0) Vs Non-dimensional Amplitude Ratio (δ^*/ε^*), Mild Steel Rotor R_1=0.01m, L=0.8m, q=12, R_D=0.055m,T_D=0.020m, M_D = 1.0kg for virtual mass effect ..... …….87

4.5 Frequency Ratio (ω/ω_0) Vs Non-dimensional Amplitude Ratio (δ^*/ε^*), Mild Steel Rotor R_1=0.01m, L=0.8m, q=12, a1/D= 0.125, a2/D=0.150, L_1/L= 0.313, L_2/L=0.563, R_D = 0.055m, T_D= 0.020m, M_D = 1.0kg for virtual mass effect..... 87

4.6 Frequency Ratio (ω/ω_0) Vs Non-dimensional Amplitude Ratio (δ^*/ε^*), Mild Steel Rotor R_1=0.01m, L=0.8m, q=12, R_D = 0.055m,T_D= 0.020m, M_D = 1.0kg for Gap ratio effect 88

4.7 Frequency Ratio (ω/ω_0) Vs Non-dimensional Amplitude Ratio (δ^*/ε^*), Mild Steel Rotor R_1=0.01m, L=0.8m, q=12, a1/D= 0.125, a2/D=0.150, L_1/L= 0.313, L_2/L=0.563, R_D=0.055m,T_D= 0.020m, M_D = 1.0kg for 44-Direction..... 88

4.8 Frequency Ratio (ω/ω_0) Vs Non-dimensional Amplitude Ratio (δ^*/ε^*), Mild Steel Rotor R_1=0.01m, L=0.8m, q =12,a1/D=0.250,a1/D=0.225, L_1/L=0.313, L_2/L=0.563, R_D=0.055m, T_D=0.020m, M_D=1.0kg for 44- Direction.....89

4.9 Frequency Ratio (ω/ω_0) Vs Non-dimensional Amplitude Ratio (δ^*/ε^*), Mild

Steel Rotor R_1=0.01m, L=0.8m, q =12,a1/D=0.225,a1/D=0.150, L_1/L = 0.313, L_2/L=0.563, R_D =0.055m, T_D=0.020m, M_D=1.0kg for 44- Direction 89

4.10 Frequency Ratio (ω/ω0) Vs Non-dimensional Amplitude Ratio (δ*/ε*), Mild Steel Rotor R_1=0.01m, L=0.8m, q=12,a1/D=0.150,a1/D=0.125, L_1/L=0.313, L_2/L=0.563, R_D = 0.055m, T_D= 0.020m, M_D = 1.0kg for 44- Direction 90

4.11 Frequency Ratio (ω/ω_0) Vs Non-dimensional Amplitude Ratio (δ*/ε*), Mild Steel Shaft R_1=0.01m, L=0.8m, q=12,a1/D=0.250,a1/D=0.225, L_1/L = 0.313, L_2/L=0.563, R_D = 0.055m, T_D= 0.020m, M_D = 1.0kg for 55- Direction ..... …90

4.12 Frequency Ratio (ω/ω_0) Vs Non-dimensional Amplitude Ratio (δ*/ε*), Mild Steel Shaft R1=0.01m, L=0.8m, q =12, a1/D=0.225, a1/D=0.150, L_1/L = 0.313, L_2/L=0.563, R_D = 0.055m, T_D= 0.020m, M_D =1.0kg for 55- Direction ..... …….91

4.13 Frequency Ratio (ω/ω_0) Vs Non-dimensional Amplitude Ratio (δ*/ε*), Mild Steel Rotor R_1=0.01m, L=0.8m, q =12, a1/D=0.150, a1/D=0.125, L_1/L = 0.313, L_2/L=0.563, R_D = 0.055m, T_D= 0.020m, M_D = 1.0kg for 55- Direction ..... …….91

5.1(a) Triangular membership function ..... …….100

5.1(b) Gaussian membership function 100

5.1(c) Trapezoidal membership function 100

5.2 General structure of fuzzy logic system 102

5.3(a) Triangular fuzzy controller model 104

5.3(b) Gaussian fuzzy controller model 104

5.3(c) Trapezoidal fuzzy controller model 105

5.4 Membership function for traingular fuzzy controller model ..... …109

5.5 Membership function for gaussian fuzzy controller model 110

5.6 Membership function for trapzoidal fuzzy controller model 111

5.7 Resultant values of first and second relative crack depth and crack locations from triangular membership function while activated the fuzzy rules no 5 and 18 of Table 5.2 for the rotor 112

5.8 Resultant values of first and second relative crack depth and crack locations from Gaussian membership function while activated the fuzzy rules no 5 and 18 of Table 5.2 for the rotor 113

5.9 Resultant values of first and second relative crack depth and crack locations from Trapezoidal membership function while activated the fuzzy rules no 5 and 18 of Table 5.2 for the rotor 114

5.10 Zero-order T-S fuzzy Logic system with two inputs and two rules [208] ..... …116

5.11 Hybrid fuzzy architecture for crack identification 117
6.1 Model of neuron of artificial neural network 129
6.2 Back propagation Technique 132
6.3 Multi-layer feed forward back propagation neural network model for crack identification 133
6.4 RBFNN model for identification of crack 139
6.5 Hybrid BPNN-RBFNN neural network architecture for multiple crack identification 141
7.1 Bell-shaped membership function 152
7.2(a) Representation of multiple ANFIS controller for crack identification 154
7.2(b) Adaptive Neuro-fuzzy inference system (ANFIS) for crack identification 155
8.1 Rule base controller for identification of multiple crack 163
8.2 Hybrid fuzzy-rule base technique for identification of multiple cracks 164
9.1 View of experimental setup 172
9.1(a) Ultrasonic sensor 172
9.1(b) Aurdino micro-controller 173
9.1(c) Bread board 173
9.1(d) Variac 173
9.1(e) Power motor 174
9.1(f) Tachometer 174
9.1(g) Display device 174
A1 FEA model of crack rotor 189
A2 FEA model of rotor with fluid medium 189
A3 FEA solution of Rotor with fluid medium in axisymmetric position 190
A4 FEA solution of Rotor with fluid medium 190

List of Tables

3.1 Physical properties of cantilever rotor 45

3.2 Properties of three different type of viscous fluid 45

3.3 Comparison between numerical and experimental results for effect of different viscous medium 76

3.4 Comparison between theoretical and experimental results for ν=0.541 stokes & M*=0.136 for virtual mass effect (non-cracked rotor) 77

3.5 Comparison between theoretical and experimental results for ν=0.541 stokes, M*=0.0.136, L_1/L=0.313,L_2/L=0.563, a1/D=0.125, a2/D=0.150 for virtual mass effect 77

3.6 Comparison between theoretical and experimental results for ν=0.541stokes, M*=0.136 77

3.7 Comparison between theoretical and experimental results for crack positionL_1/L=0.313,L_2/L=0.563,a1/D=0.125,a2/D=0.150,ν=0.541 stokes, M*=0.136 for 44- Direction 77

3.8 Comparison between Theoretical and experimental results for crack position L_1/L=0.313, L_2/L=0.563 78

4.1 Material properties of mild steel rotor 85

4.2 Physical properties of viscous fluid medium (for water) 86

4.3 Comparison between theoretical, experimental and FEA results for effect of different viscous medium 92

4.4 Comparison between theoretical, experimental and FEA results for ν=0.541stokes, M*=0.136 92

4.5 Comparison between theoretical, experimental and FEA results for a1/D= 0.125, a2/D=0.150, L_1/L = 0.313, L_2/L=0.563, ν=0.541stokes, M*=0.0.136 (virtual mass effect) 92

4.6 Comparison between theoretical, experimental and FEA results for ν =0.541 stokes, M*=0.136 (Non-cracked rotor) 93

4.7 Comparison between theoretical and experimental results for a1/D= 0.125, a2/D=0.150, L_1/L = 0.313, L_2/L=0.563, ν=0.541stokes, M*=0.136 (44-Direction of crack) 93

4.8 Comparison between theoretical, experimental and FEA results for

$L_1/L = 0.313$, $L_2/L=0.563$ 94
5.1 Description of fuzzy linguistic variable 106
5.2 Example of some fuzzy rules out of several fuzzy rules for the rotor 108
5.3 Comparison of the results obtained from Mamdani fuzzy gaussian, Mamdani fuzzy trapezoidal, Mamdani fuzzy triangular model and experimental analysis for the rotor 120
5.4 Comparison of the results obtained from fuzzy gaussian, FEA, theoretical and experimental analysis for the rotor 121
5.5 Comparison of the results obtained from Sugeno fuzzy gaussian, Sugeno fuzzy trapezoidal, Sugeno fuzzy traingular model and experimental analysis for the rotor 122
5.6 Comparison of the results obtained from Sugeno fuzzy, FEA, theoretical and experimental analysis for the rotor 123
5.7 Comparison of the results obtained from Mamdani fuzzy, Sugeno fuzzy, Hybrid fuzzy model and experimental analysis for the rotor 124
6.1 Comparison of the results obtained from BPNN, FEA and experiment analysis for the rotor 143
6.2 Comparison of the results obtained from RBFNN, FEA and experimental analysis for the rotor 144
6.3 Comparison of the results obtained from BPNN, RBFNN, Mamdani fuzzy gausian model and experimental analysis for the rotor. 145
6.4 Comparision of the results obtained from BPNN, RBFNN, Hybrid BPNN-RBFNN model and experimental analysis for the rotor 146
7.1 Comparison of the results obtained from MANFIS, RBFNN, Sugeno gaussain fuzzy model and experimental analysis for the rotor 157
7.2 Comparison of the results obtained from MANFIS, FEA, theoretical and experimental analysis for the rotor 158
8.1 Comparison of the results obtained from rule-base technique, Hybrid fuzzy-rule base, MANFIS and experimental analysis for the rotor 167
8.2 Comparison of the results obtained from Hybrid fuzzy-rule base model, FEA, theoretical, MANFIS and experimental analysis for the rotor 168
9.1 Detail Description and Specifications of the apparatus used in the experiments 171

Nomenclatures

a1 a2	Depth of crack
A_1	Cross-sectional area
B	Width of Beam
b	Half width of crack in case of rotor
D	Diameter of rotor
E	Young's modulus of rotor
EI	Bending stiffness of rotor
F_x, F_y	Fluid forces on rotor in x and y-axis direction respectively
G	Shear modulus
I	Moment of inertia
J	Strain energy release rate
K_s	Stiffness of rotor
K_{44}	Stiffness of cracked rotor in 44-direction
K_{55}	Stiffness of cracked rotor in 55-direction
$K_{1,i}$	Stress intensity factor for Pi loads
K_{ij}	Load flexibility matrix elements
L	Length of rotor
L_1 L_2	Location of crack in rotor
m	Fluid mass displaced by the rotor par unit length
m_s	Mass of the rotor per unit length
M	Equivalent mass of fluid displaced by a rotor
M_s	Equivalent mass of rotor
$M_{s1}=M_D$	Mass of disc
M_{s2}	Mass of rotor
M_1M	Equivalent mass of fluid displaced by a cracked rotor in 44-direction
M_2M	Equivalent mass of fluid displaced by a cracked rotor in 55-direction
M_1M_S	Equivalent mass of a cracked rotor in 44-direction
M_2M_S	Equivalent mass of a cracked rotor in 55-direction

M_i	Compliance constant
P	Fluid Pressure
P_i	Load
q	Gap ratio $((R_2-R_1)/R_1)$
R_1	Radius of rotor
R_2	Radius of fluid filled container
R_D	Radius of disc
u_a	Radial flow velocity at point 'A'
v_a	Tangential flow velocity at point 'A'
β	Relative crack depth (a1/D)
α	Relative crack location (L_1/L)
δ	Whirling radius
δ^*	Dimensionless amplitude $\left(\delta^* = \delta_n^* = 1,2\left(\delta_1^*, \delta_2^*\right)\right)$
ε	Eccentricity
ε_1	Eccentricity along 44-direction
ε_2	Eccentricity along 55-direction
ν	Coefficient of kinematics viscosity
ν_1	Poisson's ratio
ρ	Density of fluid
ρ_1	Mass density of material
ω	Rotating speed
ω_0	Fundamental natural frequency of the rotor without disc
ω_n	Natural frequency
ω_{0r}	Critical speed (1^{st}) of the rotor
ω_{xx}	Fundamental natural frequency of a cracked shaft in x-direction
ω_{yy}	Fundamental natural frequency of cracked shaft in y-direction
ω_{44}	Fundamental natural frequency of a cracked shaft in 44- direction

ω_{55}	Fundamental natural frequency a cracked shaft in 55- direction
ω_{crack}	Natural frequency of cracked rotor
Ω	Angular velocity of whirling
44-direction	Direction perpendicular to the crack
55 direction	Direction along the crack
ANN	Artificial Neural Network
BPNN	Back propagation neural network
RBFNN	Radial basis function neural network
MANFIS	Multiple Adaptive Neuro-Fuzzy Inference System

Note: - The symbols and abbreviations other than above have been explained in the text.

Chapter 1

Introduction

The rotating device plays a significant role in many industries and several engineering fields. Not only it's used in large machines such as pumps or turbines in power generation plants and large vehicles such as ships or airplanes, but it is also used in small machines in factories, automobiles, and computer hard drives. One of the dangerous components in the rotating machinery is the rotor since it is an important part that conveys power to the other device to do work on the machines. Cracks can arise on the rotor from a variety of causes, such as bending and torsion stresses. Accordingly machine failure due to cracked rotor can compromise the safety of human beings and also due to crack occurrence more maintenance and operating costs are required. The current chapter highlights the methodology that is being used for analysis of cracked rotor. The first section introduces the motivation in the area of analysis of dynamic behavior of faulty rotor. The final segment of the present chapter provides an outline of each chapter of the dissertation.

1.1 Motivation of the Research Work

The vibration analysis of the rotor has been given great significance in the area of vibration due to the frequent catastrophe of such rotor in engineering applications. The development of health monitoring techniques is most significant to avoid sudden and unexpected failure of the rotor systems. The rotor is one of the most important elements of the machines. Any distraction present in this rotor may lead to the loss of assets and also the loss of life. It is, therefore, most important to ensure the safe and sound performance of the rotor by periodic monitoring. In the literature survey, many methods are available for assessment of crack present in the rotor. But not reported in detailed for the analysis of rotating cracked rotor in the fluid medium. Furthermore, when a rotor rotates with transverse crack submerged in a viscous fluid medium, then it is very difficult and complicated to analyses the rotor. In the present analysis, an effort has been taken to develop a tool using the vibration response of non-cracked and cracked rotor with the help of theoretical analysis, experimental analysis, FE analysis and artificial intelligence

technique.The AI techniques are modeled with an objective of fast and accurate measurement of cracks present in the rotor. Fuzzy logic system (FLC), neural network model and multiple ANFIS models have been designed and analyzed in current research for prediction of multiple cracks present in the rotor partially submerged in the viscous medium to ensure the smooth and safe operation by arresting the vibration response. To develop experimental setup to perform the experimental exercises for validating the results obtained from the above mentioned soft computing techniques.

1.2 Aims and Objectives of the Proposed Research Work

It is essential that rotor must be safe and function properly throughout service life but cracks commence a breakdown in the rotor. The presence of crack is a crucial threat in the rotor. It is a well-known circumstance that vibration characteristics of the rotor change because of an existence of crack and viscous fluid. It has been noticed that the existence of the cracks in rotor leads to catastrophic failure, operative failure as well as early failure. The numbers of researches are reported on the dynamic analysis of rotor and mostly on the vibration analysis of cracked rotor. The vibration behaviour (i.e. Natural frequency and amplitude) of the rotor varies due to the occurrence of crack and viscosity of the fluid medium. The change in vibration response has been used by the investigator as one of the principles of the fault diagnosis for the rotor. In general, this technique can be very helpful for crack identification in the rotor partially submerged in the fluid medium. In the present examination, many literatures available so far have been studied and investigated.The aims and objectives for the research towards analysis of dynamic behaviour of rotor with multiple transverse cracks partially submerged in the viscous fluid are summarized below:

- Theoretical investigations of the cantilever and fixed-fixed rotor with multiple transverse cracks partially submerged in the viscous fluid medium have been accomplished to evaluate the dynamic responses.
- To measure the vibration signature of non-cracked and cracked cantilever rotor, influence coefficient strain energy method has been used.
- To analyse the influence of fluid forces on the rotor, Navier-Stokes equation has been used.
- Development of the experimental test rig to perform experimental exercises to obtain the vibration behaviour (i.e. Natural frequency and amplitude) of the

cantilever rotor with multiple transverse cracks immersed in the different fluid medium.

- Finite element analysis using ANSYS 14.0 tool to determine the dynamic responses of the non-cracked and cracked cantilever rotor partially submerged in the viscous fluid medium are to be applied.
- Design and development of the fault diagnosis tool for multiple crack identification in rotor using the intelligent expert systems such as fuzzy logic system, adaptive neural network, MANFIS and rule-base technique are to be carried out.

1.3 Methodologies Applied for Proposed Research Work

The methodologies with the particular steps applied for proposed research work is summarized as follows:

- Study of the various techniques applied to vibration analysis of rotor with transverse cracks in the literature survey is carried out.
- Theoretical investigation of the cantilever and fixed-fixed rotor with multiple transverse cracks partially submerged in the viscous fluid medium has been accomplished to evaluate the dynamic responses in both transverse directions (i.e. 44 and 55-direction) of crack in rotor.
- Measuring the vibration signature of non-cracked and cracked cantilever rotor using Influence coefficient strain energy method.
- Consideration at the variation of the crack orientation of the rotor to find out their effect on the dynamic characteristics of rotor immersed in the viscous fluid medium.
- Analyse the influence of fluid forces on the rotor using Navier-Stokes equation.
- Determination of the local flexibility at the vicinity of crack positions in rotor using the stiffness matrix.
- Application of Finite element analysis using ANSYS 14.0 tool to determine the dynamic responses of the non-cracked and cracked cantilever rotor partially submerged in the viscous fluid medium.
- Development of the Mamdani fuzzy and Takagi-Sugeno fuzzy architecture for finding the multiple cracks in the rotor.
- Hybridization of the Mamdani fuzzy and Takagi-Sugeno fuzzy to adjust and tune the input/output membership function parameters of the fuzzy controller. This developed

hybrid fuzzy system improves the performance of fault diagnosis tool for finding the multiple cracks in rotor in viscous fluid.

- Design of an adaptive neural network (i.e. BPNN and RBFNN) architecture for identify the multiple crack in rotor.
- Development of the MANFIS controller for detecting the cracks in rotor.
- Integration of the fuzzy controller model with the rule-base technique called as hybrid fuzzy-rule base technique for detecting the multiple crack locations and depths in cantilever rotor.
- Building an experimental setup for performing the experiments to evaluate the vibration behaviour of cracked cantilever rotor submerged in the viscous medium.
- The obtained results from the proposed techniques which cited above are to be authenticated with the developed experimental setup.

1.4 Novelty of Proposed Research Work

In literature survey, it is found that the most of the researchers have applied the various methods for vibration analysis of the static or dynamic behaviour of the rotor with transverse crack in air medium. However, few researchers have reported the vibration analysis of damaged structures in viscous fluid medium in dynamic condition and have not considered the artificial intelligence system for fault diagnosis of rotating structures.

The novelty of this dissertation is dynamic analysis of rotor with multiple transverse cracks partially submerged in the viscous medium.The artificial intelligence technique such as fuzzy logic system (FLC), adaptive neural networks, multiple adaptive neuro fuzzy inference system (MANFIS) and rule-base technique have been design and developed for the identification of multiple cracks using the dynamic response of rotating multiple cracked rotor system in the viscous fluid medium.

In this research work, the application of hybrid fuzzy technique and rule-base technique for the diagnosis of multiple cracks in rotor has been carried out. Beside, this rule-base controller is integrated with the fuzzy controller to adjust and optimize the antecedent and consequent parameters of the fuzzy membership function and it is not found during the literature survey.

1.5 Outline of the Research Work

In this thesis outline of the research work is distributed into eleven chapters. The analysis carried out in the current research for investigation of the effect of multiple crack locations and depths on the mechanical impedance of the rotor partially submerged in the viscous fluid medium are depicted chapter wise as follows.

- **Chapter 1** presents the influence of transverse crack on the rotor in different engineering or industrial applications. It also discusses the methods actually implemented by the engineering and scientists to examine the faults or damages in various engineering or industrial applications. This chapter also describes the motivations and objectives of the investigation along with the prominence of the proposed research.
- **Chapter 2** introduces the literature review of the vibration analysis of rotor with transverse cracks, partially submerged in the viscous fluid medium using different methodology, FEM, and Artificial intelligent techniques. This chapter also carries the classification of methodologies in the area of vibration analysis of rotor with different type of crack (i.e. transverse and breathing crack)
- **Chapter 3** investigates the vibration behaviours of cantilever and fixed-fixed rotor with multiple transverse cracks, partially submerged in the viscous fluid medium using the influence coefficient method and the strain energy release rate. The Navier-Stokes equation is used to analyse the external fluid forces. The presence of crack generates local flexibility at the vicinity of crack.Vibration analysis has been accomplished to evaluate the dynamic behaviour of the non-cracked and cracked rotor submerged in the different viscous medium. The results and discussion have been also presented in this segment. Finally, the theoretical and experimental analysis results have been compared with the results from theoretical investigation for authentication.
- **Chapter 4** introduces the FE analysis of the cantilever rotor carrying multiple transverse cracks partially submerged in the viscous fluid medium using ANSYS 14.0 tool to measure the dynamic response. The results of FE analysis are compared with the obtained results of theoretical and experimental analysis for authentication.
- **Chapter 5** discuses the theory of the fuzzy logic system using the Mamdani, Takagi-Sugeno fuzzy and hybrid fuzzy controller system for prediction the relative crack depth and locations. Triangular, Trapezoidal and Gaussian membership functions

based intelligent system with detail design are briefly discussed. The obtained results of fuzzy controller are compared with the results from the experimental investigation.

- **Chapter 6** introduces the hybrid BPNN-RBFNN neural network methodologies for multiple crack identification in rotor. The results of the BPNN, RBFNN and hybrid BPNN-RBFNN neural network are discussed in detail.
- **Chapter 7** introduces the ANFIS method for forecasting of relative crack locations and depths by means of dynamic response of multiple cracked rotor.The obtained results from the fuzzy logic system, neural network, MANFIS, theoretical and experimental investigation have been reported.
- **Chapter 8** discusses the hybrid fuzzy-rule base technique for the detection of crack locations and crack depths in rotor.
- **Chapter 9** presents the details of the experimental procedure along with the developed experimental setup for the vibration analysis. Finally, the experimental analysis results have been obtained and discussed in detail.
- **Chapter 10** presents a comprehensive review and analysis of outcomes obtained from various proposed methods cited in the proposed investigation.
- **Chapter 11** depicts the conclusions obtained from the investigation carried out in the present research and recommendations for the future scope of research work in the similar field.

Chapter 2

Literature Review

This chapter presents the review of research work associated with the analysis of dynamic behavior of the cracked structure (i.e. rotor, beam, plate) and the progress of crack identification tool in damaged structures. In the last few decades, improvement has been made in the field of crack diagnosis of rotor partially submerged in a viscous medium has been described. Finally, the applications of artificial intelligence techniques for crack identification and prediction are discussed from the past and recent developments.

2.1 Introduction

The literature review section introduces the investigation of the available research work constrained to the field of damage detection and characterization approach and model testing for engineering structure. The review commences with the depiction of altered dynamic analysis technique employed for identification of crack. Subsequently, vibration analysis of rotating cracked rotor, damage detection approaches to develop fault diagnosis tool utilizing the classical method, finite element method, Hilbert-Huang transform method and wavelet techniques are discussed. The artificial intelligence techniques (i.e. Fuzzy logic system, neural network, MANFIS, rule base technique and hybrid technique) can be designed and developed for the crack identification of the vibrating structure(i.e. rotor, plate, and beam).

The main goal of the current research is to propose an artificial intelligence methodologies, which is able to predict the existence of multi-crack in the rotor with considerably high precision and less computational time.The potential directions for investigation can be acquired from the exploration of the literatures mentioned in current chapter. From the available research works, it is perceived that the knowledge related to crack identification in various systems differs extensively.In spite of all, there is an extensive discrepancy in the enhancement of crack detection technique.

2.2 Analysis of Differnent Methodologies for Crack Identification in Rotor

2.2.1 Classical Methods for Identification of Crack

The enhancement of methodology for crack identification in real world establishes the most significant inclination in the present research work on crack identification. Investigators have concentrated on many methods based on the vibration analysis for detection of damage in several sectors of engineering structure which is efficiently used for health monitoring in a faulty system.The recent methods adapted for fault diagnosis are outlined below.Dimarogonas [1] has presented a review article on several fault detection techniques reported by the researcher (1971-1993).Doebling et al. [2] have presented the detailed review of vibration based damage identification and structural health diagnosis methods up to 1996. Kastsikadelis and Tsiatas [3] have done the nonlinear dynamic analysis of the bernouli-eular beam with variable stiffness undergoing large deflections and nonlinear boundary conditions.They have derived the governing equations in both deformed, and undeformed configuration and error of the two approaches are studied.Gams et al.[4] have presented the vibration analysis of highly flexible elastic planar beams using finite element analysis. They have developed the equation of motion from the Hamilton principle including only strain variable, and Galerkin type finite element discretization is applied.

Chung and Yoo [5] have discussed the vibration based analysis of a cantilever beam using the finite element formulation. They have applied the stretched deformation instead of the conventional axial deformation based upon the dynamic modelling and obtained the three differential equation using the Hamilton's principle.Cai et al. [6] have applied the Hamilton theory and Finite element method for the vibration based analysis of a flexible hub beam system carrying a mass at the tip of free end..Chang and Liu [7] have employed the finite element analysis with consideration of effect of longitudinal deflection and inertia for analysis of vibration characteristics of non-linear beam subjected to moving load.Coupled equation of longitudinal and transverse deflection calculated based on the Bernoulli-Euler hypothesis. Galerkin method with the finite element method is used to calculate the statical dynamic response of beam. They have used implicit direct integration method for calculating the non-linear system differential equation.Li et al. [8] have developed a finite element formulation with generalized degree of freedom for the

dynamic analysis of plates and beam with varying cross-section in a continuous or discontinuous manner. They have simplified the derivations of finite element or finite strip formulation applying the second order polynomial. The local displacement and global displacement field of an element are modeled using interpolating polynomials and quadratic B-spline respectively.Fedeliński [9] has reported the analysis of cracked structure using boundary element method. However, the crack growth of structure with variable and constant velocity, which is depends upon the fracture condition of model. Orhan [10] has developed the free and forced vibration based analysis method to finding the crack position and crack depth in the cracked beam. Natural frequencies are obtained from the free vibration analysis.Harmonic response has been obtained on the force appliance point.The changes in the natural frequency and harmonic responses corresponding to changes in crack depth and location. Ghoneam [11] has reported the numerical and experimental methodologies for the analysis of dynamic behavior of the cracked laminated composite beam.They have considered crack location, crack depth, various number laminates and boundary conditions as main variable parameters.

Lin [12] has reported the vibration based analysis of multiple span beam carrying a different concentrated element using the numerical assembly method. He has derived the coefficient matrices for the pinned support, intermediate concentrated elements, applied force, right-end and left-end support of a beam. Lin and Wu [13] have discussed an Eigen analysis problem regarding planar closed frame structure which is dynamically analyzed by applying the hybrid numerical method.This is useful for numerical execution of a transfer matrix solution to the analytical equation of motion. Eigen value can be calculated by the continuation of the non-trivial solution and considered for the correlation between the first section and the last section of the closed structure. Fotouhi [14] has studied the vibration analysis of uniform cantilever beam with large deflection using the Finite Element approach. He has set the three objectives for this investigation. The first objective was to detail the behavior of the problem as it converts the linear to a nonlinear problem and the Second objective was to implement the finite element code for the particular problem. The third objective was to investigate the stability of particular evenness position with the help of a nonlinear dynamic analysis.They have evaluated the stresses, strains, forces and time varying displacements in the flexible beam due to transient, harmonic and static load. Banerjee [15] has presented the proposed the dynamic stiffness method, for vibration based analysis of beam moving mass system and combined the stiffness dynamic matrix and spring mass element of the beam, which is used to prepare the eigen value

problem for free vibration analysis. He has determined the vibration response (i.e.natural frequencies and mode shape) of a cantilever beam attached with spring-mass at the tip of free end using the wittrick-Williams algorithm for.Xiang et al.[16] have proposed the combination of wavelet based element and genetic algorithm(GA) method to identified the crack in the shaft. The cracked shaft is modeled using the wavelet based element to acquire a definite frequencies. They have used the three definite measured frequencies to identify the crack location and crack depth with the help of a genetic algorithm. For the inverse problem analysis, GA is used to rectify the error in frequencies which is obtained by the numerical and experimental analysis. El-saeidy [17] has employed the finite element formulation for vibration based analysis of a spinning shaft with or without non-linear boundary condition subjected to a moving mass load. The equation of motion is derived by utilizing the Lagrange's equations, which is sequentially decoupled using modal analysis articulate in the normal co-ordinate representation.

Fu et al. [18] have investigated the non-linear dynamic stability of a spinning cracked shaft carrying a disk in mid span. The standard unstable region is established by Floquet theory and Runge-Kutta method.They found that by increasing the thickness of the disc, the critical speed of shaft and area of an unsteady region are slightly decreased. Sekhar and Prasad [19] have studied the vibration behavior of the rotor-bearing system with slant crack using the finite element analysis. They have developed the stiffness matrix of a slant cracked element. It is successfully utilized in the Finite Element Method analysis of the rotor bearing system. Jun [20] has reported the vibration based analysis of rotor with transverse crack subjected to bending moment at crack location. Complex transfer matrix is used to expresses the equation of motion. The additional slope is considered as an excitation source. The dynamic and gravity–induced static bending moment are systematically articulated as the function of the additional slope at the crack. Han and Chu [21] have employed the Bolotin's and Harmonic balance method to investigate the steady-state response and instability of a rotating shaft including an elliptical front crack. In this article the breathing effect on the crack shaft studied. They have developed the local flexibility matrix on the crack of the shaft and the equation of motion of cracked shaft system formulated using the assumed mode method.Rajab and Al-Sabeeh [22] have investigated the vibration behavior of the crack Timoshenko shaft. They have developed the analytical expressions by crack modelling as shear load and bending moment agreements of incremental strain energy using J-integral concept from fracture mechanics. They have computed the vibration response of the shaft having transverse crack using

characteristics equation of the cracked shaft. Tsai and wang [23] have proposed a novel methodology to detect the position and size of the stationary cracked shaft. They have employed the transfer matrix method which is solved based on the Timoshenko beam theory to determine the dynamic response of the shaft and predicted the crack from the difference of the fundamental modes between the uncracked and cracked shaft. Additionally, the size of crack is recognisesd from the deviations of the crossponding natural frequency. Singh and Tiwari [24] have discussed the transverse frequency response function for investigating a multi-cracked shaft system.They have developed two-stage identification method which recognizes a number of cracks, sizes of crack and their location in the shaft. The finite element methods based on the Timoshenko beam theory are utilized to analyze the transverse forced vibrations of a non-rotating cracked shaft in two orthogonal planes.

Papadopoulos and Dimarogonas [25] have studied a coupling of longitudinal and bending vibration of a rotating shaft carrying a transverse surface crack. Nerantzaki and katsikadelis [26] have discussed the nonlinear vibration based analysis of round plates with changeable thickness with large deflection using boundary element technique.This technique is based upon the theory of analog equation which changes the principal coupled non-linear equation with flexible constant. Hashemi et al. [27] have presented a vibration based dynamic analysis of spinning thick plate using the FEM formulation and also used the Mindlin plate theory and second order strain displacement combined for modeling the plate.They have derived the non-linear governing equation of motion by the Kane dynamic method which includes Coriolis effect and coupling between in plane and out of plane deformation.

Si et al. [28] have suggested the Rayleigh-Ritz technique for analysis of dynamic behavior of baffled rectangular cracked plate subjected to an infinite water region. Displacement trail function is expressed by adding mass density which is found by using the Green function approach. Hsu [29] has proposed the differential quadrature method to developed the equation of motion for a Bernoulli's Euler beam with a single transverse crack under condition of axial loading. Jun et al.[30] have reported the dynamic analysis of rotor with breathing crack. The equation of motion is developed for breathing cracked rotor based upon the fracture mechanics. The circumstances for crack opening and closing are derived with the help of switching crack model. They have estimated the cross-coupled stiffness's and direct stiffness using the concept of fracture mechanics by considering the partial opening and closing behavior of a breathing crack. Darpe et al.[31] have presented an

analysis of the Jeffcott rotor carrying two transverse cracks. Based on the concepts of fracture mechanics stiffness of the rotor is determined. They have studied the influence of the interface of the two transverse cracks on the and on the unbalance response and breathing behavior of the rotor.Takahasi [32] has applied the transfer matrix approach for the vibration and instability analysis of a cracked non-uniform Timosinko shaft subjected tangential force which is concentrated over the center line with an axial force. They have determined the natural frequency, critical flutter load considers the effect of varying cross-section, crack depth, crack position and stiffness of the cantilever cracked beam. Buśkiewicz [33] has presented the dynamic analysis of the beam with moving boundary conditions using the Finite Difference Method. Also, they have studied the transfer of energy between the vibrating beam and moving support under assumption zero slopes of the elastic beam line at the moving support. Hamilton's principle are used to express the equation of motion to depict the interaction between elements the system. Nahvi and Jabbari [34] have developed a method to identify the crack position in the beams based on experimental modal analysis results.The finite element model of the beam was updated using the obtained result of experimental analysis.They have formulated the stiffness matrix of a cracked beam element consideration of bending and shearing forces.

Hwang and Kim [35] have proposed the frequency response method to detect the locations and intensity of crack.This method detects the position and severities of crack by reducing the difference between the test and analytical FRFs. Binici [36] has proposed the novel method for determining the Eigen frequency and mode shapes of multiple cracked beams, which subjected to axial force.Çam et al.[37] have reported the vibration based analysis of the cracked beam structure. They have determined the position and depth of cracks with the help of analyzing the vibration signal.Also, they have used the ANSYS software to simulate the problem. Jun and Gadala [38] have examined the dynamic characteristics of the rotor carrying breathing crack. The additional slop is used to consider the breathing crack and equation of motion as one of the input to create the bending moment at the crack position. They have evaluated the additional slope by integration on the crack position based on the concept of fracture mechanics and transfer matrix method is employed to obtain the response of the crack rotor.

Prokić and Lukić [39] have proposed the Benscoter's theory for analyzing the dynamic response of thin-walled beam of the closed cross-section. They have derived the differential equation of motion considering the virtual work due to variation in displacement. Saavedra and Cuitino [40] have established an innovative element stiffness

matrix on the crack element using the theory of linear fracture mechanics for the analysis of the cracked multi-beam system. The function of Strain energy density is employed to determine the flexibility that the crack generates in its area.They have used the Hilbert,-Hughes -Taylors (HHT)integration technique for deriving the equation of motion. Chen and Chen [41] have investigated the instability of cracked rotor subjected to an axial compressive force the and also, considered the influence of the crack on the whirling speeds of the shaft. They have employed Finite element method (FEM) to achieve the numerical results.Qian et al. [42] have suggested the finite element formulation for analysis the dynamic behavior of the cracked beam. They have used stress intensity factor to developed the element stiffness matrix of a cracked beam.

Sinou et al.[43] have discussed the effect of transverse breathing crack on the nonlineaner behavior of rotating shaft using the alternate frequency /time domain technique. They have determined the non-linear behavior of cracked rotor by modelling the crack with truncated Fourier series. Song et al.[44] have applied the scaled boundary finite element method to determine the transient response of finite biomaterial plates with interface crack.They have determined the complex dynamic stress intensity factor from the crack opening displacements of the singular stress term. Arruda and Castro[45] have proposed a hybrid–mixed stress finite element model for the linear dynamic analysis of structure. HMS model has considered two independent approximations for the stress and the displacement in the region of each element. Time integration techniques are used to perform the linear dynamic analysis.Eshmatow et al. [46] have presented the effect of properties of structure material (i.e. viscoelastic and in homogenous) on the stability of the plate.They have determined the results by applying the bubnow-galerkin procedure combined with a numerical method based on the quadrature formulas.

Cheng and Hatam [47] have presented the vibration analysis of the point coupled structure using the finite element method. Also, they have studied the effect of biased compliance measurement on the accuracy of the prediction. Patil and Maiti [48] have suggested a technique for fault recognition in a slender Euler-Bernoulli beam using frequency measurement and the transfer matrix method. They have considered cracks as rotating springs in the analytical method for identification of cracks.Ebersbach and Peng [49] have proposed an enhance technique for the condition monitoring of fixed plant machinery, using proven industry method. They have observed that developed system can be used to detect failure with high precision using the dynamic response of the system.Finite element methods and wavelets transform method are used to find the size and severity of

cracks.Cerri et al. [50] have presented theoretical analysis for the vibration based analysis of a circular arc in both faulty and non-faulty models to design a damage detection method. They have compered the obtained results of theoretical analysis with the results of experimental analysis for validation. They have used the mode shapes and natural frequencies to develop the damage detection model with the assumption, the arch act as a torsion spring on the cracked section. Humar et al. [51] have presented a survey on some of the common vibration base crack detection techniques and discovered the drawbacks in them. The presence of cracks in the structure has badly affected the modal response, stiffness, and damping.They have found that the vibration-based damage detection techniques, fail to perform when applied to real structures due to the inherent complications.

He et al. [52] have presented a method to determine the local flexibility matrix and stress intensity factor of cracked beam to formulate a technique for crack dection. Zou et al. [53] have reported a developed method of the local flexibility of a cracked rotor system. They have examined the vibration characteristics of the rotor with transverse crack to design for forward application as a crack diagnostic model. Patel and Drape [54] have dicussed the analysis of nonlinear dynamic behaviour of the shaft containing breathing crack. They have proposed the response–dependent breathing crack model and switching crack model to investigated the nonlinear dynamic analysis of cracked rotor. Bachschmid et al. [55] have invstigated accuratly the breathing crack mechanism in rotating shaft with the help of the 3D non-linear models. Also invatigated the effect of crack on the cross section of the rotor due to mutual action of the torsion and bending.They have developed the model, which consider the linear stress and strain allocations for established the breathing mechanism.

Sawicki et al. [56] have presented the analysis of dynamic behavior of rotor of machines with transverse breathing crack that is open and closed due to self-weight. They have applied auxiliary magnetic bearing (AMB) for detection of crack in the rotor. Xiao-feng et al. [57] have presented the nonlinear vibration analysis of the cracked rotor with or without whirling.Authors have found distinct differences in bifurcation, orbit and amplitude while carrying on this comparision.Zhu [58] has analyzed theoretically the vibration based analysis of a cracked rotor with an active magnatic bearing. He has discussed the influence of crack on the stability of the active control system. Bovsunovskii [59] has analyzed the influence of crack depth and location on the vibration behavior of the cantilever beam by considering the changes in the cross-section. Rayleigh

method is used to obtained the frequency of the first mode of cantilever beam with breathing crack(i.e. open and close crack) due to vibration of longitudinal and bending loading.Müller et al.[60] have discussed the vibartion based nonlinear dynamic analysis of the rotating cracked shaft. Theory of lyapunov exponents is developed for the nonlinear dynamical systems, chaotic motions and strange attractors in the case of a faulty rotor.They have used Model-based technique to crack dection in shaft. Zhou et al. [61] have investigated the vibration based nonlinear dynamic behaviour of the cracked rotor by numerical and experimental analysis. The eccentricity, depth of crack and angle of crack are taken as an influence parameters for the analysis of cracked rotor.

Ishida et al.[62] have proposed the method to identify the crack in the rotor based on the nonlinear vibration diagnosis by means of harmonic excitation force. They have employed piecewise linear function for modeling the open and close crack mechanism.Qin et al. [63] have proposed a Piecewise linear function employed to model the cracked rotor for vibration based nonlinear dynamic analysis of a cracked rotor. They have developed the differential equations of motion for the non-smooth system.Sinha [64] has investigated the nonlinear dynamic behavior of the mechanical system for detecting the presence of higher harmonics spectra in a signals obtained from the system applying higher order spectra tools. He has found the misaligned axis of rotation of the shaft and crack exhibits a nonlinear behavior because of the existence of greater harmonics spectra in the indicator. According to author, the higher order spectra tool in indicator can be actually utilized for monitoring condition of rotatory mechanical arrangements.

Babu et al. [65] have discussed the transient analysis of a cracked rotor system with transverse breathing crack for the flexural vibrations using Hilbert hung transform method. Guo and Peng [66] have suggested the Hilbert hung transform (HHT) method for analysis the non-linear response of the cracked rotor. They have applied the FEM and dimarogonas methods to develop the model of rotor with a growth crack. Han et al. [67] have discussed the dynamic behaviour of a geared rotor- bearing system carrying a breathing crack. They have developed the slant crack geared-rotor model using the FEM and also used the stress intensity factor based on fracture mechanics for calculating the flexibility matrix for the slant crack. Khanlo et al. [68] have investigated the effect of lateral torsional coupling on the dynamic characteristics of the a spinning shaft-disk system. They have used Rayleigh beam theory to develop the equation of motion. Guo et al. [69] have reported the analysis of dynamic behaviour of the Jeffcot rotor carrying transverse breathing crack.They have employed the Floquet theory for evaluating the

stability of the rotor system considering the spinning speed and crack depth. Auciello and Nole [70] have presented the vibration analysis of the cantilever beams containing a mass at the free end. In this study authors have assumed two different calculation methods. First is an exact method which has solved the problem using the Bessel function, and another one is Rayleigh-Ritz method using orthogonal polynomials as test functions. Caddemi et al. [71] have investigated the non-linear dynamic behavior of the beam with multiple concentrated switching cracks (i.e. cracks are either fully open or fully closed). They have developed crack model employing Dirac'c deltas which permit the closed-form estimation of the mode shape of the beam for general crack configuration. Presas et al. [72] have analyzed the effect of the rotation on the vibration response (i.e.natural frequencies and amplitude) of the imeresed-confined disc in the fluid filled container by analytically, experimentally and numerically.Thin plate theory are used for modelling the disc, and Laplace equation are used for the fluid flow velocities on the lower and upper parts of the disc.Computation fluid dynamic (CFD) simulation has been done for the fluid flow inside the container in order to evaluate the average speed of water on the lower and upper area of the disc for changed velocities.

2.2.2 Finite Element Method used for Identification of Crack

Darpe et al. [73] have proposed the transient anlaysis of the dynamics of bowed rotor carrying a transverse crack. They have analysed the transient response of the transversed cracked rotor considered with and without gravity. Also investigated the effect of bow on the open and closed crack mechanism of the rotor for the different intensity value of bow. Georgantzinos and Anifantis [74] have proposed a nonlinear finite element method for simulation of quasi-static crack breathing mechanism in rotating shaft. This process can predict successfully the contact between the crack surfaces by means of the anagle of crack rotation. Bachschmid and Tanzi [75] have presented the analysis of circular cross section cracked beam with different crack depths subjected to shear, axial and torsion loads. Sekhar [76] has investigated the dynamic behavior of the rotor carrying double transverse crack using developed finite element modeling of a rotor-bearing system. He has determined the changes in stability and eigen frequencies with parameters of crack for shaft parameters such as slenderness ratio.

Chasalevris and Papadopoulos [77] have presented the vibration based analysis of a beam with doubled transverse crack. They have considered the crack location, crack depth, and relative crack angle as a variable parameter for this analysis. The compliance matrix is

calculated using the integration method of strain energy density function on the open crack area. Nandi [78] has proposed an effective analysis of rotor instability. They have used the standaraed method of assumed solution for solving the above rotor stability analysis. Mohamed et al. [79] have reported the analysis of vibration characteristics of rotor with two different types of crack, a notch cut to changeable depths and actual crack growth from a pre-crack. The vibration based condition health monitoring technique is employed to evaluate and monitored the begning of fatigue crack and propagation in a pre-cracked of high carbon steel rotor. Baviskar and Tungikar [80] have proposed the inverse technique for fault detection in moving parts. The model of beam is developed with the help of finite element method.

Hossain et al. [81] have developed the experimental test rig for the vibration analysis of a cantilever beam partially immersed in air and fluid medium and vibration response is measured with the help of Polytech scanning vibrometer. Also, they have used the finite element analysis (FEA) method to forecast the dynamic response of the same beam.The alteration in the vibration response of the beam such as frequency, amplitude and resonant frequency are compared as functions of the rheological properties of viscous fluid. Georgantzinos and Anifantis [82] have examined the effect of the breathing crack mechanism on the rotating crack shaft assuming the quasi-static approximation. The nonlinear contact–FEM method are used for the analysis of circular cross-sectional cracked cantilever beam subjected to torsion load. Kerboua et al.[83] have reported the analysis of the vibration characteristic of the rectangular plates coupled with the fluid.They have developed the mathematical model of the plate using the Sander's shell theory and finite element method. The fluid pressure is analyzed with the help of velocity potential and Bernoulli's equation. Darpe [84,85,86] has proposed innovative technique to identify the crack size and location in the rotating shaft carrying the breathing crack subjected the transient torsional excitation. Author has determined the instability behavior of the rotor with slant crack using the nonlinear breathing crack model. He has considered the finite element model of the disc rotor containing the six degrees of freedom per node for the cracked area and formulated the stiffness matrix turns into account all the coupling phenomenon (i.e.Longitudinal-torsion,bending-torsion,bending-longitudinal) that occurs in the area of crack on the rotor.

Silania et al. [87] have reported the vibration based analysis of dynamic behavior of rotating shaft system with breathing crack. Modified integration method is used to compute the stiffness matrix of cracked element. They have employed the Finite element

formulation for breathing crack modelling and frequency/time domain methods are used to calculate the vibration characteristic of the rotor with breathing crack. Kulesza [88] have suggested a technique for identification of crack in the rotor using a multisine technique. Authors have employed the finite element analysis for the flexible spinning shaft modelling. Sekhar and Prasad [89] have reported the flexural vibration based analysis of the rotor-bearing system with a cracked shaft using Finite element method. They have developed the flexibility matrix and stiffness matrix of a crack element to be employed in the FEM investigation of the rotor bearing system.

2.2.3 Wavelet Transform and Wavelet Finite Element Method used for Identification of Crack

Nguyen and Tran [90] have repoerted a novel technique for crack identification of the structure based on the wavelet transform of the vibration response obtained from a moving vehicle.Ren et al. [91] have investigated the vibration behaviour of the rotor with transverse crack using wavelate scalogram method based on the 3-D water fall spectrum.Yang et al.[92] have examined the non-linear dynamic behaviour of model-based rotor with transverse crack using wavelet based algorithm that is efficiently identifying the mechanical chaotic response.Xiang et al. [93] have proposed a novel methodology for recognizing the crack size and crack location in the rotor using finite element method of B-spline wavelet on the interval (FEM BSWI). They have developed the disc and slender shaft model using BSWI Rayleigh-Timosinko beam element and BSWI Rayleigh–Euler beam element respectively.

Jibing et al. [94] have suggested the harmonic wavelet transform (HWT) and Poincare map technique for identifying the various types of motion of the existing system due to change in parameters of nonlinear vibration system. The HWT is useful to recognize the quasiperiod from chaos and Poincare map method is used to recognize the periodic motion of the system. Ma et al. [95] have proposed the new wavelet based beam element method for analyzing the complicated beam such as those with uneven cross section, local load. They have developed Wavelet based beam element method using the daubechies scaling element functions.Li et al. [96] have proposed a wavelet Finite element method (FEM) to recognized crack size and crack location in beam. They have discretized the beam into the a set of wavelet finite element to correctly determined the vibration response (i.e. natural frequency) of the beam with different crack size and crack location. Gómez et al. [97]

have reported the wavelet transform theory (WTT) for crack identification in jeffcot rotor of the rotating machinery.

2.2.4 Other Approaches are used for Identification of Crack

Gasch [98] has investigated the dynamic behaviour of a cracked rotor carrying a disc in the mid span. He has formulated the non-linear equation of motion for the crack rotor model and only concentrated on the lateral vibration. Floquets method are used for the stability analysis of the rotor. Sino et al. [99] have presented the vibration based anlaysis of dynamic behaviour of rotating composite shaft with internal damping. They have estimated the natural frequency and instability thresholds using the Homogenized finite element beam model with considering the internal damping and also compared the urbanized simplified homogenized beam theory with the equivalent beam modulus theory (EMBT).Wang et al. [100] have presented the vibration analysis of the horizontal axis wind turbine using the thin walled structure theory. Stress-displacement field, dynamic displacement and stress distribution of the wind tower blade rotor are estimated from the forced response analysis.

Szolc et al.[101] have suggested the stochastic method for crack identifying cracks in the rotating shaft of the machines.This method is based on the Monte Carlo simulation of the rotor torsional-lateral-longitudinal vibration with open crack at arbitrarily selected locations and depths on the shaft. Gomez-Mancilla et al. [102] have invetigated the effect of transverse crack in a orbital position of cracked rotating shaft. Shulzhenko and Ovcharova [103] have presented the numerical analysis for the influence of the break of the elastic axis of rotor with transverse crack on its vibrational. Dong et al. [104] have proposed a wavelet finite element model and high precision model parameter identification method for identifying the crack location and crack depth in rotor carrying transverse crack. Simultaneously a new method Laplace wavelet based and empirical mode decomposition is developed to obtain the high precision model parameters, which is employed to progress the accuracy of crack recognition.Stoisser and Audebert [105] have discussed theoretically the three-dimensional beam model with transverse crack and also presented the numerical and experimental approach for crack identification in rotating machinery of power plant.

Mueller et al.[106] have studied the different methods for estimating the initiation of creep crack.They have compared the two Criteria Diagram (2CD), Nikbin-Smith-Webster (NSW) model and Time Dependent Failure Assessment Diagram (TDFAD) method for

predicting the creep crack commencement.Chen et al. [107] have reported a novel approach for investigating the nonlinear behavior of a cracked rotor system including an effect of crack size. Mass of the rotating shaft carrying a disc in mid-span, the nonlinearity of the rotor and additional displacement of the rotor due to the presence of transverse crack are considered for establishing the method.Also, they have investigated the dynamic stability of rotor system. Pennacchi and Vania [108] have discussed the model based analysis of the gasturbine shaft (100MW) because of the propagation of transverse crack with coupling load. Shahgholi et al. [109] have discussed the analysis of the dynamic behaviour of a nonlinear spinning simply supported shaft.They have considered the rotary inertia and gyroscopic effect for the modelling of the system. Extended Hamilton principle is used to formulate the equation of motion of the system. Phan et al. [110] have discussed the vibration analysis of rectangular cross sectional cantilever beam partially submerged in a viscous fluid medium under harmonic base excitation.The interaction between fluid and structure (i.e.cantilever beam) are developed using a complex hydrodynamic function.

Curadelli et al.[111] have presented the experimental and numerical investigation of the vibration behavior of spherical tanks under horizontal motion.The main aim is to find the natural frequencies of the modes which contribute to the dynamic behavior of this certain structure.Chouksey et. Al [112] have discussed the model analysis of rotor with consideration the effect of internal damping of rotor material and the fluid-film forces.They have formulated the equation of motion using the 2-noded finite Rayleigh beam elements. Liang et al.[113] have proposed a methodology to define the vibration mode shapes and frequencies of cantilever plates which are submerged in the fluid medium on the basis of empirical added mass formulation. Uscilowska and Kołodziej [114] have reported the vibration based analysis of an offshore structure.The structure is modelled as a uniform Bernoulli- Euler cantilever beam fixed at the bottom end with an intense mass at the top. Arruda and Castro [115] have proposed an FE model of hybrid-mixed stress for the vibration based analysis of the dynamic behavior of the structure assuming a geometrically and physically linear manner. They have used time integration technique to accomplish the linear dynamic analysis.

Singh and Tiwari [116] have presented experimental analysis to validated the multi-crack detection and localization (MCDLA) algorithm for the multi-crack identification and localization of the simply supported shaft. The performance of the algorithm is totally based on the identification of slope discountinuity. Rubio et al.[117] have discussed the

static analysis of the vibration response of the shaft in bending with elliptical shape of crack at a different position of the shaft by using the polynomial expressions of the flexibility. Vaziri and Nayeb-Hashemi [118] have determined the effective third mode stress intensity factor for multi-cracked circular shaft subjected to torsional load using the asperity-interlocking mechanism.Gubran and Sinha [119] have investigated experimentally the dynamic behaviour of the bladed disc due to instantaneous angular speed which is transmitted to the shaft as a torsional vibration. Eftekharnejad et al. [120] have employed the many techniques such as motor current signature analysis, acoustic emission and vibration analysis for the identification of existing crack in the pinion shaft of a gear box.

Liong and Proppe [121] have developed the cohesive zone model (CZM) for calculating the the stiffness losses in a rotor carrying transverse breathing crack.The breathing crack is modelled by a parabolic shape. Also they have analyzed the effect of breathing transverse crack mechanism on the rotor system which is performed because of self-weight and inertia forces. Abuzeid and Dado [122] have presented the analysis of the shaft with the transverse crack under pure bending considering the irregular surface at the crack position. Cheng et al. [123] have studied the effect of breathing crack and imbalance orientation angle on the dynamic behavior of the critical speed of the jeffcot rotor. Yadykin et al. [124] have presented the numerical study of cantilever plate with additional mass submerged in the fluid region. They have used the Airfoil Theory for analysis of an incompressible fluid flow forces. Fu and Price [125] have reported the vibration analysis of the cantilever plate which is partially or fully immersed inside the fluid. They have used the hydro-elastic theory for performing the interaction analysis between the vibrating the cantilever plate and fluid.

2.2.5 Artificial Intelligence Technique used for Identification of Crack

In this current section introduces the various types of Artificial intelligence techniques (ANN) used in the field of identification of fault in present in faulty structure (i.e. rotor, beam, plate) have been described.

2.2.5.1 Fuzzy Logic Technique

Wada and oka [126] have presented a fuzzy logic technique with the triangular membership functions for the image processing the governor level of granular inside the hopper. Ganguli [127] has developed a fuzzy logic system for ground-based structural

health monitoring system to detect the fault in helicopter for measuring rotating and non-rotating frequency in the vacuum. De Miguel and Blázquez [128] have proposed a fuzzy system based on prediction module for damage detection application. Chen [129] have presented Takagi-Sugeno (T-S) Fuzzy Models for the stability condition and controller design of the structural and mechanical system.They have designed the fuzzy logic controller by using the design procedure of the controller and parallel-distributed compensation. Boutros and Liang [130] have developed the fault identification technique using efficient fuzzy fusion method based on the Sugeno inference engine.They have validated the fuzzy-based method in two different approaches (i.e. Bearing condition valuation and milling tool conditioning monitoring of milling operation).

Zhang et al. [131] have proposed mechanical fault diagnosis technology based on the fuzzy grey optimizing prediction method with multi-dimensional fault characteristics parameter model for the rotating parts of the machines.Kim et al. [132] have proposed a fault identification system for reinforced concrete structures using the fuzzy system. The environmental condition, numeric data of concrete and symptoms of crack are considered as an input parameter in the fuzzy inference system. Angelov et al. [133] have suggested two novel methodologies (i.e. eClass and FLEXFIS) for progress the performance of on line fuzzy classifier. The eClass methods have a multi-input and multi-output with multiple hyper planes to build the fuzzy rule. Chandrashekhar et al. [134] have studied the measurement uncertainty and geometric for damage identification.They have studied the variation in the fault indication because of the ambiguity in the geometric properties of the structure using Monte Carlo simulation technique, and these simulation results are used for developing the fuzzy inference system.

Saravanan et al. [135] have reported a vibration signal based methodology for condition monitoring of remote moving parts in the machines. The decision tree and fuzzy classifier to form the rules automatically are used to design the suggested method.Wu and Law [136] have discussed wavelet function based fuzzy robust wavelet support vector classifier (FRWSVC) and established an adaptive gaussian particle swarm optimization algorithm to pursue the peak unidentified parameter for the FRWSVC. Experimental results are validated with the obtained results of hybrid model. Parhi and Choudhury [137] have investigated a transverse crack of beam using the fuzzy logic system and finite element method. They have used hybrid membership function (i.e. combination of the trapezoidal, triangular and gaussain) as an input parameter and trapezoidal membership functions as an output parameter in the fuzzy controller system.Choi and Jung [138] have proposed the

Takagi-Sugeno fuzzy method based on fuzzy speed controller for an analyzing permanent magnet synchronous motor. They have formulated existence conditions in term of Linear Matrix inequalities (LMI) for designing the T-S Fuzzy speed controller. Hasanzadeh et al. [139] have proposed a non-phenomenological technique to resolve the inverse problems, particularly for the electromagnetic alternative current field measurement method to recognize the metal surface crack.They have shown that the combination of technique of adaption and fuzzy inference method for altered crack natures delivers adequate means as a previous observed information for the training system. Sugumaran and Ramachandran [140] have used the decision tree for picking the bin ranges which will distinguish the faulty circumstance of the bearing system from a definite train models and rules forms from the decision tree. The vibration signal receives from the piezoelectric transducer for various kinds of earing fault conditioning is used to form the fuzzy rules. Mohanta et al. [141] have established a model of fuzzy Markov for the captive power plant maintenance planning taking into account the several parameters that develops the disaster repair cycle. Parhi [142] has described a mobile robot path planning control system based on fuzzy inference system.

2.2.5.2 Artificial Neural Network Technique

In curent segment altered types of Artificial Neural Network (ANN) based techniques used for crack detection are described. ANN is used as a capable technique for fault identification. This segment describes the different types of Neural Network technique used for the identification of crack. The ANN has been used as an auspicious methodology in the field of an inverse problem for crack dectection. Liu et al. [143] have proposed an inverse analysis to simulate scan ultrasonic nondestructive testing using the back propagation neural network (BPNN) and computational mechanics combining the finite element method with boundary integration equation.The trained neural networks are utilized for the classification and identification of the crack in the medium to evaluate the type, position, and length of the crack.

Fang et al. [144] have presented structural fault diagnosis method by using FRFs as an input data to train the BPNN.They have studied the effect of three various algorithms; FSD, TSD and DSD in neural network training. Mehrjoo et al. [145] have established an inverse algorithm for crack identification to evaluate the severity and location of the damages in combined truss and bridge structure using the BPNN approach. Mode shapes and natural frequencies are used as a input parameters.Wu et al. [146] have presented the

fault identification method for IC engine using the artificial neural network and discrete wavelet transform. Just-Agosto et al. [147] have proposed neural network method with a permutation of thermal and vibration damage identification signature to established a fault detection device.Authors have developed the method for the crack detection on the sandwich composite.

Wu et al. [148] have discussed a fault dectction technique for gears of rotating machinery applying the neural network and wavelet transform technique. Gears sound emissions are used along with the continuous wavelet transform method and the assortment of the feature of energy spectrum to develop the fault identification tool based on neural network method. Ghate et al.[149] have proposed a multi-layer neural network technique for identification of damages in induction motor. They have utilized numerical parameters as an input to trained the neural network controller. Fan et al. [150] have discussed a fault diagnosis and detection approach for air handling division. Their methods comprise two phases which are the related to fault detection stages. In first stage, they have used the neural network fault detection model for producing the sensors values, and it is compared to actual value to generate remaining values. The mentioned fault detection neural network controller has been trained using the historical data of the HAVC system. Wang et al. [151] have presented a novel fault identification method based on BPNN. The results obtained by them are compared by the three different methods, which contain the variation of the autoregressive coefficient with BPNN and the distance of autoregressive coefficient technique for several samples. They have obtained that the variation of autoregressive coefficients with the BPNN was greater then the autoregressive coefficient with BPNN and distance of autoregressive coefficient method.

Saravanan et al. [152] have discussed a wavelet-based technique for fault diagnosis of gearbox using proximal support vector machine and ANN. The J48 algorithms are used to classified the statistical feature vectors from the Morlet wavelet coefficients.The main features are used as an input for the proximal support vector signature and ANN.Paviglianiti et al. [153] have developed an arrangement for identifying and isolating sensor faults in manipulators of an industrial robot. They have implemented a Radial basis function method to improve the dynamics of the proposed arrangement. Schlechtingen and Santos [154] have studied a comparison of results between the two artificial neural network based methodologies and the regression-based model. For conditioning monitoring of bearing in a wind turbine used an auto-aggressive normal behavior model. Eski et al. [155] have reported the experimental analysis of the robot manipulator using

the artificial neural network for investigating the joints vibration.They have established an experimental test rig to accumulate the associated values which have six degrees of freedom.The obtained results indication that the suggested Radial Basis Neural Network is used to analyzed the acceleration of joints of manipulators because of a given trajectory.

Thatoi and Jena [156] have discussed the analysis of dynamic response of a cracked shaft with the help of experimental analysis and ANN system.The obtained experimental analysis data are used as an input parameter to feed in BPNN system. Oberholster and Heyns [157] have proposed a method for online structure health monitoring of axial flow for blades using ANN system. Extracted vibration characteristic from the experimental test of the structure is used as an input parameter for train the ANN. Rakideh et al. [158] have developed and design the BPNN technique for condition monitoring of cracked beam.They have extracted the natural frequencies of the beam using the analytical method and fed these natural frequencies to BPNN model to forecast the size and location of the crack. According to them, the neural network is a powerful way to determine the crack size and depth. Also, the capability of prediction has increased with increasing the numbers of the natural frequencies.

Kao and Hung [159] have presented structural condition monitoring using a supervised learning type of Neural System Identification Networks (NSINs).They first identified the uncracked and cracked conditions of a structural system using NSINs then trained NSINs has been used to develop free vibration responses with the same condition of structures.Quteishat and Lim [160] have proposed a Fuzzy Min-Max (FMM) network structure, which is a trained Neural network controller that construct hyper-boxes for prediction the problems. This method is applied to the removal of rule set from the Fuzzy Min-Max to permit the predicted results. The outputs of FMM are compared with results measured from a plant of power generation for fault recognition with the help of sensors.

Hajnayeb et al. [161] have designed and developed a feature selection based network system to diagnose the various types of faults in the gearbox. The authenticity of the proposed method is verified by experimental analysis. The results of feature selection method are compared with genetic algorithm results. They have found a close proximity to the results.Samanta [162] has presented a study on gear fault identification using ANNs and Support Vector Machines (SMVs). The vibration parameters of a rotating machine with damage and non-damage gears are sort out for extraction of features. He has used extracted features from damage and non-damage gears as an inputs to both classifiers (i.e. ANNs and SVMs) for the state recognition of gear box. Haykin [163] has defined that the

neural network has associated processing units called neurons, which can adopt the knowledge from available information and to make it available for use.Samanta et al. [164] have presented a comparative study of the performance of the bearing fault recognition techniques using two classifiers namely ANNs and SVMs. The vibration analysis performed to get the vibration signal of a spinning machine with defective and non-defective bearing processes for extraction of features. The extracted features from original and processed signals are used as an inputs to the classifier for two senses (i.e. normal and fault) detection. The nodes of in hidden layers of ANN and width of radial basis function (RBFN) along with selected input features are optimized using a genetic algorithm.

2.2.5.3 Adaptive Neuro-Fuzzy Interference System (ANFIS)

In curent section different types of Adaptive neuro fuzzy interference system (ANFIS) based techniques used for fault identification are described. ANFIS is used as a capable technique for damage detaction.Wang et al. [165] have reported the assessment of the execution of the two different damage identification method that is neuro-fuzzy and recurrent neural network systems using the two standard time series data sets. According to them, it is observed that the neural network fault identification system is less authentic for health condition monitoring of machine then the neuro-fuzzy predictive system.

Kuo and Chang [166] have suggested damage dignosis method based on fuzzy neural diagnosis approach for identification of damages in propeller shaft of marine propulsion. They have conducted experiment an analysis the fault behavior of the propeller shaft system. The results obtained from the experimentation have been used as training data and input/output rule generation of fuzzy neural network.Ye et al. [167] have described a novel online diagnosis process to evaluate the mechanical problem of the electrical mechanism using Adaptive Neuro-Fuzzy Inference System (ANFIS) and wavelet packet decomposition. Zio and Gola [168] have proposed a fault identification technique using fuzzy neuro approach. Authors have applied this technique for the determination of a great rate of exact categorisation and to find the explainable classified model.

Yang et al. [169] have proposed ANFIS based fault identification technique incorporated with the decision tree for the induction motor. They have used the hybrid of square algorithm and back propagation to train the membership function. The data set found from the current signals and vibration signals of the induction motors.Eslamaloueyan [170] has proposed hierarchical neural network method for separating the damages of the

Tennessee Eastman Process being accomplished through the Eastman chemical company to offer an industrialized development for achieve monitoring and process planning control technique.They have used Fuzzy clustering algorithm to split the fault patterns space into a sub spaces. Salahshoor et al. [171] have proposed an advanced damage detection method based on the distributed arrangement of three ANFIS classifier for the steam turbine power plant (i.e. 440MW power generation capacity). A suitable choice of four calculated variable has been organized to provide in each ANFIS classifier with the greatest significant diagnostic data. Sadeghian and Fatehi [172] have proposed a fault dignosis method for forecasting the faulty progression of cement rotary kiln in the White Saveh cement factory. The authors have employed the Linear neuro-fuzzy (LNF) based model trained by the LOLIMOT algorithm for identifying the several operation points in the kiln.

Beena and Ganguli [173] have proposed an innovative algorithm based on the fuzzy logic and artificial neural network approach for fault detection in structure. Authors have used the finite element analysis to calculate the natural frequencies due to fault in structure. The deviations are measured because of the damage are fuzzified and designed to a set of the fault using fuzzy cognitive map. The frequency deviation is used as an input parameter and damage locations of the beam are used as output parameters for the fuzzy cognitive map. Zhu et al. [174] have discussed a fault identification method based on the combine ANFIS, interval modelling method and wavelet real time filtering algorithm to process signals of structural behavior and excitation data. Here ANFIS was used to model structural response, wavelet transform algorithm to strain the arbitrary noise and interval modelling method to quantify damage index precisely.

Chen et al. [175] have proposed ANFIS based on the prior knowledge for the wind turbine fault diagnosis.They have used the data of the 6 known WT pitch faults to train the model with prior information integrated.Bachi et al. [176] have reported an ANFIS technique for predicting the vibration behaviour of beam due to the effect of large displacements and axial forces. They have used the finite element method and experimental analysis for calculating nonlinear vibration responses of the single and multiple- stepped beam. Al-Shammari et al. [177] have investigated the efficient approach to obtain the wake wind speed at any location of the wing farm using ANFIS.They have developed the Simulink model using the MATLAB with the ANFIS network to the estimation of wake wind speed.Petkovic et al. [178] have investigated new methodology based on the ANFIS for achieving the contact position of the proposed tactile sensing structure.They have used the

experimentally obtained results as a testing and trained data for the ANFIS network. Zhang et al. [179] have been proposed a bearing fault identification technique based on the ANFIS and multi-scale entropy to evaluate the nonlinearity existing in bearing system.They have used the experimental data to arrange and train the ANFIS structure for fault diagnosis.

Boyacioglu and Avci [180] have presented an ANFIS based mechanism for predicting the stock price index return of the Istanbul Stock Exchange (ISE). They have concluded that the economists can be apply ANFIS successfully for forecasting the return of stock price index. Zhang et al. [181] have investigated a forecasting the continuation of chaotic signals in time-based on the delay co-ordinate embedding technique by using the multi-input and multi-output ANFIS controller.Gradient descent algorithms have been used to trained the MANFIS method. They have used back-propagation algorithm to generate the set of the membership functions with the embedded phase space vector. Hinojosa and Doménech-Asensi [182] have presented modeling method of microwave devices based on the space mapping (SM) methodology by using the multiple neuro-fuzzy inference system (MANFIS). Authors have used the micro-genetic algorithm to find the nonlinear multi-dimensional mapping functions.

Lei et al. [183] have proposed a novel methodology based on the static analysis, improved distance evaluation technique, empirical mode decomposition (EMD) and MANFIS for intelligent fault identification of rotating machinery.Doménech-Asensi et al. [184] have developed an accurate analog circuit macro model sizing using a fuzzy logic system. According to them, the suggested technique forecast the performance characteristics (i.e. bandwidth and gain) of a differential telescopic trans-conductance amplifier (OTA) based on the MANFIS. Güneri et al. [185] have presented a novel approach based on ANFIS for overcoming the problem of supplier selection. They have minimized the problem using the ANFIS input selection technique. Dash and Parhi [186] have developed a novel tool to identifying the multi-crack in the dynamic structures using MANFIS. They have considered the difference of the first three average relative mode shapes, first three natural frequencies as input parameters and crack depths and crack locations are used as output parameters for the fuzzy and neural controllers of the MANFIS model.

Ghaffari et al. [187] have proposed the new prediction models based on the multiple adaptive neuro-fuzzy systems (MANFIS) for an overtaking behavior of human.They have used kinematic features of driver vehicle units (DVUs) such as acceleration, velocity, and distance. Field data are used as inputs and outputs of MANFIS to be models. The result

obtained are compared and validated with the actual traffic data sets and found that very closer. Saeed et al. [188] have proposed the fault identification method in Francis turbine using different Artificial intelligence technique, MANFIS and multiple ANNs.They have used the changes in vibration characteristics as inputs and position, the size of fault in the runner as output parameters to train the proposed artificial intelligence technique for evaluating the turbine operating conditions.

Linh and Long [189] have proposed a hybrid approach using the MANFIS and Fuzzy clustering method (FCM) to recover the compression ratio of the state of the art compression algorithm-DCRA. They have found the coefficient of nonlinear transform for sliding window using the MANFIS. Subhi Al-batah et al. [190] have proposed an intelligent computer system for the classification of cervical cancer. The proposed Intelligent system consists of two main stages. The first stage is based on the automatic features extraction (AEF) algorithm and in the second stage, MANFIS is used for the identification process.

2.2.5.4 Rule Base Technique

This section discusses the literatures related to rule base technique used for various problems. Takagi et el. [191] have reported the rule base technique to design and develop mobile robot to carry a rectangle from one place to another place. Authors have addressed a classified architecture in rules. These rules are used to achieve the angle among the box and robot. They used total 120 rules in their experiment. Gaeta et al. [192] have presented the rule base technique for finding the age groups. They have proposed that there is an age related decline in the effectiveness of incorporating several sources in a single auditory sense. De Souze et al. [193] have discussed the reusable structure for rule base technique pronounced using design patterns. The design patterns are used to organize a catalog of design that can be used by designers to recognize and generate novel rule base methods, thus endorsing reuse in this systems. Dietrich et al. [194] have reported a typical structure for rule based agents and clarified the technique to understand the navigation mechanism using semantic web languages.

Tunstel et al. [195] have described the functional safety and health condition monitoring of complex matters of self- governing mobile robots. Mc Intosh et al.[196] have proposed a simple theory of rule base method. Authors have implemented a method to provide systematic management-oriented modelling of vegetated landscapes. Pfeiffer et al. [197,198,199] have used a rule base visual language to control a small LEGO mobile

robot. Fei et al.[200] have introduces the rule base method for adapting an environmental condition. Gilmore et al. [201] have reported a rule base method to forecast the dynamic characteristics of operations of feeders and manipulator. Bonner et al. [202,203,204] have applied rules which are based on the free space cell, to determine the sustaining accident free paths in an organized environment for mobile robot navigation.

2.3 Summary

From the above-described literature survey, it is found that the dynamic response of the cracked rotor partially immersed in the viscous medium is determined by the strain energy release rate. Different Artificial intelligence technique may be employed for fault diagnosis of many engineering structure applications. It is observed from the literature survey that the artificial intelligence technique is not applied potentially for fault diagnosis of the rotating cracked rotor. So, in the present research, an organized effort has been made to develop artificial intelligent based system for health condition monitoring of spinning rotor with multiple transeverse crack partially submerged in the viscous medium using fuzzy system, neural network, MANFIS and rule base method. The parameters are necessary to design and train the artificial intelligence model using the data from theoretical, finite element and experimental analysis of the multiple cracked rotor.

Chapter 3

Theoretical Analysis of DynamicResponse of Rotor with Multiple Transverse Crack Partially Submerged in Viscous Medium

The presence of the crack in structures or machine component is a serious threat to the integrity of structures as well the safety of human life. Throughout the world, many researchers are working on structural dynamics and particularly on dynamic characteristics of structure with multiple transverse cracks. Numerous techniques are available in literature to detect the crack at the primary stage of final failure of structures. The vibration-based methods are effectively applied for crack identification in structures (i.e. rotor, beam and plate). It is observed that dynamic response, e.g. natural frequencies and amplitude of vibration changes due to presence of crack in structure.

3.1 Introduction

Vibration analysis of spinning rotor is playing a vital role in the area of vibration due to the frequent catastrophe of such rotors in engineering applications.The vibration analysis of the spinning rotor with transverse crack has been investigated successfully by several researchers with the help different methodologies. The vibration response is very sensitive to crack location and its intensity. The researchers and scientists have analyzed that effect of cracks on vibration responses of the cracked rotor.These changes in vibration responses can be efficiently utilized for developing the crack detection technique. When a rotor rotates in a viscous medium with crack on it, the dynamic analysis of such system becomes more complex and difficult. The investigations done so far on the vibration behavior of rotor with transverse crack are presented in the literature survey in detail. Still there is no detailed research has been described the performance of the spinning rotor with transverse crack partially submerged in the viscous fluid medium.In this chapter a systematic theoretical approach is used to investigate the influence of multiple cracks on

vibration responses of rotor partially submerged in the viscous medium. This analysis has been divided into two parts first part contains the analysis for solid rotor without any crack rotating in viscous medium. Whereas second part deals with the rotor with crack rotating in viscous fluid. The dynamic response of multiple cracked rotor partially submerged in the viscous medium with attached extra mass (i.e. Disc) has been calculated by using influence coefficient method. The external fluid forces on the rotor are calculated by the Navier-Stokes equation. The strain energy release rate at the crack section of the rotor has been used for evaluating the local stiffness and is dependent on the crack depth. The Simpson's 1/3 rule is used in the theoretical analysis. Finally, the proposed theoretical model results have been compared with results of the experimental analysis for the authentication.

The present investigation for rotating rotor partially submerged in viscous medium with multiple transverse crack can have extensive applications in industries such as, condition monitoring of rotating shafts in various machineries with detection of crack, design of high speed rotors used in centrifuges, boring machines as well as rotors used for extracting oil from sea bed etc.

3.2 Theoretical Analysis of Spinning Rotor with Transverse Crack Submerged in Viscous Medium

This segment introduces the methodology employed to devlop the proposed theoretical model for calculating the vibration response (i.e. natural frequency and amplitude) of non-cracked rotor and multiple transverse cracked rotor partially submerged in viscous medium for different relative crack positions and depths. From the analysis of theoretical results, it is found that a visible change in the natural frequency and amplitude have been marked due to an existence of crack and viscosity of the viscous fluid.

3.2.1 Dynamic Analysis of Rotating Non-cracked Cantilever Rotor with Additional Mass Partially Submerged in the Viscous Medium

For theoretical analysis a cantilever rotor with a disc at its free end rotating in viscous medium is considered.

3.2.1.1 Equation of Fluid Velocites

Figure 3.1 shows the whirling speed of the rotor. The length shaft 'L' and radius 'R_1' rotates at the center indicated by 'O' with the rotating speed 'ω'.Whirling radius and speed of the shaft indicated by 'δ' and 'Ω' signifies respectively.

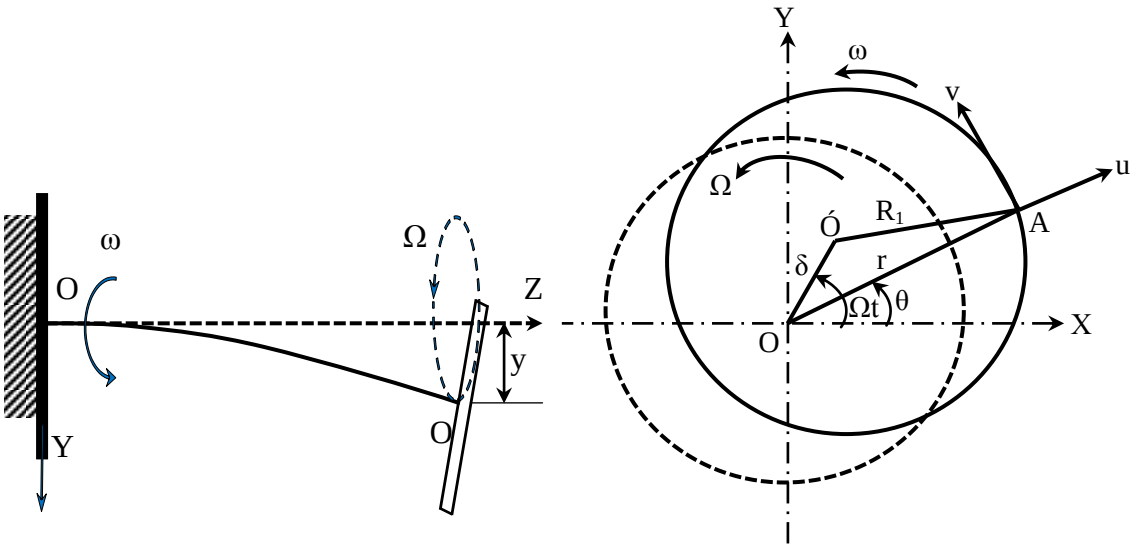

Figure 3.1**:** Representation of whirling position of cantilever rotor

The polar coordinates of the Navier-Strokes equation can be expressed as

$$\frac{\partial u}{\partial t}=-\frac{1}{\rho}\frac{\partial p}{\partial r}+\nu\left(\frac{\partial^2 u}{\partial r^2}+\frac{1}{r}\frac{\partial u}{\partial r}-\frac{u}{r^2}+\frac{1}{r^2}\frac{\partial^2 u}{\partial \theta^2}-\frac{2}{r^2}\frac{\partial v}{\partial \theta}\right) \tag{3.1a}$$

$$\frac{\partial v}{\partial t}=-\frac{1}{\rho r}\frac{\partial p}{\partial \theta}+\nu\left(\frac{\partial^2 v}{\partial r^2}+\frac{1}{r}\frac{\partial v}{\partial r}-\frac{v}{r^2}+\frac{1}{r^2}\frac{\partial^2 v}{\partial \theta^2}+\frac{2}{r^2}\frac{\partial u}{\partial \theta}\right) \tag{3.1b}$$

In the above equation 'u' and 'v' denote the fluid flow velocity in radial and tangential direction respectively and 'P' is the fluid pressure with the help of stream function $\psi(r,\theta,t)$ and eliminating the pressure term, the above equation can be written as;

$$\nabla^4\psi-\left(\frac{1}{\nu}\right)\frac{\partial}{\partial t}\left(\nabla^2\psi\right)=0 \tag{3.2}$$

Where $\nabla^2=\dfrac{\partial^2}{\partial r^2}+\dfrac{1}{r}\dfrac{\partial}{\partial r}+\dfrac{1}{r^2}\dfrac{\partial^2}{\partial \theta^2}$

Equation 2 can be divided into two parts i.e.

$$\nabla^2\psi=0,\ \nabla^2\psi-\left(\frac{1}{\nu}\right)\left(\frac{\partial\psi}{\partial t}\right)=0 \tag{3.3}$$

The solution of equation (3.2) can be given by

$\psi = \psi_1 + \psi_2$

Where ψ_1 and ψ_2 are solution of equation (3.3)

The radial and tangential component of flow velocity at point 'A' in Figure 3.1 are;

$$u_A = R_1\omega \sin a - \delta\Omega \sin(\Omega t - \theta) \tag{3.4a}$$

$$v_A = R_1\omega \cos a - \delta\Omega \cos(\Omega t - \theta) \tag{3.4b}$$

Where 'A' is the angle between O'A and OA

$\sin a = (\delta / R_1)\sin(\Omega t - \theta)$ and $\cos a = 1$ for $\delta << R_1$

For $r = R_1$ the equation (3.4) can be rewritten as;

$$u_{r=R_1} = \delta(\omega - \Omega)\sin(\Omega t - \theta) = \mathrm{Re}\left[-j\delta(\omega - \Omega)e^{j(\Omega t - \theta)}\right] \tag{3.5a}$$

$$v_{r=R_1} = \delta\cos(\Omega t - \theta) + R_1\omega = \mathrm{Re}\left[\delta\Omega e^{j(\Omega t - \theta)}\right] + R_1\omega \tag{3.5b}$$

Where $j = \sqrt{1}$ and $\mathrm{Re}[.]$ denotes a real part of $[.]$.

For a special (i.e. For synchronous whirl, which is used in practice) case $\omega = \Omega$ equation (3.5) is reduced to

$$u_{r=R_1} = 0 \; v_{r=R_1} = \mathrm{Re}\left[\delta\omega e^{j(\omega t - \theta)}\right] + R_1\omega \tag{3.6}$$

When the rotor is immersed in an infinitely extending fluid region, the boundary condition for $r \to \infty$ are;

$$u_{r=\infty} = v_{r=\infty} = 0 \tag{3.7}$$

When the rotor is immersed in a finite extending fluid region the boundary conditions for $r = R_2$ (i.e. the container radius is taken as R_2) are taken as;

$$u_{r=R_2} = v_{r=R_2} = 0 \tag{3.8}$$

Under these conditions, non-stationary components of the solution ψ_1 and ψ_2 can be expressed as;

$$\psi_1(r,\theta,t) = F_1(r)e^{j(\omega t - \theta)} \tag{3.9a}$$

$$\psi_2(r,\theta,t) = F_2(r)e^{j(\omega t - \theta)} \tag{3.9b}$$

From equation (3.9a and 3.9b) and equation (3.3) we obtain;

$$\nabla^2 F_1(r)e^{i(\omega t - \theta)} = \left(\frac{\partial^2}{\partial r^2} + \frac{1}{r}\frac{\partial}{\partial r} + \frac{1}{r^2}\frac{\partial}{\partial \theta}\right)\left(F_1(r)e^{i(\omega t - \theta)}\right)$$

$$= \frac{\partial^2 F_1(r)}{\partial r^2} e^{i(\omega t-\theta)} + \frac{1}{r}\frac{\partial^2 F_1(r)}{\partial r^2} e^{i(\omega t-\theta)} - \frac{1}{r^2} F_1(r) e^{i(\omega t-\theta)} = 0$$

$$= \frac{d^2 F_1(r)}{dr^2} + \frac{1}{r}\left(\frac{dF_1(r)}{dr}\right) - \frac{1}{r^2} F_1(r) = 0 \tag{3.10a}$$

and

$$\left(\nabla^2 - \frac{1}{\nu}\frac{\partial}{\partial t}\right) F_2(r) e^{i(\omega t-\theta)} = \left(\frac{\partial^2}{\partial r^2} + \frac{1}{r}\frac{\partial}{\partial r} + \frac{1}{r^2}\frac{\partial}{\partial \theta} - \frac{1}{\nu}\frac{\partial}{\partial t}\right)\left(F_2(r) e^{i(\omega t-\theta)}\right)$$

$$= \frac{\partial^2 F_2(r)}{\partial r^2} e^{i(\omega t-\theta)} + \frac{1}{r}\frac{\partial F_2(r)}{\partial r} e^{i(\omega t-\theta)} - \frac{1}{r^2} F_2(r) e^{i(\omega t-\theta)} - K^2 F_2(r) e^{i(\omega t-\theta)} = 0$$

$$= \frac{d^2 F_2(r)}{dr^2} + \frac{1}{r}\left(\frac{dF_2(r)}{dr}\right) - \left(\frac{1}{r^2} + K^2\right) F_2(r) = 0 \tag{3.10b}$$

Where $\left(k = \sqrt{\frac{j\omega}{\nu}}\right)$

Since equation (3.10a) is a Euler's equation and equation.(3.10b) is Bessel's equation, the general solution of these equations are easily derived as;

$$F_1(r) = \delta\omega\left(\frac{AR_1^2}{r} + Br\right), \tag{3.11a}$$

$$F_2(r) = \delta\omega R_1\left(CI(Kr) + DK(Kr)\right) \tag{3.11b}$$

Where A, B, C and D are arbitrary constants, and $I_1(Kr)$ and $K_1(Kr)$ modified Bessel functions of the 1st and 2nd kinds, respectively. Thus the non-stationary components of flow velocities induced by the whirling motion of a rotor are given as follows:

$$u_r = -\frac{1}{r}\frac{\partial \varphi}{\partial \theta} = -\frac{1}{r}\frac{\partial}{\partial \theta}\left(\delta\omega\left(\mathrm{A}_q R_1^2/r + B_q r\right) + \delta\omega R_1\left(C_q I_1(Kr) + D_q K_1(Kr)\right)\right) e^{i(\omega t-\theta)}$$

$$= i\delta\omega\left[A_q\left(\frac{R_1}{r}\right)^2 + B_q + C_q\frac{R_1}{r} I_1(Kr) + D_q\frac{R_1}{r} K_1(Kr)\right] e^{i(\omega t-\theta)} \tag{3.12a}$$

$$V_r = \frac{\partial \varphi}{\partial \theta} = \frac{\partial}{\partial r}\left(\delta\omega\left(\mathrm{A}_q R_1^2/r + B_q r\right) + \delta\omega R_1\left(C_q I_1(Kr) + D_q K_1(Kr)\right)\right) e^{i(\omega t-\theta)}$$

$$= \delta\omega\begin{bmatrix} -A_q\left(\frac{R_1}{r}\right)^2 + B_q + C_q\left(-\frac{R_1}{r} I_1(Kr) + KR_1 I_0(Kr)\right) \\ + D_q\left(-\frac{R_1}{r} K_1(Kr) - KR_1 K_0(Kr)\right) \end{bmatrix} \tag{3.12b}$$

3.2.1.2 Analysis of Fluid Forces

Substituting the flow velocities given by equation (3.12) into the equation (3.1), the non-stationary component of pressure p can be written as;

$$p = \int \frac{\partial p}{\partial \theta} \partial\theta = \delta\rho\omega^2 \left\{ \frac{-A}{r} R_1^{\,2} + Br \right\} e^{i(\omega t - \theta)} \tag{3.13}$$

Normal stress τ_{rr} and tangential stress $\tau_{r\theta}$ due to flow can be obtained as,

$$\tau_{rr} = -p + 2\mu \frac{\partial u_i}{\partial r} \text{ and } \tau_{r\theta} = \mu \left(r \frac{\partial}{\partial r}\left(\frac{v_i}{r} \right) + \frac{1}{r} \frac{\partial u_i}{\partial \theta} \right) \tag{3.14}$$

Fluid forces acting on the surfaces (i.e. $r = R$) per unit length of the rotor in the x and y-axis direction are obtained.

$$F_x = \int_0^{2\pi} \left(\tau_{rr} \cos\theta - \tau_{r\theta} \sin\theta \right) R_1 d\theta = m\delta\omega^2 \left\{ A - B - CI_1(\alpha) - DK_1(\alpha) \right\} e^{i\omega t} \tag{3.15a}$$

$$F_y = \int_0^{2\pi} \left(\tau_{rr} \sin\theta + \tau_{r\theta} \cos\theta \right) R_1 d\theta = -im\delta\omega^2 \left\{ A - B - CI_1(\alpha) - DK_1(\alpha) \right\} e^{i\omega t} \tag{3.15b}$$

Where $\alpha = kR_1 m = \rho\pi R_1^2$

Only the real part of equation (3.15) is meaning full, so F_x and F_y after simplification can be expressed as;

$$F_x = m\delta\omega^2 \left(\mathrm{Re}(H)\cos(\omega t) - \mathrm{Im}(H)\sin(\omega t) \right) \tag{3.16a}$$

$$F_y = m\delta\omega^2 \left(\mathrm{Re}(H)\sin(\omega t) - \mathrm{Im}(H)\cos(\omega t) \right) \tag{3.16b}$$

Where $\mathrm{H} = \mathrm{A} - \mathrm{B} - \mathrm{CI}_1(\alpha) - \mathrm{DK}_1(\alpha)$ and $\mathrm{Re(H)}, \mathrm{Im(H)}$ denotes the real and imaginary part of H. The coordinates of the center of the rotor (as shown in the Figure 3.1) is $\mathrm{x} = \delta\cos\omega\mathrm{t}$ and $\nu = \delta\sin\omega\mathrm{t}$.

$$F_x = -m\,\mathrm{Re}(H)\frac{d^2x}{dt^2} + m\omega\,\mathrm{Im}(H)\frac{dx}{dt} \tag{3.17a}$$

$$F_y = -m\,\mathrm{Re}(H)\frac{d^2y}{dt^2} + m\omega\,\mathrm{Im}(H)\frac{dx}{dt} \tag{3.17b}$$

In equation $\mathrm{m\,Re(H)}$ denotes the virtual or added mass to the inertia force of the rotor and $-\mathrm{m}\omega\,\mathrm{Im(H)}$ symbolizes the viscous damping coefficient. In equation (3.17) $\mathrm{m\,Re(H)}$ denotes the virtual or added mass of the fluid relating to the inertia force of the rotor and $-\mathrm{m}\omega\,\mathrm{Im(H)}$.

3.2.1.3 Dynamic Response of the Spinning Rotor System

In order to avoid mathematical complicacy , the spinning cantilever rotor attached disc at the tip of free end has been considered as a lumped system with mass of the disc as well as equivalent mass of the rotor lumped at its free end. For the analysis of dynamic response of the above system, mass of the disc is considered as Ms_1 which is attached at the free end of the rotor.

The mass of rotor is considered as Ms_2. Equivalent mass at the free end of the above rotor system which will produce same natural frequency as that of the original system may be considered as,

$$Ms = Ms_1 + \alpha_{eq} Ms_2$$

Where $\alpha_{eq} = \dfrac{Ks}{\omega\phi^2 Ms_2}$

Ks and $\omega\phi$ are stiffness and natural frequency of the rotor (without disc) respectively.

The equation of the motion of the equivalent lumped system rotating in fluid medium is given by;

$$M_s \frac{d^2\left(x + \varepsilon\cos\omega t\right)}{\partial t^2} + K_s x = F_x \tag{3.18a}$$

$$M_s \frac{d^2\left(y + \varepsilon\sin\omega t\right)}{\partial t^2} + K_s y = F_y \tag{3.18b}$$

The fluid forces from equation (3.17) can be written as;

$$F_x = -m\,\mathrm{Re}\left(H\right)\frac{d^2x}{dt^2} + m\omega lm\left(H\right)\frac{dx}{dt} \tag{3.19a}$$

$$F_y = -m\,\mathrm{Re}\left(H\right)\frac{d^2y}{dt^2} + m\omega lm\left(H\right)\frac{dy}{dt} \tag{3.19b}$$

Where;

$$\left.\begin{aligned} M\,\mathrm{Re}\left(H\right) &= M_1\,\mathrm{Re}\left(H\right) + \alpha_{eq} M_2\,\mathrm{Re}\left(H_2\right) \\ M\,\mathrm{Re}\left(H\right) &= M_1 lm\left(H_1\right) + \alpha_{eq} M_2 lm\left(H_2\right) \\ M &= M_1 + \alpha_{eq} M_2 \end{aligned}\right\} \tag{3.20}$$

Where M_1 and M_2 mass of the fluid displaced by the rotor and disc respectively.

From equation (3.18) and (3.19) we have;

$$\left(M_s + M\,\mathrm{Re}\left(H\right)\frac{d^2x}{dt^2} - M\omega lm\left(H\right)\frac{dx}{dt} + K_s x = M_s\varepsilon\omega^2\cos\omega t\right) \tag{3.21a}$$

$$\left(M_s + M\,\mathrm{Re}(H)\frac{d^2y}{dt^2} - M\omega lm(H)\frac{dy}{dt} + K_s y = M_s \varepsilon \omega^2 \sin\omega t \right) \tag{3.21b}$$

Equation (3.21) in dimensionless from can be written as

$$\left(1 + M^*\,\mathrm{Re}(H)\frac{d^2\xi}{d\tau^2} - M^*\omega^* lm(H)\frac{d\xi}{dt} + \xi = \varepsilon^* \left(\omega^*\right)^2 \cos\left(\omega^* t\right) \right) \tag{3.22a}$$

$$\left(1 + M^*\,\mathrm{Re}(H)\frac{d^2\eta}{d\tau^2} - M^*\omega^* lm(H)\frac{d\eta}{dt} + \eta = \varepsilon^* \left(\omega^*\right)^2 \sin\left(\omega^* t\right) \right) \tag{3.22b}$$

Where $\xi = \frac{x}{R_1}, \eta = \frac{y}{R_1}, \omega^* = \frac{\omega}{\omega_0 r}, \varepsilon^* = \frac{\varepsilon}{R_1}, M^* = \frac{M}{M_s}, \tau = \omega_0 r$ or $\omega_0 r = \sqrt{\frac{K_s}{M_s}}$

The steady state solution of the above equation can be obtain in dimensionless form as;

$$\xi = \delta^* \cos\left(\omega^*\tau - \phi\right) \tag{3.23}$$

Where $\delta^* = \frac{\delta}{R_1}$ and (3.24a)

$$\delta^* = \frac{A}{\sqrt{\left(K - \left(\omega^*\right)^2\right)^2 + \left(C\omega^*\right)^2}}, \tag{3.24b}$$

$$\phi = \tan^{-1}\left[\frac{c\omega^*}{K - \left(\omega^*\right)^2}\right], \tag{3.24c}$$

$$C = -\frac{M^*\omega^* lm(H)}{1 + M^*\,\mathrm{Re}(H)}, \tag{3.24d}$$

$$K = -\frac{1}{1 + M^*\,\mathrm{Re}(H)}, \tag{3.24e}$$

$$A = \frac{\varepsilon^*\left(\omega^*\right)^2}{1 + M^*\,\mathrm{Re}(H)} \tag{3.24f}$$

Where; δ = Maximum dimensionless amplitude

Figure 3.1 shows the whirling motion of the cantilever rotor with attached disc during rotating condition, in a magnified view. Theoretical analysis for the rotor system is carried out taking the data mentioned above into account using the expression (3.1 to 3.23) with the help of computer programming (i.e. MATLAB). The "Simpson's 1/3 rule for integration algorithm" is used in numerical analysis.

The results obtained from the theoretical analysis for various aspects (i.e. Frequency ratio vs. non-dimensional amplitude ratio, Virtual mass effect, Gap ratio) are plotted in Figures 3.2 to 3.6 for finite region and Figures 3.7 to 3.10 for an infinite region. The effects of rotating speed on the amplitude of vibration are presented in Figures 3.2 and 3.3 in non-dimensional form. It is observed that as the viscosity of the external fluid increases, there is a shift in critical speed and decreases in amplitude of vibration. When to increase the length of the rotor, decrease the amplitude of vibration.

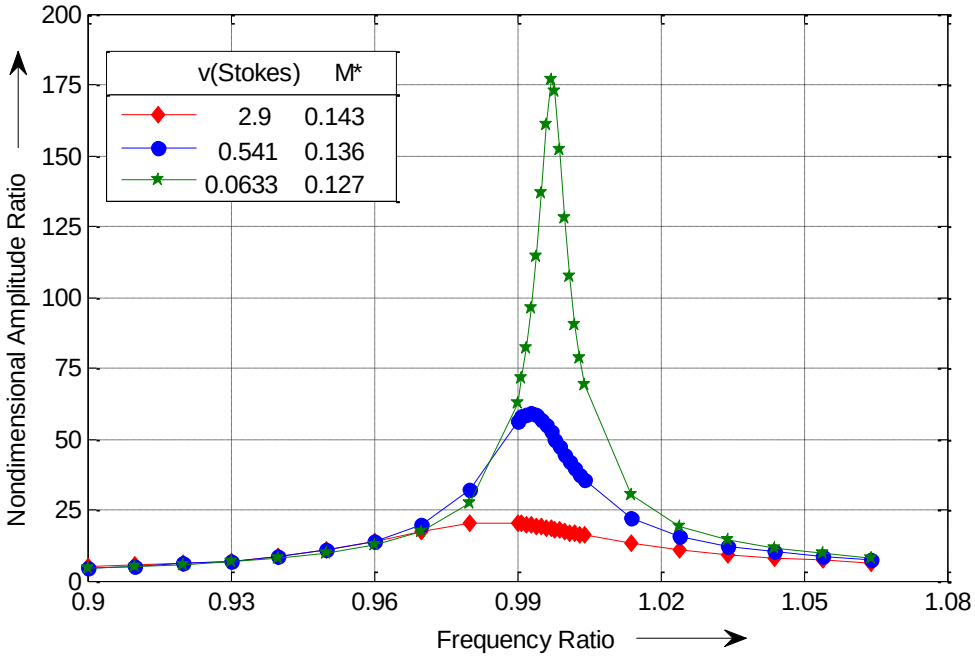

Figure 3.2: Frequency Ratio (ω/ω_0) Vs Non-dimensional Amplitude Ratio (δ^*/ε^*), Mild Steel Rotor R_1=0.01m, L=1.0m, q=12, R_D=0.055m,T_D= 0.020m, M_D = 1.0kg for finite region.

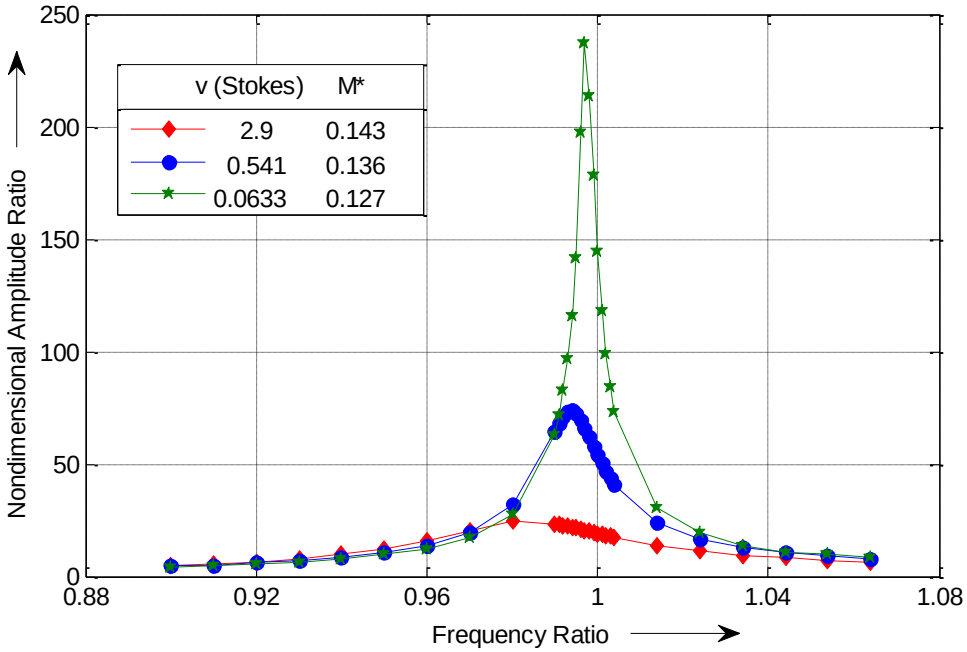

Figure 3.3: Frequency Ratio (ω/ω_0) Vs Non-dimensional Amplitude Ratio (δ^*/ε^*), Mild Steel Rotor R_1=0.01m, L=0.8m, q=12, R_D=0.055m, T_D=0.020m, M_D=1.0kg for finite region.

Figure 3.4 shows the effect of gap ration on the amplitude of vibration. When to increase the radius of the container,decrease the amplitude of vibration.

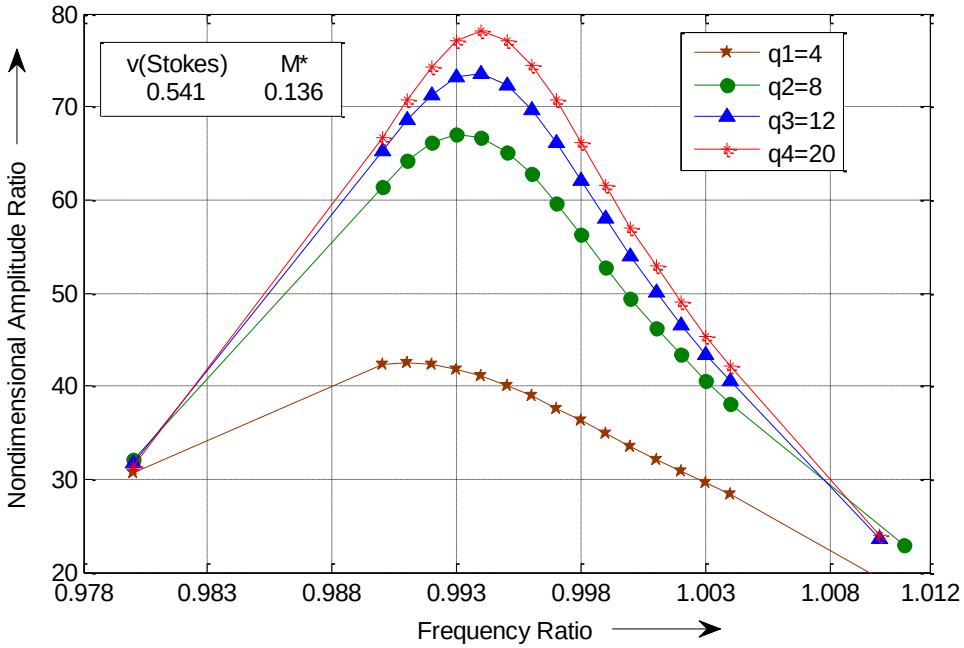

Figure 3.4: Frequency Ratio (ω/ω_0) Vs Non-dimensional Amplitude Ratio (δ^*/ε^*), Mild Steel Rotor R_1=0.01m, L=0.8m, R_D=0.055m, T_D=0.020m, M_D=1.0kg for finite region.

The effect of virtual mass and damping can be observed from Figures 3.5 and 3.6. From Figure 3.5 is noticed that with the increase in virtual mass effect $\left(\left|m\,\mathrm{Re}\left(H\right)\right|\right)$ at a fixed damping. The critical speed of the rotor system decreases and the corresponding dimensionless amplitude of vibration also decrease. Due to damping effect for a fixed virtual mass. The dimensionless amplitude is affected in a more prominent way. Due to increase in damping effect amplitude of vibration for the corresponding system decreases, which can be observed from Figure 3.6.

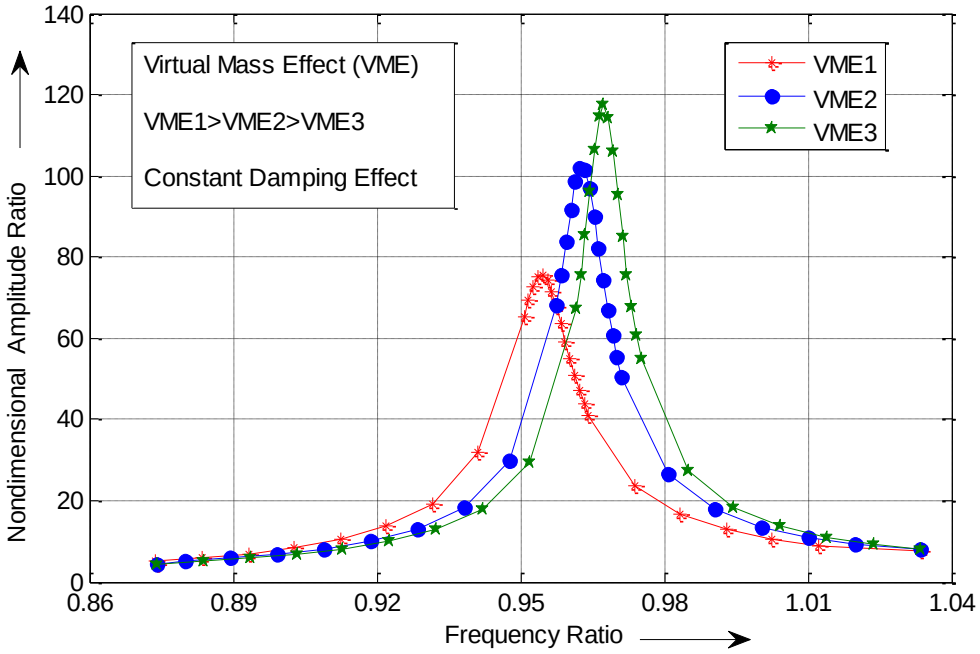

Figure 3.5: Frequency Ratio (ω/ω_0) Vs Non-dimensional Amplitude Ratio (δ^*/ε^*), Mild Steel Rotor R_1=0.01m,L=0.8m,q=12,ν=0.541stokes & M*=0.136, M_{D1} = 1.0kg, M_{D2}=0.75kg , M_{D3}=0.50kg for finite region.

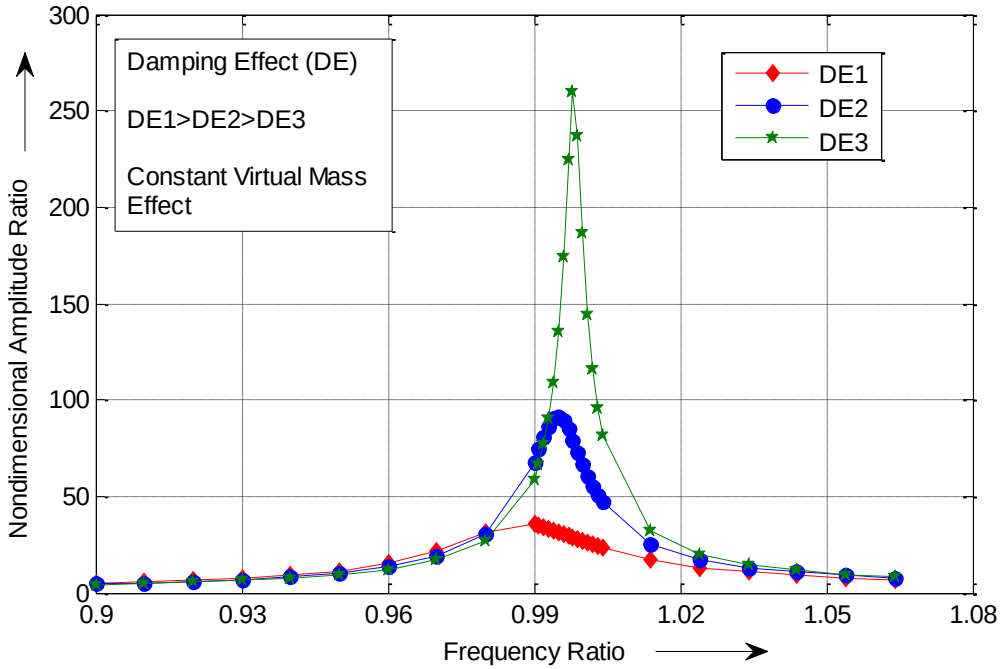

Figure 3.6: Frequency Ratio (ω/ω_0) Vs Non-dimensional Amplitude Ratio (δ^*/ε^*), Mild Steel Rotor R_1=0.01m,L=0.8m,q =12,ν=0.0633,0.541, 2.9 stokes & M*=0.127, 0.136, 0.146, R_D = 0.055m,T_D= 0.020m, M_D = 1.0kg for finite region.

Figures 3.7 and 3 .8 shows the non-dimensional amplitude of vibration with respect to frequency ratio in different viscous medium. It is observed that as the viscosity of the fluid increases the amplitude of vibration and resonant frequency decreases. A peculiar effect is observed from the comparison of Figures 3.7 and 3.8 for a particular viscous fluid when two different length of rotor are considered. It is found that the dimensionless amplitude is smaller in case larger rotor. The above phenomenon can be attributed for the higher value of virtual mass coefficient and damping coefficient for longer rotor system. The increase in virtual mass effect at a fixed damping decreases the critical speed and also decrease the amplitude of vibration.

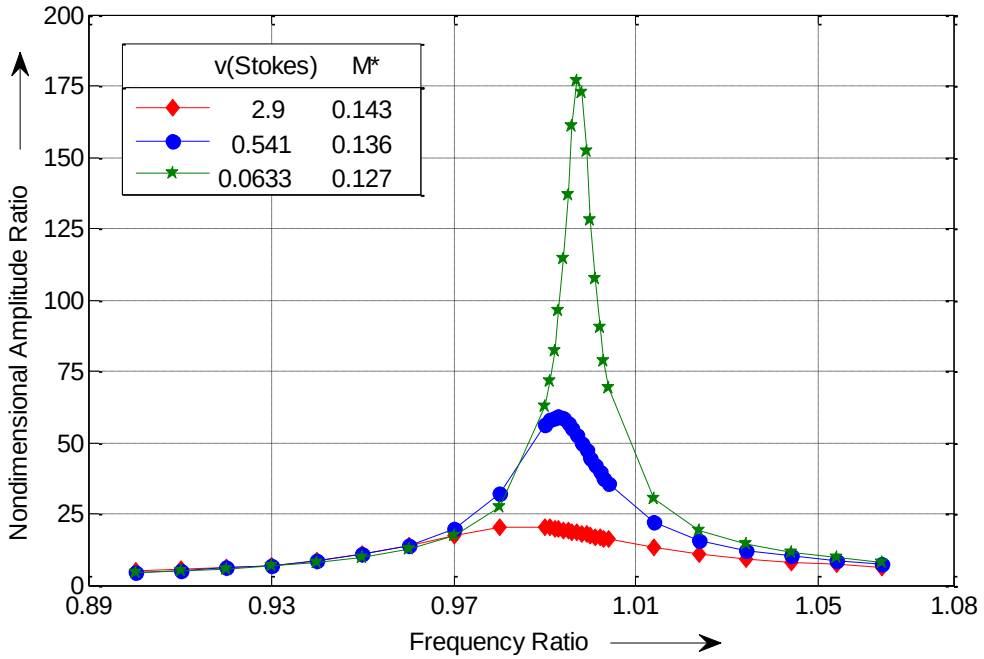

Figure 3.7: Frequency Ratio (ω/ω_0) Vs Non-dimensional Amplitude Ratio (δ^*/ε^*), Mild Steel Rotor R_1=0.01m,L=1.0m,q=12, R_D=0.055m,T_D= 0.020m, M_D = 1.0kg for infinite region.

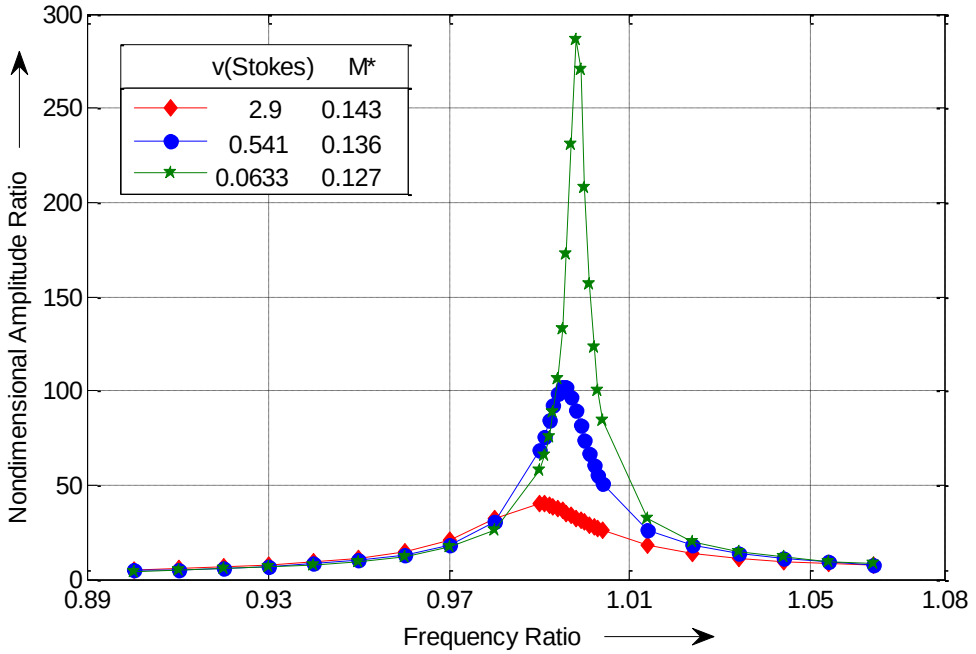

Figure 3.8: Frequency Ratio (ω/ω_0) Vs Non-dimensional Amplitude Ratio (δ^*/ε^*), Mild Steel Rotor R_1=0.01m, L=0.8m, q=12, R_D = 0.055m,T_D= 0.020m, M_D = 1.0kg, for infinite region.

This effect can be visualized from Figure 3.9. From Figure 3.10, it is observed that the damping effect at a fixed virtual mass is responsible for reducing the amplitude of vibration without shifting the critical speed to the noticeable extent.

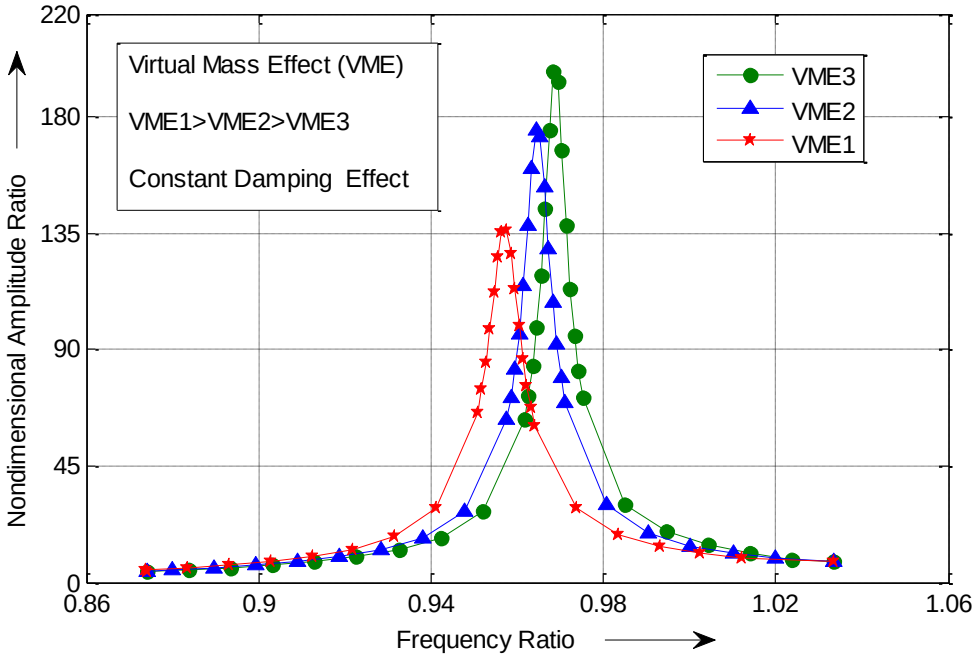

Figure 3.9: Frequency Ratio (ω/ω_0) Vs Non-dimensional Amplitude Ratio (δ^*/ε^*), Mild Steel Rotor R_1=0.01m, L=0.8m, q=12, ν=0.541stokes & M*=0.136, M_{D1} = 1.0kg, M_{D2}=0.75kg, M_{D3}=0.50kg for infinite region.

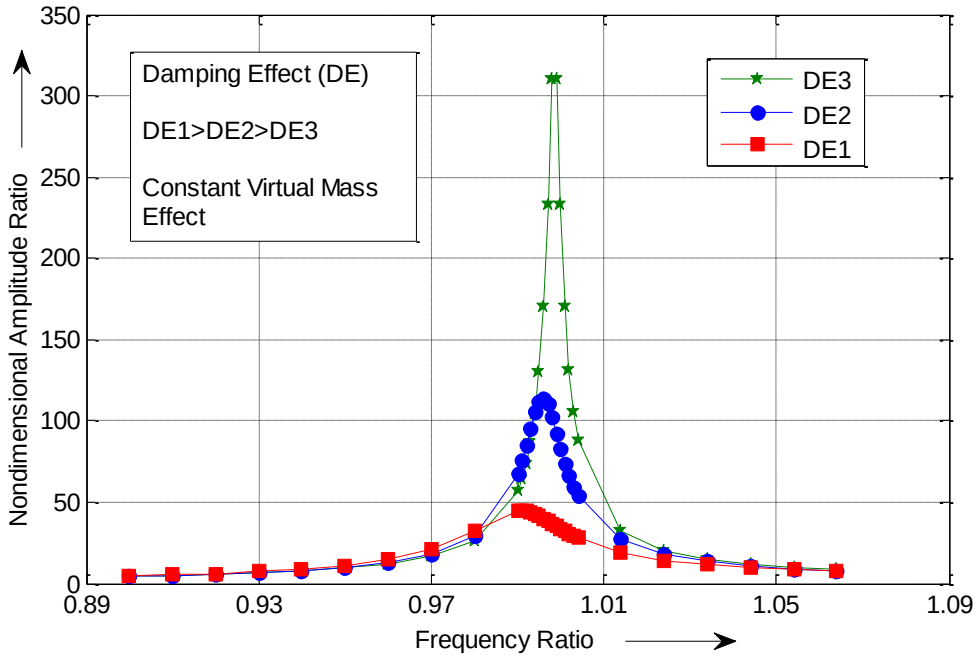

Figure 3.10: Frequency Ratio (ω/ω_0) Vs Non-dimensional Amplitude Ratio (δ^*/ε^*), Mild Steel Rotor R_1=0.01m, L=0.8m, q=12, R_D=0.055m, T_D=0.020m, M_D=1.0kg, for infinite region.

Table 3.1 shows the physical properties of cantilever rotor. Table 3.2 represented the properties of three different type of viscous fluid.

Table 3.1: Physical properties of cantilever rotor

Sl. No.	Parameters	Values (unit)
1	Material of cantilever rotor	Mild steel
2	Modulus of elasticity (E)	200GPa
3	Length of rotor (L)	0.8/1.0m
4	Material Density of rotor	ϱ=7800kg/m^3
5	Radius of rotor (R_1)	0.01m
6	Radius of disc (R_D)	R_{D1} =0.04m; R_{D2} =0.05m; R_{D3} =0.055m
7	Thickness of disc (T_D)	T_{D1}=0.01m;T_{D2}=0.015m;T_{D3}=0.020m
8	Mass of disc (M_D)	M_{D1}=0.50kg; M_{D2}=0.75kg; M_{D3}=1.0kg
9	Inside radius of vessel(R_2)	0.13m
10	Eccentricity (ε)	1.14x10^{-5}cm
11	Gap Ratio (i.e. container to rotor ratio) (q)	$q_{1,2,3,4}$=4,8,12,20
12	Operating condition temperature	25^{0}C
13	Relative crack depth of rotor (β)	$\beta_{1,2,3,4}$=0.125,0.175,0.225,0.275
14	Relative Crack position of rotor(α)	$\alpha_{1,2}$=0.313,0.563

Table 3.2: Properties of three different type of viscous fluid

Sl. No.	Fluid Name	Kinematic viscosity ν(Stokes)	Ratio of density(M*)
1	Lubricant oil 2T	2.9	0.158
2	Palm oil	0.541	0.153
3	Water (Sea)	0.0633	0.144

3.2.2 Dynamic Analysis of Rotating Multiple Cracked Cantilever Rotor Partially Submerged in the Viscous Medium

3.2.2.1 Determination of the Local Flexibility and Local Stiffness Matrix of a Cracked Rotor under Axial and Bending Loading

A multi cracked rotor of radius ' R_1' shown in Figure 3.11 is considered for the analysis. The release rate of strain energy can be calculated using the Equation (3.25).

$$J = \frac{1}{\mathrm{E}'}\left[\left(\sum_{i=1}^{6} K_{Ii}\right)^2 + \left(\sum_{i=1}^{6} K_{IIi}\right)^2 + \mathrm{m}\left(\sum_{i=1}^{6} K_{IIIi}\right)^2\right] \tag{3.25}$$

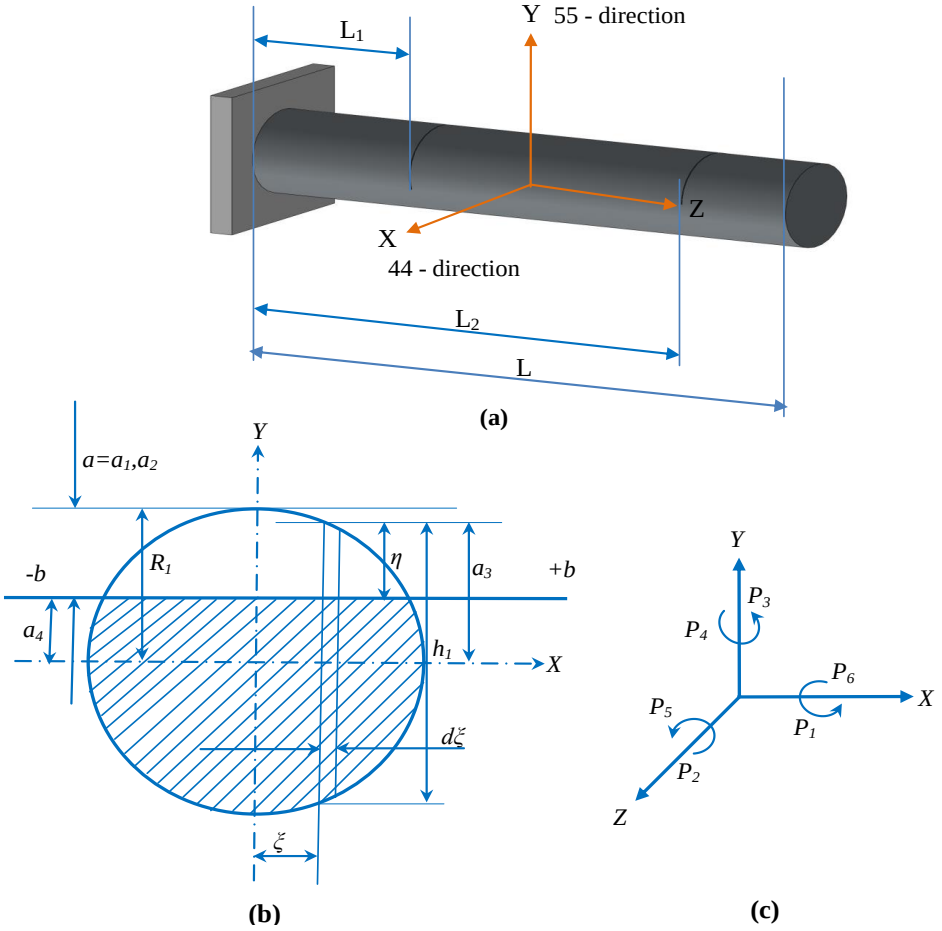

Figure 3.11: **(a)** Geometry of a cantilever rotor with crack element **(b)** Cross section of crack element **(c)** Coupling force on the crack element.

Where; $\frac{1}{E'} = \frac{1-\nu 1^2}{E}$

ν1 is the Poisson's Ratio

E is the Young's Modulus of Elasticity

The strain energy u_i can be calculated using Equation (3.26).

$$u_i = \frac{\partial U_t}{\partial P_i} \tag{3.26}$$

Local flexibility (C_{ij}) due to crack per unit width can be written as,

$$C_{ij} = \frac{\partial u_i}{\partial P_j} \tag{3.27}$$

From Tada et al. [205] it can be written

$$K_{I4} = \left\{4P_4\, x/(\pi R_1^{\,4})\right\}(\pi\, a3)^{0.5}\, F_1(a3/h1) \tag{3.28}$$

$$K_{II6} = \left\{2P_6\, x/(\pi R_1^4)\right\}(\pi\, a3)^{0.5}\, F_{II}(a3/h1) \tag{3.29}$$

$$K_{III2} = \left\{P_2 x/(\pi R_1^2)\right\}(\pi\, a3)^{0.5}\, F_{III}(a3/h1) \tag{3.30}$$

$$K_{III6} = \left\{2P_6\,(R_1^2 - x^2)^{0.5}/(\pi R_1^4)\right\}(\pi\, a3)^{0.5}\, F_{III}(a3/h1) \tag{3.31}$$

where

$$F_I\left(\frac{a3}{h1}\right) = (tanl\lambda/\lambda)^{0.5}\left[0.752 + 2.02\frac{a3}{h1} + 0.37(1 - sin\lambda)^3\right]/(cos\lambda) \tag{3.32}$$

$$F_{II}\left(\frac{a3}{h1}\right) = \left[1.122 + 0.561\frac{a3}{h1} + 0.085\left(\frac{a3}{h1}\right)^2 + 0.18\left(\frac{a3}{h1}\right)^3\right]/\left(1 - \frac{a3}{h1}\right)^{0.5} \tag{3.33}$$

$$F_{III}\left(\frac{a3}{h1}\right) = (tan\lambda/\lambda)^{0.5} \tag{3.34}$$

From the above equations the non-dimensional compliance can be written as

$$\bar{C}_{22} = \frac{\pi E R_1 C_{22}}{1 - \nu 1^2} = 4\int_{\frac{\bar{h}1}{2}-\bar{a}3}^{\frac{\bar{h}1}{2}}\int_0^{\bar{b}} \bar{y}\, F_{III}^{\,2}(\bar{h}1)\, d\bar{x}\, d\bar{y} \tag{3.35}$$

$$\bar{C}_{44} = \frac{\pi E R_1^{\,3} C_{44}}{1 - \nu 1^2} = 64\int_{\frac{\bar{h}1}{2}-\bar{a}3}^{\frac{\bar{h}1}{2}}\int_0^{\bar{b}} \bar{x}\, \bar{y}\, F_I^{\,2}(\bar{h}1)\, d\bar{x}\, d\bar{y} \tag{3.36}$$

$$\bar{C}_{62} = \frac{pE R_1^{\,2} C_{62}}{1 - \nu 1^2} = 8\int_{\frac{\bar{h}1}{2}-\bar{a}3}^{\frac{\bar{h}1}{2}}\int_0^{\bar{b}} \left(1 - \bar{x}^2\right)^{0.5}\, \bar{y}\, F_{III}^{\,2}(\bar{h}1)\, d\bar{x}\, d\bar{y} \tag{3.37}$$

$$\bar{C}_{66} = \frac{\pi E R_1^{\,3} C_{66}}{1 - \nu 1^2} = 16\int_{\frac{\bar{h}1}{2}-\bar{a}3}^{\frac{\bar{h}1}{2}}\int_0^{\bar{b}} \left(a_{1,2} + m a_4\right) d\bar{x}\, d\bar{y} \tag{3.38}$$

Where $a_{1,2} = \bar{x}^2 \bar{y} F_{II}^{\,2}(\bar{h}1)$, $a_4 = (1 - \bar{x}^2)\bar{y} F_{III}^{\,2}(\bar{h}1)$ and $\bar{x} = \frac{x}{R_1}, \bar{y} = \frac{y}{R_1}, \lambda = \frac{\pi\, a3}{2\, h1}$

$$\bar{h}1 = \frac{h1}{R_1}, \bar{b} = \frac{b}{R_1}, \bar{a}3 = \frac{a3}{R_1}, a3 = \frac{h1}{2} - a_4, h1 = 2\left(R_1^2 - x^2\right)^{0.5}$$

The dimensionless compliance matrix can be written as;

$$\bar{C}_{ij} = \begin{bmatrix} \bar{C}_{22} & \bar{C}_{26} & 0 \\ \bar{C}_{62} & \bar{C}_{66} & 0 \\ 0 & 0 & \bar{C}_{44} \end{bmatrix} \tag{3.39}$$

The local stiffness matrix can be obtained by taking the inversion of the compliance matrix, i.e.

$$K = \begin{bmatrix} K_{22} & K_{26} & 0 \\ K_{62} & K_{66} & 0 \\ 0 & 0 & K_{44} \end{bmatrix} = \begin{bmatrix} \bar{C}_{22} & \bar{C}_{26} & 0 \\ \bar{C}_{62} & \bar{C}_{66} & 0 \\ 0 & 0 & \bar{C}_{44} \end{bmatrix}^{-1} \tag{3.40}$$

In the proposed theoretical analysis a lumped mass at the free end of the rotating cantilever rotor partially immersed in the infinite fluid region is considered. To make the analysis easier the system is treated as a lumped system. In the first step the equivalent lumped mass of the cracked rotor is calculated and then the disc mass is added to it to find out the total lumped mass.Equivalent lumped masses of a spining cracked rotor are given by K_{55}/ω_{55}^2 and K_{44}/ω_{44}^2 (in two directions as shown in Figure 3.11a)

Where K_{55}, K_{44} and ω_{55}, ω_{44} are the stiffness's and fundamental natural frequencies in those direction respectively. 44-direction and 55-direction coincide with x and y-axis direction respectively. ω_{44} and ω_{55} can be derived from Chapter 3. K_{44} and K_{55} can also be derived with the help of global stiffness matrix [K_g] and Chapter 3.

The global stiffness matrix [K_g] can be written as [205,206];

$$\left[K_g\right] = \begin{bmatrix} K_{55} & K_{54} & K_{51} \\ K_{45} & K_{44} & K_{41} \\ K_{15} & K_{14} & K_{11} \end{bmatrix} = \left[\left[G_1\right]\left[C_{cr}\right]\left[G_2\right] + \left[C_s\right]\right]^{-1} \tag{3.41}$$

Where $\left[G_1\right] = diag\left[L_1, L_1, 1\right]$, (3.42a)

$$\left[G_2\right] = diag\left[L - L_1, L - L_1, 1\right], \tag{3.42b}$$

$$\left[C_s\right] = diag\left[\frac{L^3}{3EI}, \frac{L^3}{3EI}, \frac{L}{EA_1}\right] \text{ and} \tag{3.42c}$$

$$\left[C_{cr}\right] = \frac{1}{F_0} 1 \begin{bmatrix} \frac{\bar{C}_{55}}{R_1} & \frac{\bar{C}_{54}}{R_1} & \bar{C}_{51} \\ \frac{\bar{C}_{45}}{R_1} & \frac{\bar{C}_{44}}{R_1} & \bar{C}_{41} \\ \bar{C}_{15} & \bar{C}_{14} & \frac{\bar{C}_{11}}{R_1} \end{bmatrix} \tag{3.42d}$$

Where $F_0 = \frac{A_1 E}{1 - V_1^2}$, diag[.....] = diagonal matrix

The ratios of the equivalent lumped mass to the total mass of the rotor in two main directions are given by the expressions;

$$\alpha_{eq1} = \frac{K_{44}}{\omega_{44}^2 M_{s2}} \tag{3.43a}$$

$$\alpha_{eq2} = \frac{K_{55}}{\omega_{55}^2 M_{s2}} \tag{3.43b}$$

Where M_{s2} is the mass of the rotor

If a disc with mass M_{s1} is attached at the tip of the rotor, a total lumped mass of the rotor in 44 & 55- direction become.

$$M_1 M_s = M_{s1} + \alpha_{eq1} M_{s2} \text{ and } M_2 M_s = M_{s1} + \alpha_{eq2} M_{s2} \tag{3.44}$$

The equation of motion of an equivalent single degree of freedom system of the whirling multiple cracked rotor in fluid is reduced to in the form of equation (3.43a) and (3.43b).

$$M_1 M_s \frac{d^2\left(x + \varepsilon\cos\omega t\right)}{dt^2} + K_{44} x = F_x \tag{3.45a}$$

$$M_2 M_s \frac{d^2\left(y + \varepsilon\sin\omega t\right)}{dt^2} + K_{55} y = F_y \tag{3.45b}$$

The fluid forces from equation (3.17) can be written as

$$F_x = -M_1 M\ \mathrm{Re}(H)\frac{d^2x}{dt^2} + M_1 M_\omega lm(H)\frac{dx}{dt} \tag{3.46a}$$

$$F_y = -M_2 M\ \mathrm{Re}(H)\frac{d^2y}{dt^2} + M_2 M_\omega lm(H)\frac{dy}{dt} \tag{3.46b}$$

$$\left.\begin{aligned}
\text{Where; } M_1 M\ \mathrm{Re}(H) &= M_1\ \mathrm{Re}(H_1) + \alpha_{eq1} M_2\ \mathrm{Re}(H_2)\\
M_2 M\ \mathrm{Re}(H) &= M_1\ \mathrm{Re}(H_1) + \alpha_{eq2} M_2\ \mathrm{Re}(H_2)\\
M_1 M lm(H) &= M_1 lm(H_1) + \alpha_{eq1} M_2 lm(H_2)\\
M_2 M lm(H) &= M_1 lm(H_1) + \alpha_{eq2} M_2 lm(H_2)\\
M_1 M = M_1 + \alpha_{eq1} M_2 &\text{ and } M_2 M = M_1 + \alpha_{eq2} M_2
\end{aligned}\right\} \tag{3.47}$$

Where M_1 and M_2 mass of the fluid displaced by the disc and rotor respectively. Taking the eccentricity ε_1 (perpendicular to the crack, i.e. along 44- direction) and ε_2 (along the crack, i.e. along 55- direction). The analysis for amplitude is down. First ε_1 is taken and the contribution in x and y-axis direction are found out in the following procedure.

From equation (3.45) and (3.46), we get;

$$M_1M_s + M_1M\,\mathrm{Re}(H)\frac{d^2x}{dt^2} - M_1M_\omega lm(H)\frac{dx}{dt} + K_{44}X = M_1M_s\varepsilon_1\omega^2\cos\omega t \tag{3.48a}$$

$$M_2M_s + M_2M\,\mathrm{Re}(H)\frac{d^2y}{dt^2} - M_2M_\omega lm(H)\frac{dy}{dt} + K_{55}Y = M_2M_s\varepsilon_2\omega^2\sin\omega t \tag{3.48b}$$

The equation (3.48) in dimensionless form can be written as;

$$\left(1 + M_1^*\,\mathrm{Re}(H)\frac{d^2\xi_2}{d\tau_1} - M_1^*\omega_1^* lm(H)\frac{d\xi}{d\tau_1} + \xi = \varepsilon_1^*\left(\omega_1^*\right)^2\cos\left(\omega_1^*\tau_1\right)\right) \tag{3.49a}$$

$$\left(1 + M_2^*\,\mathrm{Re}(H)\frac{d^2\eta_2}{d\tau_2} - M_2^*\omega_2^* lm(H)\frac{d\eta}{d\tau_2} + \xi = \varepsilon_2^*\left(\omega_2^*\right)^2\sin\left(\omega_2^*\tau_2\right)\right) \tag{3.49b}$$

The steady state solution of the above equation can be obtained in dimensionless form as

$$\xi = \delta\delta_1^*\cos\left(\omega_1^*\tau_1 - \phi_1\right) \text{ and } \eta = \delta\delta_2^*\sin\left(\omega_2^*\tau_2 - \phi_2\right) \tag{3.50}$$

Where $\xi = \frac{x}{R_1}, \eta = \frac{y}{R_1}, \varsigma = \frac{z}{R_1}, \omega_1^* = \frac{\omega}{\omega_{01}}, \omega_2^* = \frac{\omega}{\omega_{02}}, \varepsilon_1^* = \frac{\varepsilon_1}{R_1}, \varepsilon_2^* = \frac{\varepsilon_2}{R_1}, M_1^* = \frac{M_1M}{M_1M_s}$,

$M_2^* = \frac{M_2M}{M_2M_s}, \tau_1 = \omega_{01}t, \tau_2 = \omega_{02}t, \delta\delta_n^* = \frac{\delta\delta_n}{R_1}, \omega_{01} = \sqrt{\frac{K_{44}}{M_1M_s}}, \omega_{02} = \sqrt{\frac{K_{55}}{M_2M_s}}$,

$$\left.\begin{aligned}\delta\delta_n^* &= \frac{A_n}{\sqrt{\left(K_n - \left(\omega_n^*\right)^2\right)^2 + \left(C_n\omega_n^*\right)^2}}, \phi_n = \tan^{-1}\left[\frac{C_n\omega_n^*}{K_n - \left(\omega_n^*\right)^2}\right] \\ C_n &= \frac{M_n^*\omega_n^* lm(H)}{1 + M_n^*\,\mathrm{Re}(H)}, K_n = \frac{1}{1 + M_n^*\,\mathrm{Re}(H)}, A_n = \frac{\varepsilon_1^*\left(\omega_n^*\right)^2}{1 + M_n^*\,\mathrm{Re}(H)}\end{aligned}\right\} \tag{3.51}$$

For n=1 and 2

When the 44-direction coincide with x- axis the amplitude contribution of ε_1 in x and y-axis direction are;

$\xi_{44} = \delta_1^*\cos\left(-\phi_n\right)$ in x-axis direction; (3.52a)

$$\eta_{44} = \delta_2^*\sin\left(\omega_2^*\tau_2 - \phi_n\right) \tag{3.52b}$$

When $\omega_2^*\tau_1 = 0$ in Y-axis direction;

Similarly the expression for ξ and η due to the eccentricity. ε_2 (Eccentricity in the direction of the crack 55-direction) can be found out adopting above procedure. When the 55-direction coincide with y-axis.The amplitude contribution of ε_1 in x and y- axis direction are ξ_{55} and η_{55} respectively.

The total dimensionless deflection in x and y-axis direction. When the 44-direction (perpendicular to crack) and 55-direction (along the crack) coincide with x and y- axis respectively are;

$\delta_{n=1}^{*} = \delta_{44}^{*} = \xi_{44} + \xi_{55}$ along the x-axis direction (3.53a)

$\delta_{n=2}^{*} = \delta_{55}^{*} = \eta_{44} + \eta_{55}$ along the y-axis direction (3.53b)

$\delta_1^* \left(= \delta_{44}^{*}\right)$ and $\delta_2^* \left(= \delta_{55}^{*}\right)$ is the dimensionless amplitude of the rotor.

When 44-direction and 55-direction coincide with x and y-axis respectively.

Figure 3.11(a) describes the full detail of the cantilever rotor with crack element taken for theoretical analysis. Figure 3.11(b) deals with the cross-sectional view of the cracked shaft. This figure also shows the depth of crack, width of the crack. Figure 3.11(c) shows the coupling forces on the crack element. The theoretical analysis is carried out for finding out for finding out the effect of multiple crack depths and multiple crack positions on the natural frequency of the cracked rotor on both transverse directions (i.e. 44-direction and 55-direction).

Figures 3.12 and 3.13 shows that the vibration response of multi cracked rotor in two transverse directions of crack (i.e.44-direction and 55-direction) with the different viscous fluid medium. It is observed that as the density and viscosity of the fluid increases, the amplitude as well as whirling speed decreases of the rotor. Also, it is seen that the due to increasing the multiple crack depth on the multiple crack location, the amplitude and frequency of the rotor decrease under same viscous medium.

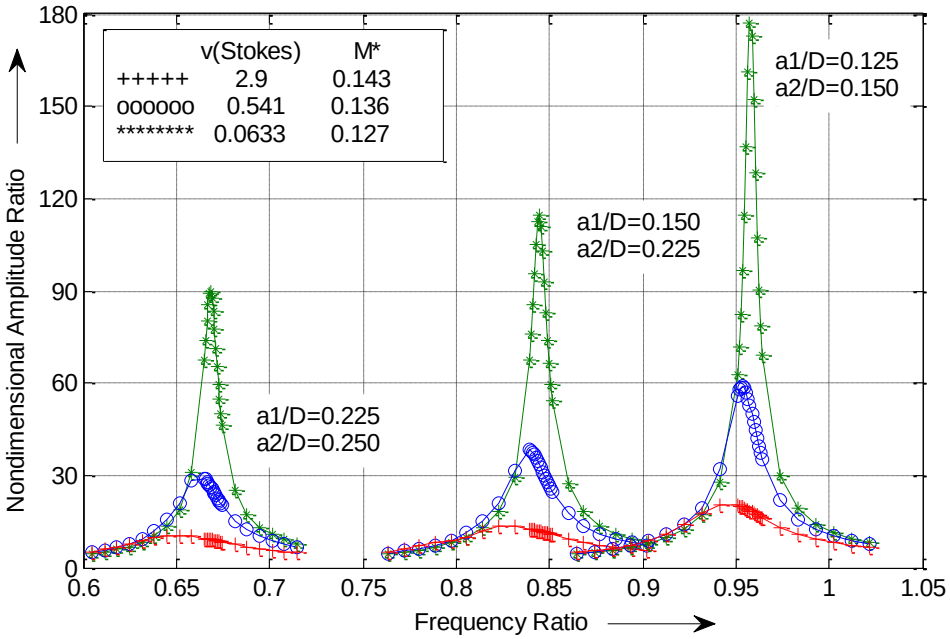

Figure 3.12: Frequency Ratio (ω/ω_0) Vs Non-dimensional Amplitude Ratio (δ^*/ε^*), Mild Steel Rotor R_1=0.01m,L=0.8m,q=12,L_1/L=0.313, L_2/L=0.563, R_D=0.055m,T_D = 0.020m, M_D = 1.0kg for 44-Direction.

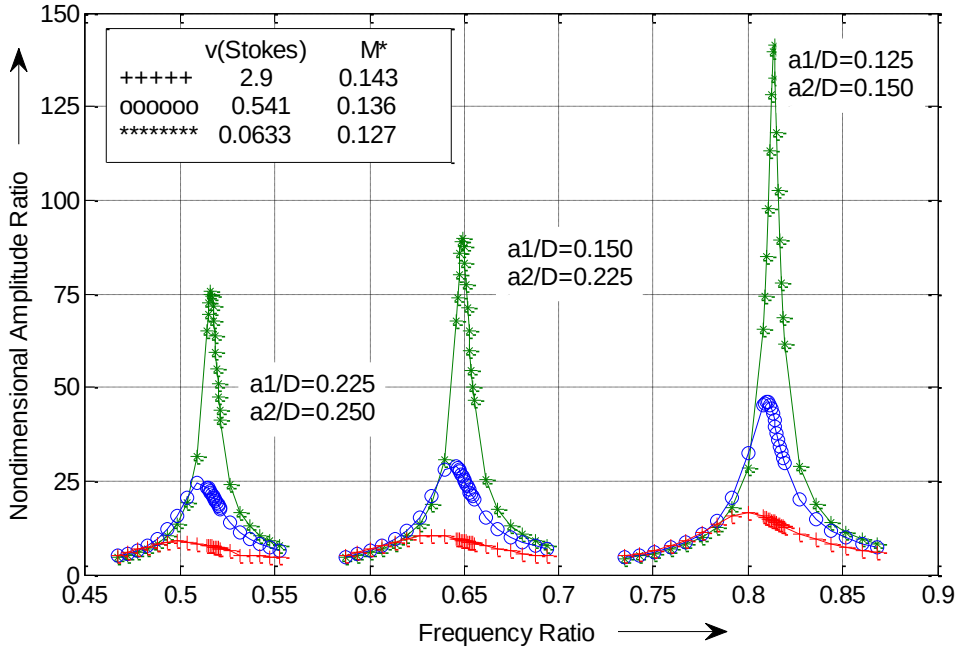

Figure 3.13: Frequency Ratio ($\omega/\omega 0$) Vs Non-dimensional Amplitude Ratio (δ^*/ε^*), Mild Steel Rotor R_1=0.01m,L=0.8m,q=12,L_1/L=0.313, L_2/L=0.563, R_D =0.055m,T_D = 0.020m, M_D=1.0kg for 55-Direction.

It is observed that the amplitude of vibration fall down by increasing the viscosity of fluid. In addition, it is found that the depth of cracks increases the fundamental natural frequency From Figure 3.14 it is observed that the cracked cantilever rotor at the 55-dierction (i.e. along the crack) ensure the less stiffness as compare to crack rotor at the 44-direction (i.e. Perpendicular to the crack).The cracked rotor stiffness are lesser than the non-cracked rotor. Because of whirling speed, the damping coefficient of cracked rotor system is increased for which the amplitude of the cracked shaft is minimized and it is maximum for the non-cracked rotor in the same fluid medium.

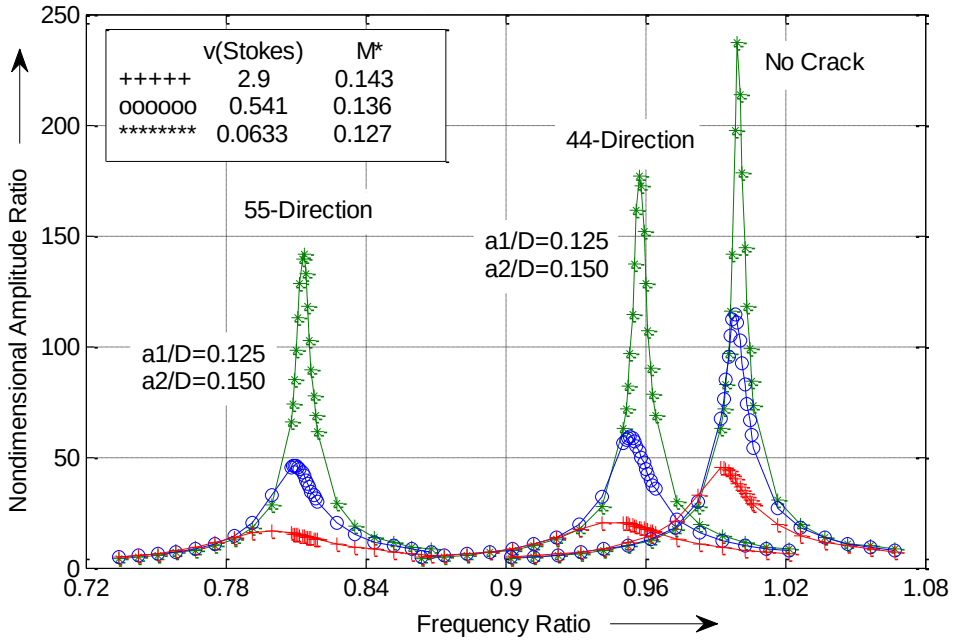

Figure 3.14: Frequency Ratio (ω/ω_0) Vs Non-dimensional Amplitude Ratio (δ^*/ε^*), Mild Steel Rotor R_1=0.01m, L=0.8m, q=12, L_1/L= 0.313, L_2/L=0.563, R_D = 0.055m, T_D= 0.020m, M_D = 1.0kg.

Figure 3.15 show the effect of gap ratio on the non-dimensional amplitude of the system on two main direction (i.e. 44- direction and 55-direction).It is observed that as the gap ratio increases (i.e. fluid container radius increases) the amplitude of vibration also increases.

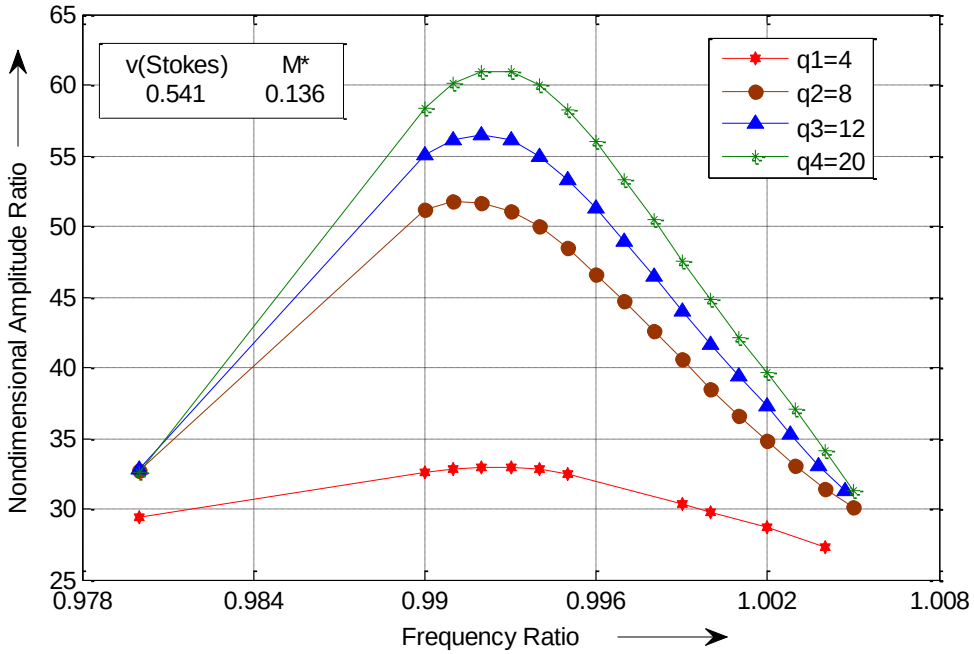

Figure 3.15: Frequency Ratio (ω/ω_0) Vs Non-dimensional Amplitude Ratio (δ^*/ε^*), Mild Steel Rotor R_1=0.01m, L=0.8m, a1/D=0.125, a2/D=0.150, L_1/L=0.313, L_2/L=0.563, R_D=0.055m,T_D=0.020m, M_D=1.0kg for 44-Direction.

From Figure 3.16 it is observed that as the virtual mass effect increases the amplitude of vibration decreases and the resonance frequency for the rotor is shifted towards left. From Figure 3.16 it is observed that as the virtual mass effect increases the amplitude of vibration decreases and the resonance frequency for the rotor is shifted towards left.

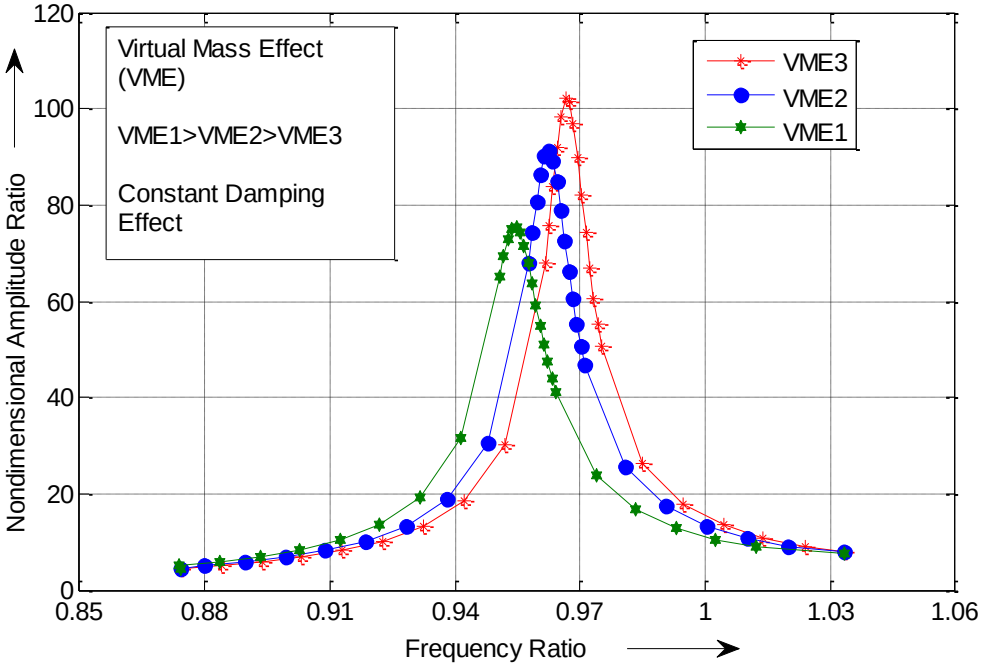

Figure 3.16: Frequency Ratio (ω/ω_0) Vs Non-dimensional Amplitude Ratio (δ^*/ε^*), Mild Steel Rotor R_1=0.01m, L=0.8m, q=12, a1/D=0.125, a2/D=0.150, L_1/L=0.313, L_2/L=0.563, ν=0.541stokes & M*=0.136,M_{D1}=1.0kg,M_{D2}=0.75kg, M_{D3}=0.50kg.

For theoretical analysis is also carried out for finding out the effect of crack depth and crack position on the natural frequency of cracked rotor in two main directions (44-direction and 55-direction). They are presented in Figures 3.17 and 3.18.

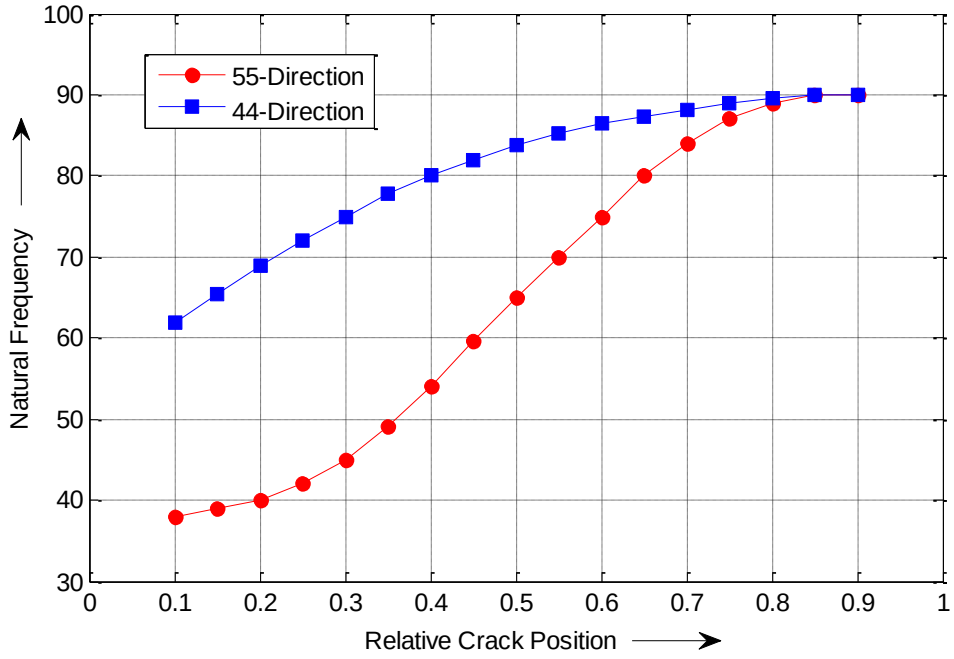

Figure 3.17: Relative Crack Position Vs Natural Frequency Mild Steel Rotor R_1=0.01m, L=0.8m, Relative crack depths a1/D=0.225, a2/D=0.250, R_D= 0.055m,T_D= 0.020m, M_D = 1.0kg.

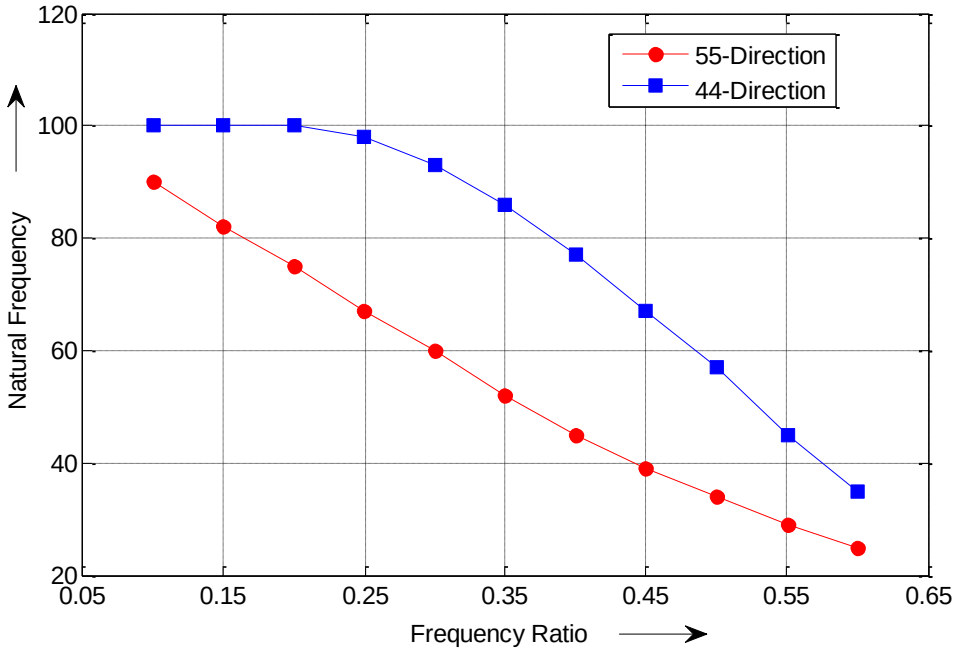

Figure 3.18: Relative Crack Depth Vs Natural Frequency, Mild Steel Rotor R_1=0.01m, L=0.8m, Relative crack location L_1/L= 0.313, L_2/L= 0.563, R_D = 0.055m,T_D= 0.020m, M_D = 1.0kg.

3.2.3 Dynamic Response of Rotating Fixed-Fixed Rotor with Additional Mass at Mid Span Submerged in the Viscous Medium

3.2.3.1 Analysis of Rotating Non-cracked Fixed-Fixed Rotor

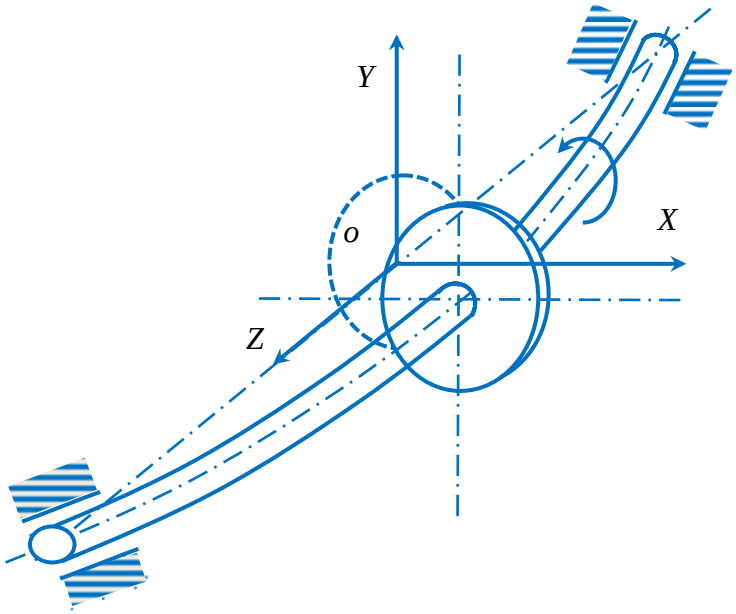

Figure 3.19: Full view of fixed-fixed rotor.

A fixed-fixed uniform spinning rotor immersed in a finite fluid region is considered in this analysis.For equation of motion and analysis of fluid forces the section 3.2.1.1 and 3.2.1.2 can be referred.

The equation of motion for the rotor having uniformly distributed mass and stiffness are;

$$M_s \frac{d^2\left(x+\varepsilon\cos\omega t\right)}{dt^2} + EI\frac{d^4x}{dz^4} = F_x \tag{3.54a}$$

$$M_s \frac{d^2\left(x+\varepsilon\sin\omega t\right)}{dt^2} + EI\frac{d^4y}{dz^4} = F_y \tag{3.54b}$$

Where; M_s = Mass of the rotor per unit length

M= Fluid mass displaced by the rotor per unit length.

EI= Bending stiffness of the rotor.

From equation (3.54) and equation (3.17) we obtain;

$$\left(m_s + m\,\mathrm{Re}\left(H\right)\right)\frac{d^2x}{dt^2} - m\omega lm\left(H\right)\frac{dx}{dt} + EI\frac{d^4x}{dz^4} = m_s\varepsilon\omega^2\cos\omega t \tag{3.55a}$$

$$\left(m_s + m\,\mathrm{Re}(H)\right)\frac{d^2y}{dt^2} - m\omega lm(H)\frac{dy}{dt} + EI\frac{d^4y}{dz^4} = m_s\varepsilon\omega^2\sin\omega t \tag{3.55b}$$

Equation (3.55) can be written in dimensionless form as;

$$\left(1+m^*\,\mathrm{Re}(H)\right)\frac{d^2\xi}{d\tau^2} - m^*\omega^* lm(H)\frac{d\xi}{d\tau} + \frac{L^{*4}}{\pi^4}\frac{d^4\xi}{d\varsigma^4} = \varepsilon^*\left(\omega^*\right)^2\cos\left(\omega^*\tau\right) \tag{3.56a}$$

$$\left(1+m^*\,\mathrm{Re}(H)\right)\frac{d^2\xi}{d\tau^2} - m^*\omega^* lm(H)\frac{d\eta}{d\tau} + \frac{L^{*4}}{\pi^4}\frac{d^4\eta}{d\varsigma^4} = \varepsilon^*\left(\omega^*\right)^2\sin\left(\omega^*\tau\right) \tag{3.56b}$$

Where; $\xi = \frac{x}{R_1}, \eta = \frac{y}{R_1}, \varsigma = \frac{z}{R_1}, \omega^* = \frac{\omega}{\omega_0 r}, \varepsilon^* = \frac{\varepsilon}{R_1}, M^* = \frac{m}{m_s}, \tau = \omega_0 r, L^* = \frac{L}{R_1}$,

$$\omega_0 = \pi^2\left[\frac{EI}{m_s L^4}\right]^{0.5}$$

ω_0 is the fundamental natural frequency of the rotor.

Applying the Fourier transformation to both sides of equation (3.56a and 3.56b), we obtain;

$$\ddot{X}_v(\tau) + C_0\ddot{X}_v + K_v X_v = A_v\cos\left(\omega^*\tau\right) \tag{3.57}$$

Where $X_v(\tau) = \int_0^{L^*}\xi(\varsigma_1\tau)\sin\left(\frac{v\pi\varsigma}{L^*}\right)d\varsigma_1$ (v=1, 2, ----------) (3.58a)

$$C_0 = -\frac{M^*\omega^* lm(H)}{1+M^*\,\mathrm{Re}(H)}, \tag{3.58b}$$

$$K_v = \frac{v^4}{1+M^*\,\mathrm{Re}(H)}, \tag{3.58c}$$

$$A_v = \frac{\frac{2}{v\pi}\varepsilon^*\left(\omega^*\right)^2 L^*\sin^2\left(\frac{v\pi}{2}\right)}{1+M^*\,\mathrm{Re}(H)} \tag{3.58d}$$

and $\xi = \frac{d^2\xi}{d\zeta^2} = 0$ for $\varsigma = 0, L^*$ (boundary condition at two ends of the rotor)

The steady state solution of equation (3.55) is easily obtained as;

$$X_v = \left(\frac{1}{2}\right)\delta_v^*\cos\left(\omega^*\tau - \phi_v\right) \qquad \text{(For v=1, 2, ----------)} \tag{3.59}$$

Where; $\delta_v^* = \frac{2A_v}{\sqrt{\left(K_v - \left(\omega^*\right)^2\right)^2 + \left(C_0\omega^*\right)^2}}$, (3.60a)

$$\phi_v = \tan^{-1}\left[\frac{C_0\omega^*}{K_v - \left(\omega^*\right)^2}\right] \tag{3.60b}$$

Taking the inverse Fourier transform of X_v we get;

$$\xi(\varsigma,\tau) = 2\sum_{v=1}^{\infty} X_v(\tau)\sin\left(\frac{v\pi\varsigma}{L^*}\right) = \sum_{v=1}^{\infty}\delta_v^*\cos\left(\omega^*\tau - \phi_v\right)\sin\left(\frac{v\pi\varsigma}{L^*}\right) \tag{3.61}$$

From the above equation the whirling fundamental bending mode at the rotor mid span can be written as;

$$\xi\left(\frac{L^*}{2},\tau\right) = \delta_1^*\cos\left(\omega^*\tau - \phi_1\right) \tag{3.62}$$

Where; $\delta_1^* = \dfrac{\frac{4}{v\pi}\varepsilon^*\left(\omega^*\right)^2 L^*}{\sqrt{\left(1-\left(\omega^*\right)^2\left(1+m^*\,\mathrm{Re}(H)\right)\right)^2 + \left(m^*\left(\omega^*\right)^2 lm(H)\right)^2}}$, (3.63a)

$$\phi_1 = \tan^{-1}\left[\frac{-m^*\left(\omega^*\right)^2 lm(H)}{1-\left(\omega^*\right)^2\left(1+m^*\,\mathrm{Re}(H)\right)}\right] \tag{3.63b}$$

δ_1^*/ε^* is the maximum dimensionless amplitude that the rotor exhibits in fundamental mode.

The results obtained from numerical analysis using the expression 3.53 with the help of MATLAB program are plotted graph between frequency ratio and non-dimensional amplitude ratio in Figure 3.20 to 3.24 to illustrate the effect of various parameters (i.e. kinematic viscosities of different fluid, virtual mass effect, damping coefficient effect and gap ratio). Figures 3.20 and 3 .21 shows the non-dimensional amplitude of vibration with respect to frequency ratio in different viscous medium. It is observed that as the viscosity of the fluid increases the amplitude of vibration and critical speed of rotor decreases. A peculiar effect is observed from the comparison of Figures 3.20 and 3.21 for a particular viscous fluid when two different length of rotor are considered. It is found that the dimensionless amplitude is smaller in case larger rotor.

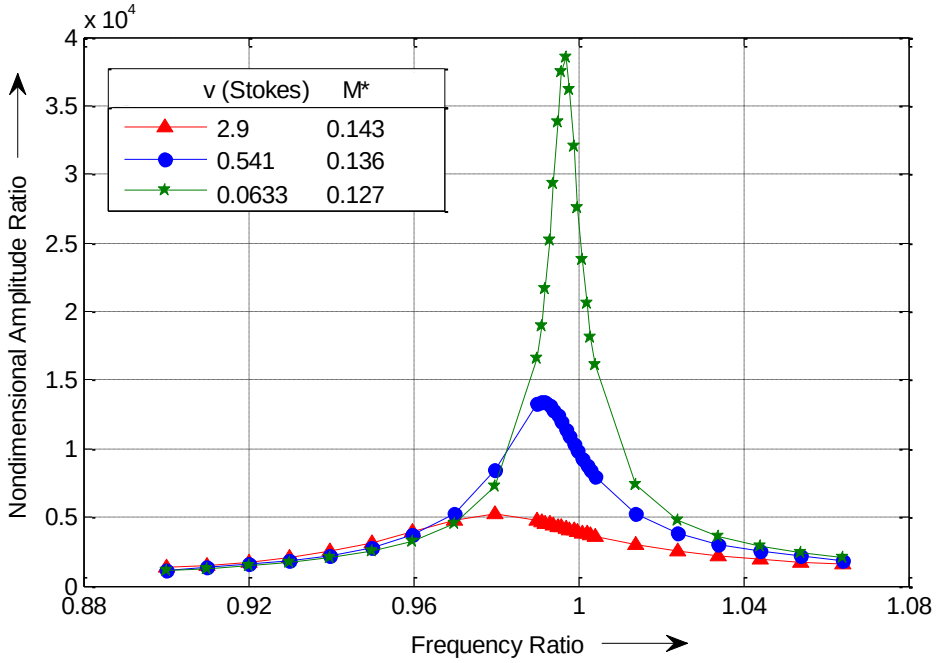

Figure 3.20: Frequency Ratio (ω/ω_0) Vs Non-dimensional Amplitude Ratio (δ^*/ε^*), Mild Steel Rotor R_1=0.01m, L=1.0m, q=12, R_D = 0.055m,T_D= 0.020m, M_D = 1.0kg.

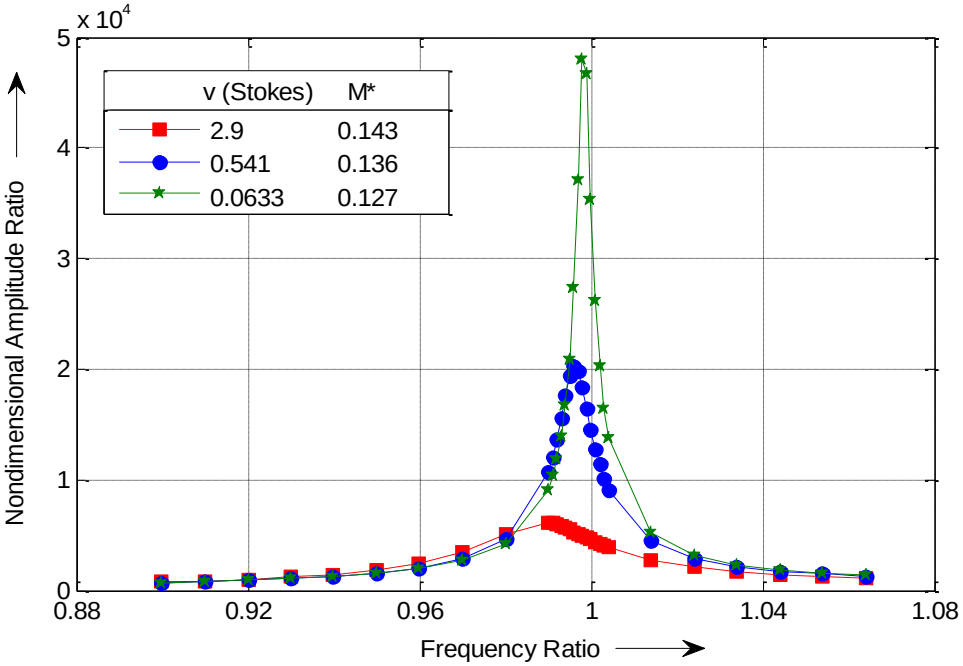

Figure 3.21: Frequency Ratio (ω/ω_0) Vs Non-dimensional Amplitude Ratio (δ^*/ε^*), Mild Steel Rotor R_1=0.01m, L=0.8m, q=12, R_D=0.055m,T_D=0.020m, M_D=1.0kg.

The effect of gap ratio is presented in Figure 3.22. It is observed that the increase in fluid container radius the corresponding non-dimensional amplitude increase.

The effect of virtual mass and damping coefficient can be seen in Figure 3.23 and 3.24. From Figure 3.23 it is observed that the with the increase in virtual mass effect $\left(\left|m\,\mathrm{Re}\left(H\right)\right|\right)$ at affixed damping the critical speed of the rotor decreases and the corresponding dimensionless amplitude of vibration also decreases due to damping effect at affixed virtual mass, the dimensionless amplitude is affected in a more prominent way. With the increase in damping effect, amplitude of vibration for the corresponding system decreases, which can be observed from Figure 3.24.

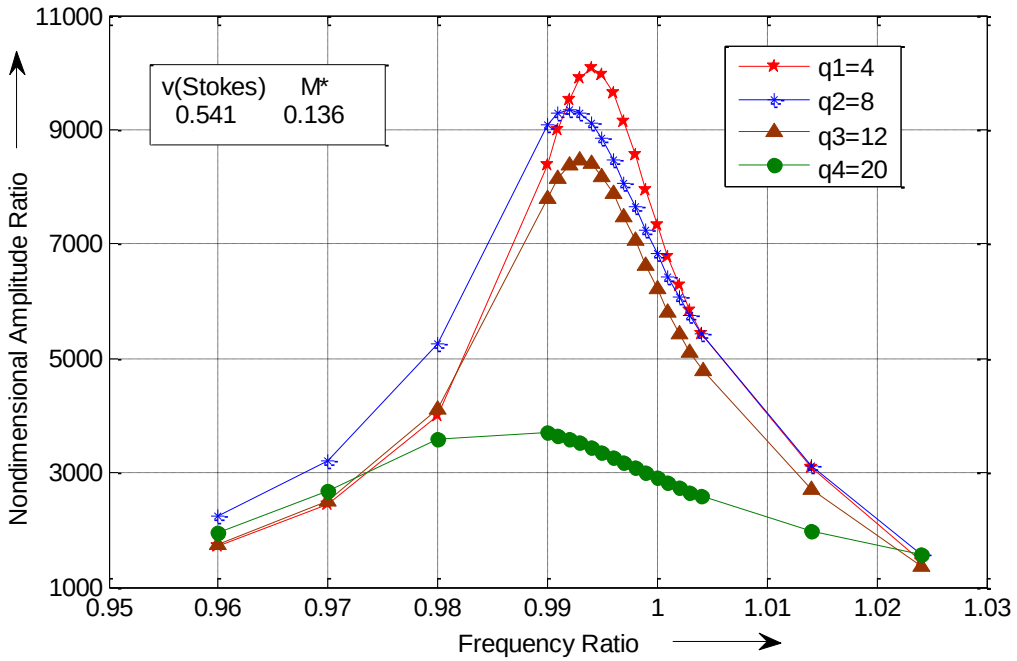

Figure 3.22: Frequency Ratio (ω/ω_0) Vs Non-dimensional Amplitude Ratio (δ^*/ε^*), Mild Steel Rotor R_1=0.01m, L=0.8m, R_D = 0.055m,T_D= 0.020m, M_D = 1.0kg.

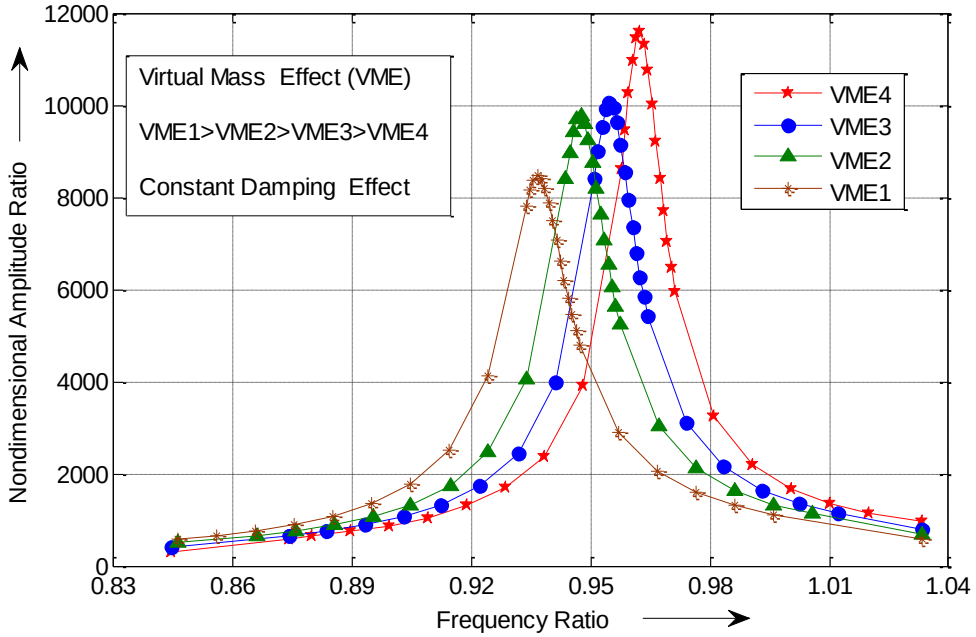

Figure 3.23: Frequency Ratio (ω/ω_0) Vs Non-dimensional Amplitude Ratio (δ^*/ε^*), Mild Steel Rotor R_1=0.01m, L=0.8m, q=12, ν=0.541stokes & M^*=0.136,M_{D1}=1.0kg,M_{D2}=0.75kg, M_{D3}=0.60kg, M_{D4}=0.50kg.

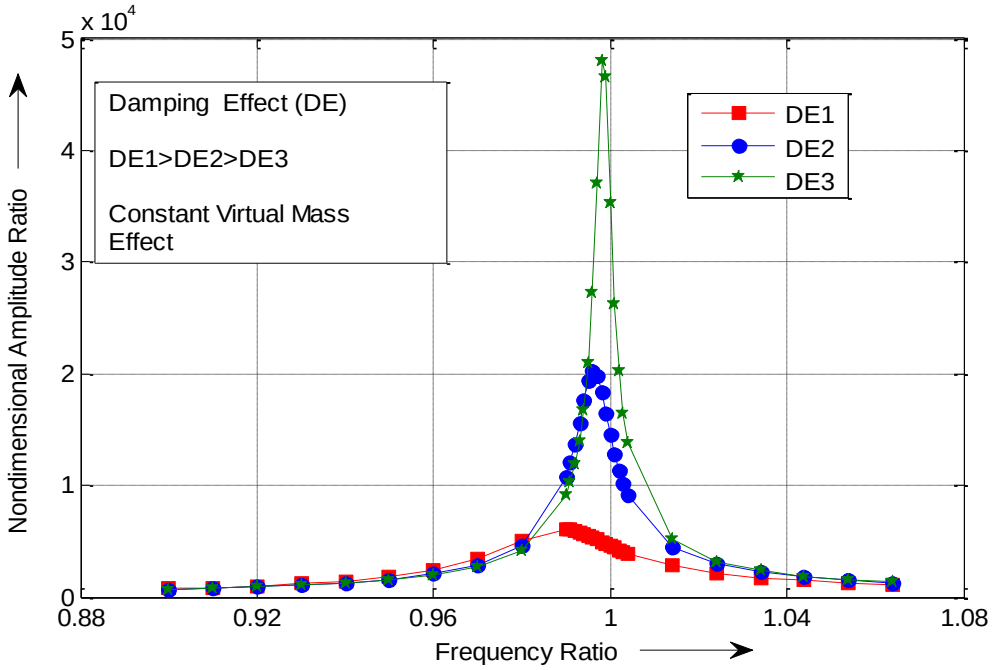

Figure 3.24: Frequency Ratio (ω/ω_0) Vs Non-dimensional Amplitude Ratio (δ^*/ε^*), Mild Steel Rotor R_1=0.01m, L=0.8m, q=12, ν=0.0633, 0.541, 2.9 stokes & M^*=0.127, 0.136,0.146, R_D=0.055m, T_D= 0.020m, M_D=1.0kg.

3.2.3.2 Analysis of Rotating Multiple Cracked Fixed-Fixed Rotor

A rotating multiple cracked fixed-fixed rotor submerged in fluid region is considered.

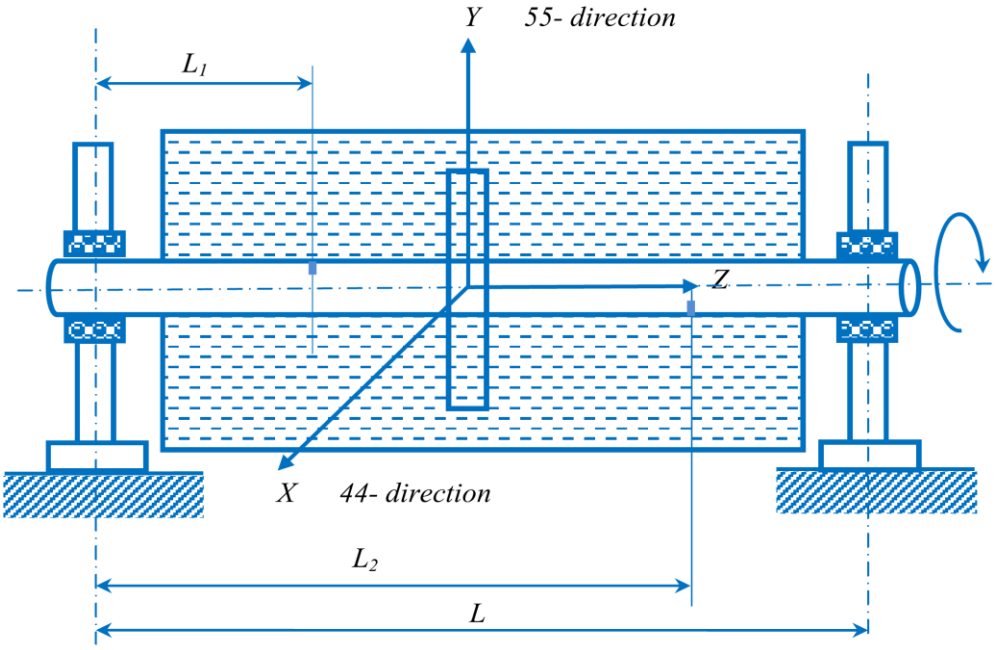

Figure 3.25: Schematic representation of multiple cracked fixed-fixed rotor submerged in the viscous fluid.

$$M_s \frac{d^2\left(x+\varepsilon\cos\omega t\right)}{dt^2} + EI\frac{d^4x}{dz^4} = F_x \tag{3.64a}$$

$$M_s \frac{d^2\left(x+\varepsilon\sin\omega t\right)}{dt^2} + EI\frac{d^4y}{dz^4} = F_y \tag{3.64b}$$

Where; m_s = Mass of the rotor per unit length

m= Fluid mass displaced by the shaft per unit length.

EI= Bending stiffness of the shaft.

From equation (3.64) and equation (3.17) we obtain;

$$\left(m_s + m\,\mathrm{Re}\left(H\right)\right)\frac{d^2x}{dt^2} - m\omega lm\left(H\right)\frac{dx}{dt} + EI\frac{d^4x}{dz^4} = m_s\varepsilon\omega^2\cos\omega t \tag{3.65a}$$

$$\left(m_s + m\,\mathrm{Re}\left(H\right)\right)\frac{d^2y}{dt^2} - m\omega lm\left(H\right)\frac{dy}{dt} + EI\frac{d^4y}{dz^4} = m_s\varepsilon\omega^2\sin\omega t \tag{3.65b}$$

Taking the eccentricity ε_1 (perpendicular to the crack, i.e.along 44-direction) and ε_2 (along the crack, i.e. along 55- direction).

The analysis for amplitude is drawn. At first ε_1 is taken and its contribution in x and y-axis direction are found out in the following procedures.

Introducing dimensionless quantities;

Where $\xi = \frac{x}{R_1}$, $\eta = \frac{y}{R_1}$, $\varsigma = \frac{z}{R_1}$, $\omega_1^* = \frac{\omega}{\omega_{xx}}$, $\omega_2^* = \frac{\omega}{\omega_{yy}}$, $\varepsilon_1^* = \frac{\varepsilon_1}{R_1}$, $M^* = \frac{m}{m_s}$, $\tau_1 = \omega_{xx} t$,

$\tau_2 = \omega_{yy} t$, $L^* = \frac{L}{R_1}$, $F_1 = \left(\frac{\omega_0}{\omega_{xx}}\right)^2$, $F_2 = \left(\frac{\omega_0}{\omega_{yy}}\right)^2$, $m^* = \frac{m}{m_s}$

ω_{xx}, ω_{yy} are the fundamental natural frequency in x and y-axis direction respectively of the cracked rotor as shown in Figure 3.25.

Where as ω_0 is the fundamental natural frequency of the non-cracked rotor

$\omega_0 = \pi^2 \left(EI/\left(M_s L^4\right)\right)^{0.5}$

$$\left(1 + m^* \operatorname{Re}(H)\right)\frac{d^2\xi}{d\tau_1^2} - m^*\omega^* lm(H)\frac{d\xi}{d\tau} + F_1\frac{L^{*4}}{\pi^4}\frac{d^4\xi}{d\varsigma^4} = \varepsilon_1^*\left(\omega_1^*\right)^2\cos\left(\omega_1^*\tau_1\right) \tag{3.66a}$$

$$\left(1 + m^* \operatorname{Re}(H)\right)\frac{d^2\xi}{d\tau_2^2} - m^*\omega_2^* lm(H)\frac{d\eta}{d\tau_2} + F_2\frac{L^{*4}}{\pi^4}\frac{d^4\eta}{d\varsigma^4} = \varepsilon_1^*\left(\omega_2^*\right)^2\sin\left(\omega_2^*\tau_2\right) \tag{3.66b}$$

Applying the Fourier transform to both side of equation (3.66), we obtain;

$$\ddot{X}_v(\tau_1) + C_{01}\ddot{X}_v + K_{v1}X_v = A_{v1}\cos\left(\omega_1^*\tau_1\right) \tag{3.67a}$$

$$\ddot{Y}_v(\tau_2) + C_{02}\ddot{Y}_v + K_{v2}Y_v = A_{v2}\cos\left(\omega_2^*\tau_2\right) \tag{3.67b}$$

Where;

$$C_{0n} = -\frac{M_n^*\omega_n^* lm(H)}{1 + M_n^* \operatorname{Re}(H)}, \quad K_{vn} = \frac{F_n}{1 + M_n^* \operatorname{Re}(H)}, \tag{3.68a}$$

$$A_{v1} = \frac{\frac{2}{v\pi}\varepsilon_1^*\left(\omega_1^*\right)^2 L^* \sin^2\left(\frac{v\pi}{2}\right)}{1 + M_1^* \operatorname{Re}(H)}, \tag{3.68b}$$

$$A_{v2} = \frac{\frac{2}{v\pi}\varepsilon_1^*\left(\omega_2^*\right)^2 L^* \cos^2\left(\frac{v\pi}{2}\right)}{1 + M_2^* \operatorname{Re}(H)} \tag{3.68c}$$

[For n=1 &2 & V=1, 2, ----------]

$F_n = F_{1 \text{ or }} F_2$ for n=1 or 2

The steady state solution of equation is easily obtained as;

$$X_v = (1/2)\delta_v^* \cos\left(\omega_1^* \tau_1 - \phi_1\right) \tag{3.69a}$$

$$Y_v = (1/2)\delta_v^* \cos\left(\omega_2^* \tau_2 - \phi_2\right) \tag{3.69b}$$

For v=1, 2

Where $\delta_{vn}^* = \dfrac{A_{vn}}{\sqrt{\left(K_{vn} - \left(\omega_n^*\right)^2\right)^2 + \left(C_{0n}\omega_n^*\right)^2}}$, $\phi_{vn} = \tan^{-1}\left[\dfrac{C_{0n}\omega_n^*}{K_{vn} - \left(\omega_n^*\right)^2}\right]$ (3.70)

For V=1, 2, ----------; n=1&2

Taking the inverse fourier transform of X_v, we get;

$$\xi(\varsigma\ \tau_1) = 2\sum_{v=1}^{v} X_v(\tau_1)\sin\left(\frac{v\pi\varsigma}{L^*}\right) \tag{3.71}$$

Similarly for Y_v it can be done

From the above equation the whirling motion for fundamental bending mode in X and Y-axis direction can be written respectively as;

$$\xi\left(\frac{L^*}{2}, \tau_1\right) = \delta_{11}^* \cos\left(\omega_1^* \tau_1 - \phi_{11}\right) \tag{3.72a}$$

$$\eta\left(\frac{L^*}{2}, \tau_2\right) = \delta_{12}^* \sin\left(\omega_2^* \tau_2 - \phi_{12}\right) \tag{3.72b}$$

ξ and η are the dimensionless deflection in x and y-axis direction respectively due to eccentricity ε_1 (Eccentricity in the direction perpendicular to the crack , 44- direction) when the 44- directin axis coincides with x-axis direction the amplitude contribution of ε_1 in x and y-axis direction are ;

$$\xi_{44}\left(\frac{L^*}{2}, \tau_1\right) = \delta_{11}^* \cos\left(-\phi_{11}\right) \quad \text{in x-axis direction} \tag{3.73a}$$

$$\eta_{44}\left(\frac{L^*}{2}, \tau_2\right) = \delta_{12}^* \sin\left(\omega_2^* \tau_2 - \phi_{12}\right) \quad \text{in y- axis direction} \tag{3.73b}$$

Similarly the expression for $\xi\left(\frac{L^*}{2}, \tau_1\right)$ and $\eta\left(\frac{L^*}{2}, \tau_2\right)$ due to eccentricity ε_2 (Eccentricity in the direction of crack, 55- direction) can be found out adopting above procedure.When the 55- direction coincide with y- axis the amplitude contribution of ε_1 in x and y direction are $\xi_{55}\left(\frac{L^*}{2}, \tau_1\right)$ and $\eta_{55}\left(\frac{L^*}{2}, \tau_2\right)$ respectively.

The total dimensionless deflection in x and y-axis direction. When the 44-direction (Perpendicular to the crack) and 55-direction (along the crack) coincide with x and y-axis respectively are;

$$\delta_1^* = \delta_{44}{}^* = \xi_{44}\left(\frac{L^*}{2},\tau_1\right)+\xi_{55}\left(\frac{L^*}{2},\tau_1\right) \text{ along the x-axis direction (44- direction)} \qquad (3.74a)$$

$$\delta_2{}^* = \delta_{55}{}^* = \eta_{55}\left(\frac{L^*}{2},\tau_1\right)+\eta_{55}\left(\frac{L^*}{2},\tau_1\right) \text{ along the y-axis direction (55- direction)} \qquad (3.74b)$$

$\delta_1^*(=\delta_{44}{}^*)$ and $\delta_2{}^*(=\delta_{55}{}^*)$ are the dimensionless amplitude of the cracked rotor. When 44-direction and 55-direction coincide with x-axis and y-axis respectively.

Figures 3.26 and 3.27 shows that the vibration response of multi cracked rotor in two transverse directions of crack (i.e.44-direction and 55-direction) with the different viscous fluid medium. It is observed that as the density and viscosity of the fluid increases, the amplitude as well as whirling speed decreases of the rotor. Also, it is seen that the due to increasing the multiple crack depth on the multiple crack location, the amplitude and frequency of the rotor decrease under same viscous medium.

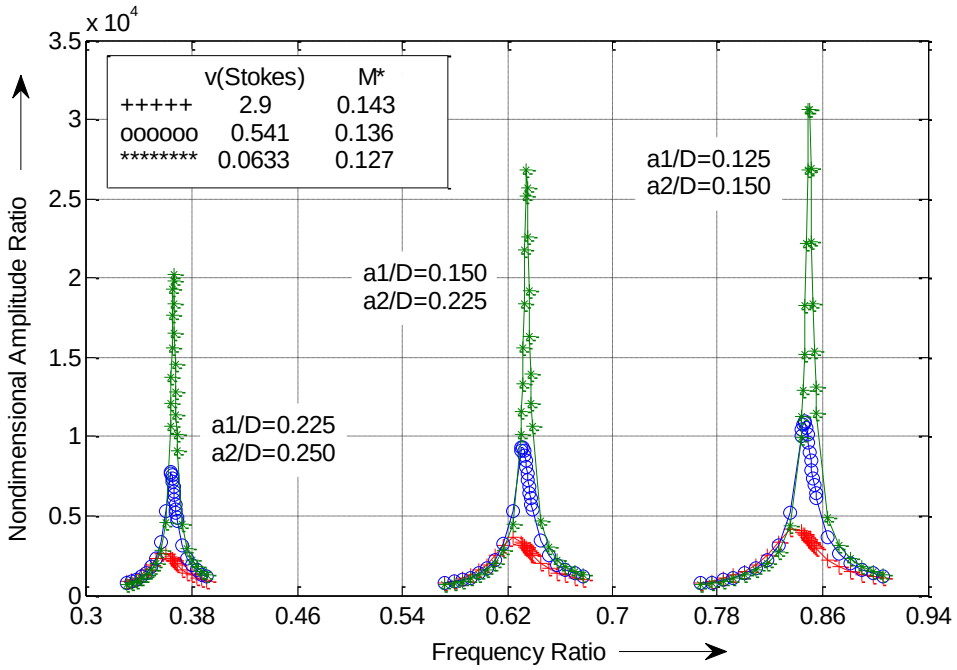

Figure 3.26: Frequency Ratio (ω/ω_0) Vs Non-dimensional Amplitude Ratio (δ^*/ε^*), Mild Steel Rotor R_1=0.01m, L=0.8m, q=12, L_1/L=0.313, L_2/L=0.563, R_D=0.055m,T_D=0.020m, M_D=1.0kg for 44-Direction.

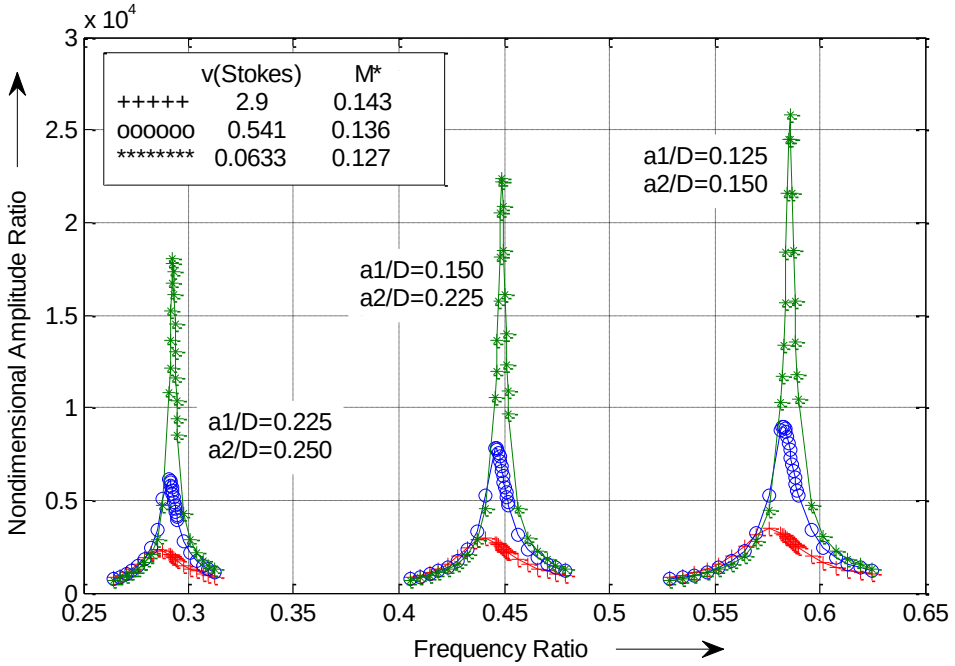

Figure 3.27: Frequency Ratio (ω/ω_0) Vs Non-dimensional Amplitude Ratio (δ^*/ε^*), Mild Steel Rotor R_1=0.01m, L=0.8m, q=12, L_1/L=0.313, L_2/L=0.563, R_D=0.055m, T_D=0.020m, M_D=1.0kg for 55-Direction.

Figure 3.28 shows that the comparison between the both transverse directions of crack with the non-cracked rotor. It is found that the amplitude of vibration at 44- direction is higher than the 55- direction. But it is lesser than the amplitude of the non- cracked rotor under the same parameters. From Figure 3.29 it is evident that as the virtual mass effect increase the critical speed decreases remarkably as compared to that of amplitude of vibration.

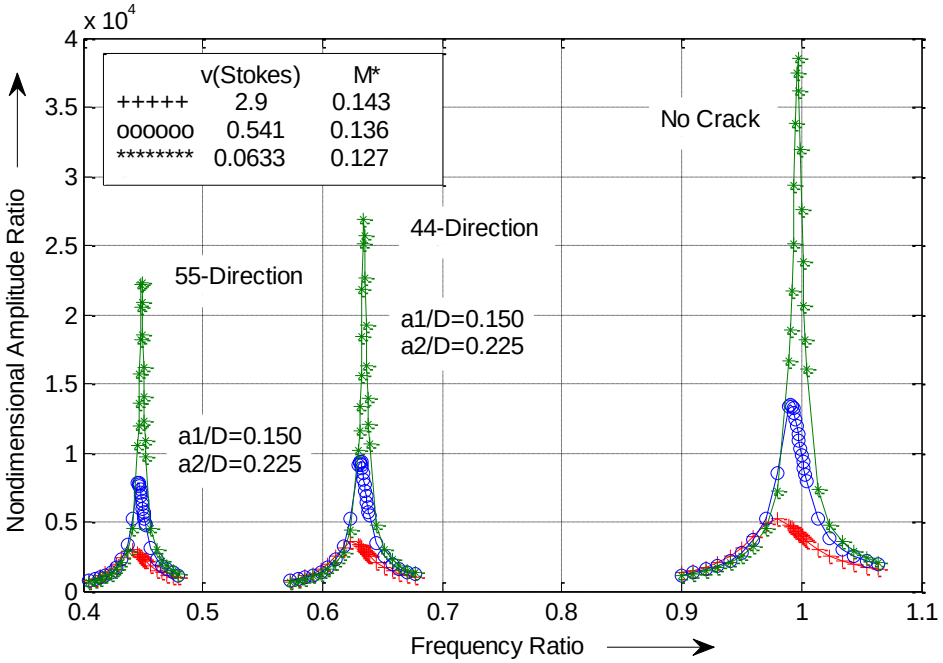

Figure 3.28: Frequency Ratio (ω/ω_0) Vs Non-dimensional Amplitude Ratio (δ^*/ε^*), Mild Steel Rotor R_1=0.01m, L=0.8m, q=12, L_1/L=0.313, L_2/L=0.563, R_D = 0.055m, T_D= 0.020m, M_D = 1.0kg.

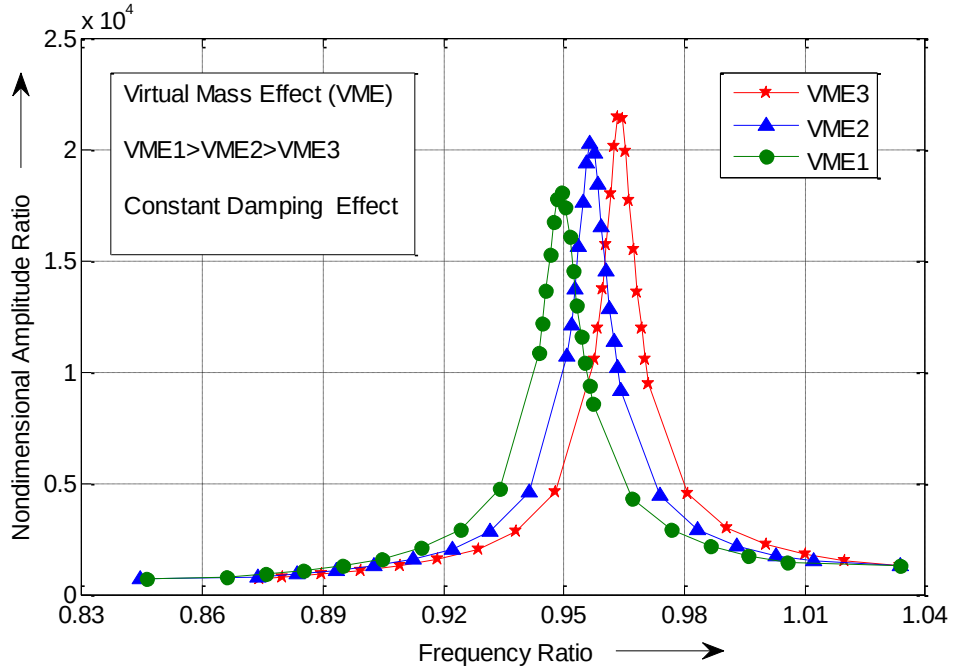

Figure 3.29: Frequency Ratio (ω/ω_0) Vs Non-dimensional Amplitude Ratio (δ^*/ε^*), Mild Steel Rotor R_1=0.01m, L=0.8m, q=12, a1/D=0.125, a2/D=0.150, L_1/L=0.313, L_2/L=0.563, ν=0.541Stokes, M*=0.136, R_D=0.055m, T_D=0.020m, M_D=1.0kg.

3.3 Eavaluation and Comparison of Experimental and Theoretical Analysis Results of the Cantilever Rotor System

The rotating multiple cracked cantilever rotor partially submerged in the viscous medium has been considered in analysis for evaluation of vibration response. The numbers of experiments have been conducted on mild steel rotor in three different viscous fluids with different relative crack depths and relative crack locations for measuring the corresponding relative natural frequencies and relative amplitude of vibration. Figure 3.30 illustrates the schematic block diagram of experimental setup.

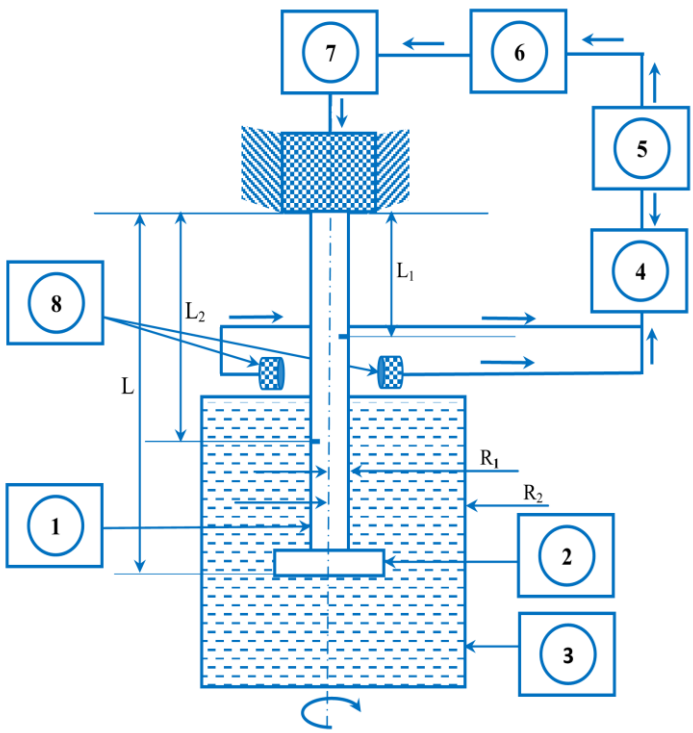

1. Cracked Cantilever Rotor
2. Disk
3. Fluid filled container
4. Arduino Micro-controller for recorded the amplitude in the computer system
5. Power supply
6. Variac
7. Power motor
8. 3-Ultrasonic Sensors.

Figure 3.30: Schematic block diagram representation of experimental set up

The performance of the theoretical model has been verified by experimental test, performed on the rotating cracked cantilever rotor with attached disk at free end submerged in the viscous medium. The results derived from theoretical and experimental observation are displayed in graphical form with changed viscosity of fluid, radius of the container and relative crack location and relative crack depth in both transverse direction (i.e. 44-direction and 55-direction) in the Figure 3.31 to 3.41 for non-cracked and multi

cracked cantilever rotor partially submerged in viscous medium. Figure 3.31 and 3.32 shows the comparison of theoretical and experimental result for effect of change in viscosity of fluid on the non-cracked and cracked cantilever rotor partially submerged in the viscous medium respectively.

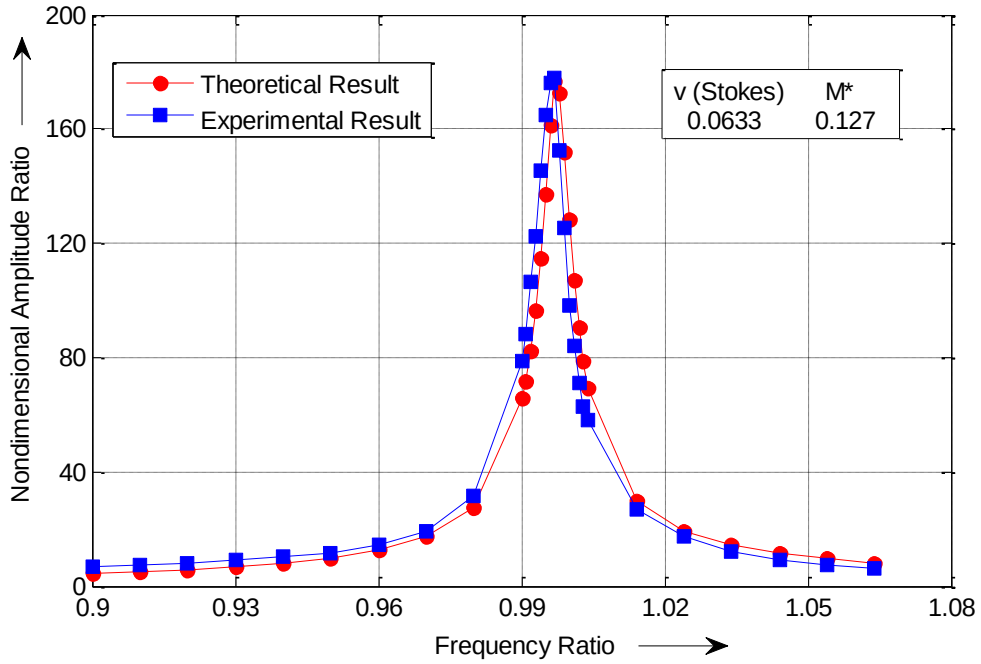

Figure 3.31: Frequency Ratio (ω/ω_0) Vs Non-dimensional Amplitude Ratio (δ^*/ε^*), Mild Steel Rotor R_1=0.01m, L=0.8m, q=12, R_D=0.055m, T_D=0.020m, M_D =1.0kg. for non-cracked rotor.

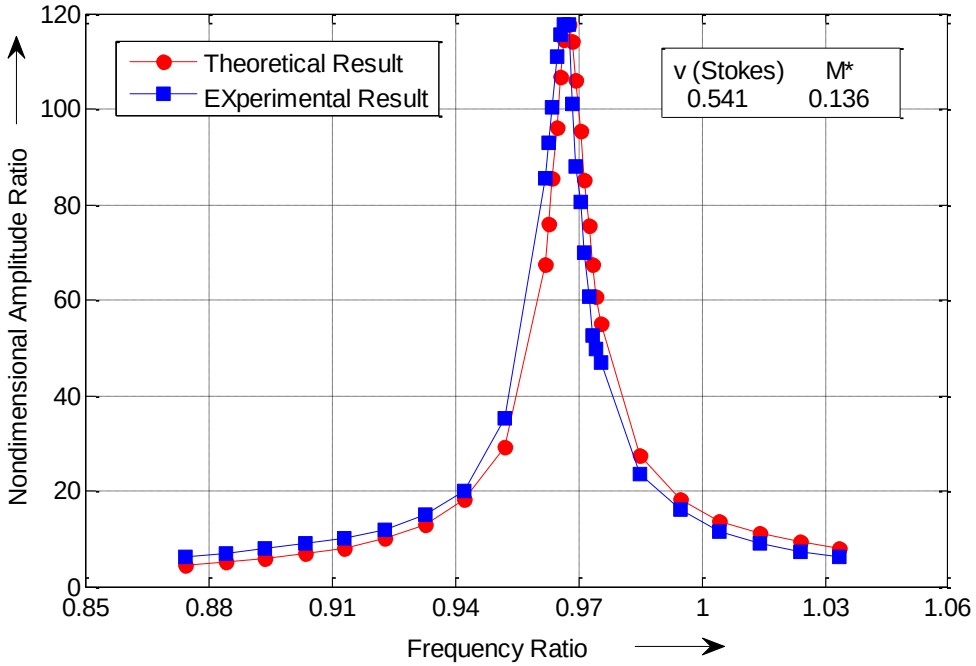

Figure 3.32: Frequency Ratio (ω/ω_0) Vs Non-dimensional Amplitude Ratio (δ^*/ε^*), Mild Steel Rotor R_1=0.01m, L=0.8m, q=12, R_D= 0.0.55m, T_D= 0.020m, M_D = 1.0kg, For non-crack rotor .

Figure 3.33 and 3.34 illustrate the comparison of theoretical and experimental result for effect of change in radius of fluid filled container on the un-crack and cracked rotor respectively.

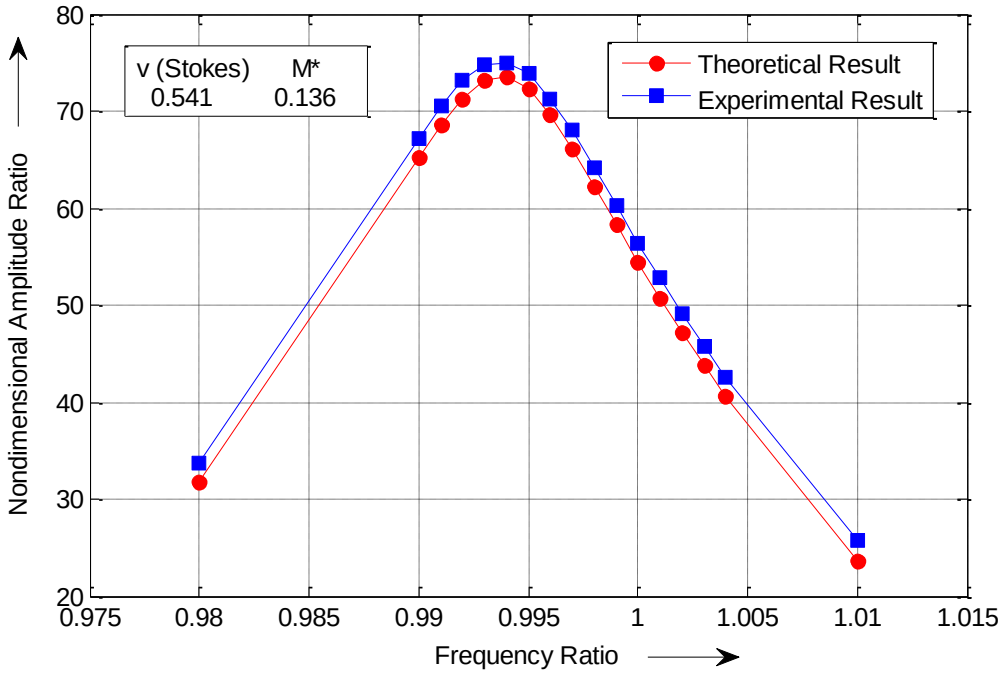

Figure 3.33: Frequency Ratio (ω/ω_0) Vs Non-dimensional Amplitude Ratio (δ^*/ε^*), Mild Steel Rotor R_1=0.01m, L=0.8m, q=12, R_D=0.55m,T_D=0.020m, M_D = 1.0kg for non-cracked rotor.

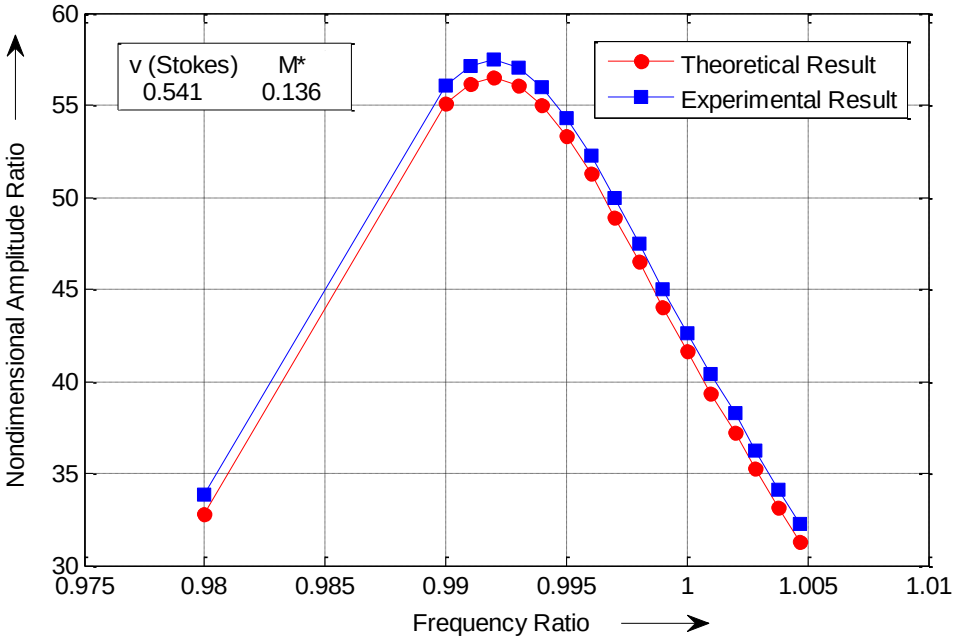

Figure 3.34: Frequency Ratio (ω/ω_0) Vs Non-dimensional Amplitude Ratio (δ^*/ε^*), Mild Steel Rotor R_1=0.01m, L=0.8m, q=12, a1/D= 0.125, a2/D=0.150, L_1/L= 0.313, L_2/L=0.563 R_D = 0.055m,T_D= 0.020m, M_D = 1.0kg for 44-Direction.

Figure 3.35 demonstrate the comparison of theoretical and experimental result for virtual mass effect on the un-cracked and cracked cantilever rotor partially submerged in the viscous medium.

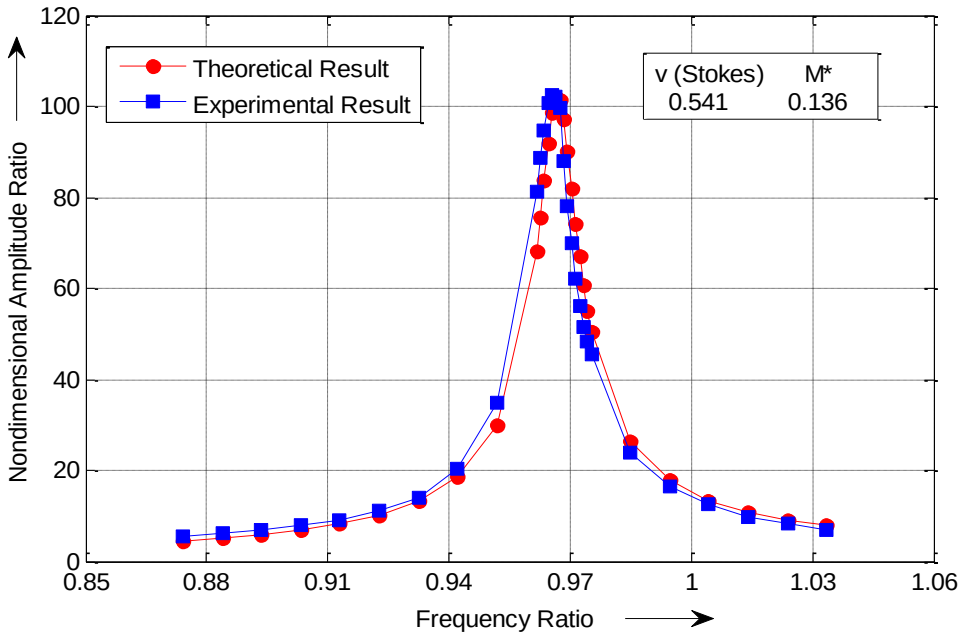

Figure 3.35: Frequency Ratio (ω/ω_0) Vs Non-dimensional Amplitude Ratio (δ^*/ε^*), Mild Steel Rotor R_1=0.01m, L=0.8m, q=12, a1/D= 0.125, a2/D=0.150, L_1/L= 0.313, L_2/L=0.563, R_D = 0.055m, T_D= 0.020m, M_D = 1.0kg.

Figure 3.36, 3.37, and 3.38 shows the comparison of theoretical and experimental result for the effect of different multiple cracks in crack location at transverse crack direction (i.e. 44-direction) of cantilever rotor which rotated in the same viscous medium.

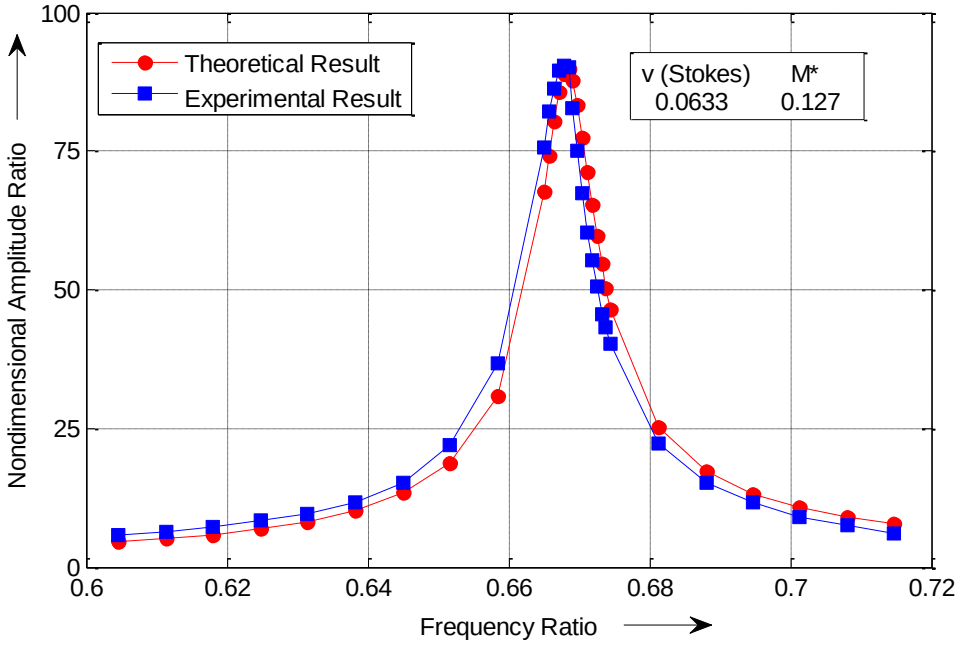

Figure 3.36: Frequency Ratio (ω/ω_0) Vs Non-dimensional Amplitude Ratio (δ^*/ε^*), Mild Steel Rotor R_1=0.01m, L=0.8m, q=12, a1/D=0.250, a2/D=0.225, L_1/L=0.313, L_2/L=0.563, R_D=0.055m, T_D=0.020m, M_D=1.0kg for 44- Direction.

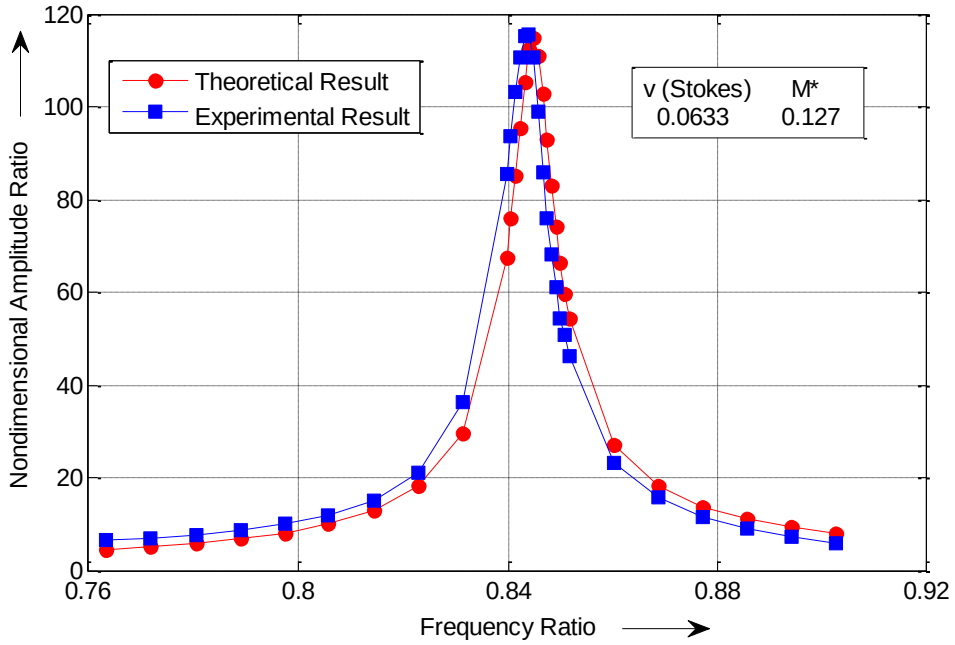

Figure 3.37: Frequency Ratio (ω/ω_0) Vs Non-dimensional Amplitude Ratio (δ^*/ε^*), Mild Steel Rotor R_1=0.01m, L=0.8m, q =12,a1/D=0.225,a2/D=0.150, L_1/L=0.313, L_2/L=0.563, R_D=0.055m, T_D=0.020m, M_D =1.0kg for 44- Direction.

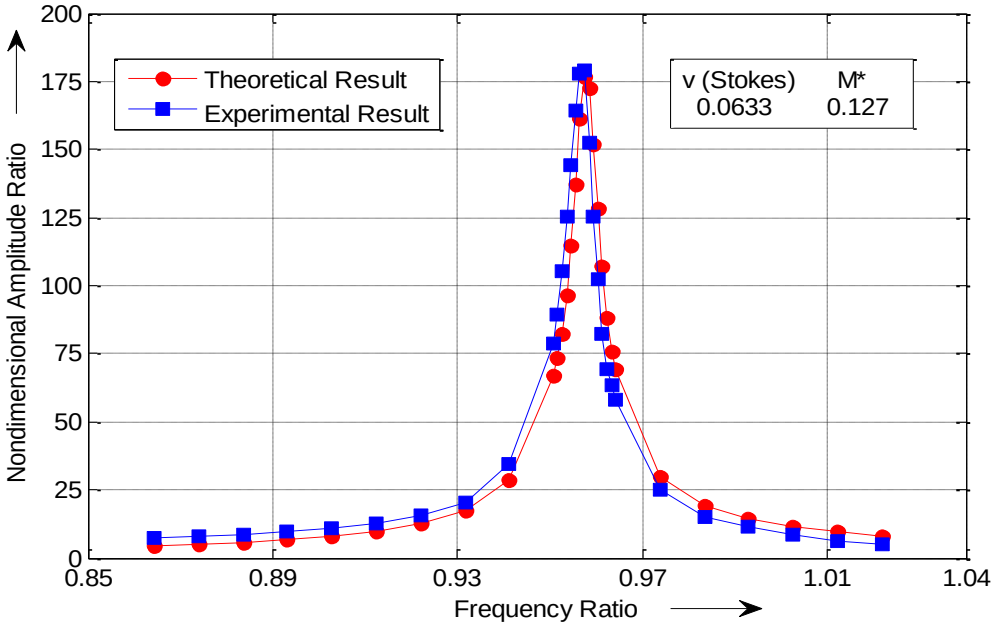

Figure 3.38: Frequency Ratio (ω/ω_0) Vs Non-dimensional Amplitude Ratio (δ^*/ε^*), Mild Steel Rotor R_1=0.01m, L=0.8m, q=12, a1/D=0.150, a2/D=0.125, L_1/L=0.313, L_2/L=0.563, R_D=0.055m, T_D=0.020m, M_D=1.0kg for 44- Direction.

Figure 3.39, 3.40, and 3.41 shows the comparison of theoretical and experimental result for the effect of different multiple cracks in crack location at transverse crack direction (i.e. 55-direction) of cantilever rotor which rotated in the same viscous medium. As can be seen, the results obtained using the theoretically show well agreement with the experimental results.

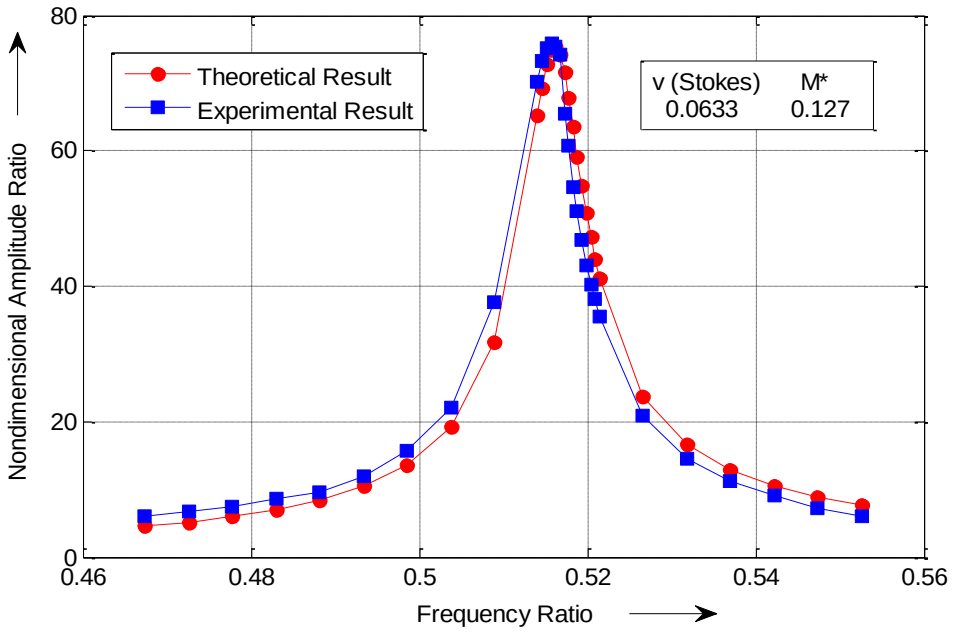

Figure 3.39: Frequency Ratio (ω/ω_0) Vs Non-dimensional Amplitude Ratio (δ^*/ε^*), Mild Steel Rotor R_1=0.01m, L=0.8m, q=12, a1/D=0.250, a2/D=0.225, L_1/L=0.313, L_2/L=0.563, R_D=0.055m, T_D= 0.020m, M_D=1.0kg for 55- Direction.

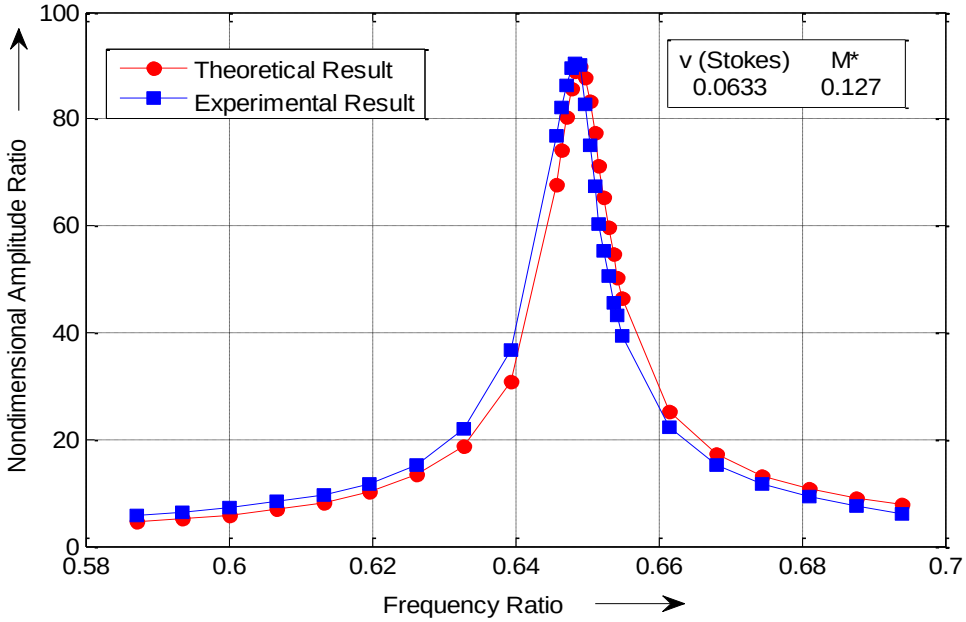

Figure 3.40: Frequency Ratio (ω/ω_0) Vs Non-dimensional Amplitude Ratio (δ^*/ε^*), Mild Steel Rotor R_1=0.01m, L=0.8m, q =12, a1/D=0.225, a2/D=0.150, L_1/L=0.313, L_2/L=0.563, R_D=0.055m, T_D=0.020m, M_D = 1.0kg for 55- Direction.

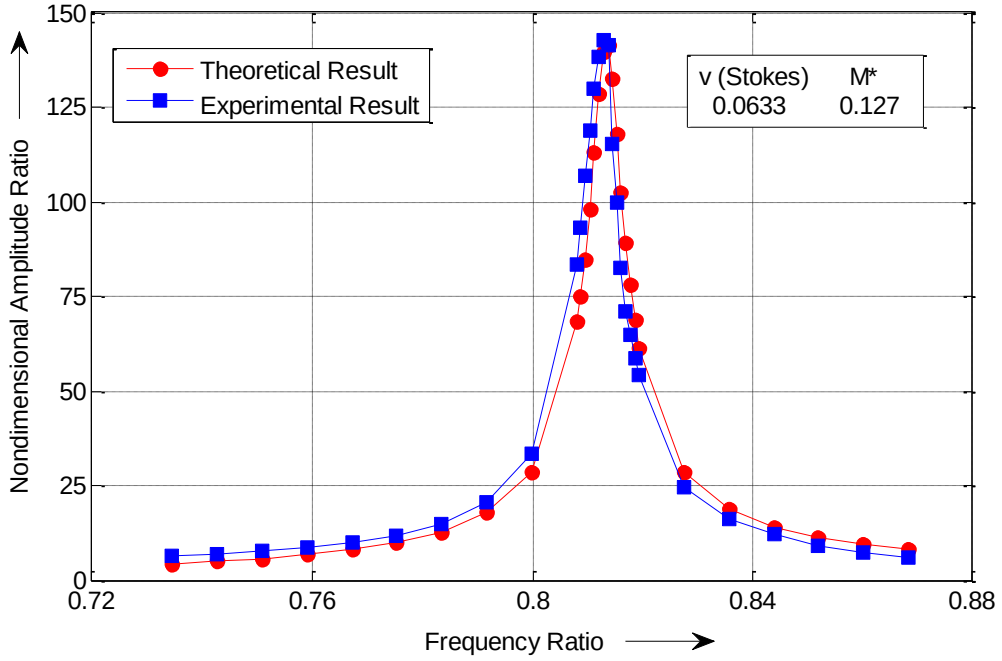

Figure 3.41: Frequency Ratio (ω/ω_0) Vs Non-dimensional Amplitude Ratio (δ^*/ε^*), Mild Steel Rotor R_1=0.01m, L=0.8m, q=12, a1/D=0.150, a2/D=0.125, L_1/L=0.313, L_2/L=0.563, R_D=0.055m, T_D=0.020m, M_D =1.0kg for 55-Direction.

3.4 Comparision and Authentication of Theoretical and Experimental Analysis Results

The fidelity and performance of the theoretical model has been verified by experimental test, performed on the rotating cracked cantilever rotor with attached disk at free end submerged in the viscous medium. The results obtained from theoretical and experimental analysis are compared for multiple cracked cantilever rotor in viscous medium is shown in Figures 3.31 to 3.41. The theoretical analysis results and experimental investigation results are compared in this section, only three results (i.e. Maximum amplitude ratio value) taken from the available data is represented in Tables 3.3 to 3.8 for cracked cantilever rotor. The relative natural frequency and relative amplitude of vibration employed in the investigation can be defined as;

$$\text{Relative natural frequency}(\omega/\omega_0) = \frac{\text{Rotating speed of cracked rotor}}{\text{Fundamental Natural frequency of non-cracked rotor}}$$

$$\text{Relative Amplitude } (\delta^*/\varepsilon^*) = \frac{\text{Whirling radius of rotor}}{\text{Eccentricity of rotor shaft}}$$

Table 3.3 shows the comparison of theoretical and experimental result for effect of change in viscosity of fluid on the non-cracked cantilever rotor.

Table 3.3: Comparison between numerical and experimental results for effect of different viscous medium

Sl. No.	Viscosity of fluid (ν) in Stokes	Theoretical analysis (Non-dimensional Amplitude (δ*/ε*))	Experimental Analysis (Non-dimensional Amplitude (δ*/ε*))	Error in Percentage (%)
1	0.0633	176.920	186.19	4.97
2	0.5410	58.947	61.792	4.60
3	2.9000	20.533	21.491	4.45

Tables 3.4 and 3.5 demonstrate the comparison of theoretical and experimental result for virtual mass effect on the un-cracked and cracked cantilever rotor partially submerged in the viscous medium respectively.

Table 3.4: Comparison between theoretical and experimental results for ν=0.541stokes & M*=0.136, for virtual mass effect (non-cracked rotor)

Sl. No.	Mass of disc (M_D) in kg	Theoretical analysis (Non-dimensional Amplitude (δ*/ε*))	Experimental Analysis (Non-dimensional Amplitude (δ*/ε*))	Error in Percentage (%)
1	1.00	117.583	123.40	4.71
2	0.75	102.032	107.34	4.94
3	0.50	75.46	79.044	4.53

Table 3.5: Comparison between theoretical and experimental results for ν=0.541 stokes, M*=0.0.136, L_1/L=0.313,L_2/L=0.563, a1/D=0.125, a2/D=0.150, for virtual mass effect.

Sl. No.	Mass of disc(M_D) kg	Theoretical analysis (Non-dimensional Amplitude (δ*/ε*))	Experimental Analysis (Non-dimensional Amplitude (δ*/ε*))	Error in Percentage (%)
1	1.00	103.03	107.92	4.53
2	0.75	91.218	96.144	5.12
3	0.50	75.463	79.195	4.71

Tables 3.6 and 3.7 illustrate the comparison of theoretical and experimental result for effect of change in radius of fluid filled container on the uncrack and cracked rotor respectively.

Table 3.6: Comparison between theoretical and experimental results for v=0.541stokes, M*=0.136, for non-Cracked rotor.

Sl. No.	Gap Ratio (q)	Theoretical analysis (Non-dimensional Amplitude (δ*/ε*))	Experimental Analysis (Non-dimensional Amplitude (δ*/ε*))	Error in Percentage (%)
1	q1	42.5346	44.286	3.95
2	q2	66.999	70.576	5.06
3	q3	73.582	76.790	4.17
4	q4	78.069	80.910	3.51

Table 3.7: Comparison between theoretical and experimental results for crack position L_1/L = 0.313, L_2/L=0.563, a1/D= 0.125, a2/D=0.150, v=0.541stokes, M*=0.136, for 44-Direction.

Sl. No.	Gap Ratio(q)	Theoretical analysis (Non-dimensional Amplitude (δ*/ε*))	Experimental Analysis (Non-dimensional Amplitude (δ*/ε*))	Error in Percentage (%)
1	4	32.9397	34.625	4.86
2	8	51.7353	54.151	4.46
3	12	56.4638	58.924	4.17
4	20	60.9867	63.815	4.43

Table 3.8 shows the comparison of theoretical and experimental result for the effect of multiple cracks in crack location at both transverse crack direction (i.e. 44-direction and 55-direction) of cantilever rotor which rotated in the different viscous medium. As can be

seen, the results obtained using the theoretically show well agreement with the experimental results.

Table 3.8: Comparison between theoretical and experimental results for crack position $L_1/L = 0.313$, $L_2/L=0.563$.

	Relative crack depth(β)	44-Direction			55-Direction		
		Viscosity of fluid (ν) Stokes			Viscosity of fluid (ν) Stokes		
		0.0633	0.541	2.9	0.0633	0.541	2.9
Theoretical Analysis (Non-dimensional Amplitude (δ*/ε*))	β_1=0.250 β_2=0.225	89.791	29.073	10.528	75.463	24.521	8.855
	β_1=0.225 β_2=0.150	110.98	37.943	13.535	89.791	29.073	10.528
	β_1=0.150 β_2=0.225	176.92	58.947	20.531	141.24	46.105	15.561
Experimental Analysis (Non-dimensional Amplitude (δ*/ε*))	β_1=0.250 β_2=0.225	94.127	30.224	10.978	78.496	25.533	9.303
	β_1=0.225 β_2=0.150	116.79	39.749	14.148	94.083	30.648	11.009
	β_1=0.150 β_2=0.225	185.07	61.297	21.594	148.18	48.258	16.172
Error in Percentage (%)	β_1=0.250 β_2=0.225	4.46	3.80	4.09	3.48	3.96	4.81
	β_1=0.225 β_2=0.150	4.97	4.54	4.33	4.56	5.13	4.36
	β_1=0.150 β_2=0.225	4.40	3.83	4.92	4.68	4.46	3.77

3.5 Discussion

This section is subjected to discussion on analysis of results derived during the theoretical and experimental evaluation.This chapter presents the theoretical analysis of cantilever rotor with multiple transverse crack which partially submerged in the viscous medium then its experimental validation. Figure 3.30 presents schematic block diagram of experiment setup for the cantilever cracked rotor submerged in the viscous fluid. Comparison and verification of the results derived from theoretical model are plotted with results of experimental examination and are plotted in Figures 3.31 to 3.41.The results derived from theoretical and experimental observation are displayed in tabular form with changed viscosity of fluid, mass of disc, radius of the cantainer and relative crack location and relative crack depth in both transverse direction (i.e. 44-direction and 55-direction) in the Tables 3.3 to 3.8 for non-cracked and multi cracked cantilever rotor partially

submerged in viscous medium.Table 3.3 shows the comparison of theoretical and experimental result for effect of change in viscosity of fluid on the non-cracked cantilever rotor. Tables 3.4 and 3.5 demonstrate the comparison of theoretical and experimental result for virtual mass effect on the un-cracked and cracked cantilever rotor partially submerged in the viscous medium respectively. Tables 3.6 and 3.7 illustrate the comparison of theoretical and experimental result for effect of change in radius of fluid filled container on the uncrack and cracked rotor respectively.Table 3.8 shows the comparison of theoretical and experimental result for the effect of multiple cracks in crack location at both transverse crack direction (i.e. 44-direction and 55-direction) of cantilever rotor which rotated in the different viscous medium. As can be seen, the results obtained using the theoretically show well agreement with the experimental results.

3.6 Summary

The summary is outlined are drawn in this section based on the results derived from theoretical and experimental examination in this chapter. The vibration response (i.e. natural frequencies and amplitude) are changed due to altered viscosity of fluid, mass of disc, radius of fluid filled container and presence of transverse crack in the cantilever rotor.The vibration responses derived from theoretical analysis have been verified with the obtained results of experimental investigation and a close proximity is found. The percentage of error between the theoretical and experimental analysis is found within 5%.The error in the dynamic behavior of the rotor can be used as the factor for diagnosis of the crack. The proposed method can be successfully applied for the design of smart artificial intelligent techniques for online measurement of the crack present in the rotor partially submerged in viscous medium. In the successive chapters various artificial intelligent based techniques have been discussed for identification of multiple cracks present in rotor system.

Chapter 4

Finite Element Analysis of Multiple Cracked Cantilever Rotor Partially Submerged in Fluid Medium for Measurement of Dynamic Response

The presence of cracks in the rotor, beam and structural components is a serious risk to the integrity of the system. This may be because of destruction and collapse of the structures. The detection of the crack in the early stage of the system is beneficial. In the last two decades, many researchers and engineers have developed several methods and presented many models for the prediction of cracks, based on vibrational behaviors of cracked structures. The techniques based on vibration are used for identification of damage; given some benifits over other conventional methodologies. These technique can help to detect crack depth and location using vibrational data, obtained from the cracked structure. The presence of the crack in structures generates flexibility at the vicinity of crack which causes the reduction of natural frequencies and amplitude. Hence it may be possible to detect crack location and intensity by measuring the change in vibration parameters. The current chapter introduces the finite element analysis for detection the multiple cracks in the cantilever rotor partially submerged in the viscous fluid medium. The results of finite element analysis have been compared with the results of theoretical analysis and experimental analysis to secure the consistance of proposed numerical method. Finally it is concluded that proposed finite element method can be successfully applied for identification of multiple crack in structures(i.e. Rotor, beam,plates etc).

4.1 Introduction

Mechanism of damage detection techniques in different engineering system can be characterized as a organized methodology to predict and compute the damage existing in

the system. The concerned of the failure analysis of faulty beam structure is to secure the overall safety and performance of the system. The vibration characteristics of faulty structural members can be effectively used to seize the damage feature such as crack location and crack depth. The researchers have proposed various damage detection methods based on thermal radiation, energy, discreet wavelet and numerical methods such as artificial intelligent and finite element methods. In the past few decades, scientists have developed a model for single crack structure based on the finite element method and found that the enactment of finite element method is enhanced as compared to the theoretical model designed for identification of crack. Hence, this method can be employed to detect the crack parameters such as location and depth of crack in the system using the modal response of the system. In the present section finite element method has been used to find crack locations and depths for multiple cracked composites and structural steel beams. It is found that the presence of cracks in the beam structure potentially affect the dynamic behavior of the beam. The finite element result has been compared to that of theoretical and experimental analysis results and close proximity between the results is found.

4.2 Analysis of Finite Element Method using ANSYS

The finite element method is a powerful finite element method that can be used to solve the complex problem using interpolation or approximation method. The finite element method is a systematic approach for solving the complicated problems. So the finite element method can be applied in vibrating structures with different boundary conditions to get the exact solution. In the finite element analysis, the whole structure is first divided into small parts in various shapes. These small parts known as elements and method employed to split the structures in small parts is called discretization and generation of the regular shape pattern in the structure are called meshing. The efficiency of finite element method is dependent on the quality of the mesh. Convergence test is considered for choosing the appropriate size of mesh element. Each element of finite element model has corner points that connect to another element called nodes. Each finite element associated with the equation of motion and that can be easily interpolated. The solutions of each finite element are combined to get global mass and stiffness matrices, which describes the vibration response of the structure. The global mass and stiffness matrices can be analyzed to get vibrational parameters of the structure. The finite element analysis of cantilever

beam has been done using ANSYS software. ANSYS is commercially available finite element analysis software with capacity of solving wide range of complex problems. The application of ANSYS is spread over many fields of engineering and technology such as structural, thermal, mechanical, electromagnetic and computational fluid dynamics. The modelling and simulation of mild steel cantilever rotor submerged in the viscous medium has been done in ANSYS using multi-physics platform. The natural frequencies and relevant amplitude at both transverse direction (i.e. 44 and 55-axis) have been extracted from block lanczos. ANSYS involves the following steps in order to solve the problem:

(1) Preprocessing Phase: This section of the ANSYS involves the selection of type of the element with respect to problem types. The ANSYS also provides the CAD modelling facility. Meshing process is the most important feature of FE analysis. Convergence test is conducted to evaluate the suitable size of mesh element.

(2) Solution Phase: Applying the boundary conditions and load on the structural component are the most significant feature of this section. ANSYS then attempts to solve the equation of motion of the system element. The block lanczos method is taken in the present investigation.

(3) Post processing phase: This section allows the review of the results. The post processing is most significant tool for viewing the results after the solution phase. These results may be in form of color contour plot and graphical representation of the stress, thermal, buckling, electromagnetic, vibration and computation fluid dynamics analysis etc.

4.3 Analysis of Finite Element Analysis of Rotor with Transverse Cracks Partially Submerged in the Viscous Fluid

The finite element analysis is performed for studying the modal response of a rotating cracked rotor.The natural frequencies and amplitude are the most important parameters in designing a structure under the dynamic and complex loading conditions. The finite element analysis is performed using the ANSYS software in the frequency domain to find change in behaviors of vibration parameters. The presence of damage in the form of crack and different viscous fluid medium parameters alters the vibration indices. The change in

behavior of vibration characteristics can be applied to develop the structural health monitoring techniques.

4.3.1 Description of SOLID187 Element used for Solid Rotor

The selection of elements is important in the ANSYS. A higher order 3-D, 10 node element (Specified as SOLID187 in ANSYS) with three degree of freedom at each node: translation in the nodal x, y, and z directions are selected and used throughout the analysis. The SOLID187 has plasticity, hyper-plasticity, creep, stress stiffening, large deflection, and large strain capabilities.it also has mixed formulation capabilities for simulating deformations of nearly incompressible elastoplastic materials, and fully incompressible hyperplastic materials. The geometry, node locations, and the coordinate system for the element are shown in Figure 4.1.

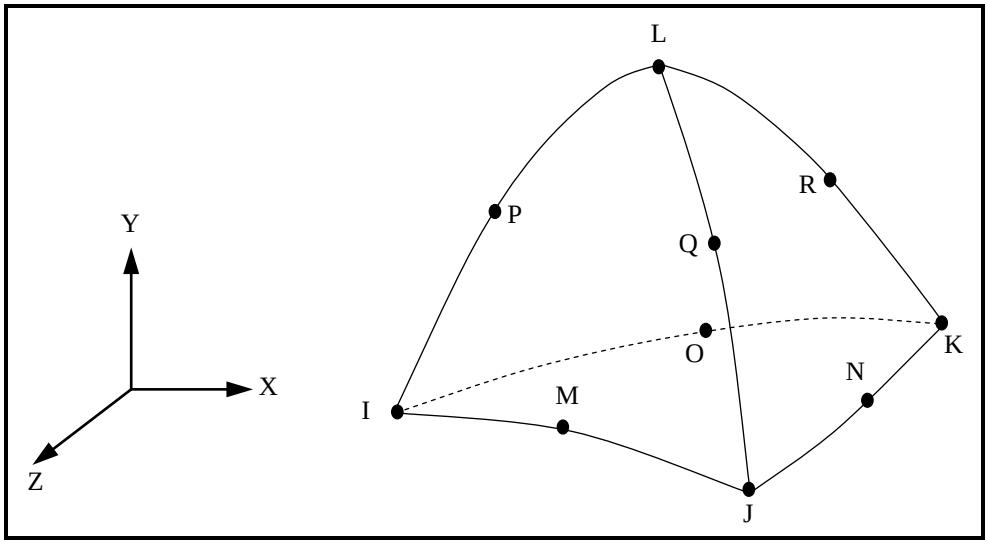

Figure 4.1: Geometry of SOLID187 element.

Assumptions and Restrictions

- The element must not have a zero volume.
- Elements may be numbered either as shown in Figure 4.1or may have node L below the I, J, K plane.
- An edge with a removed mid side node implies that the displacement varies linearly, rather than parabolically, along that edge.

- When mixed formulation is used (KEYOPT (6) = 1 or 2), no mid side nodes can be missed.
- If you use the mixed formulation (KEYOPT (6) = 1 or 2), the damped eigen solver is not supported. You must use the sparse solver (default).
- Stress stiffening is always included in geometrically nonlinear analysis.

4.3.2 Description of FLUID30 Element used for Fluid Medium

FLUID30 is used for modeling the fluid medium and the interface in fluid/structure interaction problems. Typical applications include sound wave propagation and submerged structural dynamics. The governing equation of acoustics, namely the 3-D wave equation, has been discretized taking into account the coupling of acoustic pressure and structural motion at the Interface. The element has 8-corner nodes with four degree of freedom per node: translations in the x, y and z directions and pressure. The translation, however, are applicable only at nodes that are on the interface. The element has the capability to include damping of sound absorbing material at the interface. The element can be used with other 3-D structural elements to perform unsymmetric or damped modal, full harmonic response and full transient method analysis. When there is no structural motion, the element is also applicable to static, modal and reduced harmonic response analysis.

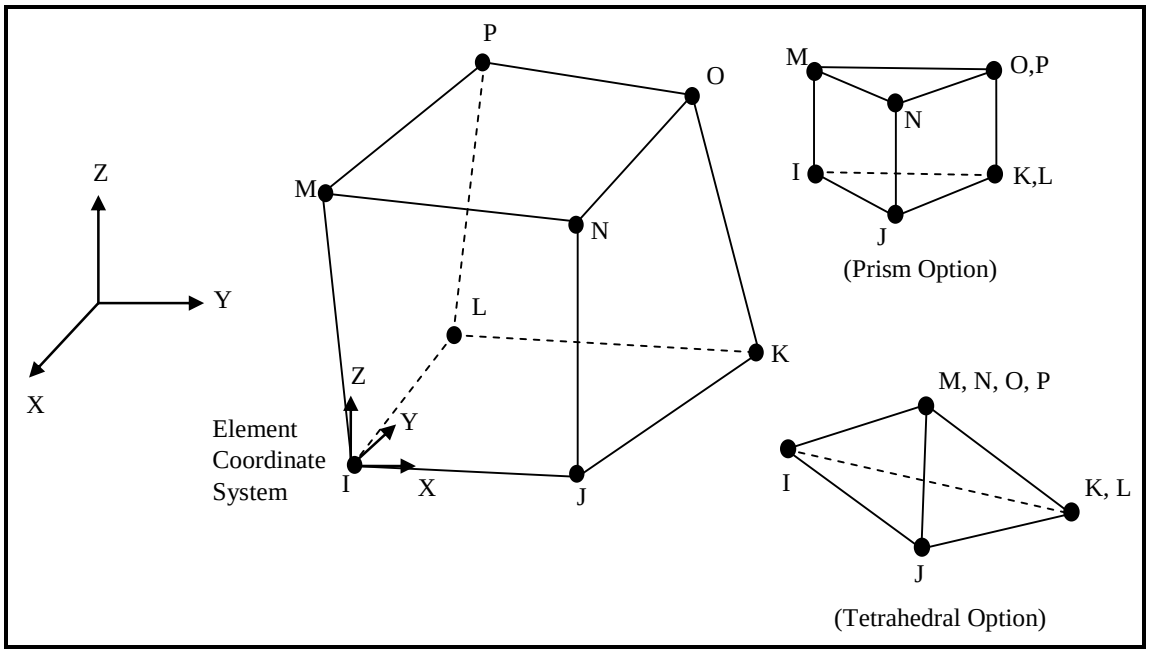

Figure 4.2: Geometry of FLUID30 (3-D acoustic fluid) element.

Assumptions and Restrictions

The element must not have a zero volume. Element nodes may be numbered either as shown in Figure 4.2 or may have planes IJKL and MNOP interchanged. Also, the element may not be twisted such that it has two separate volumes. This occurs usually when the element nodes are not in the correct sequence. All elements must have 8 nodes. A prism-shaped element may be formed by defining duplicate K and L and duplicate O and P nodes. A tetrahedron shape is also available. The acoustic pressure in the fluid medium is determined by the wave equation with the following assumptions:

- The fluid is compressible (density changes due to pressure variations).
- Inviscid fluid (no dissipative effect due to viscosity).
- There is no mean flow of the fluid.
- The mean density and pressure are uniform throughout the fluid. Note that the acoustic pressure is the excess pressure from the mean pressure.
- Analyses are limited to relatively small acoustic pressures so that the changes in density are small compared with the mean density.

The lumped mass matrix formulation is not allowed for this element.

4.3.3 Material Properties and boundary condition of Rotor and Viscous Fluid Medium

The following dimensions of the rotor are used in the current section:

Length of the rotor (L) = 800mm; radius of the rotor (R_1) = 10mm; Thickness of the disc T_{D1}=0.01m; T_{D2}=0.015m; T_{D3}=0.020m.

The material properties of the mild steel cantilever rotor used in the analysis are shown in the Table 4.1.

Table 4.1: Material properties of mild steel rotor.

Young's Modulus (E)	200Gpa
Poisson ratio's (ν)	0.3
Density (ρ)	7850 kg/m^3

The required material properties for the fluid elements were bulk modulus (K), density (ρ) and viscosity (ν) are shown in Table 4.2.The actual fluid properties used in the FE analysis depend on the type of fluid to be simulated.

Table 4.2: Physical properties of viscous fluid medium (for water).

Bulk Modulus (E)	2.05GPa
Viscosity (v)	0.01poise
Density (ρ)	1000 kg/m^3

Cantilever rotor has fixed at both x and y direction (X=0,Y=0) and rotated at z direction those are parallel direction of axis of rotor. Rotor speed has been set between the ranges of 300 to 700 rpm. Fluid container is fixed in all direction(X=0,Y=0 and Z=0) from the bottom side. Mesh size has been chosen on the basis of conversion test. Mesh size is 4710.

The natural frequency and amplitude for cracked rotor derived from finite element based finite element analysis are plotted along with theoretical and experimental analysis results of cracked cantilever rotor with viscous medium and the orientation of cracks (β_1=0.125, β_2=0.175, β_3=0.225 and β_4=0.275) is shown in the Figures 4.3 to 4.13.

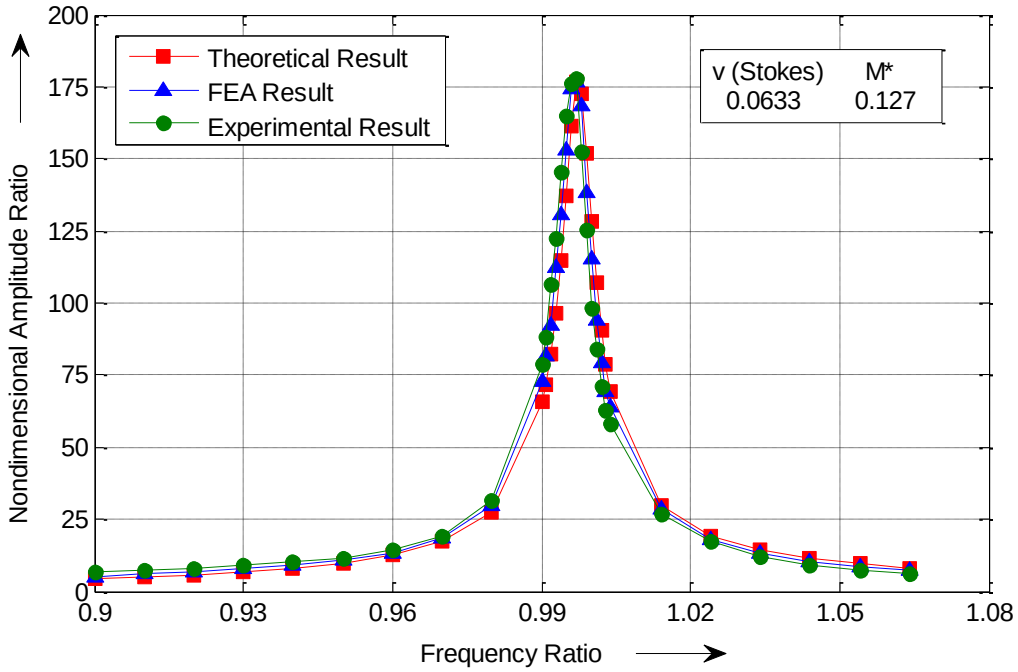

Figure 4.3: Frequency Ratio (ω/ω_0) Vs Non-dimensional Amplitude Ratio (δ^*/ε^*), Mild Steel Rotor R_1=0.01m, L=0.8m, q =12, R_D = 0.055m, T_D= 0.020m, M_D = 1.0kg .

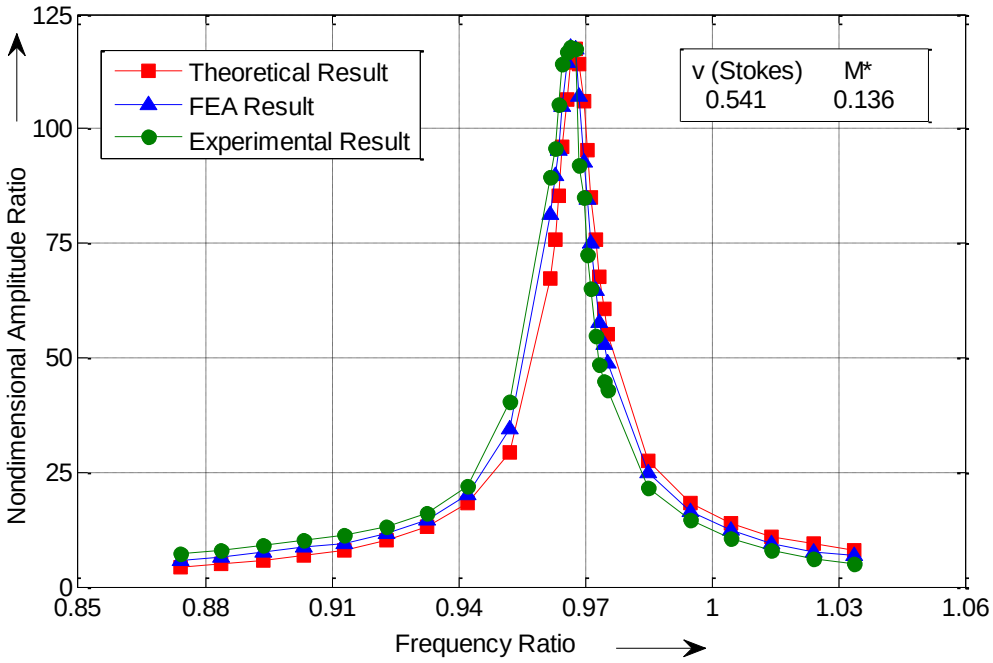

Figure 4.4: Frequency Ratio (ω/ω_0) Vs Non-dimensional Amplitude Ratio (δ^*/ε^*), Mild Steel Rotor R_1=0.01m, L=0.8m, q=12, R_D=0.055m,T_D=0.020m, M_D = 1.0kg, for virtual mass effect.

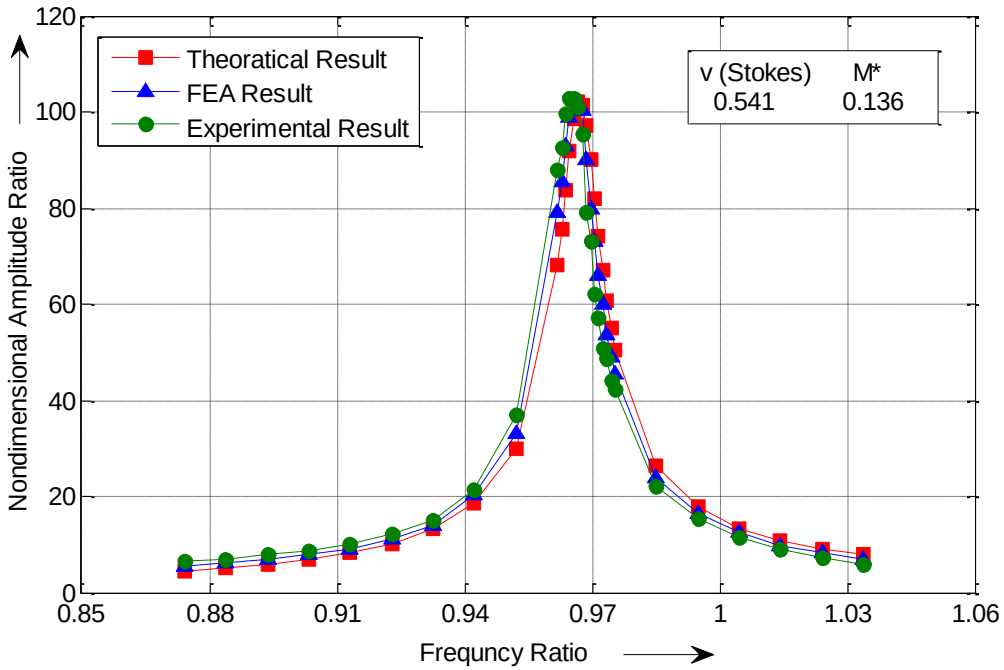

Figure 4.5: Frequency Ratio ($\omega/\ \omega_0$) Vs Non-dimensional Amplitude Ratio (δ^*/ε^*), Mild Steel Rotor R_1=0.01m, L=0.8m, q=12, a1/D=0.125, a2/D=0.150, L_1/L=0.313, L_2/L=0.563, R_D=0.055m, T_D=0.020m, M_D=1.0kg, for virtual mass effect.

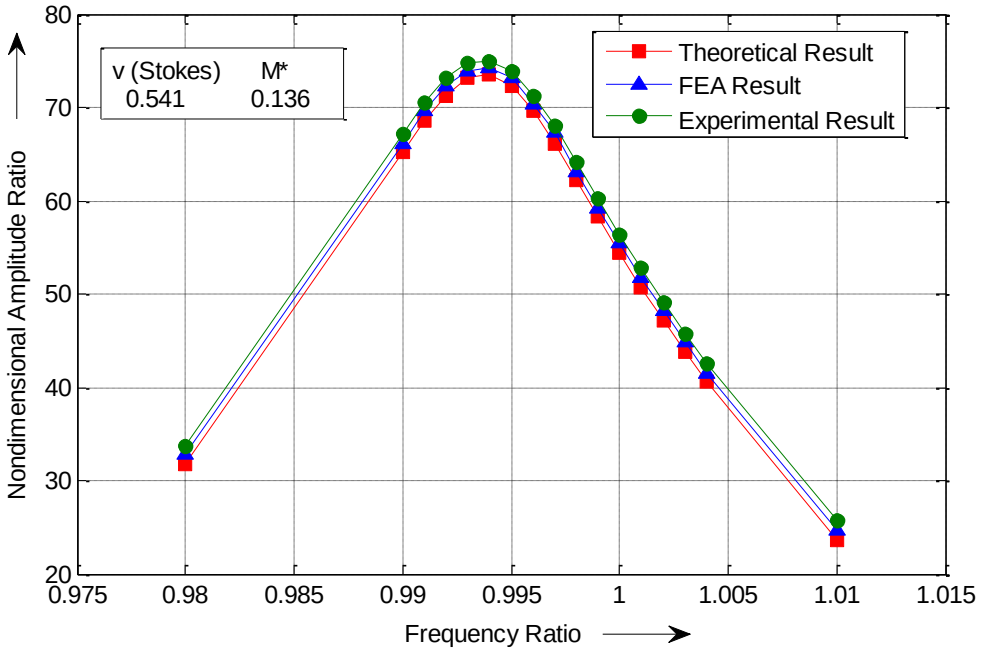

Figure 4.6: Frequency Ratio (ω/ω_0) Vs Non-dimensional Amplitude Ratio (δ^*/ε^*), Mild Steel Rotor R_1=0.01m, L=0.8m, q=12, R_D=0.055m,T_D=0.020m, M_D=1.0kg, for gap ratio effect.

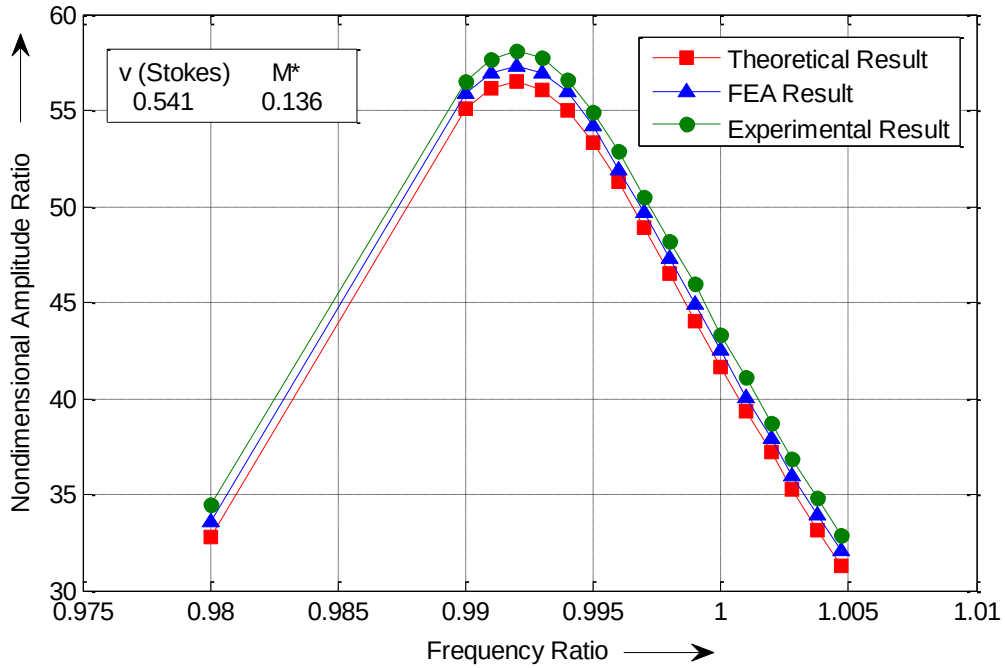

Figure 4.7: Frequency Ratio (ω/ω_0) Vs Non-dimensional Amplitude Ratio (δ^*/ε^*), Mild Steel Rotor R_1=0.01m, L=0.8m, q=12, a1/D=0.125, a2/D=0.150, L_1/L=0.313, L_2/L=0.563, R_D=0.055m,T_D=0.020m, M_D = 1.0kg, for 44-Direction.

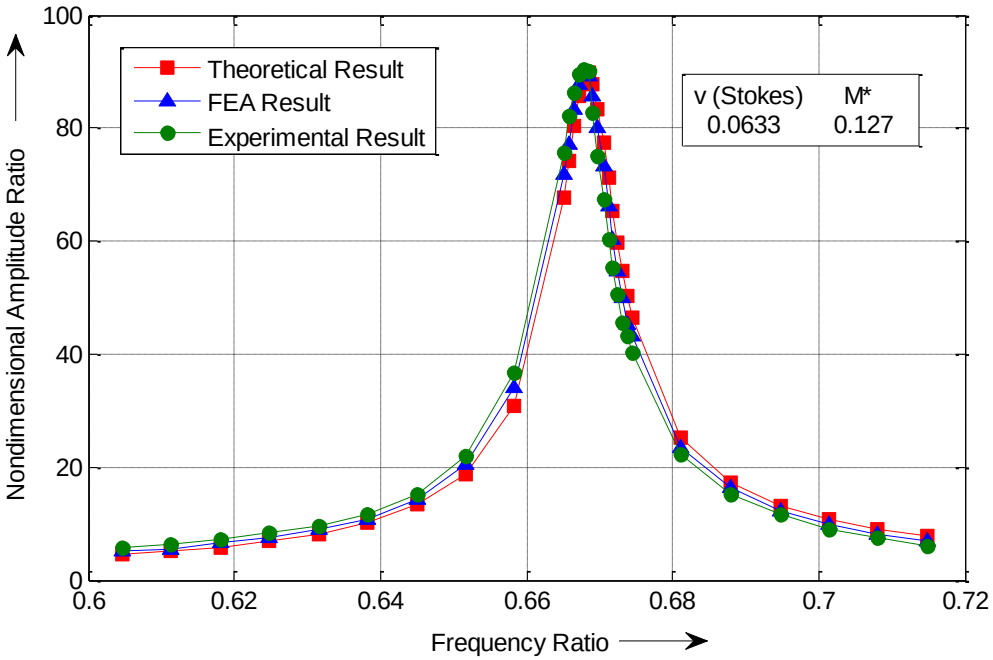

Figure 4.8: Frequency Ratio (ω/ω_0) Vs Non-dimensional Amplitude Ratio (δ^*/ε^*), Mild Steel Rotor R_1=0.01m, L=0.8m, q=12,a1/D=0.250, a1/D=0.225, L_1/L=0.313, L_2/L=0.563, R_D=0.055m, T_D=0.020m, M_D=1.0kg, for 44- Direction.

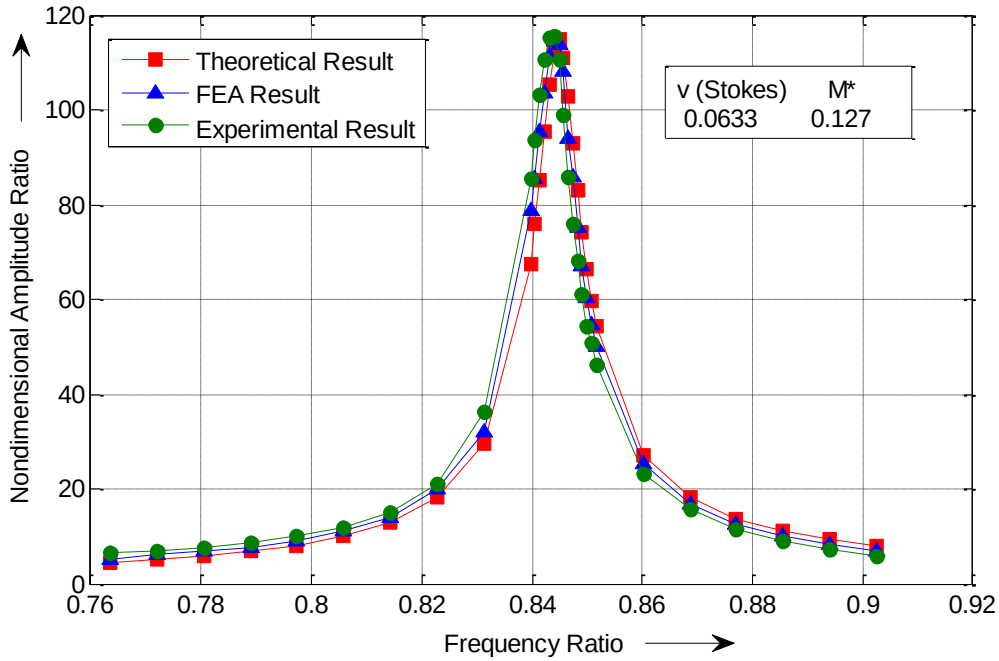

Figure 4.9: Frequency Ratio (ω/ω_0) Vs Non-dimensional Amplitude Ratio (δ^*/ε^*), Mild Steel Rotor R_1=0.01m, L=0.8m, q=12, a1/D=0.225, a1/D=0.150, L_1/L=0.313, L_2/L=0.563, R_D =0.055m, T_D=0.020m, M_D=1.0kg, for 44- Direction.

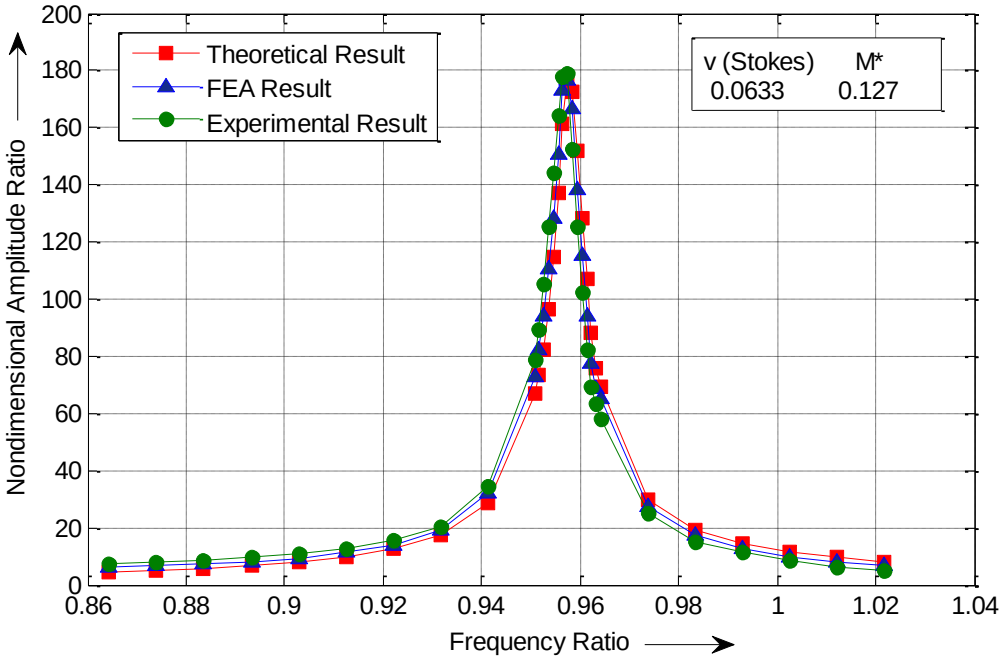

Figure 4.10: Frequency Ratio (ω/ω0) Vs Non-dimensional Amplitude Ratio (δ*/ε*), Mild Steel Rotor R_1=0.01m, L=0.8m, q=12,a1/D=0.150,a1/D=0.125, L_1/L=0.313, L_2/L=0.563, R_D=0.055m, T_D=0.020m, M_D =1.0kg, for 44- Direction.

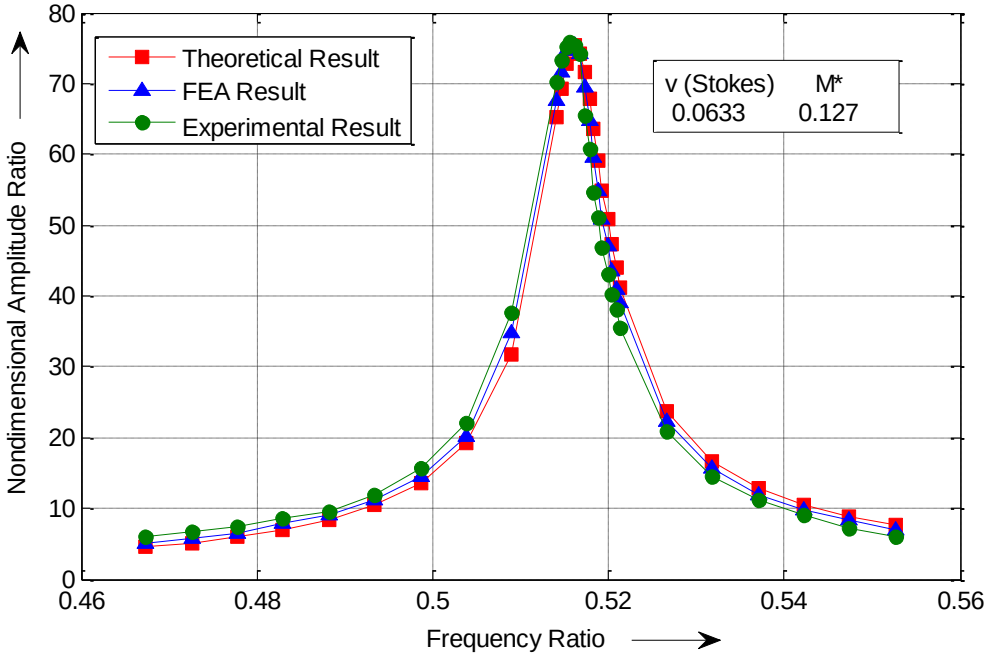

Figure 4.11: Frequency Ratio (ω/ω_0) Vs Non-dimensional Amplitude Ratio (δ*/ε*), Mild Steel rator R_1=0.01m, L=0.8m, q=12, a1/D=0.250, a1/D=0.225, L_1/L = 0.313, L_2/L=0.563, R_D=0.055m, T_D=0.020m, M_D=1.0kg, for 55- Direction.

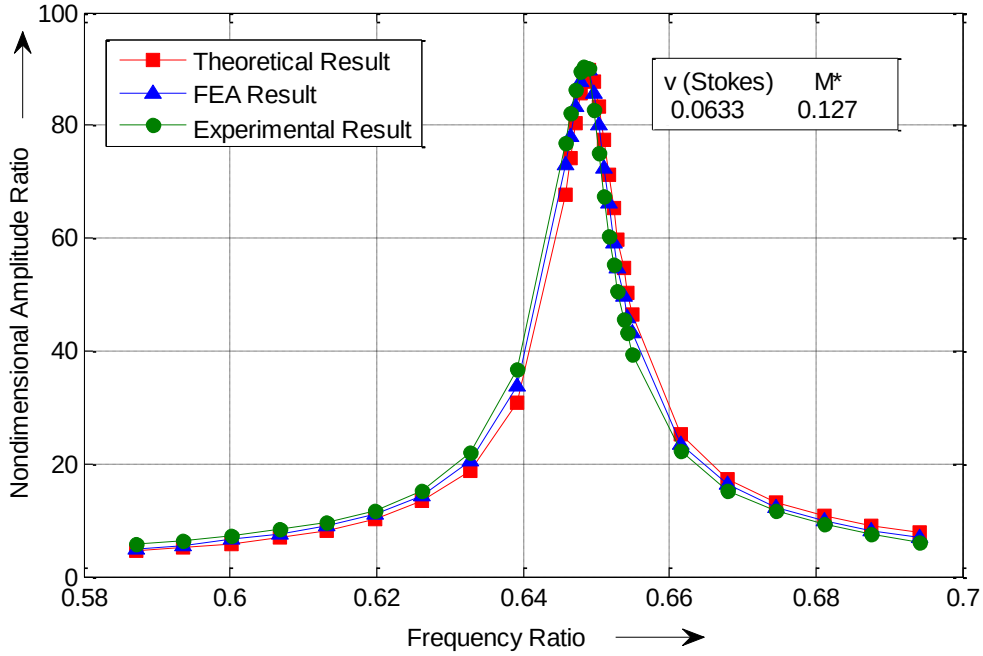

Figure 4.12: Frequency Ratio (ω/ω_0) Vs Non-dimensional Amplitude Ratio (δ^*/ε^*), Mild Steel Rotor R1=0.01m, L=0.8m, q=12, a1/D=0.225, a1/D=0.150, L_1/L=0.313, L_2/L=0.563, R_D=0.055m, T_D=0.020m, M_D=1.0kg, for 55- Direction.

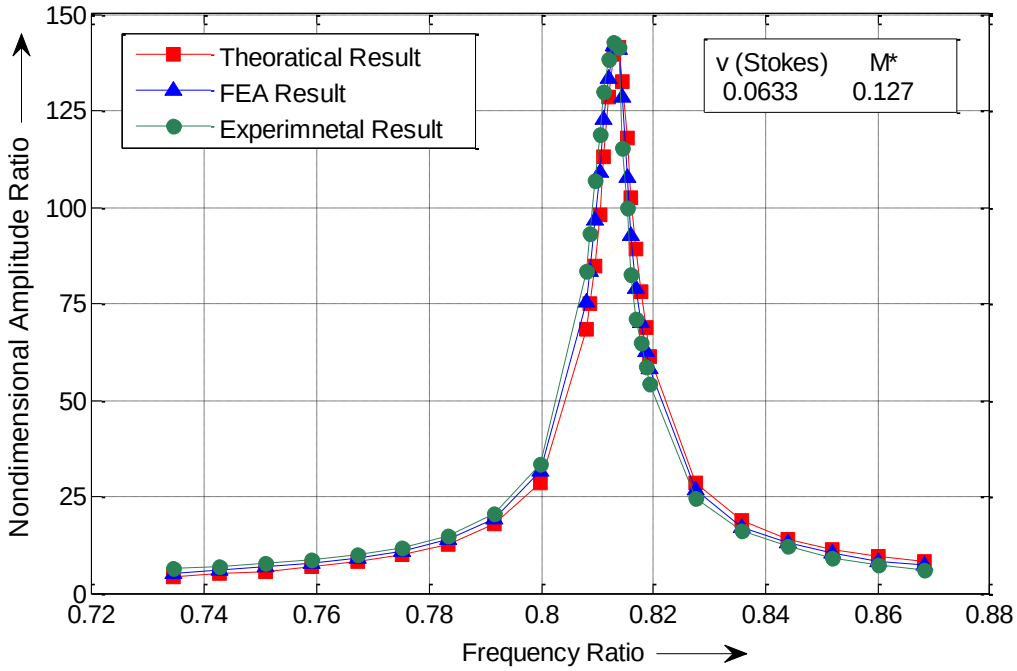

Figure 4.13: Frequency Ratio (ω/ω_0) Vs Non-dimensional Amplitude Ratio (δ^*/ε^*), Mild Steel Rotor R_1=0.01m, L=0.8m, q =12, a1/D=0.150, a1/D=0.125, L_1/L = 0.313, L_2/L=0.563, R_D = 0.055m, T_D= 0.020m, M_D = 1.0kg, for 55- Direction.

Table 4.3 shows the comparison of FEA result with theoretical and experimental result for effect of change in viscosity of fluid on the non-cracked cantilever rotor.

Table 4.3: Comparison between theoretical, experimental and FEA results for effect of different viscous medium.

Sl.No.	Viscosity of fluid (ν)	Theoretical Analysis (Non-dimensional Amplitude (δ*/ε*))	Experimental Analysis (Non-dimensional Amplitude (δ*/ε*))	FEA Analysis (Non-dimensional Amplitude (δ*/ε*))	Error in % The/ FEA	Error in % Exp/ FEA
1	0.0633	176.920	186.19	181.982	2.25	2.36
2	0.5410	58.947	61.792	60.733	3.06	1.74
3	2.9000	20.533	21.491	21.140	2.16	1.66

Tables 4.4 and 4.5 illustrate the comparison of FEA result with theoretical and experimental result for virtual mass effect on the non-cracked and cracked cantilever rotor in the viscous medium respectively.

Table 4.4: Comparison between theoretical, experimental and FEA results for ν=0.541stokes, M*=0.136.

Sl. No.	Mass of disc (M_D) in kg	Theoretical Analysis (Non-dimensional Amplitude (δ*/ε*))	Experimental Analysis (Non-dimensional Amplitude (δ*/ε*))	FEA Analysis (Non-dimensional Amplitude (δ*/ε*))	Error in % The/ FEA	Error in % Exp/FEA
1	1.00	117.583	123.40	121.051	2.41	1.94
2	0.75	102.032	107.34	104.950	2.24	2.27
3	0.50	75.46	79.044	77.663	2.31	1.77

Table 4.5: Comparison between theoretical, experimental and FEA results for a1/D= 0.125, a2/D=0.150, L_1/L = 0.313, L_2/L=0.563, ν=0.541stokes, M*=0.0.136 (virtual mass effect).

Sl.No.	Mass of disc (M_D) in kg	Theoretical Analysis (Non-dimensional Amplitude (δ*/ε*))	Experimental Analysis (Non-dimensional Amplitude (δ*/ε*))	FEA Analysis (Non-dimensional Amplitude (δ*/ε*))	Error in % The/ FEA	Error in % Exp/ FEA
1	1.00	103.03	107.40	105.21	2.07	2.07
2	0.75	91.218	95.340	93.078	1.99	2.37
3	0.50	75.463	79.044	77.206	2.25	2.32

Tables 4.6 and 4.7 show the comparison of FEA result with theoretical and experimental result for effect of change in radius of fluid filled container on the uncrack and cracked rotor respectively.

Table 4.6: Comparison between theoretical, experimental and FEA results for ν=0.541 stokes, M*=0.136 (Non-cracked rotor).

Sl. No.	Gap Ratio (q)	Theoretical Analysis (Non-dimensional Amplitude (δ*/ε*))	Experimental Analysis (Non-dimensional Amplitude (δ*/ε*))	FEA Analysis (Non-dimensional Amplitude (δ*/ε*))	Error in % The/ FEA	Error in % Exp/ FEA
1	q1	42.5346	44.286	43.516	2.25	1.73
2	q2	66.999	69.776	68.446	2.11	1.90
3	q3	73.582	76.790	75.408	2.42	1.79
4	q4	78.069	80.910	79.973	2.38	1.15

Table 4.7: Comparison between theoretical and experimental results for a1/D=0.125, a2/D=0.150, L_1/L=0.313, L_2/L=0.563, ν=0.541stokes, M*=0.136 (44-direction of crack).

Sl.No.	Gap Ratio (q)	Theoretical Analysis (Non-dimensional Amplitude (δ*/ε*))	Experimental Analysis (Non-dimensional Amplitude (δ*/ε*))	FEA Analysis (Non-dimensional Amplitude (δ*/ε*))	Error in % The/ FEA	Error in % Exp/ FEA
1	q1	32.939	34.625	33.640	2.08	2.84
2	q2	51.735	54.151	52.935	2.26	2.24
3	q3	56.463	58.924	57.840	2.38	1.83
4	q4	60.986	63.815	62.394	2.25	2.22

Table 4.8 shows the comparison of FEA result with theoretical and experimental result for the effect of multiple crack depths and crack locations on the dynamic response of the cantilever rotor in the both transverse crack direction (i.e. 44-direction and 55-direction).

Table 4.8: Comparison between theoretical, experimental and FEA results for L_1/L = 0.313, L_2/L=0.563.

	Relative crack depth	44-direction			55-direction		
		Viscosity of fluid (ν) Stokes			Viscosity of fluid (ν) Stokes		
		0.0633	0.541	2.9	0.0633	0.541	2.9
Theoretical Analysis (Non-dimensional Amplitude (δ*/ε*))	β_1=0.250 β_2=0.225	89.791	29.073	10.528	75.463	24.521	8.855
	β_1=0.225 β_2=0.150	110.98	37.943	13.535	89.791	29.073	10.528
	β_1=0.150 β_2=0.225	176.92	58.947	20.531	141.24	46.105	15.561
Experimental Analysis (Non-dimensional Amplitude (δ*/ε*))	β_1=0.250 β_2=0.225	94.127	30.224	10.978	78.496	25.533	9.303
	β_1=0.225 β_2=0.150	116.79	39.749	14.148	94.083	30.648	11.009
	β_1=0.150 β_2=0.225	185.07	61.297	21.594	148.18	48.258	16.172
FEA Analysis (Non-dimensional Amplitude (δ*/ε*))	β_1=0.250 β_2=0.225	91.865	29.753	10.805	77.228	25.192	9.041
	β_1=0.225 β_2=0.150	113.33	38.720	13.861	91.972	29.831	10.812
	β_1=0.150 β_2=0.225	181.36	60.137	21.015	144.30	47.183	15.886
Error in % The/FEA	β_1=0.250 β_2=0.225	2.25	2.28	2.56	2.28	2.66	2.05
	β_1=0.225 β_2=0.150	2.07	2.00	2.35	2.37	2.54	2.62
	β_1=0.150 β_2=0.225	2.44	1.97	2.30	2.12	2.28	2.04
Error in % Exp/FEA	β_1=0.250 β_2=0.225	2.40	1.55	1.57	1.61	1.33	2.81
	β_1=0.225 β_2=0.150	2.96	2.58	2.02	2.24	2.66	1.78
	β_1=0.150 β_2=0.225	2.00	1.89	2.68	2.61	2.22	1.76

4.4 Discussion

The brief discussion on the results of proposed finite element method has been presented in this section. It is noticed that presence of changed viscosity of fluid, mass of disc, radius of container and multiple crack in the rotor alters the vibration response.Various steps involved in the ANSYS to solve any problem are discussed. These steps are: preprocessing phase, solution phase and post processing phase. The selection of the element is very important to get the most refined results from the ANSYS. The SOLID187 element is chosen for mild steel rotor and FLUID30 has been selected for the fluid medium.The geometrical configurations (i.e. geometry of element and nodal position) of SOLID187 and FLUID30 are shown in the Figures 4.1 and 4.2 respectively. The properties of mild steel rotor and fluid medium are presented in Tables 4.1 and 4.2 respectively.Finite element model of crack rotor is illustrated in Figure A1. FE model of rotor with fluid medium is demonstrated in the Figure A2. FEA simulation result is presented in the Figures A3 and A4. The results derived from finite element method are authenticated by results obtained from theoretical and experimental test for non-cracked and multi-cracked cantilever rotor partially submerged in altered viscous medium. The results obtained from the finite element analysis are plotted with results derived from theoretical and experimental analysis for cracked cantilever rotor partially submerged in the viscous medium and are shown in Figures 4.3 to 4.13. Table 4.3 shows the comparison of FEA result with theoretical and experimental result for effect of change in viscosity of fluid on the non-cracked cantilever rotor. Tables 4.4 and 4.5 illustrate the comparison of FEA result with theoretical and experimental result for virtual mass effect on the non-cracked and cracked cantilever rotor in the viscous medium respectively. Tables 4.6 and 4.7 show the comparison of FEA result with theoretical and experimental result for effect of change in radius of fluid filled container on the uncrack and cracked rotor respectively. Table 4.8 shows the comparison of FEA result with theoretical and experimental result for the effect of multiple crack depths and crack locations on the dynamic response of the cantilever rotor in the both transverse crack direction (i.e. 44-direction and 55-direction). It is observed that results are in good agreement.

4.5 Summary

The summary is outlined from the results derived from numerical method. The simple, effective and robust finite element method is presented to analyze the multiple cracks in the cantilever rotor partially submerged in the viscous medium. It is observed that the dynamic response obtained from finite element analysis show the error between non-cracked and cracked rotor model. This can be observed in Figures 4.3 and 4.13.The dynamic response such as natural frequencies and amplitude are derived from finite element analysis and found to be of close proximity with results obtained from theoretical and experimental observations. The percentage of error of finite element analysis is within 3% for rotor. The dynamic response derived from finite element analysis can be utilized to design and develop the fault diagnosis and condition monitoring techniques based on artificial intelligent techniques such as fuzzy logic and various types of neural networks.The artificial intelligent techniques based structural health monitoring algorithms have been discussed in the upcoming chapters.

Chapter 5

Analysis of Fuzzy System for Detecting the Multiple Crack in Cantilever Rotor

The presence of a crack is a grave threat to the integrity of the system, which leads to reducing the life and may cause the failure of the system. Hence, it is needed to develop the online automated method to predict the damage effectively, present in the engineering system. It is well-established fact that the presence of the crack in the system upset the vibration parameters (e.g. Change the natural frequencies and amplitude). So these changes can be successfully used to locate fault position and intensity. On the ground of these modifications in vibration parameters, automated AI techniques can be used to detect the crack locations and depths to circumvent the catastrophic failure of engineering systems. In the current chapter, inverse techniques are employed to implement the proposed methodology using the induced vibration response parameters of the rotor for predicting the locations and depths of the multiple cracks present in the rotor.

5.1 Introduction

Fuzzy Logic System (FLS) was first developed by Mamdani and Assilan around 1975 [211], although L A Zadeh [212] has presented the concept of fuzzy set in 1965. Essentially, Fuzzy Logic System (FLS) is a multi-value logic, which permits interval qualities to be characterized by linguistic expressions like true/false, high/low, yes/no. In the most recent couple of decades, specialists are utilized the FL approach for applications, such as feature extraction, identification and classification of geometrical properties and so on. FLS can mimic the human conduct by taking the distinctive thinking modes keeping in mind the end goal to make the computer system act like humans. The investigation of the imprecision and vulnerability motivates the exceptional human being capacity to comprehend different engineering or industrial applications. FL can determine mapping principles regarding words instead of numbers. Another essential idea in FLS is fuzzy if–then rule which is for the most part utilized as a part of the advancement of the fuzzy rule-based system. FLS can show nonlinear capacities of self-assertive many-sided

quality to a desired level of precision. FLS is an advantageous approach to guide a data space to output space and is one of the apparatuses used to model multi-inputs, multi-outputs systems. Henceforth the fuzzy methodology can be adequately utilized as a crack diagnostics tool for multiple cracked systems. In the present chapter, multiple crack detection techniques using fuzzy logic system have been developed. The fuzzy inference system for identification of multiple crack tool has been designed and developed with five inputs (two relative natural frequency, two relative amplitude and viscosity of fluid) and four outputs (two relative crack locations and two relative crack depths). The proposed multiple crack identification tool has been developed using the triangular, trapezoidal and gaussian membership functions. The Mamdani fuzzy, Takagi-Sugeno fuzzy and fuzzy based hybrid system is developed for identification of crack in rotor. The dynamic characteristics acquired from the theoretical, FE and experimental analysis have been used for development of the fuzzy controller model. The results of the proposed fuzzy systems for identification of crack have been compared with the results found from the theoretical, experimental and FE analysis. It is found that the fuzzy logic models can be used excellently for crack detection in the rotor. The present chapter is organized in the seven altered sections. Section 5.1 introduces the introductory part of the fuzzy logic system. A fuzzy logic system has been discussed in Section 5.2. The investigation of the Mamdani fuzzy system used for identification of multiple crack in rotor has been described in section 5.3. The analysis of Takagi-Sugeno fuzzy system for the identification in rotor has been described in section 5.4. The analysis of gaussian fuzzy based hybrid system for the identification of multiple crack in the rotor has been introduced in section 5.5. Section 5.6 discusses the obtained results from the Mamdani fuzzy, Takagi-Sugeno fuzzy and Hybrid fuzzy model and finally, section 5.7 discuses a summary of the analysis of fuzzy system used for identification of multiple transverse crack in the rotor.

5.2 Fuzzy Logic System

The fuzzy technique is a popular computing system based on the concept of fuzzy set theory, fuzzy reasoning, and fuzzy if-then rules. The application of fuzzy logic is found successfully in wide variety of fields such as bioinformatics, pattern recognition, business, data classification, automatic control, decision analysis, robotics, expert systems and time series prediction. A fuzzy logic controller primarily takes a judgement by nonlinear mapping of the input information in a scalar output, applying fuzzy rules. The mapping

could be possible through fuzzy if–then rules, input/output membership functions, a total of output sets, and de-fuzzification. An FLC can be taken as a congregation of autonomous multi-data, single-output network. The FLC mainly comprises four parts: the inference engine, rules base, fuzzifier and de-fuzzifier. The rule base of the FLC can be created using the numeric information. When the fuzzy rules are developed, FLC becomes a system that gives output data, after processing the input data using fuzzy rules and fuzzy linguistic expressions. The fuzzifier receive data values and checks the level of relationship with each of the fuzzy sets along with membership functions. The FLC changes crisp inputs into crisp outputs. The fuzzy logic system consists of five stages to complete the operation. These are as follows;

Step 1: Feed input data to FLC

The input data is fed to FLS. The fuzzy system distinguishes the degree of association of input variables using fuzzy rule database and membership functions. That is called fuzzification of input data.

Step 2: Functions of Fuzzy Operator

The fuzzy system measures the degree of association of each fuzzified input data that fulfils for each rule of the fuzzy rule base. If the rule exists among more than one membership functions, the fuzzy operator gets a single value of the rule.

Step 3: Apply the algorithm for generation of rules

The fuzzy membership function is reshaped through an algorithm, which is a parameter of a fuzzy set. A function is associated for reshaping the output, related to the forerunner.

Step 4: Clustering the results

Each rule of the fuzzy database produces a result, that is integrated to get a decision from fuzzy logic system. The clustering of each rule base results leads to an aggregated fuzzy set as output.

Step 5: Aggregate all output

The aggregate output fuzzy set consider as an input for the defuzzification method and the output is single value. The aggregate of a fuzzy set incorporate a sort of output values and defuzzified in order to determine a single output value from the set.

5.2.1 Concept of Fuzzy Membership Function

The fuzzy membership function plays a significant role in the modeling of the fuzzy logic controller. The fuzzy membership function describes the fuzzy set and delivers an amount of the degree of similarity or inaccurate enslavements of an element to a fuzzy set.The triangular, gaussian, trapezoidal, Bell-shaped, etc. are the membership functions mostly used in the fuzzy logic analysis, but any other type of membership functions can also be used.The non-zero degree membership elements are called as support and one degree membership elements are called as core of the fuzzy set. The membership functions are usually called μ_F (x) is shown in the Figures 5.1(a), 5.1(b) and 5.1(c).Where μ is signifies as the degree of the weight of the element x in the fuzzy set F. The size of the membership function is typically stated to zero to one. Therefore, each component of the fuzzy set. Fits with a degree in the range of [0, 1]. The following three types of membership function selected in the present analysis are address below.

The Triangular membership function is shown in Figure 5.1 (a). The Triangular membership function $\mu_F(x)$ has three vertices 'p', 'q' and 'r' of the fuzzy set 'F'. The degree of membership is equivalent to zero at point 'p' & 'r' and degree of membership is equal to one at point 'q'. The mathematical exemplification of the fuzzy triangular membership function $\mu_F(x)$ can be described below.

$$\left.\begin{aligned} \mu_F(x,p,q,r) &= 0 \ if \ x \le p \\ &= \frac{(x-p)}{(q-p)} \ if \ p \le x \le q \\ &= \frac{(p-x)}{(q-p)} \ if \ q \le x \le r \\ &= 0 \ if \ x \ge r \end{aligned}\right\} \qquad (5.1)$$

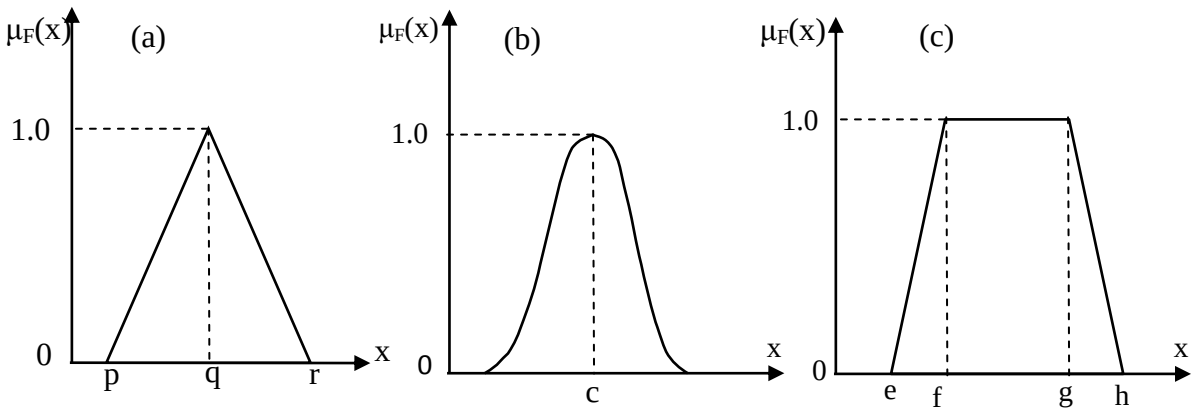

Figure 5.1: Membership functions used in FLS analysis (a) Traingular (b) Gaussian and (c) Trapezoidal

The parameter 'p' and 'r' placed at feet of the triangle and the parameter 'q' placed at the pick.

The fuzzy gaussian membership function is shown in figure 5.1 (b). The gaussian membership function is determined by the 'c' and 'α'. Where 'α' is the width of membership function and 'c' is denoted the center of membership function. The mathematical exemplification of the gaussian fuzzy membership function can be described as below.

$$(x;c,\alpha) = \exp\left(-0.5\left((x-c)/\alpha\right)^2\right) \tag{5.2}$$

The trapezoidal membership function is shown in Figure 5.1(c). It has two base points (e, h) and two shoulder point (f, g).The mathematical representations of the trapezoidal membership function are as follows.

$$\left.\begin{array}{l} \mu_F(x,e,f,g,h) = 0 \\ \text{when } x \le e \text{ and } x \ge e \\ = \dfrac{(x-e)}{(f-x)} \text{ when } e \le m \le f \\ = 1 \text{ when } g \le x \le h \\ = \dfrac{(h-x)}{(h-g)} \text{ when } g \le x \le h \end{array}\right\} \tag{5.3}$$

5.2.2 Designing of Fuzzy Logic Model using Fuzzy Rule

Fuzzy logic system is based on the permutation of fuzzy logic and fuzzy set theory. Fuzzy logic system possesses the approximation feature with the help of fuzzy IF-THEN rules and fuzzy membership functions. Figure 5.2 shows a basic model of fuzzy inference system.

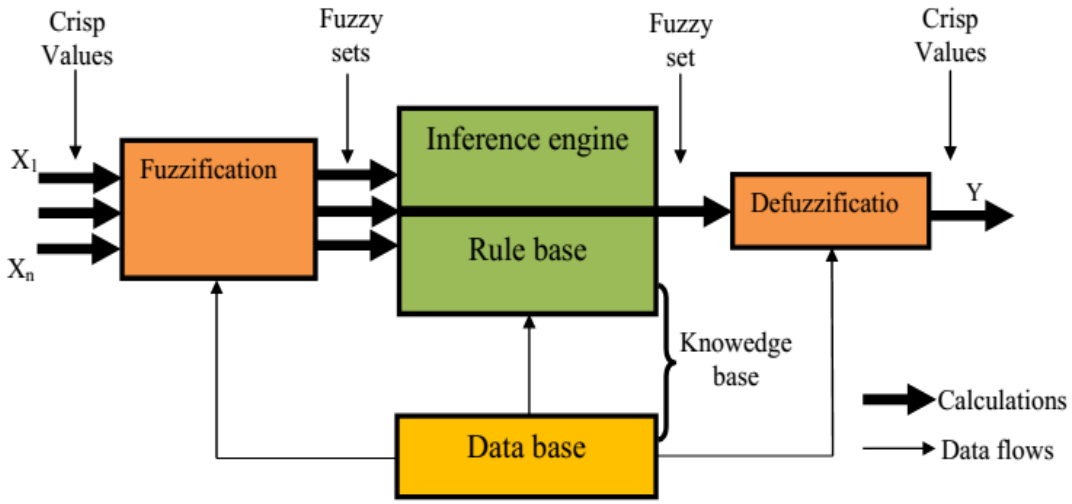

Figure 5.2: General structure of fuzzy logic system

The input and output variables intricately depend on working domain of any real complex problem, so the optimization of input and output data is necessary for the better solution of complex systems. Sometimes approximation of input and output variables of a complex application is preferable, rather than going through an elaborate process, which gets more time to solve the same problem. The fuzzy rules and membership functions have been used to perform the fuzzy system for the approximation of input and output parameters.The fuzzy membership functions are significant parameters of the fuzzy system, which are designed using proper fuzzy rules and fuzzy linguistic term.The fuzzification of input variables and defuzzification of the output variables have been performed using the conditional statement and fuzzy rules. The conditional statements like fuzzy intersection, union and complement have been used to develop the membership functions of the fuzzy system. Hence, the fuzzy model receives the input variables from the working domain to an absolute circumstances and using the fuzzy rules. It will give an organized action as preferred by the system.

5.2.3 Modeling of Defuzzification Mechanism

The conversion of fuzzy outputs into crisp output in the fuzzy system is called defuzzification. Defuzzification approach is selected based on the features of the application. The last step in modeling of fuzzy system is the transformation of fuzzy output set to a crisp output. The crisp output illustrates the possible distribution of the conditional fuzzy control action. The correlation between the fuzzy output set (K), non-fuzzy output (X_0) and defuzzifier in the following equation;

X_0 = Defuzzifier (K).

For the development of the fuzzy system, several defuzzification methods are used. The mostly used defuzzication methods are listed below;

(1) Centroid of the area method (2) Mean of maximum method

(3) Maximum membership principle (4) Weighted average method

5.3 Analysis of Mamdani Fuzzy Logic Mechanism for Identification of Multiple Crack in Rotor

In the present segment introduces the analysis of triangular, gaussian and trapezoidal membership functions for the development of Mamdani fuzzy models. The five input data are fed into fuzzy model and four variables are received as output. The linguistic variables used for the inputs are as follows;

(1) rnfx = Relative natural frequency in x-axis direction

(2) rnfy = Relative natural frequency in y-axis direction

(3) rax = Relative amplitude in x-axis direction

(4) ray = Relative amplitude in y-axis direction

(5) ν = Viscosity of fluid

The linguistic variables used for the outputs are as follows;

(1) rfcl = Relative first crack location (2) rfcd =Relative first crack location

(3) rscl =Relative second crack depth (4) rscd =Relative second crack depth

Figures 5.3(a), 5.3(b) and 5.3(c) illustrate the triangular membership, gaussian membership and trapezoidal membership fuzzy models respectively. The various fuzzy linguistic variables with detail description of the membership function name and range of linguistic term have been illustrated in the Table 5.1. Fuzzy controller has been trained with the help of many defined fuzzy rules. Twenty fuzzy rules are taken from the several

rules and described in Table 5.2. Eleven membership functions are considered for all five input parameters. Nineteen membership functions are taken for the output parameters of relative first and second crack depth. Whereas Forty-six membership functions are considered for the four output parameters (i.e. relative first crack location and depth). Figures 5.4, 5.5, and 5.6 shows the three menmbership function(i.e. Triangular, Gaussian, and Trapezoidal) of fuzzy controller model.The process of defuzzification of the Mamdani fuzzy system with three membership function (i.e. Triangular, Gaussian, and Trapezoidal) are illustrated in Figures 5.7, 5.8 and 5.9 respectively by activating the rule no. 5 and 18 from Table 5.2.

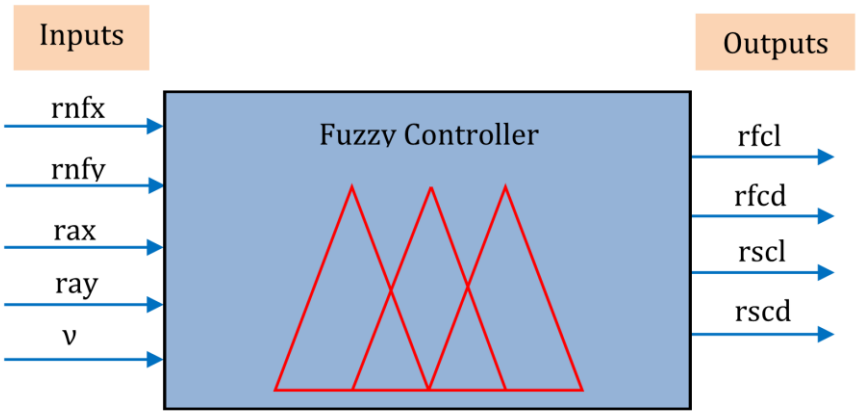

Figure 5.3(a): Triangular fuzzy controller model.

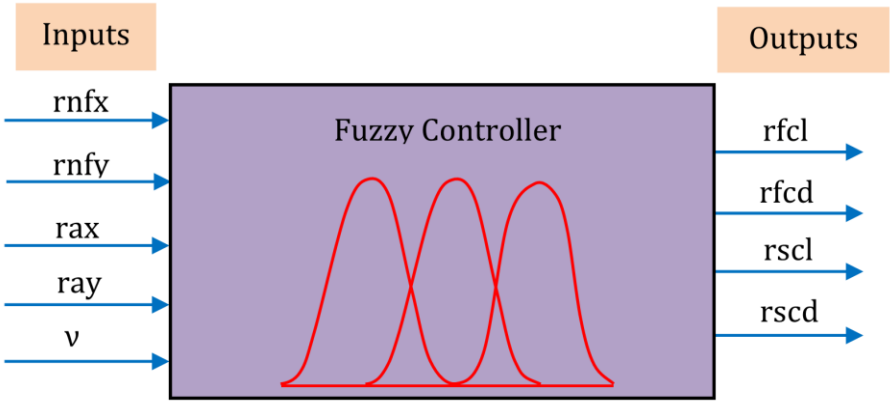

Figure 5.3 (b): Gaussian fuzzy controller model.

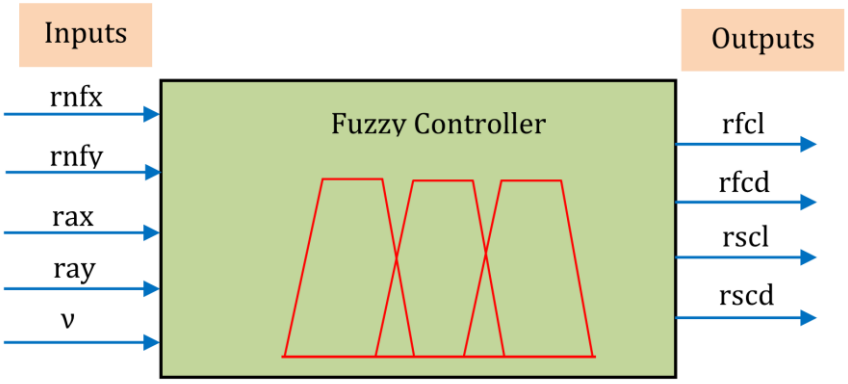

Figure 5.3 (c): Trapezoidal fuzzy controller model.

5.3.1 Designing the Mamdani Fuzzy Logic Mechanism for Multiple Crack Identification in Rotor

The rules for fuzzy mechanism can be defined, based on above fuzzy linguistic terms as follow:

IF *rfnf is* $rnfx_p$ *and rsnf is* $rnfy_q$ *and rfa is* rax_r *and rsa is* ray_s *and v is* v_t

THEN *rfcl is* $rfcl_{pqrst}$ *and rfcd is* $rfcd_{pqrst}$ *and rscl is* $rscl_{pqrst}$ *and rscd is* $rscd_{pqrst}$ (5.4)

Where p, q, r, s, t =1to11.

According to fuzzy methodology a factor, W_{pqrst} is defined in the rules as follows [142,207]:

$$W_{pqrst} = \mu\, rnfx_p\left(freq_p\right) \wedge \mu\, rnfy_q\left(freq_q\right) \wedge \mu\, rax_r\left(Amp_r\right) \wedge \mu\, ray_s\left(Amp_s\right) \wedge \mu\, v_t\left(v_t\right) \quad (5.5)$$

Where: $freq_p$ and $freq_q$ are the first and second relative natural frequencies at x and y-axis directions of the carcked cantilever rotor respectively; Amp_r and Amp_s first and second relative amplitudes at x and y-axis directions of the cracked cantilever rotor; v_t is the viscosity of fluid. The membership values of the relative carck loaction and relative crack depth, $(crack_location)_{rcli}$ and $(crack_depth)_{rcdi}$ (i=1,2) by relating the composition rule of fuzzy inference can be inscribed as [142, 207]:

$$\mu_{rcli_{pqrst}}(crack_location) = w_{pqrst} \wedge \mu_{rcli_{pqrst}}(crack_location)\ \forall_{length} \in rcli \quad (5.6a)$$

$$\mu_{rcdi_{pqrst}}(crack_depth) = w_{pqrst} \wedge \mu_{rcdi_{pqrst}}(crack_depth)\ \forall_{depth} \in rcdi \quad (5.6b)$$

The outputs of all sets of fuzzy rules combined to accomplish the comprehensive conclusions can be written as follows;

$$\mu_{rcli}(crack_location) = \mu_{rcli_{11111}}(crack_location) \vee .. \vee \mu_{rcli_{pqrst}}(crack_location) \vee .. \vee \mu_{rcli_{12121212121}}(crack_location) \quad (5.7a)$$

$$\mu_{rcli}(crack_depth) = \mu_{rcli_{11111}}(crack_depth) \vee \ldots \vee \mu_{rcli_{pqrst}}(crack_depth) \vee \ldots \vee \mu_{rcli_{12121212121}}(crack_depth) \quad (5.7b)$$

The crisp values of the first and second relative crack location and crack depth can be written using Centre of gravity approach as [142,207]:

$$\text{Re}lative\ crack\ location\ (rfcl, rscl) = = \frac{\int (crack_location) . \mu_{rcl_{1,2}}(crack_location) . d\ (crack_location)}{\int \mu_{rcl_{1,2}}(crack_location) . d\ (carck_location)} \quad (5.8a)$$

$$\text{Re}lative\ crack\ depth\ (rfcd, rscd) = = \frac{\int (crack_depth) . \mu_{rcl_{1,2}}(crack_depth) . d\ (crack_depth)}{\int \mu_{rcl_{1,2}}(crack_depth) . d\ (crack_depth)} \quad (5.8b)$$

Table 5.1: Description of fuzzy linguistic variable.

Linguistic term with range	**Membership function name**	**Description and range of the linguistic term**
$rnfx_{1\ to\ 4}$	H1NF1,H2NF1,H3NF1, H4NF4,	High ranges of relative natural frequency in X-direction of vibration in ascending order respectively.
$rnfx_{5\ to\ 7}$	M1NF1,M2NF1,M3NF1,	Medium ranges of relative natural frequency in X-direction of vibration in ascending order respectively
$rnfx_{8\ to\ 11}$	L1NF1,L2NF1,L3NF1, L4NF1	Lower ranges of relative natural frequency in X-direction of vibration in descending order respectively.
$rnfy_{1to\ 4}$	H1NF2,H2NF2,H3NF2, H4F2	Higher ranges of relative natural frequency in Y-direction of vibration in ascending order respectively.
$rnfy_{5\ to\ 7}$	M1NF2,M2NF2,M3NF2	Medium ranges of relative natural frequency in Y-direction of vibration in ascending order respectively.
$rnfy_{8to\ 11}$	L1NF2, L2NF2, L3NF2, L4NF2	Lower ranges of relative natural frequency in Y-direction of vibration in descending order respectively.
$rax_{1\ to\ 4}$	H1A1,H2A1,H3A1	Higher ranges of relative amplitude in X-direction of vibration in ascending order respectively
$rax_{5\ to\ 7}$	M1A1,M2A1,M3A1	Medium ranges of relative amplitude in X-direction of vibration in ascending order respectively

$rax_{8\ to\ 11}$	L1A1,L2A1,L3A1, L4A1	Lower ranges of relative amplitude in X-direction of vibration in descending order respectively
$ray_{1\ to\ 4}$	H1A2,H2A2,H3A3	High ranges of relative amplitude in Y-direction of vibration in ascending order respectively.
$ray_{\ 5\ to\ 7}$	M1A2,M2A2,M3A2	Medium ranges of relative amplitude in Y-direction of vibration in ascending order respectively
$ray_{8\ to\ 11}$	L1A2,L2A2,L3A2, L4A2	Lower ranges of relative amplitude in Y-direction of vibration in descending order respectively
$V_{1\ to\ 4}$	H1V1,H2V1,H3V1, H4V1	Higher ranges of viscosity of viscous medium in ascending order respectively
$V_{5\ to\ 7}$	M1V1,M2V1,M3V1	Medium ranges of viscosity of viscous medium in ascending order respectively
$V_{8\ to\ 11}$	L1V1,L2V1,L3V1, L4V1	Lower ranges of viscosity of viscous medium descending order respectively
$rfcl_{1\ to\ 21}$	S1CL1,S2CL1,S3CL 1, S4CL1…S21CL1	Smaller ranges of relative crack depth of rotor in descending order respectively
$rfcl_{22to\ 24}$	M1CL1,M2CL1, M3CL1	Medium ranges of relative crack depth of rotor in ascending order respectively
$rfcl_{25\ to\ 46}$	B1CL1, B2CL1, B3CL1… B22CL1	Bigger ranges of relative crack depth of rotor in ascending order respectively
$rfcd_{1\ to\ 9}$	S1CD1,S2CD1,S3CD 1, S4CD1 ….S9CD1	Smaller ranges of relative crack location in the rotor in ascending order respectively
$rfcd_{10}$	M1CD1	Medium ranges of relative crack location in the rotor in ascending order respectively
$rfcd_{\ 11\ to\ 19}$	L1CD1, L2CD1, L3CD1…… L9CD1	Larger ranges of relative crack location in the rotor in ascending order respectively
$rscl_{1\ to\ 21}$	S1CL2,S2CL2,S3CL 2,S4CL2 ….S21CL2	Smaller ranges of relative crack depth of rotor in ascending order respectively
$rscl_{22to\ 24}$	M1CL2,M2CL2, M3CL2	Medium ranges of relative crack depth of rotor in ascending order respectively
$rscl_{25\ to\ 46}$	B1CL2, B2CL2, B3CL2…… B22CL2	Bigger ranges of relative crack depth of rotor in ascending order respectively
$rscd_{1\ to\ 9}$	S1CD2,S2CD2,S3CD 2, S4CD2 ….S9CD2	Smaller ranges of relative crack location in the rotor in descending order respectively
$rscd_{10}$	M1CD2	Medium ranges of relative crack location in the rotor in ascending order respectively
$rscd_{\ 11\ to\ 19}$	L1CD2, L2CD2, L3CD2…… L9CD2	Larger ranges of relative crack location in the rotor in ascending order respectively

Table 5.2: Example of some fuzzy rules out of several fuzzy rules for the rotor.

Sl. No.	Few rules for fuzzy controller
1	If rnfx is H1NF1, rnfy is H2NF2, rax is H1A1, ray is H2A2, v is L2V1 then rfcl is B17CL1 and rfcd is S8CD1, and rscl is L18CL2 and rscd is S5CD2
2	If rnfx is H2NF1, rnfy is H3NF2, rax is H2A1, ray is H3A2, v is L1V2 then rfcl is B15CL1 and rfcd is S7CD1, and rscl is L16CL2 and rscd is S3CD2
3	If rnfx is H3NF1, rnfy is L1NF2, rax is H3A1, ray is L1A2, v is M1V1 then rfcl is M2CL1 and rfcd is M1CD1, and rscl is B2CL2 and rscd is S6CD2
4	If rnfx is M1NF1, rnfy is H3NF2, rax is M1A1, ray is H3A2, v is M2V1 then rfcl is B10CL1 and rfcd is S5CD1, and rscl is L4CL2 and rscd is S8CD2
5	If rnfx is M2NF1, rnfy is L3NF2, rax is M2A1, ray is L3A2, v is M3V1 then rfcl is S18CL1 and rfcd is M1CD1, and rscl is S8CL2 and rscd is L2CD2
6	If rnfx is H4NF1, rnfy is H1NF2, rax is H1A1, ray is H3A2, v is L1V1 then rfcl is B19CL1 and rfcd is S8CD1, and rscl is L7CL2 and rscd is S1CD2
7	If rnfx is L1NF1, rnfy is M2NF2, rax is M3A1, ray is H2A2, v is L2V1 then rfcl is M1CL1 and rfcd is L2CD1, and rscl is L3CL2 and rscd is S7CD2
8	If rnfx is M3NF1, rnfy is M2NF2, rax is M2A1, ray is M3A2, v is L3V1 then rfcl is S16CL1 and rfcd is S9CD1, and rscl is M2CL2 and rscd is L1CD2
9	If rnfx is H2NF1, rnfy is L2NF2, rax is H4A1, ray is L2A2, v is M1V1 then rfcl is S8CL1 and rfcd is L8CD1, and rscl is S4CL2 and rscd is L5CD2
10	If rnfx is L2NF1, rnfy is L4NF2, rax is L2A1, ray is L4A2, v is H3V1 then rfcl is S5CL1 and rfcd is L7CD1, and rscl is S2CL2 and rscd is L8CD2
11	If rnfx is M1NF1, rnfy is L4NF2, rax is M3A1, ray is L2A2, v is H2V1 then rfcl is S10CL1 and rfcd is L5CD1, and rscl is S14CL2 and rscd is L2CD2
12	If rnfx is H3NF1, rnfy is M3NF2, rax is H1A1, ray is M1A2, v is L1V1 then rfcl is B9CL1 and rfcd is L6CD1, and rscl is S20CL2 and rscd is S8CD2
13	If rnfx is L3NF1, rnfy is L1NF2, rax is L3A1, ray is L2A2, v is H2V1 then rfcl is B9CL1 and rfcd is L5CD1, and rscl is S20CL2 and rscd is S8CD2
14	If rnfx is L4NF1, rnfy is L2NF2, rax is L4A1, ray is L2A2, v is H3V1 then rfcl is S6CL1 and rfcd is L4CD1, and rscl is S8CL2 and rscd is L7CD2
15	If rnfx is H1NF1, rsnf is H2NF2, rfa is M3A1, rsa is M1A2, v is L2V1 then rfcl is B8CL1 and rfcd is S17CD1, and rscl is S18CL2 and rscd is L3CD2
16	If rnfx is M3NF1, rnfy is L3NF2, rax is L2A1, ray is L1A2, v is M1V1 then rfcl is S9CL1 and rfcd is L4CD1, and rscl is M2CL2 and rscd is L2CD2
17	If rnfx is L2NF1, rnfy is M1NF2, rax is L4A1, ray is M1A2, v is H2V1 then rfcl is S9CL1 and rfcd is L5CD1, and rscl is M2CL2 and rscd is S5CD2
18	If rnfx is H2NF1, rnfy is M2NF2, rax is H4A1, ray is L2A2, v is L3V1 then rfcl is S14CL1 and rfcd is L5CD1, and rscl is M3CL2 and rscd is S9CD2
19	If rnfx is H4NF1, rnfy is L4NF2, rax is L2A1, ray is L3A2, v is H3V1then rfcl is S20CL1 and rfcd is S8CD1, and rscl is M1CL2 and rscd is L4CD2
20	If rnfx is L1NF1, rnfy is L4NF2, rax is L3A1, ray is L2A2, v is H2V1 then rfcl is S4CL1 and rfcd is L6CD1, and rscl is S16CL2 and rscd is L8CD2

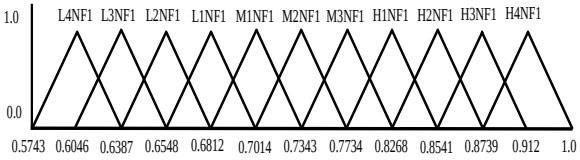

(a) Natural Frequency at x-axis direction.

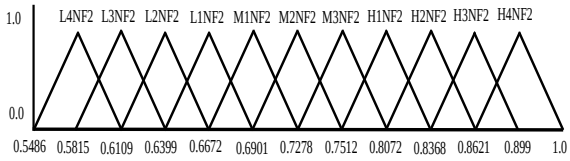

(b)NaturalFrequency at y-axis direction.

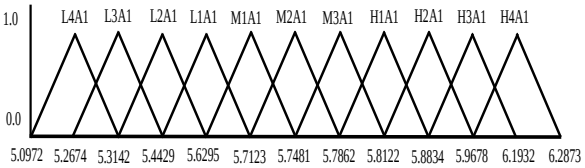

(c) Amplitude at x-axis direction.

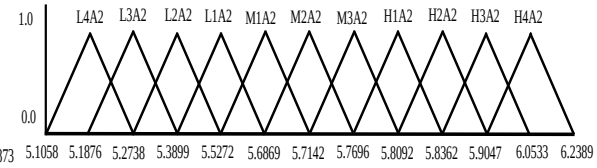

(d) Amplitude at y-axis direction.

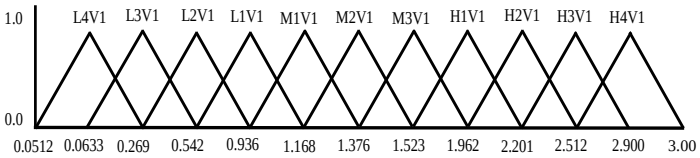

(e):Membership function for viscosity of fluid.

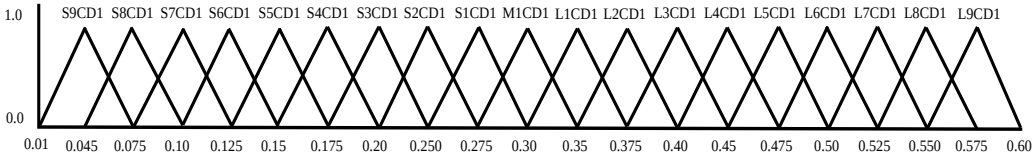

(f) Relative first crack depth.

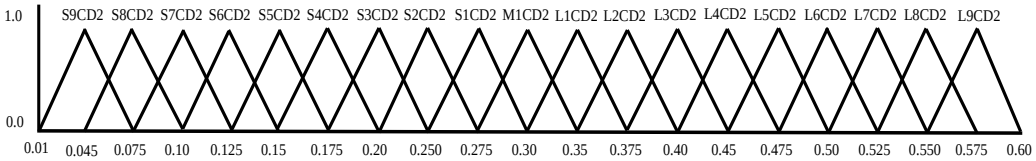

(g) Relative second crack depth.

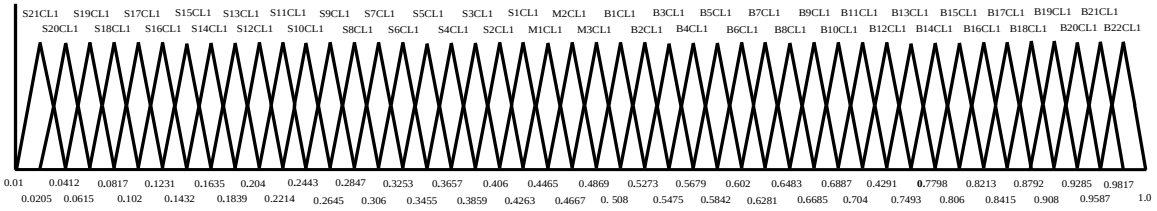

(h) Relative first crack location.

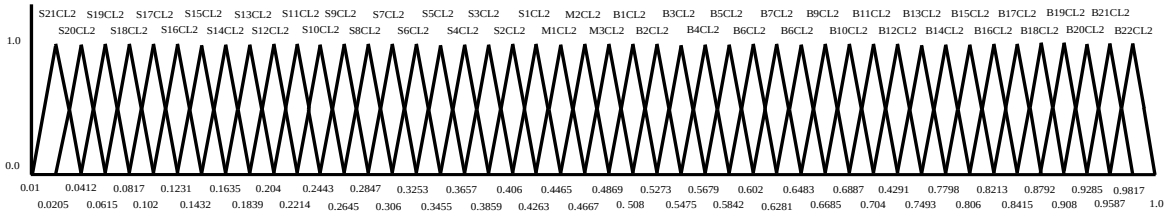

(i) Relative second crack location.

Figure 5.4: Membership functions for triangular fuzzy controller model

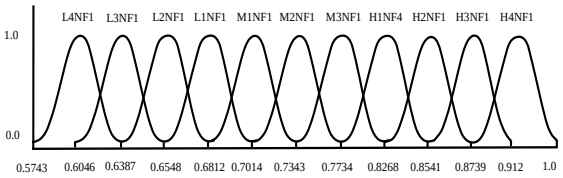

(a) Natural Frequency at x-axis direction

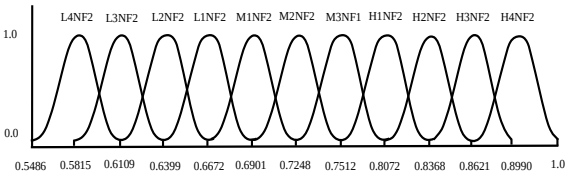

(b) Natural Frequency at y-axis direction

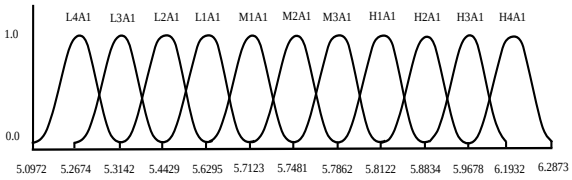

(c) Amplitude at x-axis direction.

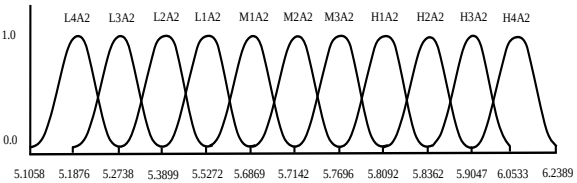

(d) Amplitude at y-axis direction.

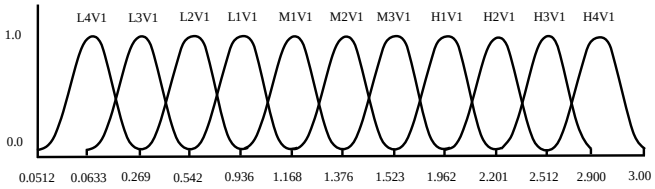

(e) Viscosity of fluid

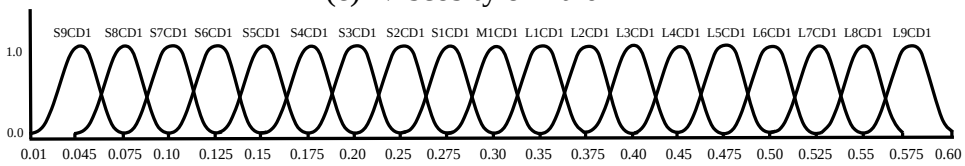

(f) First relative first crack depth.

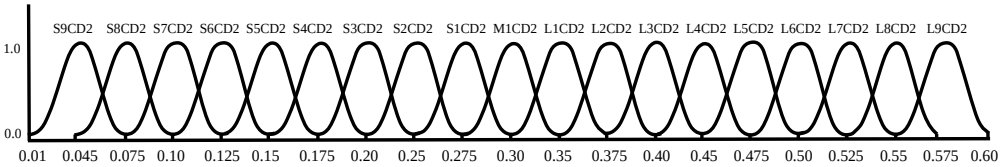

(g) First relative second crack depth.

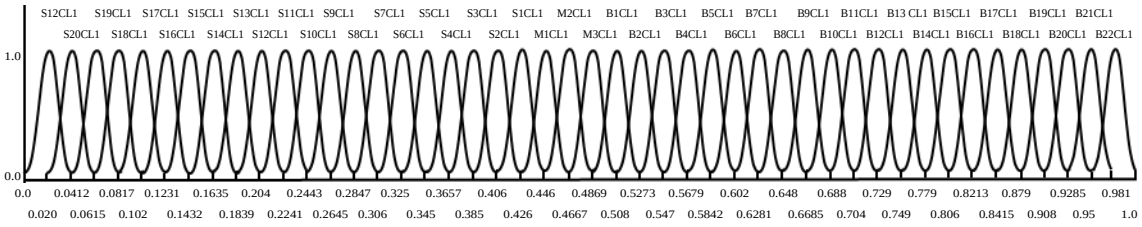

(h) Relative first crack location.

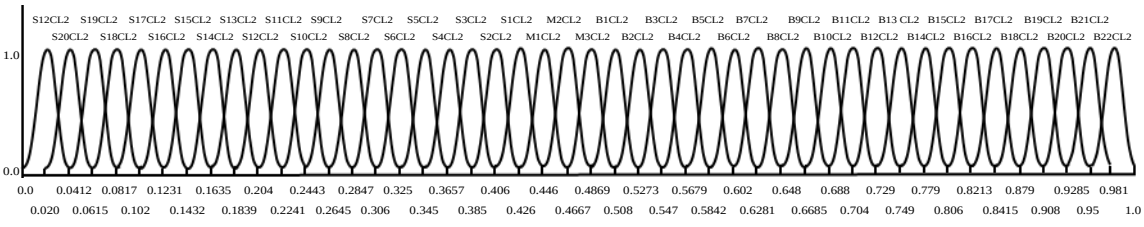

(i) Relative second crack location.

Figure 5.5: Membership functions for gaussian fuzzy controller model
(i) Relative second crack location.

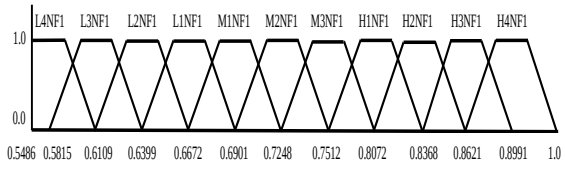

(a) Natural Frequency at x-axis direction

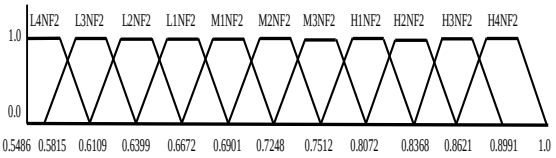

(b) Natural Frequency at y-axis direction

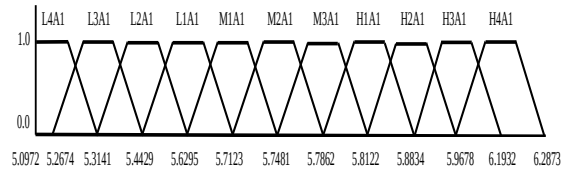

(c) Amplitude at x-axis direction

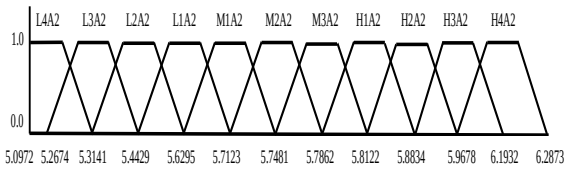

(d) Amplitude at y-axis direction

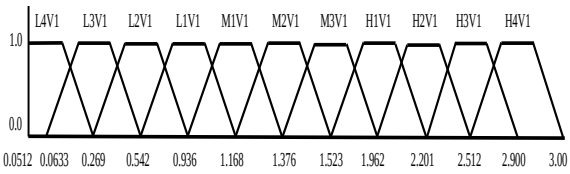

(e) Viscosity of fluid

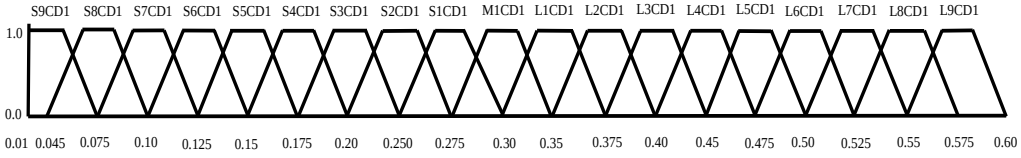

(f) Relative first crack depth

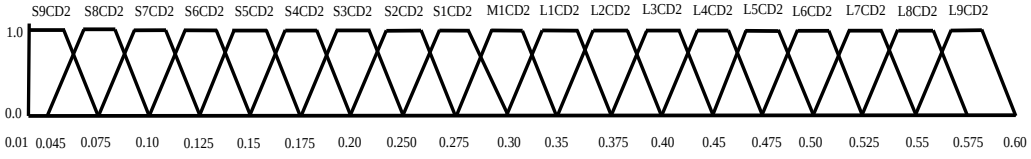

(g) Relative second crack depth

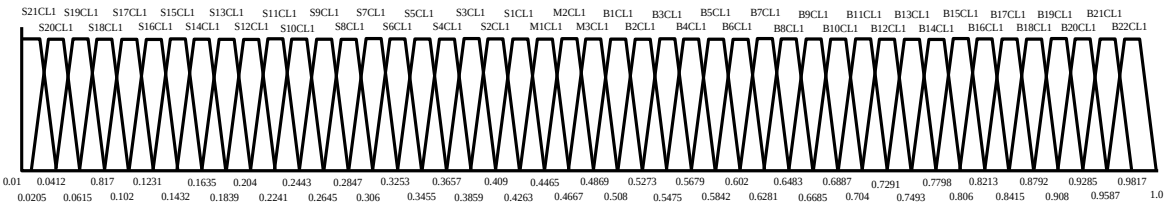

(h) Relative first crack location

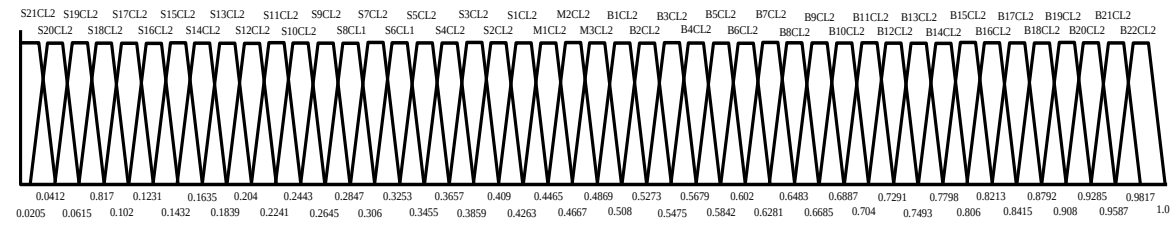

(i) Relative second crack location.

Figure 5.6: Membership functions for Trapazoidal fuzzy controller model

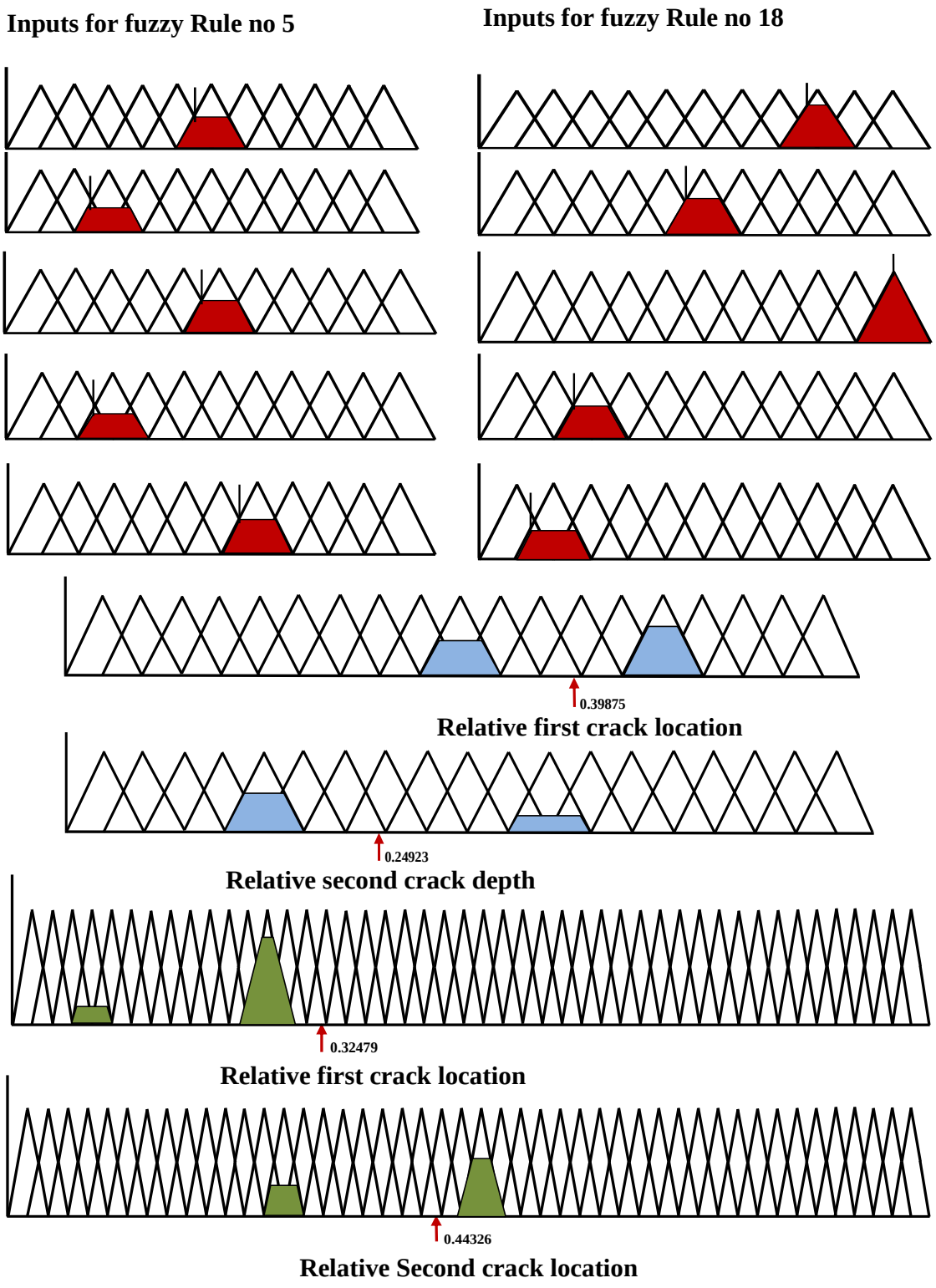

Figure 5.7: Resultant values of first and second relative crack depth and crack locations from triangular membership function while activated the fuzzy rules no 5 and 18 of Table 5.2 for the rotor.

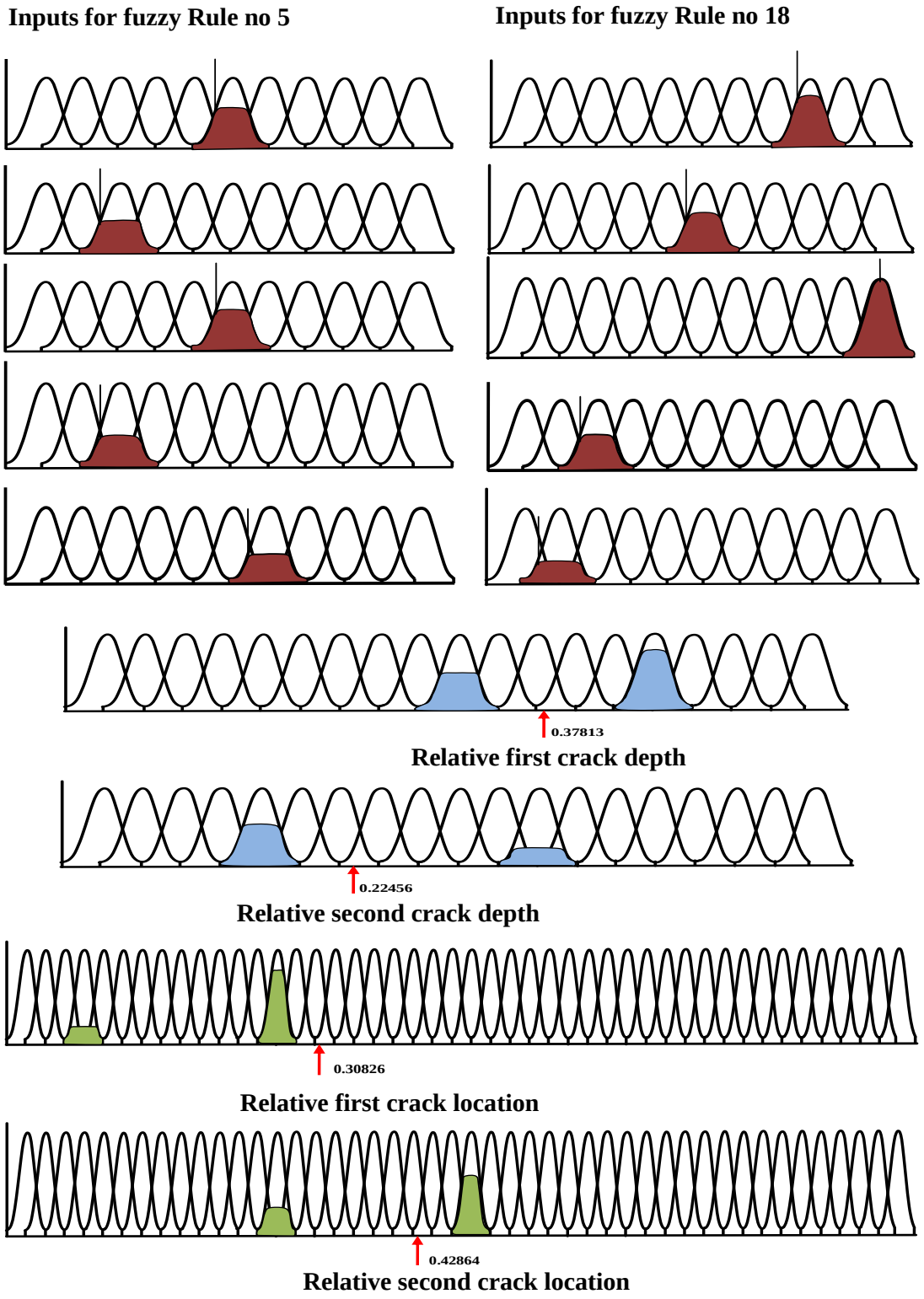

Figure 5.8: Resultant values of first and second relative crack depth and crack locations from gaussian membership function while activated the fuzzy rules no 5 and 18 of Table 5.2 for the rotor.

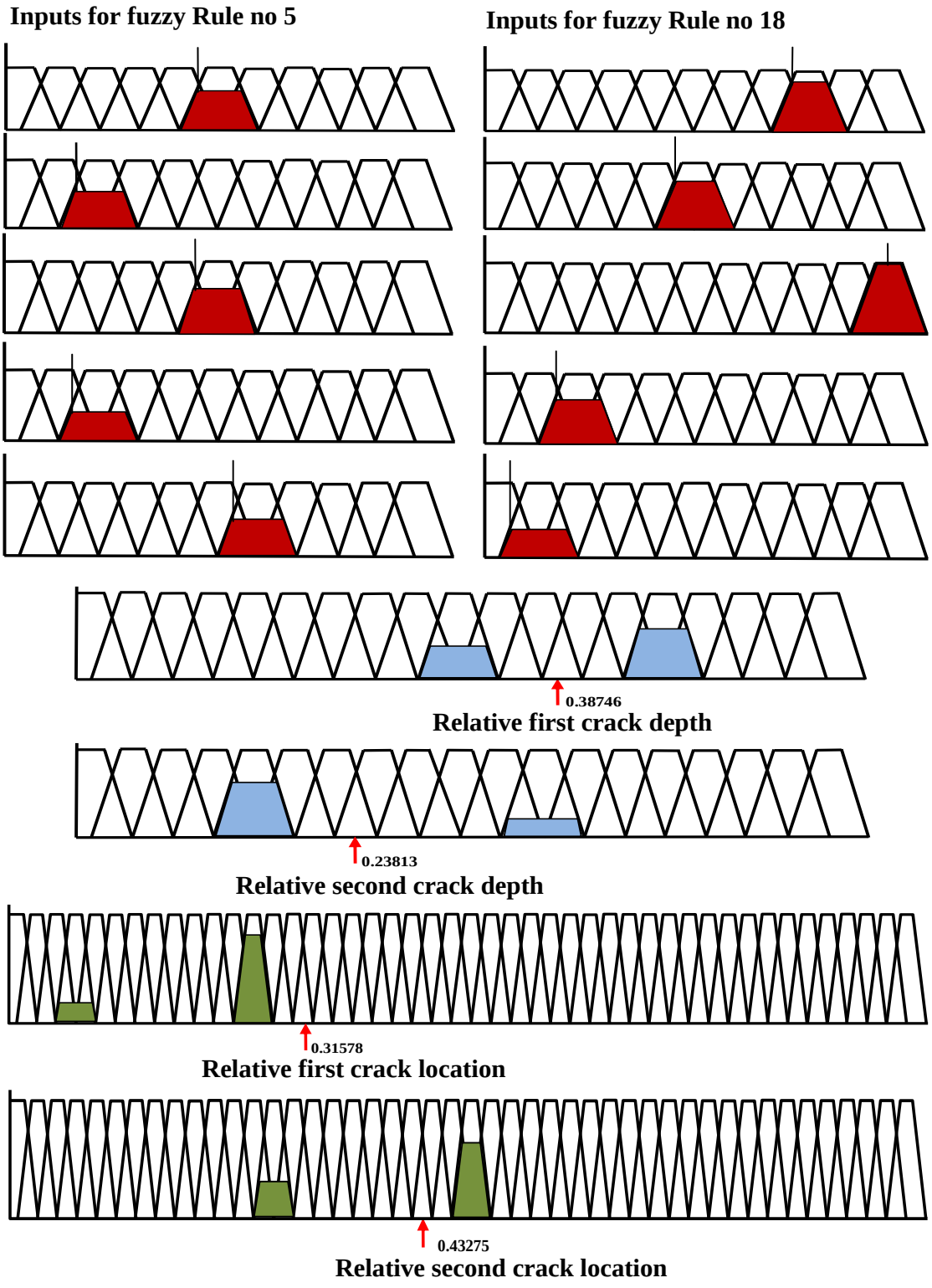

Figure 5.9: Resultant values of first and second relative crack depth and crack locations from trapezoidal membership function while activated the fuzzy rules no 5 and 18 of Table 5.2 for the rotor.

5.4 Analysis of Takagi-Sugeno Fuzzy Logic Mechanism for Identification of Crack in Rotor

In this segment, the Takagi-Sugeno fuzzy controller is used for identification of crack in cantilever rotor partially submerged in the viscous medium. The input and output variables are taken for T-S fuzzy controller system as similar as the Mamdani type fuzzy system. The Takagi-Sugeno method of fuzzy inference was introduced by the Takagi, sugeno and Kang [1985] to develop a systematic approach for producing fuzzy rules from a given input-output data set. In general, the structure of Takagi-Sugeno type fuzzy model is similar to the Mamdani type fuzzy model. The first order Takagi-Sugeno model has more degrees of freedom and hence the estimated capability is higher, with a more risk to over fit. The practice of minimum degrees of freedom is employed to control overfitting the problem. Zero-order Sugeno fuzzy is highly interpretable than the first-order Sugeno fuzzy model. Hence, the assortment of the Tagaki-Sugeno type model depend on the requirements of the problem and the probability to overfit the fuzzy system. For the n-dimensional input, m-dimensional output of the system, the rule of the T-S fuzzy inference system is described by the equation are as follows;

$$IF(y_1 \text{ is } \mathrm{P}_1^k) \text{ and} \ldots\ldots \text{and} (y_n \text{ is } \mathrm{P}_n^k) \text{ then } (u_1 \text{ is } \mathrm{Q}_1^k) \text{ and} \ldots. \text{ and} (u_m \text{is } \mathrm{Q}_m^k) \quad (5.9)$$

Where $y = (y_1, \ldots\ldots\ldots, y_n)$ are the input variables and $u = (u_1, \ldots.u_m)$ are the output variables, P_n^k are the set of fuzzy defined on the input variables and $Q_i^k \left(i = 1, \ldots., m\right)$ are fuzzy singletons defined on the output variables over the output variables u_i .When u is constant the resulting model is called as the Zero-order Sugeno fuzzy model. It can be viewed in the case of the Mamdani fuzzy logic system, in which a fuzzy singleton specifies each rule's consequent. Figure 5.10 represents the cognitive mechanism for zero-order Sugeno model. More specifically, the consequent part of this fuzzy simplified rule can be seen either as a singleton fuzzy set in the Mamdani model or as a constant output function in TS models. In this work, the membership functions have been verified based on the analysis of error (average error calculation). The three membership function (i.e. Triangular, Gaussian and Trapezoidal) employed in the zero-order Sugeno based models. Based on a set of K rules, the output of any unknown input vector y(0) is obtained by the following fuzzy cognitive formula:

$$\mu_k(Y) = \prod_{i=1}^{n} \mu_{jk}(y_i), \qquad \text{k=1,.....,K} \tag{5.10}$$

It is noted that while calculating the rule activation strength, the connective AND can be understood through changed T-norm operators: usually there is a choice between product and min operated. Here chosen the product operator as it keeps up more input statistics than the min operator and mostly provides a smoother output surface which is a required possession in any modeling application. Calculate the inferred outputs $\hat{u}_j$ by taking the weighted average of consequent values Q_j^k with respect to rule activation strength $\mu_k(y)$:

$$\hat{u}_j = \frac{\sum_{k}^{K} = 1^{\mu} k^{(y) q_{jk}}}{\sum_{k=1}^{K} \mu_k(y)}, \qquad \text{i=1,.....,m} \tag{5.11}$$

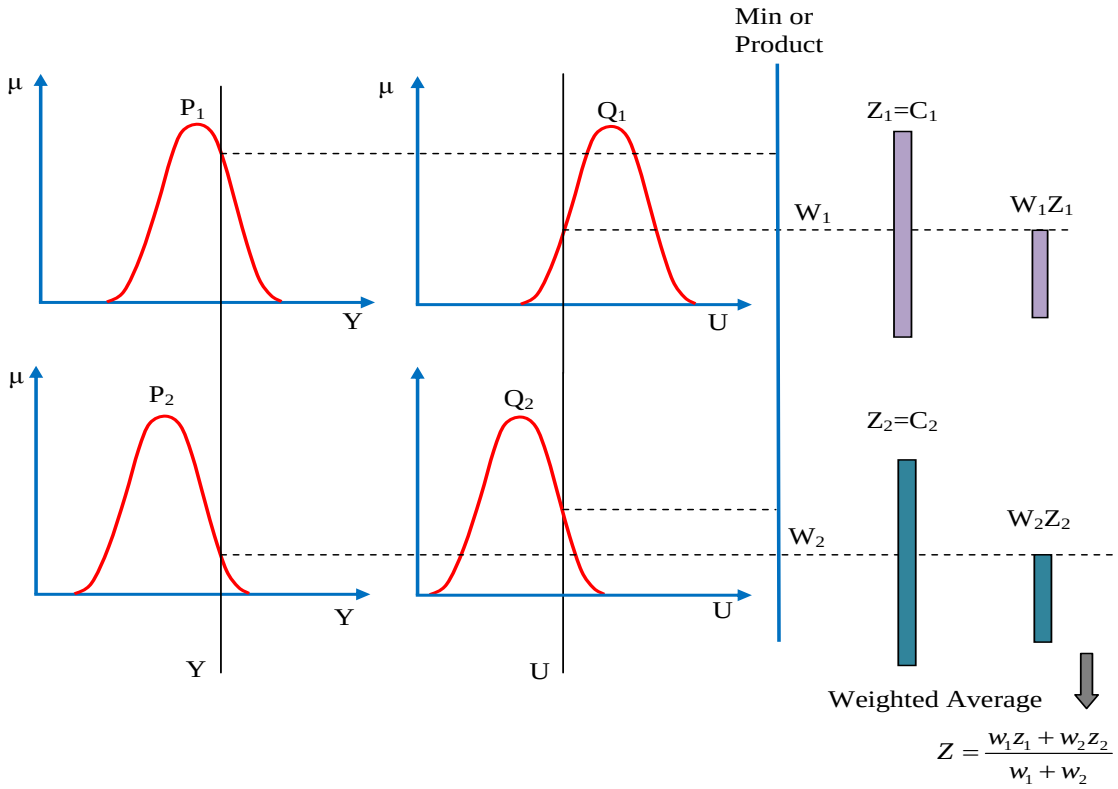

Figure 5.10: Zero-order T-S fuzzy logic system with two inputs and two rules [208].

5.5 Analysis of Hybrid Fuzzy Logic Mechanism for Identification of Multiple Crack in Rotor

This section introduces the mechanism of hybrid fuzzy controller for multiple crack identification in rotor partially submerged in the viscous fluid. To diagnose the locations and depths of multiple crack in rotor system, a novel fuzzy base hybrid model has been developed. Takagi-Sugeno type fuzzy models are more accurate than the Mamdani type fuzzy models, but they have much more parameters what sometimes might be a drawback. A hybrid approach has been offered to reduce the number of parameters and to maintain the prediction accuracy for the fault diagnosis. Figure 5.11 illustrates the structure of the hybrid fuzzy model.

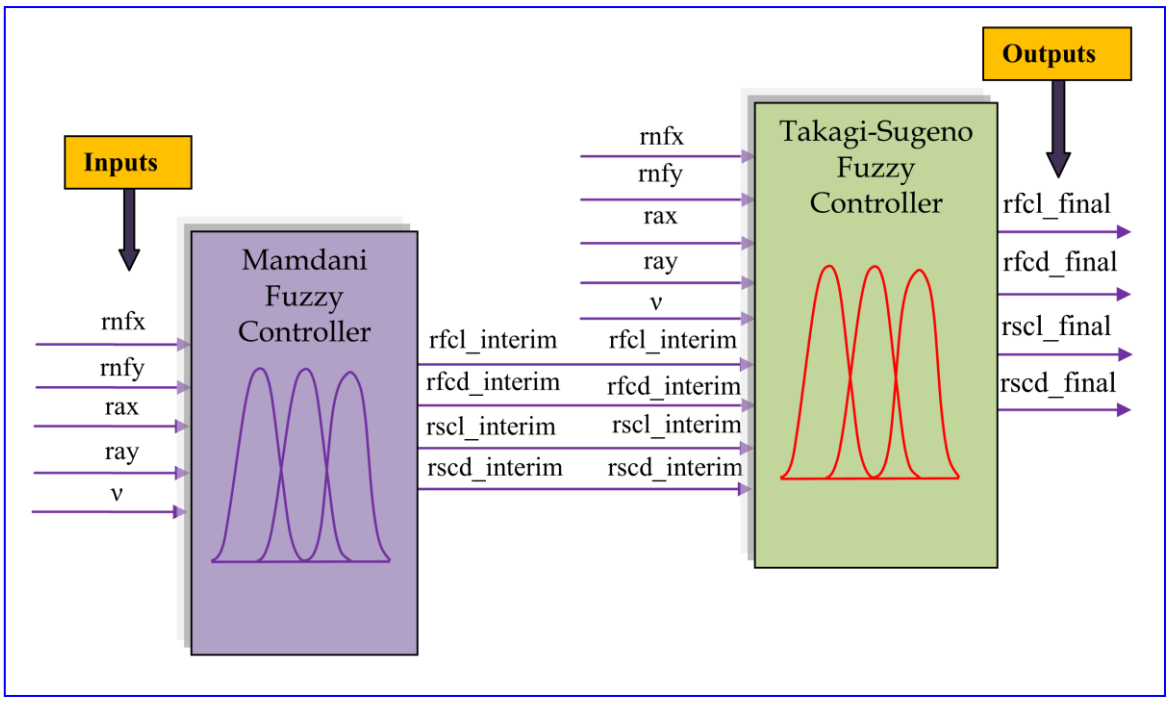

Figure 5.11: Hybrid fuzzy architecture for crack identification.

In this segment hybrid fuzzy model are designed by combination of Mamdani fuzzy and Takagi- Sugeno fuzzy system. The hybrid fuzzy controllers are trained by means of vibration characteristics which is extracted from the theoretical, experimental, and FE analysis. The first and second relative natural frequencies, first and second relative amplitude and viscosity of fluid are considered as an input parameters for hybrid fuzzy controller. Mamdani fuzzy controllers have given the output in the form of interim values (i.e. rfcl _interim, rfcd _interim, rscl_interim, rscd_interim). The Takagi-Sugeno fuzzy controller receives the interim outputs parameters from the Mamdani fuzzy controller

along with the two relative natural frequencies, two relative amplitude, and viscosity of fluid as inputs.Finally, the output parameters rfcl_final, rfcd_final, rscl_final, rscd_final are obtained from the hybrid fuzzy controller. The comparison of result obtained from the Mamdani fuzzy, Sugeno fuzzy, hybrid fuzzy and experimental analysis have been illustrated in Table 5.7 and the results are obtained to be in close agreement.

5.6 Results and Discussion

In this section analysis of results are carried out from developed Mamdani fuzzy, Takagi-Sugeno fuzzy and fuzzy based hybrid model to forcast the multiple crack locations and depths in cantilever rotor system partially immersed in the viscous fluid medium. The Mamdani and Takagi-Sugeno fuzzy model are used the triangular, gaussian and trapezoidal membership functions. The fuzzy based hybrid systems are active with the gaussian membership function. The proposed FL model with three different type of fuzzy membership function (i.e. Triangular, Gaussian and Trapezoidal) has been developed for the five input variable (two relative natural frequency, two relative amplitude and viscosity of fluid) and four output variables (first and second relative crack locations and depths). Figures 5.1(a), 5.1(b) and 5.1(c) illustrate the three type of membership function (Triangular, Gaussian and Trapezoidal) employed for the progress of the knowledge base system. The different stages incorporated in the fuzzy logic system are presented in Figure 5.2. Figures 5.3(a), 5.3(b) and 5.3(c) present the triangular, gaussian and trapezoidal membership function with linguistic term respectively. Tables 5.1 and 5.2 show the various linguistic term with range and twenty fuzzy rules used to train the fuzzy logic based crack identification system for rotor respectively. The complete structure of the Mamdani fuzzy system including three different type of membership function with the linguistic variable has been illustrated in Figures 5.4 to 5.6. The process of defuzzification for the Mamdani fuzzy model has been implemented using triangular, gaussian and trapezoidal membership functions with the help of activated rules 5 and 18 of Table 5.2 and presented in Figures 5.7 to 5.9. The obtained results from the developed Mamdani fuzzy models using triangular, gaussian and trapezoidal membership functions and experimental analysis have been compared in Table 5.3 for the rotor.Table 5.3 present the analysis result of the Mamdani fuzzy system. It has been observed that the Mamdani gaussian fuzzy gives the better results as compared to Mamdani triangular fuzzy and Mamdani trapazoidal fuzzy system. The illustrative view of mechanism of zero-order

Sugeno fuzzy model is presented in Figure 5.10. The comparison of results obtained from the implemented sugeno triangular fuzzy model, Sugeno gaussian fuzzy model, Sugeno trapezoidal fuzzy model and experimental analysis have been presented in Table 5.5. From the analysis of sugeno fuzzy model, it has been observed that the sugeno gaussain fuzzy gives the closer result as compared to sugeno trapezoidal fuzzy and sugeno triangular fuzzy model.Table 5.6 represents the comparison of results obtained from theoretical, experimental, FE analysis and Sugeno fuzzy gaussian model for the rotor. The hybrid fuzzy model is the combination of the Mamdani fuzzy and Sugeno fuzzy model with gaussian membership function has been implemented. Figure 5.11 represents the structure of the hybrid fuzzy controller. The obtained results from the developed hybrid fuzzy model with gaussian membership function and experimental analysis have been compared in Table 5.7 for the rotor. Table 5.7 represents the comparison of results obtained from Mamdani fuzzy, Sugeno fuzzy, hybrid fuzzy and experimental analysis for the rotor. It has been observed that the hybrid fuzzy model provides the better result as compared to Mamdani fuzzy and Sugeno fuzzy model.

Table 5.3: Comparison of the results obtained from Mamdani fuzzy gaussian, Mamdani fuzzy trapezoidal, Mamdani fuzzy triangular model and experimental analysis for the rotor.

Relative 1st frequency at x-axis direction 'rfnf'	Relative 2nd frequency at y-axis direction 'rsnf'	Relative 1st amplitude at x-axis direction 'rax'	Relative 2nd amplitude at y-axis direction 'ray'	Viscosity of fluid 'v'	Experimental relative				Mamdani Fuzzy Gaussian relative				Mamdani Fuzzy trapezoidal relative				Mamdani Fuzzy Triangular relative			
					1st crack location 'rfcl'	1st crack depth 'rfcd'	2nd crack location 'rscl'	2nd crack depth 'rscd'	1st crack location 'rfcl'	1st crack depth 'rfcd'	2nd crack location 'rscl'	2nd crack depth 'rscd'	1st crack location 'rfcl'	1st crack depth 'rfcd'	2nd crack location 'rscl'	2nd crack depth 'rscd'	1st crack location 'rfcl'	1st crack depth 'rfcd'	2nd crack location 'rscl'	2nd crack depth 'rscd'
					rfcl	rfcd	rscl	rscd	rfcl	rfcd	rscl	rscd	rfcl	rfcd	rscl	rscd	rfcl	rfcd	rscl	rscd
0.8735	0.7305	5.773	5.8122	0.0633	0.187	0.175	0.125	0.300	0.176	0.165	0.119	0.285	0.175	0.162	0.116	0.279	0.173	0.161	0.115	0.277
0.7804	0.6002	6.3111	6.4533	0.541	0.312	0.162	0.687	0.275	0.295	0.153	0.651	0.260	0.290	0.151	0.640	0.255	0.288	0.149	0.636	0.254
0.5777	0.4778	7.1679	6.6364	2.9	0.375	0.125	0.625	0.175	0.355	0.1185	0.592	0.166	0.348	0.116	0.583	0.145	0.347	0.115	0.578	0.161
0.8936	0.7843	5.6307	5.6839	0.0633	0.437	0.250	0.750	0.350	0.414	0.237	0.710	0.331	0.405	0.232	0.698	0.325	0.403	0.231	0.693	0.323
0.7893	0.6422	5.9889	6.1122	0.541	0.187	0.225	0.200	0.275	0.176	0.213	0.189	0.260	0.174	0.209	0.186	0.256	0.173	0.208	0.185	0.254
0.6181	0.4993	6.6179	7.0558	2.9	0.250	0.200	0.562	0.350	0.2369	0.189	0.531	0.331	0.232	0.186	0.523	0.327	0.231	0.185	0.520	0.323
0.8932	0.7385	6.7564	6.8083	0.0633	0.125	0.175	0.812	0.225	0.118	0.1659	0.768	0.213	0.116	0.162	0.756	0.209	0.115	0.161	0.751	0.208
0.7889	0.6067	7.4789	7.6605	0.541	0.625	0.150	0.875	0.325	0.198	0.1422	0.829	0.308	0.582	0.139	0.815	0.302	0.578	0.138	0.808	0.300
0.584	0.483	7.6496	7.3818	2.9	0.250	0.300	0.500	0.350	0.236	0.284	0.472	0.332	0.233	0.279	0.465	0.325	0.231	0.277	0.462	0.323
0.8739	0.7226	5.0186	5.0486	0.0633	0.500	0.225	0.750	0.275	0.4736	0.213	0.710	0.260	0.468	0.209	0.699	0.256	0.462	0.207	0.184	0.254
Average percentage of error									5.3	5.2	5.3	5.2	6.73	6.77	6.80	6.8	7.48	7.54	6.74	7.55
Total percentage of error									**5.25**				**6.77**				**7.32**			

Table 5.4: Comparison of the results obtained from fuzzy gaussian, FEA, theoretical and experimental analysis for the rotor.

Relative 1st frequency at x-axis direction 'rfnf'	Relative 2nd frequency at y-axis direction 'rsnf'	Relative 1st amplitude at x-axis direction 'rax'	Relative 2nd amplitude at y-axis direction 'ray'	Viscosity of fluid 'v'	Experimental relative				Mamdani Fuzzy Gaussian relative				FEA relative				Theoretical relative			
					1st crack location 'rfcl'				1st crack location 'rfcl'				1st crack location 'rfcl'				1st crack location 'rfcl'			
					1st crack depth 'rfcd'				1st crack depth 'rfcd'				1st crack depth 'rfcd'				1st crack depth 'rfcd'			
					2nd crack location 'rscl'				2nd crack location 'rscl'				2nd crack location 'rscl'				2nd crack location 'rscl'			
					2nd crack depth 'rscd'				2nd crack depth 'rscd'				2nd crack depth 'rscd'				2nd crack depth 'rscd'			
					rfcl	rfcd	rscl	rscd	rfcl	rfcd	rscl	rscd	rfcl	rfcd	rscl	rscd	rfcl	rfcd	rscl	rscd
0.8735	0.7305	5.773	5.8122	0.0633	0.187	0.175	0.125	0.300	0.176	0.165	0.119	0.285	0.181	0.172	0.122	0.294	0.179	0.165	0.118	0.292
0.7804	0.6002	6.3111	6.4533	0.541	0.312	0.162	0.687	0.275	0.295	0.153	0.651	0.260	0.302	0.158	0.671	0.271	0.296	0.155	0.643	0.261
0.5777	0.4778	7.1679	6.6364	2.9	0.375	0.125	0.625	0.175	0.355	0.1185	0.592	0.166	0.367	0.123	0.605	0.172	0.356	0.119	0.593	0.166
0.8936	0.7843	5.6307	5.6839	0.0633	0.437	0.250	0.750	0.350	0.414	0.237	0.710	0.331	0.432	0.246	0.733	0.342	0.41	0.238	0.718	0.34
0.7893	0.6422	5.9889	6.1122	0.541	0.187	0.225	0.200	0.275	0.176	0.213	0.189	0.260	0.183	0.219	0.195	0.267	0.175	0.214	0.191	0.262
0.6181	0.4993	6.6179	7.0558	2.9	0.250	0.200	0.562	0.350	0.2369	0.189	0.531	0.331	0.245	0.194	0.555	0.342	0.237	0.191	0.532	0.331
0.8932	0.7385	6.7564	6.8083	0.0633	0.125	0.175	0.812	0.225	0.118	0.1659	0.768	0.213	0.121	0.171	0.792	0.219	0.121	0.167	0.768	0.21
0.7889	0.6067	7.4789	7.6605	0.541	0.625	0.150	0.875	0.325	0.198	0.1422	0.829	0.308	0.612	0.146	0.853	0.317	0.612	0.142	0.854	0.314
0.584	0.483	7.6496	7.3818	2.9	0.250	0.300	0.500	0.350	0.236	0.284	0.472	0.332	0.243	0.292	0.489	0.341	0.236	0.281	0.474	0.331
0.8739	0.7226	5.0186	5.0486	0.0633	0.500	0.225	0.750	0.275	0.4736	0.213	0.710	0.260	0.484	0.216	0.726	0.266	0.479	0.212	0.711	0.258
Average percentage of error									5.3	5.2	5.3	5.2	2.51	2.47	2.43	2.36	4.73	5.1	4.94	4.76
Total percentage of error									**5.25**				**2.44**				**4.89**			

Table 5.5:Comparison of the results obtained from Sugeno fuzzy gaussian, Sugeno fuzzy trapezoidal, Sugeno fuzzy triangular model and experimental analysis for the rotor.

Relative 1st frequency at x-axis direction 'rfnf'	Relative 2nd frequency at y-axis direction 'rsnf'	Relative 1st amplitude at x-axis direction 'rax'	Relative 2nd amplitude at y-axis direction 'ray'	Viscosity of fluid 'v'	Experimental relative 1st crack location 'rfcl'				Sugeno Fuzzy Gaussian relative 1st crack location 'rfcl' 1st crack depth 'rfcd' 2nd crack location 'rscl' 2nd crack depth 'rscd'				Sugeno Fuzzy trapezoidal relative 1st crack location 'rfcl' 1st crack depth 'rfcd' 2nd crack location 'rscl' 2nd crack depth 'rscd'				Sugeno Fuzzy Triangular relative 1st crack location 'rfcl' 1st crack depth 'rfcd' 2nd crack location 'rscl' 2nd crack depth 'rscd'			
					rfcl	rfcd	rscl	rscd	rfcl	rfcd	rscl	rscd	rfcl	rfcd	rscl	rscd	rfcl	rfcd	rscl	rscd
0.8735	0.7305	5.773	5.8122	0.0633	0.187	0.175	0.125	0.300	0.178	0.168	0.117	0.282	0.172	0.167	0.116	0.275	0.172	0.165	0.119	0.279
0.7804	0.6002	6.3111	6.4533	0.541	0.312	0.162	0.687	0.275	0.299	0.154	0.649	0.266	0.293	0.154	0.656	0.265	0.291	0.152	0.643	0.255
0.5777	0.4778	7.1679	6.6364	2.9	0.375	0.125	0.625	0.175	0.352	0.12	0.599	0.169	0.362	0.118	0.581	0.167	0.359	0.115	0.581	0.162
0.8936	0.7843	5.6307	5.6839	0.0633	0.437	0.250	0.750	0.350	0.415	0.239	0.711	0.333	0.406	0.233	0.718	0.329	0.411	0.227	0.703	0.323
0.7893	0.6422	5.9889	6.1122	0.541	0.187	0.225	0.200	0.275	0.176	0.216	0.189	0.259	0.179	0.208	0.185	0.262	0.178	0.209	0.187	0.246
0.6181	0.4993	6.6179	7.0558	2.9	0.250	0.200	0.562	0.350	0.235	0.189	0.538	0.331	0.237	0.188	0.515	0.327	0.231	0.187	0.533	0.327
0.8932	0.7385	6.7564	6.8083	0.0633	0.125	0.175	0.812	0.225	0.119	0.169	0.794	0.213	0.116	0.165	0.776	0.212	0.111	0.162	0.762	0.208
0.7889	0.6067	7.4789	7.6605	0.541	0.625	0.150	0.875	0.325	0.588	0.141	0.829	0.307	0.581	0.138	0.836	0.302	0.594	0.138	0.819	0.302
0.584	0.483	7.6496	7.3818	2.9	0.250	0.300	0.500	0.350	0.233	0.284	0.479	0.328	0.229	0.282	0.469	0.331	0.231	0.281	0.465	0.324
0.8739	0.7226	5.0186	5.0486	0.0633	0.500	0.225	0.750	0.275	0.485	0.209	0.709	0.261	0.474	0.207	0.703	0.255	0.465	0.207	0.687	0.258
Average percentage of error					5.25	4.87	4.82	5.1	6.19	6.32	6.02	5.94	6.81	7.24	6.41	7.47				
Total percentage of error					**5.01**				**6.12**				**6.98**							

Table 5.6: Comparison of the results obtained from Sugeno fuzzy, FEA, theoretical and experimental analysis for the rotor.

Relative 1st frequency at x-axis direction 'rfnf'	Relative 2nd frequency at y-axis direction 'rsnf'	Relative 1st amplitude at x-axis direction 'rax'	Relative 2nd amplitude at y-axis direction 'ray'	Viscosity of fluid 'v'	Experimental relative				Sugeno fuzzy relative				FEA relative				Theoretical relative			
					1st crack location 'rfcl'	1st crack depth 'rfcd'	2nd crack location 'rscl'	2nd crack depth 'rscd'	1st crack location 'rfcl'	1st crack depth 'rfcd'	2nd crack location 'rscl'	2nd crack depth 'rscd'	1st crack location 'rfcl'	1st crack depth 'rfcd'	2nd crack location 'rscl'	2nd crack depth 'rscd'	1st crack location 'rfcl'	1st crack depth 'rfcd'	2nd crack location 'rscl'	2nd crack depth 'rscd'
					rfcl	rfcd	rscl	rscd	rfcl	rfcd	rscl	rscd	rfcl	rfcd	rscl	rscd	rfcl	rfcd	rscl	rscd
0.8735	0.7305	5.773	5.8122	0.0633	0.187	0.175	0.125	0.300	0.178	0.168	0.117	0.282	0.181	0.172	0.122	0.294	0.179	0.165	0.118	0.292
0.7804	0.6002	6.3111	6.4533	0.541	0.312	0.162	0.687	0.275	0.299	0.154	0.649	0.266	0.302	0.158	0.671	0.271	0.296	0.155	0.643	0.261
0.5777	0.4778	7.1679	6.6364	2.9	0.375	0.125	0.625	0.175	0.352	0.12	0.599	0.169	0.367	0.123	0.605	0.172	0.356	0.119	0.593	0.166
0.8936	0.7843	5.6307	5.6839	0.0633	0.437	0.250	0.750	0.350	0.415	0.239	0.711	0.333	0.432	0.246	0.733	0.342	0.41	0.238	0.718	0.34
0.7893	0.6422	5.9889	6.1122	0.541	0.187	0.225	0.200	0.275	0.176	0.216	0.189	0.259	0.183	0.219	0.195	0.267	0.175	0.214	0.191	0.262
0.6181	0.4993	6.6179	7.0558	2.9	0.250	0.200	0.562	0.350	0.235	0.189	0.538	0.331	0.245	0.194	0.555	0.342	0.237	0.191	0.532	0.331
0.8932	0.7385	6.7564	6.8083	0.0633	0.125	0.175	0.812	0.225	0.119	0.169	0.794	0.213	0.121	0.171	0.792	0.219	0.121	0.167	0.768	0.21
0.7889	0.6067	7.4789	7.6605	0.541	0.625	0.150	0.875	0.325	0.588	0.141	0.829	0.307	0.612	0.146	0.853	0.317	0.612	0.142	0.854	0.314
0.584	0.483	7.6496	7.3818	2.9	0.250	0.300	0.500	0.350	0.233	0.284	0.479	0.328	0.243	0.292	0.489	0.341	0.236	0.281	0.474	0.331
0.8739	0.7226	5.0186	5.0486	0.0633	0.500	0.225	0.750	0.275	0.485	0.209	0.709	0.261	0.484	0.216	0.726	0.266	0.479	0.212	0.711	0.258
Average percentage of error									5.25	4.87	4.82	5.1	2.51	2.47	2.43	2.36	4.73	5.1	4.94	4.76
Total percentage of error									**5.01**				**2.44**				**4.89**			

Table 5.7: Comparison of the results obtained from Mamdani fuzzy, Sugeno fuzzy, Hybrid fuzzy model and experimental analysis for the rotor

Relative 1st frequency at x-axis direction 'rfnf'	Relative 2nd frequency at y-axis direction 'rsnf'	Relative 1st amplitude at x-axis direction 'rax'	Relative 2nd amplitude at y-axis direction 'ray'	Viscosity of fluid 'v'	Experimental relative				Mamdani fuzzy relative				Sugeno fuzzy relative				Hybrid fuzzy relative			
					1st crack location 'rfcl'	1st crack depth 'rfcd'	2nd crack location 'rscl'	2nd crack depth 'rscd'	1st crack location 'rfcl'	1st crack depth 'rfcd'	2nd crack location 'rscl'	2nd crack depth 'rscd'	1st crack location 'rfcl'	1st crack depth 'rfcd'	2nd crack location 'rscl'	2nd crack depth 'rscd'	1st crack location 'rfcl'	1st crack depth 'rfcd'	2nd crack location 'rscl'	2nd crack depth 'rscd'
					rfcl	rfcd	rscl	rscd	rfcl	rfcd	rscl	rscd	rfcl	rfcd	rscl	rscd	rfcl	rfcd	rscl	rscd
0.8735	0.7305	5.773	5.8122	0.0633	0.187	0.175	0.125	0.300	0.176	0.165	0.119	0.285	0.178	0.168	0.117	0.282	0.178	0.166	0.119	0.291
0.7804	0.6002	6.3111	6.4533	0.541	0.312	0.162	0.687	0.275	0.295	0.153	0.651	0.260	0.299	0.154	0.649	0.266	0.295	0.154	0.644	0.262
0.5777	0.4778	7.1679	6.6364	2.9	0.375	0.125	0.625	0.175	0.355	0.1185	0.592	0.166	0.352	0.12	0.599	0.169	0.364	0.118	0.594	0.165
0.8936	0.7843	5.6307	5.6839	0.0633	0.437	0.250	0.750	0.350	0.414	0.237	0.710	0.331	0.415	0.239	0.711	0.333	0.421	0.235	0.719	0.341
0.7893	0.6422	5.9889	6.1122	0.541	0.187	0.225	0.200	0.275	0.176	0.213	0.189	0.260	0.176	0.216	0.189	0.259	0.175	0.213	0.192	0.265
0.6181	0.4993	6.6179	7.0558	2.9	0.250	0.200	0.562	0.350	0.2369	0.189	0.531	0.331	0.235	0.189	0.538	0.331	0.234	0.192	0.533	0.331
0.8932	0.7385	6.7564	6.8083	0.0633	0.125	0.175	0.812	0.225	0.118	0.1659	0.768	0.213	0.119	0.169	0.794	0.213	0.122	0.165	0.765	0.213
0.7889	0.6067	7.4789	7.6605	0.541	0.625	0.150	0.875	0.325	0.198	0.1422	0.829	0.308	0.588	0.141	0.829	0.307	0.613	0.143	0.853	0.311
0.584	0.483	7.6496	7.3818	2.9	0.250	0.300	0.500	0.350	0.236	0.284	0.472	0.332	0.233	0.284	0.479	0.328	0.237	0.282	0.473	0.331
0.8739	0.7226	5.0186	5.0486	0.0633	0.500	0.225	0.750	0.275	0.4736	0.213	0.710	0.260	0.485	0.209	0.709	0.261	0.478	0.213	0.712	0.252
Average percentage of error					5.3	5.2	5.3	5.2	5.25	4.87	4.82	5.1	4.35	5.27	4.8	4.85				
Total percentage of error					**5.25**				**5.01**				**4.82**							

5.7 Summary

The Mamdani fuzzy, Takagi-Sugeno fuzzy and hybrid fuzzy approaches are implemented in the present analysis.The following summary can be drawn by considering the results derived from Mamdani fuzzy, Sugeno fuzzy and hybrid fuzzy models.The two relative natural frequencies, two relative amplitude and viscosity of fluid are considered as input parameters and two relative crack locations, two relative crack depths are taken as the output parameters for proposed fuzzy models. The result derived from the developed Mamdani fuzzy model, Sugeno fuzzy model and hybrid fuzzy model have been compared with experimental test results to authenticate the effectiveness of proposed fuzzy models. The total percentage of error of the obtained result of the Mamdani triangular fuzzy model is 7.32%, for the Mamdani gaussian fuzzy model is 5.25% and for the Mamdani trapezoidal fuzzy model is 6.77%. From the analysis result of takagi-sugeno fuzzy model, It has been observed that the error of the percentage of the obtained result of the Sugeno triangular fuzzy model is 6.98%, for the sugeno gaussian fuzzy model is 5.01% and for the sugeno trapezoidal fuzzy model is 6.12%.The results found to be good in agreement. Based on above study, it is found that fuzzy model with gaussian membership function gives better results as comparison to triangular and trapezoidal models for both Mamdani and takagi-sugeno fuzzy model. Therefore, the developed gaussian membership fuzzy controller can be efficiently used as fault diagnosis tools in dynamically analysis of rotor. The fuzzy based hybrid model gives more precise result as compared to Mamdani fuzzy and Sugeno fuzzy. It is found that total percentage of error for hybrid fuzzy model is 4.82 %.

Chapter 6

Analysis of Hybrid BPNN-RBFNN Neural Network for Identification of Multiple Crack in Cantilever Rotor Partially Submerged in the Viscous Medium

The presence of damage is a serious threat to proper functioning of structures and machines. Early detection of damage now has become the subject of serious concern for the researchers to secure the performance of systems. The efficient structural fault diagnosis methodology can be a valuable technique for proper identification of crack and worsening in engineering or industrial structural members. Since the last few years, many techniques have been applied to identify the fault in the engineering system. Few of them have used the sensors (Radiograph, Magnetic field, eddy current and thermal fields) to identify damage and others based on visual method (Dye penetration method). These methods consume much time to seize the fault in the system. Since last few years, some mathematical models and experimental investigations have been proposed by the researchers to determine the crack initiation and propagation. In the current chapter, intelligent techniques have been applied based on artificial network techniques to locate the multiple crack, present in the rotor which is rotates in the viscous fluid medium. The Back Propagation Neural Network (BPNN) and Radial Basis Function Neural Network (RBFNN) have been used in the present study. Finally, the obtained results from the proposed neural network model are validated with results of experimental analysis and show a very well agreement.

6.1 Introduction

The present chapter, proposed an introduction of basic design and development of neural network controller and learning rule. In a human body, the biological neural network has a

systematized set of neurons, assist for several kinds of output (i.e. breathing, thinking etc.) The Artificial Neural Networks (ANNs) are simplified models of the biological central nervous system. ANN is a massively parallel distributed information processing system made up of highly interconnected neural computing elements that have the ability to learn and thereby acquire knowledge and make it available for use. Neural network can be used to distinguish patterns and recognize trends that are more difficult to be remarked by the humans being or other computer system. Many researchers believe neural models offer a most promising integrated approach to build truly intelligent computer system. The biological network able to process millions of input stimuli in milisec even through the process is electrochemical in nature and, therefore, propagates relatively at slow milisec rate. Some of its properties of neural network are outlined below;

a) Self-Organization: Neural network can acquire outcomes for inputs that are not used during training by producing its specific depiction of the information it obtains during learning time. This ability benefits in resolving the higher level complicated problem.

b) Adaptive learning: The neural network system has the ability to control the altering of the environment by regulating the synaptic weights and execute as per the condition. This features of the neural network system can be applied for industrial applications in non- stationary environment.

c) Real time operation: This feature of the neural network is to compile maximum number connected neurons employed in parallel to resolve a particular problem. Neural networks learn by example. For this particular hardware devices are manufactured which takes advantages of this ability.

d) Non-linearity: Artificial neural networks (ANNs) have ability to solve the non-linear problems. This capability is tremendously used in the field of structural health monitoring as the signals from multifaceted structures with inconstant loading.

e) Input-Output mapping: This is the very influential feature of the artificial neural network which includes controlled learning. The network efforts to associate a single input signal with a desire response. It revises the synaptic weights by a learning process in order to achieve the desired response.

f) Fault Tolerance: Neural network is integrally fault tolerant. In case of failure of neuron in neural network system there will be a partial damage of the network system which leads to only weakening the excellence of output instead of crumpling the entire system.

Since last few decades, many researchers have developed a health monitoring algorithm for the structural elements. The development of structural health monitoring techniques is a significant achievement of science fraternity because the existence of crack decreases the service life of the structural element and accountable for commercial damage and in few cases may be loss of human life. The various non-destructive techniques are available in the literature for predicting the structural damage, that is not efficient in term of correctness and computation time for real problems. Moreover the development of mathematical model for the complicated problems is almost impossible. In the present analysis, application of ANN with adaptive learning, self-organization capacity, real time operation, fault tolerance ability and pattern recognition capability are suitable for design of an automated intelligent system. It is capable for fault recognition with very high accuracy and less are computation time for faulty dynamic structure. In the present scenario various scientist continuously engaged for developing a damage detection tool using ANNs.In this section, three types of ANNs have been discussed (i.e. BPNN and RBFNN). All two types of ANNs are designed for five input variables (relative first and second natural frequencies & relative first and second amplitde and viscosity of fluid) and four output variables (relative first and second crack location and relative first and second crack depth). A comparison of results obtained from all three ANN models with results obtained from theoretical, numerical and experimental is done in current chapter. The RBFNN gives the best results as compared to other discussed ANNs models. Experimental investigation authenticates the fidelity of neural models.Therefore, it is decided that the proposed method can be effectively using for multiple crack identification. The current chapter has been organized into six different segments. Section 6.1 presents the introduction part of neural network technique. The analysis of the ANN model used for identification of multiple crack have been discussed in section 6.2. The representation of complete view of the BPNN is presented in section 6.3. The representation of complete view of the RBFNN is presented in section 6.4. The results and discussions of the results obtained from BPNN and RBFNN model have been discussed in section 6.5. Finally the summary of the complete chapter described in section 6.6.

6.2 Artificial Neural Network Technique

ANNs are computational parallel distributed information processing system. It is therefore effectively applied in many industrial applications such as fault diagnosis control & optimization, industrial process, and sale forecasting, etc. The ability to work under challenging environment and parallel computing ability make ANNs most efficient and robust to solve the problem easily unlike using analytical methods.

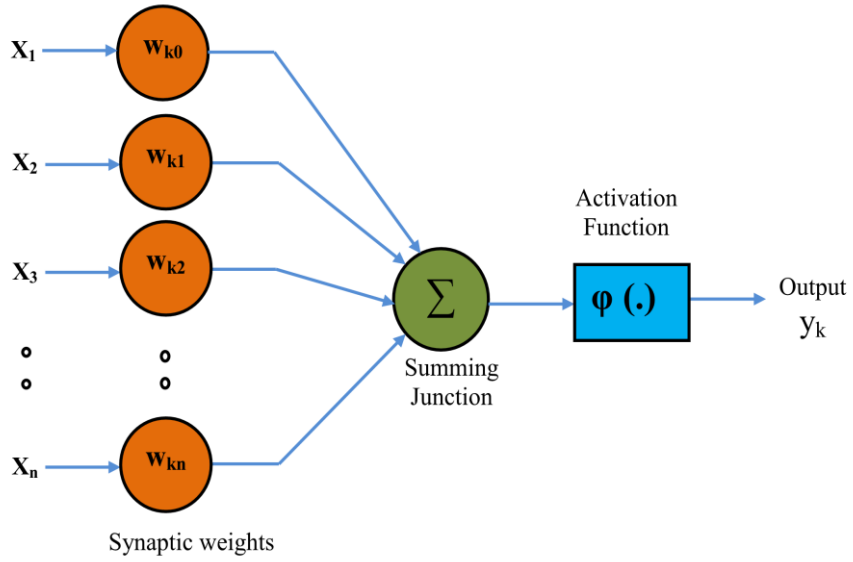

Figure 6.1: Model of neuron of artificial neural network

The important features of the ANN are described below.

(1) The input variables with synaptic weights are assigned to train neuron that turn upset the decision-making capacity of ANN. The inputs to the neuron with synaptic weight are also called weighted inputs.

(2) These weighted inputs are then summed together in summing point and if they exceed with pre-set threshold value, the neuron fires. Moreover, for any other cases neuron does not fire.

(3) For limiting the output of neuron, an activation function is provided. The most popular activation function is sigmoidal. Mostly the normalized amplitude range of the output of a neuron is given as closed unit interval [0, 1] or [-1, 1].

6.2.1 Learning Paradigms of Artificial Neural Network

The learning process of Artificial neural network is a mathematical logic which develops the performance of ANNs and frequently this rule is applied repeatedly over the network. The learning rule may accept the weights and bias of network and will compare the actual result and predicted result of network to provide better values for weights and bias. The learning rule of ANN is mainly divided into three categories;

a) Supervised learning: In this type of learning process type if the desired output for the network is also delivered with the input while training the network. An input and output pair are given the neural network and it is possible to calculate an error based on its target output and actual output. This error is used to make adjustment to the network by bring up to date its weights.

b) Unsupervised learning: In this learning process the neural network is only given a set of inputs and network's concern to find some kind of arrangement within the inputs provided without any outward assistance.

c) Reinforcement learning: Reinforcement learning is related to supervised learning in that some feedback is given, though in its place of given that a target output a reward is given based on how sound the system performed. The intention of reinforcement learning process is to make the most of the reward the system accepts through trial-and-error.

Mathematically, neuron q can be described through the following equations:

$$u_q = \sum_{j=1}^{x} w_{qj} k_j \tag{6.1}$$

$$y_q = g\left(u_q\right) \tag{6.2}$$

Where: k_1, k_2... k_x are the input signals; w_{q1}, w_{q2}... w_{qx} are the synaptic weights of neuron *q;* y_q is the output signal of the neuron; $g(\cdot)$ is the activation and u_q is the linear combined output.

6.3 Analysis of Feed Forward Back Propagation Neural Network Controller used for Multiple Crack Identification in Rotor

The proposed multilayer feed forward neural network controller trained by back-propagation algorithm has been built for the prediction of relative crack depth and relative crack location of the cantilever rotor partially submerged in the viscous medium. (Figure 6.3.). The neural network has got five input parameters (two relative natural frequency in x and y-axis directions, two relative amplitude in x and y- axis directions and viscosity of fluid) and four output parameters (first and second relative crack location and depths).Five input parameters have been taken from the experimental results.

6.3.1 Learning Back Propagation Technique

The feed forward multilayer neural network has been trained using the back propagation technique (Figure 6.2). The backpropagation technique is based on delta learning rule in which the synaptic weight modification is ended by the mean square error of the output value to the input value. This technique computes the loss function gradient for all the weights in the network. The gradient is supplied to the optimization method which uses it to bring up to date the synaptic weights, in an order to reduce the loss function. To computes the gradient of a loss function, backpropagation requires a known and desired output for each input value. Each hidden layer error in an opposite way towards the propagate movement by the network to be calculated and supply to the network using back propagation algorithm to reduce the error in the actual output value and desired output value. It is considered as a supervised learning method while it is also used in some unsupervised networks such as auto-encoders.

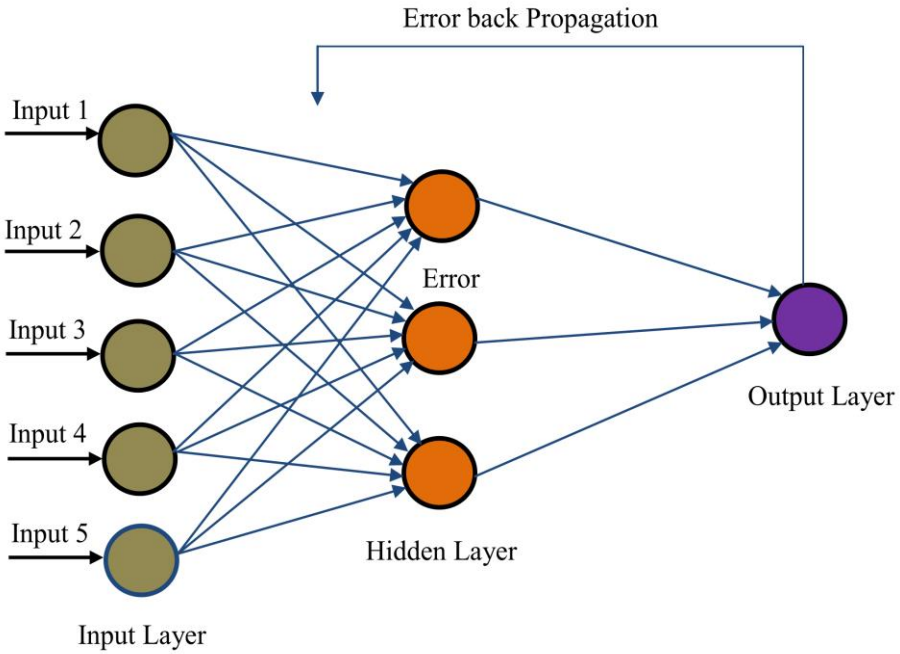

Figure 6.2: Back propagation Technique

6.3.2 Neural Controller Mechanism

A back propagation neural network has been designed for identification of multiple crack of cantilever rotor partially submerged in the viscous fluid. The BPNN model has been designed for five input and four output parameters. The input variables to the neural model are: 'rnfx', 'rnfy', 'rax', 'ray', and 'ν'. The output variables of BPNN model are: 'rfcl', 'rfcd', 'rscl' and 'rscd'. The BPNN model is made with one input layer, seven hidden layers and one output layer. The input and output layer contain five and four neurons respectively. The input layer neurons represent the relative first & second natural frequencies, first & second amplitude and viscosity of fluid. Similarly, output layer neurons represent first & second relative crack location and first & second crack depth in cantilever rotor.

The first hidden layer has 16 neurons, the second hidden layer has 50 neurons, the third hidden layer has 150 neurons, the fourth hidden layer has 300 neurons, the fifth hidden layer has 150 neurons, the sixth hidden layer has 86 neurons and the seventh hidden layer has 24 neurons. In the present investigation the number of hidden layers are framed and the number of neurons in each layer are chosen experimentally. Several neural networks with the different number of hidden layers and hidden neurons and the performance are measured for networks using cross-validation on the basis of above

experimentation is chosen. In current research, considered 1410 samples for training and testing. Out of which 900 are used for training and 510 are used for testing. Out of 900 training data 300(theoretical), 300(FEM analysis) and 300(experimentally) are used. Figure 6.3 represents multiple layers back propagation neural network architecture for identification of multiple crack. The neural network is trained with 900 patterns representing typical scenarios, some of which are illustrated in Table 6.1.

μ = Momentum coefficient (i.e. 0.2);

η = Learning rate (i.e. 0.35);

Network topology 5-16-50-150-300-150-86-24-4

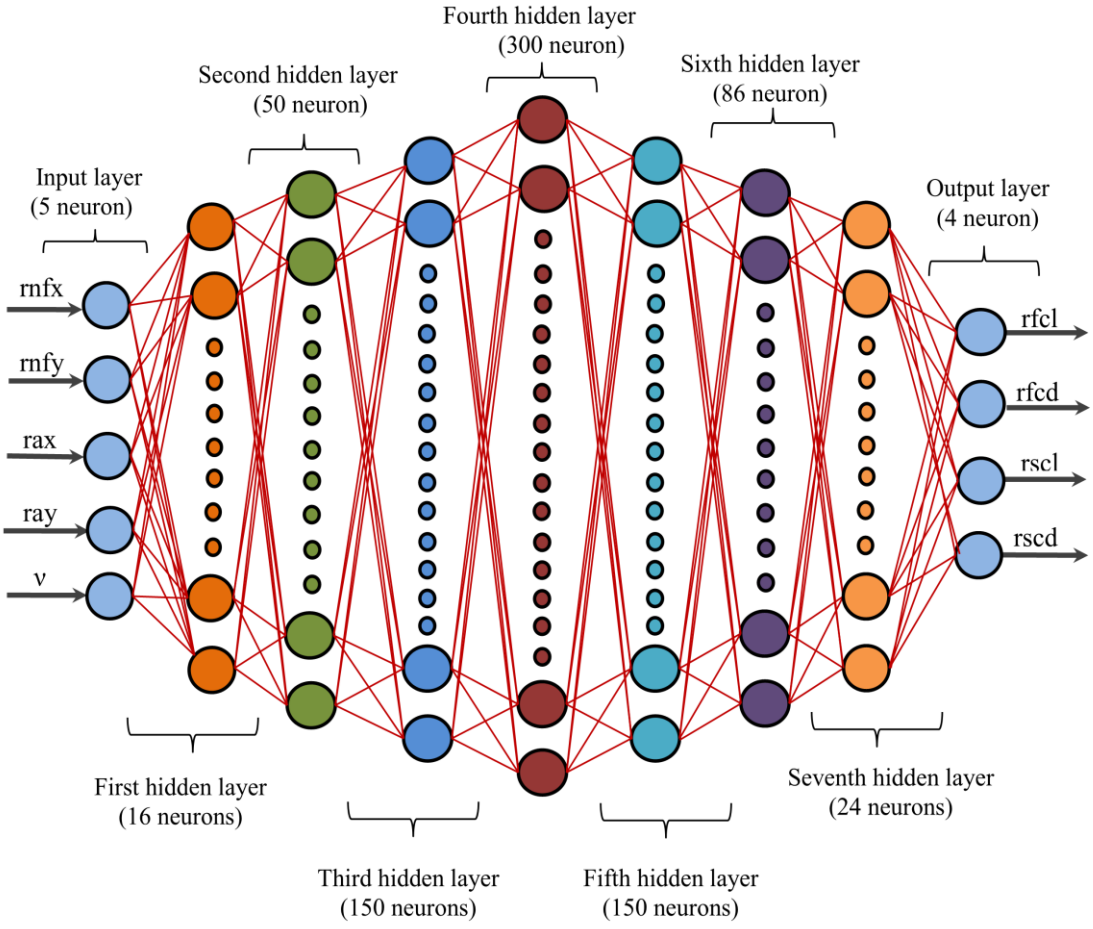

Figure 6.3: Multi-layer feed forward back propagation neural network model for crack identification

ψ_1= deviation in natural frequency in x-axis direction.

ψ_2= deviation in natural frequency in y- axis direction.

ψ_3= deviation in amplitude in x-axis direction.

ψ_4=deviation in amplitude in y-axis direction.

ψ_5=deviation in viscosity of fluid.

The output of BPNN due to sharing of input layer neuron to hidden layer neuron are given by [163];

$$f\left(z_j^{(L)}\right)=\psi_{\mathrm{i}}^{\mathrm{L}} \tag{6.3}$$

Where: $z_j^{(L)}=\sum_i W_{ji}^{(L)}.\psi_{\mathrm{i}}^{(\mathrm{L}\text{-}1)}$, (6.4)

Layer number (2 or 8) = L

j^{th} neuron in hidden layer labeled as 'L'= j

i^{th} neuron in hidden layer labeled as 'L-1'=i

$W_{ji}^{(L)}$= Weight of connection from 'i' neuron in layer 'L-1' to j neuron in layer 'L'

The activation function taken as;

$$f(x)=\frac{e^{x}-e^{-x}}{e^{x}+e^{-x}} \tag{6.5}$$

In the training process output of the neural network $\Phi_{actual,\,n}\left(i=1\ to\ 4\right)$ may be differ from actual output $\Phi_{desired,\,n}\left(i=1\ to\ 4\right)$ as presented in training pattern of neural network. The measure of the performance of neural network is instantaneous sum-squared difference between $\Phi_{actual,\,n}$ and $\Phi_{desired,\,n}$ for the set of given training patterns.

$$E_{error}=\frac{1}{2}\sum_{\substack{all\ training\\ pattern}}\left(\Phi_{desired,\,n}-\Phi_{actual,\,n}\right)^2 \tag{6.6}$$

Where;

Relative first crack location (rfcl) is represented by parameter $\Phi_{actual,\,n(n=1)}$

Relative second crack location (rscl) is represented by parameter $\Phi_{actual,\,n(n=2)}$

Relative first crack depth (rfcd) is represented by parameter $\Phi_{actual,\,n(n=3)}$

Relative second crack depth (rscd) is represented by parameter $\Phi_{actual,\,n(n=4)}$

Feed forward back propagation model, error back propagation method is applied to train the network [163]. This model calculates local error gradients to evaluate suitable rectifications to reduce error. The error gradient for output layer is;

$$\Delta^{(7)}=f\left(z_1^7\right)\left(\Phi_{desired,\,n}-\Phi_{actual,\,n}\right) \tag{6.7}$$

Hence local gradients for hidden layer (L) neuron is represented by;

$$\Delta_j^{(L)} = f'\left(z_J^{(L)}\right)\left(\sum_k \Delta_k^{(L+1)}\ W_{kj}^{(L+1)}\right) \tag{6.8}$$

The weights are modified as per the following terms;

$$W_{ji}(\varphi+1) = W_{ji}(\varphi) + \delta W_{ji}(\varphi+1) \tag{6.9}$$

$$\delta W_{ji}(\varphi+1) = \alpha\delta W_{ji}(\varphi) + \eta\delta W_{ji}(\varphi) + \eta\Delta_j^L \psi_{\mathrm{j}}^{(\mathrm{L}\text{-}1)} \tag{6.10}$$

Where α (momentum co-efficient) = 0.2 (chosen statically)

η (learning rate) = 0.35 (chosen statically)

φ = iteration number

The final output of the feed forward back propagation can be expressed as;

$$\Phi_{actual,\,n} = f\left(z_n^9\right) \tag{6.11}$$

Where $\left(z_n^9\right) = \sum_i W_{ni}^9\ \psi_{\mathrm{i}}^8$

6.4 Analysis of Radial Basis Function Neural Network used for Multiple Crack Identification in Rotor

The radial basis function neural network, as a type of feed-forward neural network has recently attracted extensive research interest because of its simple architecture, high approximation and regularization capability, and good local specialization and global generalization ability. RBFNN is a powerful technique for interpolation in multi-dimensional space. The RBFNN chosen is usually a gaussian-kernel transfer function, the response of such a function is positive for all input values.

6.4.1 RBFNN Mechanism for Identification the Multiple Crack

Radial basis function neural network (RBFNN) model typically have three layers. The first layer is linear and only distributes the input signal, while the next layer is nonlinear and uses gaussian functions. The third layer linearly combines the gaussian outputs. The nodes of each layer are completely linked to the previous layer. Each node of the input layers have been assigned by the input variable and transformed directly towards the hidden layer without weights. RBF contained by the hidden nodes, called as the transfer functions. RBF is symmetrical about a given center point in a multi-dimensional space. Number of hidden node of layer with RBF activation functions are connected in a feed

forward parallel manner in the RBFN model. The RBFs related parameters are enhanced for the duration of training. These values of parameter are not essentially the same all over the network nor are they directly associated by the actual training vectors. When the training vectors are supposed to be precise and it is required to implement a smooth interpolation between them, then a linear combination of RBFs can be established which provide no error at the training vectors. The methods of fitting RBFs to data, for function approximation, are closely related to distance weighted regression.

$$Y_k(x) = \sum_{j=1}^{G} w_{kj} \exp\left(-\|c_j - x\|\right)\sigma_j^2 \tag{6.12}$$

Where $Y_k(x) = k^{th}$ output, w_{kj} = weight from the j^{th} kernel node to the k^{th} output node, c_j = centroid of the i^{th} kernel node, σ_j =width of the j^{th} kernel node and G = number of kernel nodes. Generally c_j are selected constantly by the parameters w_{kj}, c_j and σ_j.The singular value decomposed (SVD) are employed to solve the w_{kj} and σ_j. Leonard et al [209] have proposed the enhance and better methodology include using K-means clustering for finding the c_j. K-nearest heuristic to evaluate the e_j. w_{kj} is evaluated using multiple linear regression. The K-means clustering algorithm determine a set of cluster centers and splits the training data into subsets. Every center of cluster is then linked with one of the centers presented in the hidden layer.

After the centers are established the width of each kernel is determined to cover the training points. To allow a smooth fit of the desired network outputs. The width is selected so that σ_j is greater than the distance to the nearest kernel center but also as small as possible to keep its distance of influence to its local region. For designing the radial basis function unit algorithms are used which are discussed in detail below. Consider training a model that has 'r' inputs. Because all inputs are associated to the hidden node, each node has r-dimensions center but only one width value is used to scale all r-dimensions.The prearrangement of the value of these centers and widths is discussed below.

Let x_t be the received vector with modules $x_{1t}, x_{2t}, \ldots\ldots\ldots, x_{rt}$. The output of the j^{th} unit, $u_j(x_t)$, in the hidden layer for this input pattern is;

$$u_j(x_t) = \exp\left(-\sum_{i=1}^{r}\left[x_{it} - \hat{x_{ij}}\right]^2 \Big/ \sigma_j^2\right) \tag{6.13}$$

Where $x_{ij}^{\wedge}$ is the center of j^{th} radial basis function unit for input variable i, σ_j is the width of the j^{th} RBF unit and x_{it} is the i^{th} variable of the pattern. The connection between the hidden layer units and output layer units are weight sums. The output value (Y_{mt}) of the m^{th} output node is equal to the summation of the weighted outputs of the hidden units, given by;

$$Y_{mt} = \exp\left(-\sum_{j=1}^{H} w_{jm} u_j \left(x_k \right) \right) \tag{6.14}$$

Where H is denoted the quantity of hidden nodes, Y_{mt} is represented the output value of the m^{th} node in the third layer(i.e. output layer) for the t^{th} received pattern, w_{jm} is the weight between the j^{th} unit of radial basis function which is calculated by three steps of the training action:

(1) The centers of RBF unit are identified by a 'K-means' clustering algorithm.
(2) The nearest-neighbor approaches are used to find the width.
(3) By applying the multiple linear regression techniques to determine the output unit and also the weights linking the RBF units.

6.4.1.1 Finding the Centers of RBF Unit

We can use any clustering algorithm for evaluation of RBF unit centers. The K-means clustering algorithm has been used to determined a set of cluster from a particular data. The numbers of input variable of the first layer (i.e. input layer) are used to calculate the dimensions of the RBF unit centers. The centers of the RBF units are coincident to the clusters centers. The K-means clustering algorithm begins as follows:

1. Altered arbitrarily selected training pattern has been used for adjusting the development of each cluster.
2. Allocate each training pattern to closest cluster. It can be completed by determining the Euclidean distance between the cluster centers and the training patterns.
3. Compute the average location for each other center after allocating all the training patterns. Then they become a fresh cluster centers.
4. The steps 2 and 3 repeats, until the cluster centers do not changed for the period of the successive iteration.

6.4.1.2 Finding the Width of RBF Unit

After allocating the centers of RBF unit, the width of RBF unit can be detrmined. The width of any RBF distance to the closest q of RBF units.

Where q is represent as a design parameter for the RBFN network, for unit is given by

$$\sigma_j = \sqrt{\left[\frac{1}{Q}\sum_{i=1}^{q}\sum_{k=1}^{r}\left(x_{kj}^{\wedge} - x_{ki}^{\wedge}\right)^2\right]} \tag{6.15}$$

Where $x_{kj}^{\wedge}$ and $x_{ki}^{\wedge}$ are the k^{th} items of the centers of the j^{th} and i^{th} hidden RBF units.

This algorithm section determines the required centers and width of the RBF unit.

6.4.1.3 Finding the Weights

When the centers and widths of the RBF units have been selected, then the N training patterns are processed through the hidden nodes to generate an NxN matrix, called D. Let T be the MxN desired output nodes. The aim is to determine the weights that decreases the error between the actual output and the desired output of the RBF network.

Essentially, we are trying to minimize the objective function.

$$\|z - WD\| \tag{6.16}$$

Where W is the T × N matrix of weights on the links between the hidden node and output nodes of the network. The selection of weights between the hidden layer and the output layer of network is determined using linear least square regression.The result to the earlier equation can be acquired using the pseudo-inverse of D and is given by;

$$W = ZD^T(DD^T)^{-1} \tag{6.17}$$

6.4.1.4 Selection of H and q

The design parameters, i.e. the number of RBF units in the hidden layer 'H' and the value of overlap parameter 'q' for the nearest neighbor method, are selected by the model builder to achieve the optimal RBF network structure for better performance. The parameters can be easily determined by using an S-fold cross-validation method (SFCV) [210], the procedure is as follows:

(1) Training data are arbitrarily separated into P equal sized sets.

(2) RBFNN is trained using P -1 data sets for a given set H and q.

(3) The remaining subset is used to test the network's local specialization and global generalization ability.

(4) The mean square difference between the target output and the predicted output is the error associated with test subsets.

(5) This procedure is repeated several times using different P–1 subsets for training and a different subset for testing at each time.

(6) The mean square error is the error for all the testing set for the proposed RBF network.

(7) This procedure is repeated several times with different values of H and q to obtain the optimum network structure with minimum mean square error.

6.4.2 Radial Basis Function Neural Network Mechanism for Finding the Crack Locations and Depths in Rotor

A radial basis function neural network is designed for identification of multiple crack of mild steel cantilever rotor submerged in the viscous fluid. The RBF neural network designed for five input and four output variables. The input variable parameters to the neural model are rnfx, rnfy, rax, ray, ν and the output variable are rfcl, rfcd, rscl and rscd.The RBFNN architecture for identification of multiple crack in rotor has been illustrated in Figure 6.4.

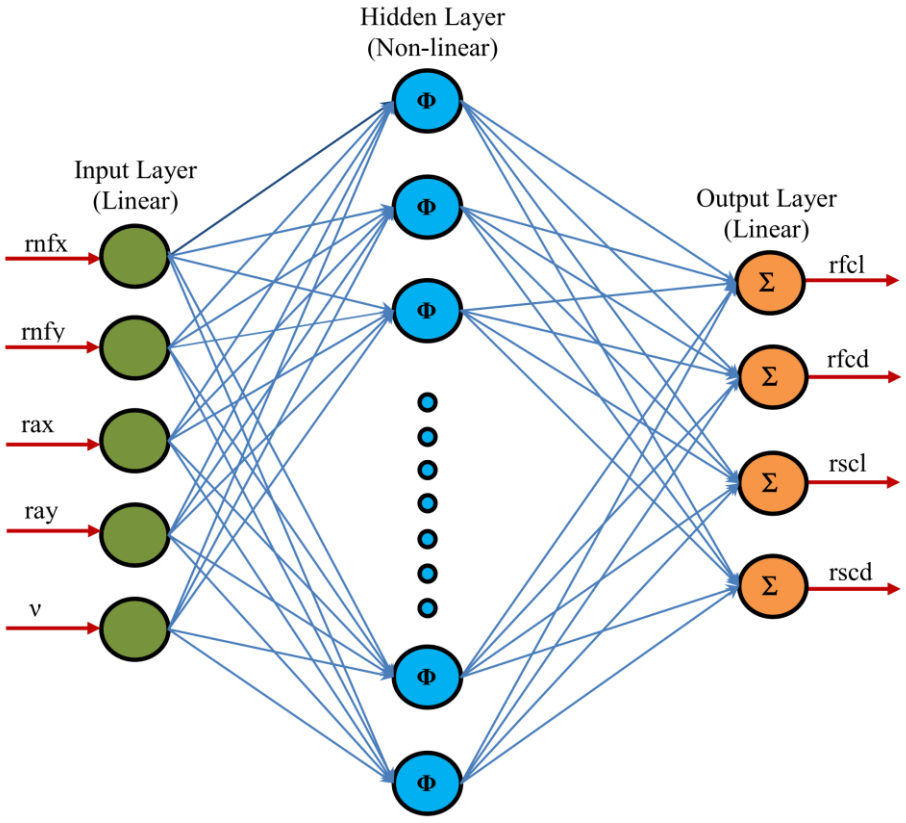

Figure 6.4: RBFNN model for identification of crack

6.5 Hybrid BPNN-RBFNN Neural Network Mechanism for Finding the Multiple Crack Locations and Crack Depths

This section introduces the mechanism of hybrid BPNN-RBFNN neural network for finding the multiple crack in cantilever rotor partially immersed in the viscous fluid medium. A novel hybrid BPNN-RBFNN neural network technique has been designed to identifying the locations and depths of multiple crack in cantilever rotor. Hybrid BPNN-RBFNN neural network controller has been designed with combination of BPNN and RBFNN controller. The extracted dynamic response from the theoretical, finite element and experimental analysis are used to train the hybrid BPNN-RBFNN neural network model.first & second relative natural frequency, first & second relative amplitude and viscosity of fluid are used as input parameters to a BPNN controller and rfcl_interim, rfcd_interim, rscl_interim, rscd_interim are the outputs from the BPNN controller. The output from the BPNN controller along with first & second relative natural frequency, first & second relative amplitude and viscosity of fluid are fed to the RBFNN controller. Finally, rfcl_final, rfcd_final, rscl_final, rscd_final are the output parameters from the hybrid BPNN-RBFNN model. The detail architecture of the hybrid fuzzy-rule base controller model has been shown in Figure 6.6.

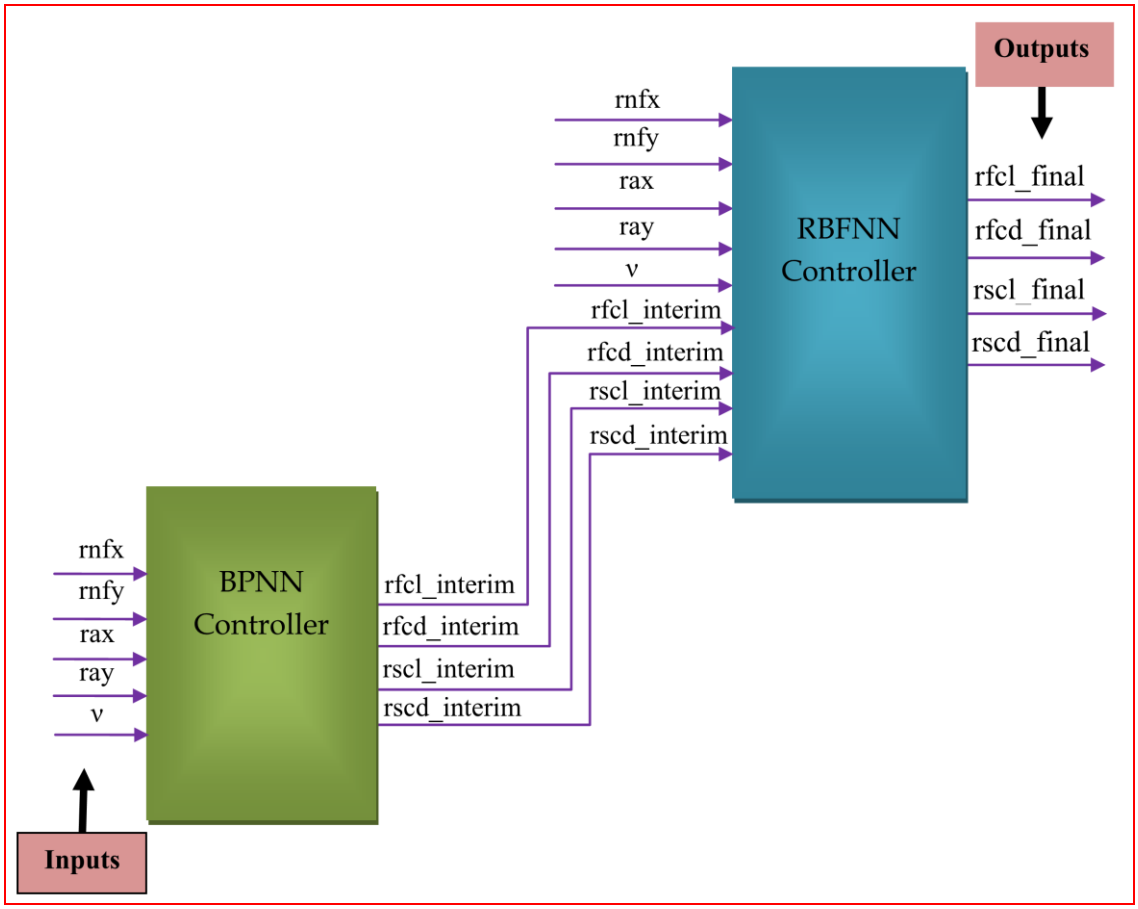

Figure 6.5: Hybrid BPNN-RBFNN neural network architecture for crack identification

6.6 Results and Discussion

This section depicts the discussion on analysis of results derived from various neural models such as BPNN and RBFNN. Figure 6.1 presents the general architecture of an artificial neural network. The architecture of BPNN mechanism has been illustrated in Figure 6.2. The nine layered back propagation neural network technique for identification of first and second relative crack locations and depths is presented in Figure 6.3. The input variables two relative natural frequency, two relative amplitude and viscosity of fluid are used for the input layer of feed forward back propagation neural network. These input variables process through seven hidden layers then the output layer gives first and second relative crack locations and depths. The RBFNN is a feed forward supervised learning type of neural network.It has approximation and regularization capacity. In present work, the RBFNN has been employed for localization and quantification of cracks present in the mild steel cantilever rotor. Similar to BPNN model, RBFNN consists of one input layer and output layer, but RBFNN has only one hidden layer. The input data is fed into input

layer. Output layer gives relative crack locations and relative crack depths. Figure 6.4 illustrates the architecture of RBFNN for identification of multiple crack. The hybrid BPNN-RBFNN model is the combination of the BPNN and RBFNN controller has been implemented. Figure 6.5 represents the architecture of the hybrid BPNN-RBFNN controller for finding the multiple crack in rotor.The results obtained from BPNN model, FEA, theoretical compared with the experimental analysis are presented in Table 6.1.The results obtained from RBFNN model, FEA, theoretical compared with the experimental analysis are presented in Table 6.2. The results obtained from BPNN, RBFNN, Mamdani fuzzy gaussian model and experimental analysis has been compared in Tables 6.3. The results obtained from the BPNN, RBFNN, hybrid BPNN-RBFNN model and experimental analysis has been compared in Table 6.4. The results obtained from BPNN, RBFNN, hybrid BPNN-RBFNN model and experimental test are compared, and close agreement is observed between each other. It is observed that the hybrid BPNN-RBFNN model gives better results as compared to BPNN, RBFNN and Mamdani fuzzy gaussian model for cracked rotor.The obtained results from the developed hybrid BPNN-RBFNN model, BPNN, RBFNN and experimental analysis has been compared in Table 6.4 for the rotor and proximity found between them. It has been observed that the hybrid BPNN-RBFNN model provides the better result as compared to BPNN and RBFNN model.

Table 6.1: Comparison of the results obtained from BPNN, FEA and experimental analysis for the rotor.

Relative 1st frequency at x-axis direction 'mfx'	Relative 2nd frequency at y-axis direction 'mfy'	Relative 1st amplitude at x-axis direction 'rax'	Relative 2nd amplitude at y-axis direction 'ray'	Viscosity of fluid 'v'	Experimental relative				BPNN relative				FEA relative				Theoretical relative			
					1st crack location 'rfcl'	1st crack depth 'rfcd'	2nd crack location 'rscl'	2nd crack depth 'rscd'	1st crack location 'rfcl'	1st crack depth 'rfcd'	2nd crack location 'rscl'	2nd crack depth 'rscd'	1st crack location 'rfcl'	1st crack depth 'rfcd'	2nd crack location 'rscl'	2nd crack depth 'rscd'	1st crack location 'rfcl'	1st crack depth 'rfcd'	2nd crack location 'rscl'	2nd crack depth 'rscd'
					rfcl	rfcd	rscl	rscd	rfcl	rfcd	rscl	rscd	rfcl	rfcd	rscl	rscd	rfcl	rfcd	rscl	rscd
0.8735	0.7305	5.773	5.8122	0.0633	0.187	0.175	0.125	0.300	0.175	0.165	0.119	0.286	0.181	0.172	0.122	0.294	0.179	0.165	0.118	0.292
0.7804	0.6002	6.3111	6.4533	0.541	0.312	0.162	0.687	0.275	0.299	0.155	0.652	0.261	0.302	0.158	0.671	0.271	0.296	0.155	0.643	0.261
0.5777	0.4778	7.1679	6.6364	2.9	0.375	0.125	0.625	0.175	0.363	0.117	0.593	0.166	0.367	0.123	0.605	0.172	0.356	0.119	0.593	0.166
0.8936	0.7843	5.6307	5.6839	0.0633	0.437	0.250	0.750	0.350	0.414	0.239	0.711	0.3297	0.432	0.246	0.733	0.342	0.41	0.238	0.718	0.34
0.7893	0.6422	5.9889	6.1122	0.541	0.187	0.225	0.200	0.275	0.175	0.213	0.189	0.259	0.183	0.219	0.195	0.267	0.175	0.214	0.191	0.262
0.6181	0.4993	6.6179	7.0558	2.9	0.250	0.200	0.562	0.350	0.237	0.189	0.532	0.331	0.245	0.194	0.555	0.342	0.237	0.191	0.532	0.331
0.8932	0.7385	6.7564	6.8083	0.0633	0.125	0.175	0.812	0.225	0.118	0.167	0.767	0.213	0.121	0.171	0.792	0.219	0.121	0.167	0.768	0.21
0.7889	0.6067	7.4789	7.6605	0.541	0.625	0.150	0.875	0.325	0.594	0.143	0.835	0.311	0.612	0.146	0.853	0.317	0.612	0.142	0.854	0.314
0.584	0.483	7.6496	7.3818	2.9	0.250	0.300	0.500	0.350	0.237	0.285	0.478	0.331	0.243	0.292	0.489	0.341	0.236	0.281	0.474	0.331
0.8739	0.7226	5.0186	5.0486	0.0633	0.500	0.225	0.750	0.275	0.479	0.211	0.705	0.261	0.484	0.216	0.726	0.266	0.479	0.212	0.711	0.258
Average percentage of error									5.06	5.21	5.15	5.22	2.51	2.47	2.43	2.36	4.73	5.1	4.94	4.76
Total percentage of error									**5.16**				**2.44**				**4.89**			

Table 6.2: Comparison of the results obtained from RBFNN, FEA , theoretical and experimental analysis for the rotor.

Relative 1st frequency at x-axis direction 'mfx'	Relative 2nd frequency at y-axis direction 'mfy'	Relative 1st amplitude at x-axis direction 'rax'	Relative 2nd amplitude at y-axis direction 'ray'	Viscosity of fluid 'v'	Experimental relative				RBFNN relative				FEA relative				Theoretical relative			
					1st crack location 'rfcl'	1st crack depth 'rfcd'	2nd crack location 'rscl'	2nd crack depth 'rscd'	1st crack location 'rfcl'	1st crack depth 'rfcd'	2nd crack location 'rscl'	2nd crack depth 'rscd'	1st crack location 'rfcl'	1st crack depth 'rfcd'	2nd crack location 'rscl'	2nd crack depth 'rscd'	1st crack location 'rfcl'	1st crack depth 'rfcd'	2nd crack location 'rscl'	2nd crack depth 'rscd'
					rfcl	rfcd	rscl	rscd	rfcl	rfcd	rscl	rscd	rfcl	rfcd	rscl	rscd	rfcl	rfcd	rscl	rscd
0.8735	0.7305	5.773	5.8122	0.0633	0.187	0.175	0.125	0.300	0.179	0.164	0.119	0.297	0.181	0.172	0.122	0.294	0.179	0.165	0.118	0.292
0.7804	0.6002	6.3111	6.4533	0.541	0.312	0.162	0.687	0.275	0.296	0.157	0.639	0.258	0.302	0.158	0.671	0.271	0.296	0.155	0.643	0.261
0.5777	0.4778	7.1679	6.6364	2.9	0.375	0.125	0.625	0.175	0.356	0.119	0.599	0.167	0.367	0.123	0.605	0.172	0.356	0.119	0.593	0.166
0.8936	0.7843	5.6307	5.6839	0.0633	0.437	0.250	0.750	0.350	0.424	0.235	0.703	0.329	0.432	0.246	0.733	0.342	0.41	0.238	0.718	0.34
0.7893	0.6422	5.9889	6.1122	0.541	0.187	0.225	0.200	0.275	0.178	0.216	0.192	0.269	0.183	0.219	0.195	0.267	0.175	0.214	0.191	0.262
0.6181	0.4993	6.6179	7.0558	2.9	0.250	0.200	0.562	0.350	0.235	0.187	0.528	0.328	0.245	0.194	0.555	0.342	0.237	0.191	0.532	0.331
0.8932	0.7385	6.7564	6.8083	0.0633	0.125	0.175	0.812	0.225	0.121	0.166	0.779	0.219	0.121	0.171	0.792	0.219	0.121	0.167	0.768	0.21
0.7889	0.6067	7.4789	7.6605	0.541	0.625	0.150	0.875	0.325	0.588	0.141	0.822	0.299	0.612	0.146	0.853	0.317	0.612	0.142	0.854	0.314
0.584	0.483	7.6496	7.3818	2.9	0.250	0.300	0.500	0.350	0.231	0.289	0.479	0.325	0.243	0.292	0.489	0.341	0.236	0.281	0.474	0.331
0.8739	0.7226	5.0186	5.0486	0.0633	0.500	0.225	0.750	0.275	0.474	0.215	0.721	0.262	0.484	0.216	0.726	0.266	0.479	0.212	0.711	0.258
Average percentage of error									5.01	4.99	5.04	4.87	2.51	2.47	2.43	2.36	4.73	5.1	4.94	4.76
Total percentage of error									**4.98**				**2.44**				**4.89**			

Table 6.3: Comparison of the results obtained from BPNN, RBFNN, Mamdani fuzzy gausian model and experimental analysis for the rotor.

Relative 1st frequency at x-axis direction 'rnfx'	Relative 2nd frequency at y-axis direction 'rnfy'	Relative 1st amplitude at x-axis direction 'rax'	Relative 2nd amplitude at y-axis direction 'ray'	Viscosity of fluid 'v'	Experimental relative				BPNN relative				RBFNN relative				Mamdani Fuzzy Gaussian relative			
					1st crack location 'rfcl'	1st crack depth 'rfcd'	2nd crack location 'rscl'	2nd crack depth 'rscd'	1st crack location 'rfcl'	1st crack depth 'rfcd'	2nd crack location 'rscl'	2nd crack depth 'rscd'	1st crack location 'rfcl'	1st crack depth 'rfcd'	2nd crack location 'rscl'	2nd crack depth 'rscd'	1st crack location 'rfcl'	1st crack depth 'rfcd'	2nd crack location 'rscl'	2nd crack depth 'rscd'
					rfcl	rfcd	rscl	rscd	rfcl	rfcd	rscl	rscd	rfcl	rfcd	rscl	rscd	rfcl	rfcd	rscl	rscd
0.8735	0.7305	5.773	5.8122	0.0633	0.187	0.175	0.125	0.300	0.175	0.165	0.119	0.286	0.179	0.164	0.119	0.297	0.176	0.165	0.119	0.285
0.7804	0.6002	6.3111	6.4533	0.541	0.312	0.162	0.687	0.275	0.299	0.155	0.652	0.261	0.296	0.157	0.639	0.258	0.295	0.153	0.651	0.260
0.5777	0.4778	7.1679	6.6364	2.9	0.375	0.125	0.625	0.175	0.363	0.117	0.593	0.166	0.356	0.119	0.599	0.167	0.355	0.1185	0.592	0.166
0.8936	0.7843	5.6307	5.6839	0.0633	0.437	0.250	0.750	0.350	0.414	0.239	0.711	0.3297	0.424	0.235	0.703	0.329	0.414	0.237	0.710	0.331
0.7893	0.6422	5.9889	6.1122	0.541	0.187	0.225	0.200	0.275	0.175	0.213	0.189	0.259	0.178	0.216	0.192	0.269	0.176	0.213	0.189	0.260
0.6181	0.4993	6.6179	7.0558	2.9	0.250	0.200	0.562	0.350	0.237	0.189	0.532	0.331	0.235	0.187	0.528	0.328	0.236	0.189	0.531	0.331
0.8932	0.7385	6.7564	6.8083	0.0633	0.125	0.175	0.812	0.225	0.118	0.167	0.767	0.213	0.121	0.166	0.779	0.219	0.118	0.1659	0.768	0.213
0.7889	0.6067	7.4789	7.6605	0.541	0.625	0.150	0.875	0.325	0.594	0.143	0.835	0.311	0.588	0.141	0.822	0.299	0.198	0.1422	0.829	0.308
0.584	0.483	7.6496	7.3818	2.9	0.250	0.300	0.500	0.350	0.237	0.285	0.478	0.331	0.231	0.289	0.479	0.325	0.236	0.284	0.472	0.332
0.8739	0.7226	5.0186	5.0486	0.0633	0.500	0.225	0.750	0.275	0.479	0.211	0.705	0.261	0.474	0.215	0.721	0.262	0.473	0.213	0.710	0.260
Average percentage of error					5.06	5.21	5.15	5.22	5.01	4.99	5.04	4.87	5.3	5.2	5.3	5.2				
Total percentage of error					**5.16**				**4.98**				**5.25**							

Table 6.4: Comparison of the results obtained from BPNN, RBFNN, Hybrid BPNN-RBFNN model and experimental analysis for the rotor.

Relative 1st frequency at x-axis direction 'mfx'	Relative 2nd frequency at y-axis direction 'mfy'	Relative 1st amplitude at x-axis direction 'rax'	Relative 2nd amplitude at y-axis direction 'ray'	Viscosity of fluid 'v'	Experimental relative 1st crack location 'rfcl'			1st crack depth 'rfcd'		2nd crack location 'rscl'		2nd crack depth 'rscd'		BPNN relative 1st crack location 'rfcl'			1st crack depth 'rfcd'		2nd crack location 'rscl'		2nd crack depth 'rscd'		RBFNN relative 1st crack location 'rfcl'			1st crack depth 'rfcd'		2nd crack location 'rscl'		2nd crack depth 'rscd'		Hybrid BPNN-RBFNN relative 1st crack location 'rfcl'			1st crack depth 'rfcd'		2nd crack location 'rscl'		2nd crack depth 'rscd'	
					rfcl		rscl		rfcd		rscl		rscd	rfcl			rfcd		rscl		rscd		rfcl			rfcd		rscl		rscd		rfcl			rfcd		rscl		rscd	
0.8735	0.7305	5.773	5.8122	0.0633	0.187		0.125		0.175		0.300			0.175			0.165		0.119		0.286		0.179			0.164		0.119		0.297		0.179			0.165		0.121		0.288	
0.7804	0.6002	6.3111	6.4533	0.541	0.312		0.687		0.275		0.350			0.299			0.155		0.652		0.261		0.296			0.157		0.639		0.258		0.299			0.158		0.658		0.266	
0.5777	0.4778	7.1679	6.6364	2.9	0.375		0.625		0.175		0.175			0.363			0.117		0.593		0.166		0.356			0.119		0.599		0.167		0.365			0.118		0.599		0.164	
0.8936	0.7843	5.6307	5.6839	0.0633	0.437		0.750		0.350		0.350			0.414			0.239		0.711		0.3297		0.424			0.235		0.703		0.329		0.426			0.238		0.725		0.334	
0.7893	0.6422	5.9889	6.1122	0.541	0.187		0.200		0.275		0.275			0.175			0.213		0.189		0.259		0.178			0.216		0.192		0.269		0.179			0.213		0.189		0.267	
0.6181	0.4993	6.6179	7.0558	2.9	0.250		0.562		0.350		0.350			0.237			0.189		0.532		0.331		0.235			0.187		0.528		0.328		0.235			0.184		0.536		0.335	
0.8932	0.7385	6.7564	6.8083	0.0633	0.125		0.812		0.225		0.225			0.118			0.167		0.767		0.213		0.121			0.166		0.779		0.219		0.118			0.164		0.761		0.215	
0.7889	0.6067	7.4789	7.6605	0.541	0.625		0.875		0.325		0.325			0.594			0.143		0.835		0.311		0.588			0.141		0.822		0.299		0.598			0.145		0.831		0.315	
0.584	0.483	7.6496	7.3818	2.9	0.250		0.500		0.350		0.350			0.237			0.285		0.478		0.331		0.231			0.289		0.479		0.325		0.235			0.274		0.479		0.341	
0.8739	0.7226	5.0186	5.0486	0.0633	0.500		0.750		0.275		0.275			0.479			0.211		0.705		0.261		0.474			0.215		0.721		0.262		0.469			0.217		0.712		0.266	
Average percentage of error														5.06			5.21		5.15		5.22		5.01			4.99		5.04		4.87		4.6			5.37		4.56		3.86	
Total percentage of error														**5.16**									**4.98**									**4.60**								

6.7 Summary

This chapter discusses the summary drawn from the analysis carried out in the present section. The neural network models (BPNN and RBFNN) and Hybrid BPNN-RBFNN neural network model has been designed and developed on the basis of the change of dynamic behavior such as amplitude and natural frequency because of the presence of the crack in the mild steel cantilever rotor. The two natural frequencies, two relative amplitude and viscosity of fluid have been employed as inputs to neural network model and the final outputs of the neural model are relative first and second crack location and crack depth. For the prediction of crack, two hundred training pattern have been taken to train the BPFNN and RBFNN model. BPNN model has a several number of neurons in the nine layers for treating the input data such as relative natural frequency and relative amplitude. It is found that the error in the output of the controller is significantly decreased from the preferred output by applying BPNN and RBFNN. The obtained results from the developed neural network have been compared with the obtained results of the theoretical analysis, experimental analysis, finite element analysis and Mamdani fuzzy gaussian method to examine the success of the model. The total percentage of error for BPNN is 5.16% , for RBFNN is 4.98% and for hybrid BPNN-RBFNN model is 4.60%. From the investigation of the operation of the developed BPNN, RBFNN and hybrid BPNN-RBFNN controller for multiple crack identification, it is observed that the hybrid BPNN-RBFNN controller can predict the crack locations and their intensities very close to the results as compared to BPNN, RBFNN and hybrid fuzzy model. In the next sections, the artificial neural network model has been to construct to several hybrid technique like as adaptive neuro-fuzzy inference system, Multi-adaptive neuro-fuzzy inference system methodology for online structural monitoring conditioning.

Chapter 7

Analysis of MANFIS For Identification of Multiple Crack in Rotor

The presence of crack is a serious threat to proper functioning of structures (i.e. rotor, beam, and shaft etc.) and structures suffers a prospective risk of failure. The catastrophe in structures produces the high expenses of maintenance. The influence of crack on the dynamic response of the structure depends mainly on the location and size of crack.In this chapter a novel technique is introduced to detect the multiple crack locations and depths in the rotor partially submerged in the viscous fluid medium using multiple adaptive neuro fuzzy-interference system (MANFIS). The proposed MANFIS controller comprises with the five layers. The first layer has the five inputs named as adaptive layer. The fourth and fifth layers are also called as adaptive layer. The fifth layer has provided the four output parameters. The second and third layers are fixed layer. The four input parameters two relative natural frequencies and two relative amplitudes at both transvers direction (i.e. 44 and 55-axis direction) and viscosity of fluid and four output parameters first and second relative crack depths and locations are utilized for the performance of proposed MANFIS controller. MANFIS is a prolonged form of the ANFIS to provide a multiple output for the required system. This methodology can be employed efficiently for modeling functions with complexity and nonlinearities without the use of precise measurable analysis. This approach has been utilized to diagnose the cracked cantilever rotor submerged in the viscous fluid medium and the results are favorable. The input and output parameters are extracted using the Takagi-Sugeno fuzzy model. The extracted data are used to train the FL model [199]. Through combination of excellent feature of both Fuzzy logic system and neural networks have been used to develop the ANFIS model. The proposed MANFIS method has been observed to be in agreement with the obtained results of experiment analysis.

7.1 Introduction

Many research work has been carried out by researchers to improve the methodology for fault diagnosis of structure. It has been analyzed that the AI based techniques such as FL System, ANNs etc. have been used to implement the well-organized intelligent techniques for detection of damages in faulty structures. Currently the science and engineering community have been used the multiple adaptive neuro-fuzzy inference system for design and development of the expert system.The combined features of neural network and fuzzy system of the multiple ANFIS model have been provided the robust stand to implement the controller for various application in engineering or industrial field. The present chapter introduces a method based on the MANFIS which is a postponement of ANFIS system to identify a multiple transverse crack in a rotor system.The recognized MANFIS controller model consists of single input layer, single output layer and three hidden layer. From the five layers of MANFIS system, the first layer name as input layer has been trained using the FL system. The residual four layers are trained using the ANNs. Many fuzzy rule and various fuzzy linguistic terms have been incorporated for the values of the five input parameters (first and second relative natural frequencies, first and second relative amplitude and viscosity of fluid) and four output parameters (first and second relative crack locations and depths) to train the fuzzy layer of the MANFIS controller. Many training patterns have been implemented to train the layer based on the neural network of the MANFIS controller. The first layer based on the fuzzy uses the two relative natural frequencies, two relative amplitude and viscosity of fluid as the inputs. The output of the fuzzy model fed to the hidden layer and Finally output parameters first and second relative crack locations and depths have been received from the MANFIS controller. From the analysis of predictive result of proposed technique. It has been observed that the output values agree well with the result of experimental investigation. Based on the analysis it is confirmed that the proposed technique reveals its capability to be an appropriate non-destructive method for identification of damages in vibrant structure. The present chapter has been organized into four different sections. First Section 7.1 discusses the introductory part of the proposed MANFIS and explains the application of MANFIS in advance computing. The analysis of MANFIS applied for identification of crack in rotor has been described in section 7.2. The comparison of the results obtained from MANFIS model with the results obtained from the techniques discoursed in the earlier chapters have been

presented and discussed in section 7.3. Finally, section 7.4 provides conclusions made by analysis of MANFIS for multiple crack identification in the rotor.

7.2 Analysis of Multiple Adaptive Neuro-Fuzzy Inference System For Identification of Crack

The Multiple adaptive neuro fuzzy inference system (MANFIS) is a combined arrangement of Fuzzy inference system (FIS) and artificial neural network (ANN). The MANFIS incorporate fuzzy inference system with the artificial neural network to improve the performance of model by means of precise and rapid estimation of the complex function. MANFIS controller employs fuzzy rules for adjustment of a set of parameters and the ANN for training and updating these parameters. The artificial neural networks give available high accuracy input- output mapping for nonlinear modelling system. The demerit of the artificial neural network is that they are black box modes which is unable to clarify the particular. The ANFIS controller is functioning under the first order Takagi Sugeno Fuzzy Model [207]. In this investigation, there are five inputs and four outputs. The inputs of the network model are as follows;

(1) rnfx = Relative natural frequency in x-axis direction
(2) rnfy = Relative natural frequency in y-axis direction
(3) rax = Relative amplitude in x-axis direction
(4) ray = Relative amplitude in y-axis direction
(5) ν = Kinematic viscosity of fluid

The output parameters are as follows;

(1) rfcl = Relative first crack location (2) rfcd = Relative first crack location
(3) rscl = Relative second crack depth (4) rscd = Relative second crack depth

For the Multiple ANFIS architecture, 'if and then rules' are defined as below;

$$\left.\begin{array}{l}\text{IF } y_1 \text{ is } P_l,\ y_2 \text{ is } Q_k,\ y_3 \text{ is } R_m,\ y_4 \text{ is } S_o, y_5 \text{ is } T_p, \\ \text{THEN } k_{j,i} = a_{j,i}y_1 + b_{j,i}y_2 + c_{j,i}y_3 + d_{j,i}y_4 + e_{j,i}y_5 + x_{j,i}\end{array}\right\} \quad (7.1)$$

Where

$$
\left.
\begin{array}{l}
k_{1,i} = rcl1, i = a_{1,i}y_1 + b_{1,i}y_2 + c_{1,i}y_3 + d_{1,i}y_4 + e_{1,i}y_5 + x_{1,i} \\
\text{For first relative crack location;} \\
k_{2,i} = rcd1, i = a_{2,i}y_1 + b_{2,i}y_2 + c_{2,i}y_3 + d_{2,i}y_4 + e_{2,i}y_5 + x_{2,i} \\
\text{For first relative crack depth;} \\
k_{3,i} = rcl2, i = a_{1,i}y_1 + b_{1,i}y_2 + c_{1,i}y_3 + d_{1,i}y_4 + e_{1,i}y_5 + x_{1,i} \\
\text{For second relative crack location;} \\
k_{4,i} = rcd2, i = a_{2,i}y_1 + b_{2,i}y_2 + c_{2,i}y_3 + d_{2,i}y_4 + e_{2,i}y_5 + x_{2,i} \\
\text{For second relative crack depth;}
\end{array}
\right\} \quad (7.2)
$$

The symbols are as follows; j =1 to 4; l=1 to n_1; k =1to n_2; m=1to n_3; o=1 to n_4; p=1 to n_5;and i=1 to y_1, y_2, y_3, y_4, y_5. The symbols n_1, n_2, n_3, n_4, and n_5 are the number of membership functions for the fuzzy systems for the inputs y_1, y_2, y_3, y_4, and y_5 respectively. The symbols P, Q, R, S and T are the fuzzy membership sets defined for the input variables y_1(rnfx), y_2(rnfy), y_3(rax), y_4(ray), and y_5(v). The symbols $a_{1,i}, b_{1,i}, c_{1,i}, d_{1,i}, e_{1,i}, x_{1,i}, a_{2,i}, b_{2,i}, c_{2,i}, d_{2,i}, e_{2,i}$ and $x_{2,i}$ are the consequent parameters of the ANFIS fuzzy model. The abbreviation "rfcl," "rfcd," "rfcl,"and "rscd," are the linear consequent functions defined in terms of the inputs (y_1, y_2, y_3, y_4, and y_5). The ANFIS consists of five layers as discussed below.

Layer 1: is the input layer. Each node in this layer is a square node with a specific fuzzy membership functions (Mode functions) identifying the degrees to which the inputs fulfill the quantifier. For five inputs, the output from the nodes are given as follows;

$$
\left.
\begin{array}{l}
O_{1,h,j} = \alpha_{P_h}(y) \text{ For } h = 1,....,n_1 \text{ (for input } y_1 \text{);} \\
O_{1,h,j} = \alpha_{Q_h}(y) \text{ For } h = n_1+1,.....,n_1+n_2 \text{ (for input } y_2 \text{);} \\
O_{1,h,j} = \alpha_{R_h}(y) \text{ For } h = n_1+n_2+1,.....,n_1+n_2+n_3 \text{ (for input } y_3 \text{);} \\
O_{1,h,j} = \alpha_{S_h}(x) \text{ For } h = n_1+n_2+n_3+1,.....,n_1+n_2+n_3+n_4 \text{ (for input } y_4 \text{);} \\
O_{1,h,j} = \alpha_{T_h}(y) \text{ For } h = n_1+n_2+n_3+n_4+1,.....,n_1+n_2+n_3+n_4+n_5 \text{ (for input } y_5 \text{);}
\end{array}
\right\} \quad (7.3)
$$

Here α_{P_h}, α_{Q_h}, α_{R_h}, $\alpha_{S_h}, \alpha_{T_h}$ are the membership functions, these can have various shapes, like triangular, trapezoidal, gaussian or some other shape. Here the membership function is selected as the bell shaped function (Figure 7.1) for P, Q, R, S and T.

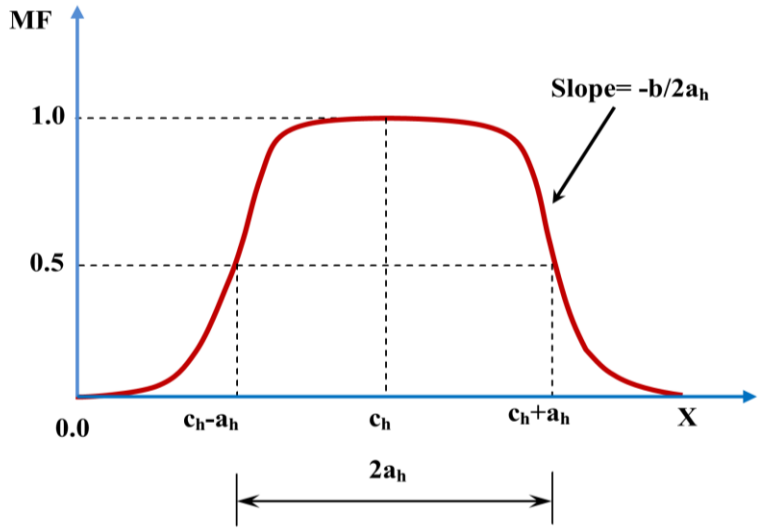

Figure 7.1: Bell-shaped membership function

The membership functions for P, Q, R, S and T are considered in 'layer 1' and are defined as follows;

$$\mu_{Ph}(y) = \frac{1}{1+\left\{\left(\frac{y-c_h}{a_h}\right)^2\right\}^{b_h}};\ h = 1,.....,n_1 \qquad (7.4(i))$$

$$\mu_{Qh}(y) = \frac{1}{1+\left\{\left(\frac{y-c_h}{a_h}\right)^2\right\}^{b_h}};\ h = n_1+1,....., n_1+n_2 \qquad (7.4(ii))$$

$$\mu_{Rh}(y) = \frac{1}{1+\left\{\left(\frac{y-c_h}{a_h}\right)^2\right\}^{b_h}};\ h = n_1+n_2+1,....., n_1+n_2+n_3 \qquad (7.4(iii))$$

$$\mu_{Sh}(y) = \frac{1}{1+\left\{\left(\frac{y-c_h}{a_h}\right)^2\right\}^{b_h}};\ h = n_1+n_2+n_3+1,....., n_1+n_2+n_3+n_4 \qquad (7.4(iv))$$

$$\mu_{Th}(y) = \frac{1}{1+\left\{\left(\frac{y-c_h}{a_h}\right)^2\right\}^{b_h}};\ h = n_1+n_2+n_3+1,....., n_1+n_2+n_3+n_4 \qquad (7.4(v))$$

Where b_h , c_h , a_h are the parameters that control the slope, center and width of bell shape function of node 'h' respectively. It is also known as premise parameter.

Layer 2: is the fuzzification layer. Neurons in this layer perform fuzzification. Fuzzification comprises the process of transforming crisp values into grades of membership for linguistic terms of fuzzy sets. Each node in this layer is a circular node, labeled as "Π." which multiplies the incoming signals and sends the product out. The output is denoted by $O_{2,i,j}$.

$$O_{2,i,j} = w_{i,j} = \alpha_{Ph}(y)\alpha_{Qh}(y)\alpha_{Rh}(y)\alpha_{Sh}(y)\alpha_{Th}(y) \tag{7.5}$$

For $i = 1,.....,n_1.n_2.n_3.n_4.n_5$ and $h = 1,.....,n_1 + n_2 + n_3 + n_4 + n_5$

Layer 3: is the rule layer. Each node in this layer is a fixed node (circular), labeled as "N." The output of the i^{th} node is calculated by talking the ratio of firing strength of i^{th} rule $\left(w_{i,j}\right)$ to the sum of all rules firing strength:

$$O_{3,i,j} = \bar{w}_{i,j} = \frac{w_{i,j}}{\sum_{r=1}^{r=n1,n2,n3,n4,n5} w_{r,j}} \tag{7.6}$$

This output gives a normalized firing strength.

Layer 4: is the normalization layer. Each neuron in this layer receives inputs from all neurons in the rule layer, and calculates the normalized firing strength of a given rule. The normalized firing strength is the ratio of the firing strength of a given rule to the sum of firing strengths of all rules. It represents the contribution of a given rule to the final result. Each node in this layer is a square node with a node function.

$$O_{4,i,j} = \bar{w}_{i,j}\, k_{i,j} = \bar{w}_{i.j}\left(a_{i,j}y_1 + b_{i,j}y_2 + c_{i,j}y_4 + d_{i,j}y_5 + x_{i,j}\right) \tag{7.7}$$

Where $\bar{w}_{i,j}$ a normalized firing strength from is (output) from layer 3, and $\left\{a_{i,j} + b_{i,j} + c_{i,j} + d_{i,j} + x_{i,j}\right\}$ is the parameter set for relative crack location $\left(j = 1\right)$ and relative crack depth $\left(j = 2\right)$.

Layer 5: is represented by a single summation neuron. The single node in this layer is a fixed node (circular), labeled as "Σ," which computes the overall outputs as the summation of all incoming signals:

$$O_{5,i,j} = \sum_{i=1}^{i=y_1.y_2.y_3.y_4.y_5} \bar{w}_{i,j}k_{j,i} = \frac{\sum_{i=1}^{i=n_1.n_2.n_3.n_4.n_5} w_{i,j}k_{j,i}}{\sum_{i=1}^{i=n_1.n_2.n_3.n_4.n_5} \omega_{i,j}} \tag{7.8}$$

The present developed structure of ANFIS model has five dimensional space partitions which are $n_1.n_2.n_3.n_4.n_5$. Each region has a fuzzy "if and then" rule. The current developed

ANFIS architecture have five dimensional space partition and has "y_1 x y_2 x y_3 x y_4 x y_5" regions. Fuzzy IF THEN rule has been governed each region. 1st layer of ANFIS is reffered to fuzzy sub space. The variables of 4th layer are mentioned as consequent parameters and have been used to optimized the network. During the forward pass of the hybrid learning algorithm node outputs go forward until layer four and the consequent parameters are identified by least square method. In the backward pass, error signals propagate backwards and the premise parameters are updated by a gradient descent method.The architecture of MANFIS is presented in Figure 7.2(a) for multiple crack identification. Figure 7.2(b) illustrates the architecture of ANFIS for identification of crack in rotor.

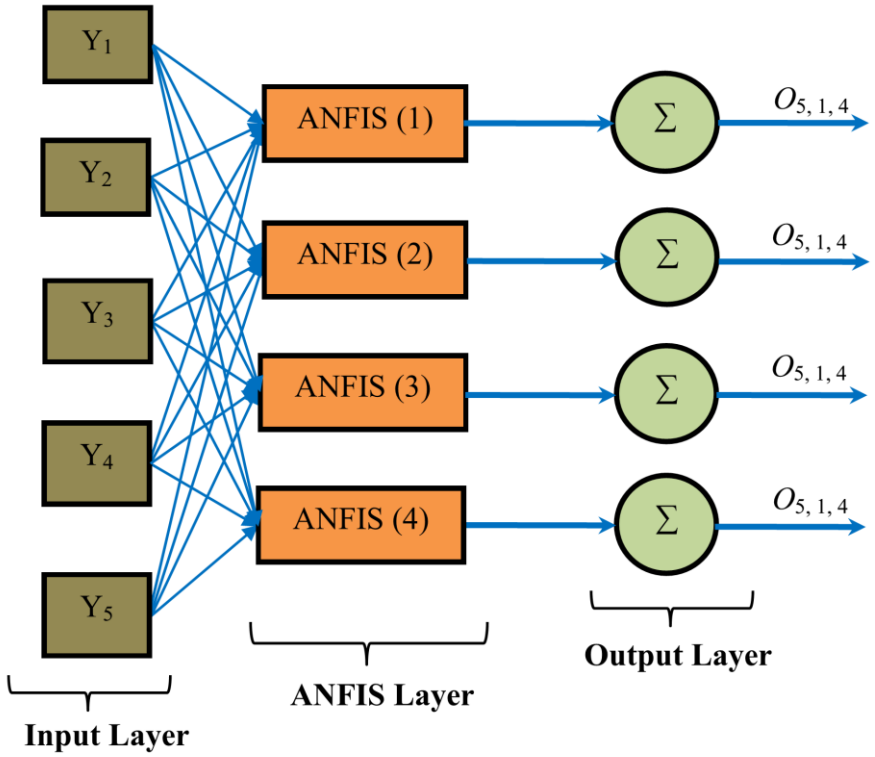

Figure 7.2(a): Representation of Multiple ANFIS controller for crack identification.

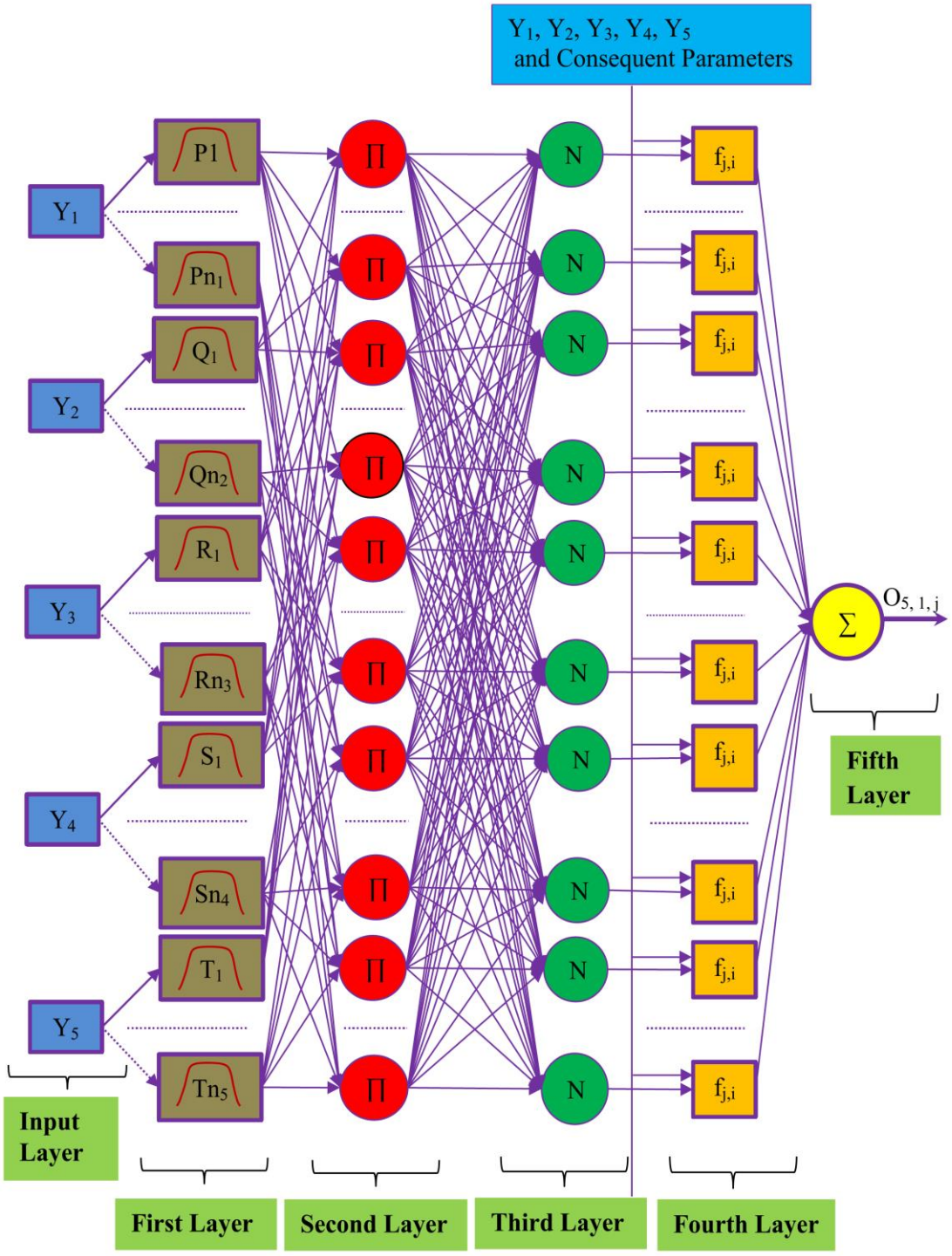

Figure 7.2(b): Adaptive Neuro-fuzzy inference system (ANFIS) for crack identification.

7.3 Results and Discussion

This section depicts the obtained results from developed Multiple adaptive neuro-fuzzy inference system (MANFIS) for identification of multiple crack in cantilever rotor system partially submerged in the viscous fluid medium. The obtained results from the current

analysis exhibit the effect of crack locations and depths on the vibration response of the cantilever rotor. Figure 7.1 illustrates the model of Bell shaped membership functions employed for developing ANFIS model. The structure of the proposed MANFIS model for multiple crack detection and the complete structure with altered layers of the ANFIS system for crack identification have been presented in Figure 7.2(a) and Figure 7.2(b) respectively.Table 7.1 presents the comparison of obtained results from the theoretical analysis, FEA and MANFIS model.The appropriateness of the MANFIS approach has been tested by comparing the results with the hybrid Fuzzy models of Chapter-5, hybrid BPNN-RBFNN neural network models of Chapter-6 and experimental analysis of Chapter-8. Comparison have been illustrated in the Table 7.2. Ten sets of inputs (two relative natural frequencies, two relative amplitudes and viscosity of fluid) from the many sets of inputs have been taken for the proposed technique and the corresponding outputs (relative first and second crack locations and depths) are presented in the Tables 7.1 and 7.2. The first five columns of Tables 7.1 and 7.2 presents the inputs for the MANFIS technique i.e. first relative natural frequency at x-axis direction (rnfx), second relative natural frequency at y-axis direction (rnfy), first relative amplitude at x-axis direction (rax), second relative natural frequency (ray) and viscosity of fluid (v).The remaining columns from the Table represent the outputs such as first relative crack location, first relative crack depth, second crack location and second crack depth from the respective techniques.

Table 7.1: Comparison of the results obtained from MANFIS, FEA, theoretical and experimental analysis for the rotor.

Relative 1st frequency at x-axis direction 'rnfx'	Relative 2nd frequency at y-axis direction 'rnfy'	Relative 1st amplitude at x-axis direction 'rax'	Relative 2nd amplitude at y-axis direction 'ray'	Viscosity of fluid 'v'	Experimental relative 1st crack location 'rfcl' 1st crack depth 'rfcd' 2nd crack location 'rscl' 2nd crack depth 'rscd'				MANFIS relative 1st crack location 'rfcl' 1st crack depth 'rfcd' 2nd crack location 'rscl' 2nd crack depth 'rscd'				FEA relative 1st crack location 'rfcl' 1st crack depth 'rfcd' 2nd crack location 'rscl' 2nd crack depth 'rscd'				Theoretical relative 1st crack location 'rfcl' 1st crack depth 'rfcd' 2nd crack location 'rscl' 2nd crack depth 'rscd'			
					rfcl	rfcd	rscl	rscd	rfcl	rfcd	rscl	rscd	rfcl	rfcd	rscl	rscd	rfcl	rfcd	rscl	rscd
0.8735	0.7305	5.773	5.8122	0.0633	0.187	0.175	0.125	0.300	0.179	0.165	0.128	0.289	0.181	0.172	0.122	0.294	0.179	0.165	0.118	0.292
0.7804	0.6002	6.3111	6.4533	0.541	0.312	0.162	0.687	0.275	0.296	0.155	0.645	0.259	0.302	0.158	0.671	0.271	0.296	0.155	0.643	0.261
0.5777	0.4778	7.1679	6.6364	2.9	0.375	0.125	0.625	0.175	0.359	0.129	0.605	0.165	0.367	0.123	0.605	0.172	0.356	0.119	0.593	0.166
0.8936	0.7843	5.6307	5.6839	0.0633	0.437	0.250	0.750	0.350	0.419	0.237	0.71	0.326	0.432	0.246	0.733	0.342	0.41	0.238	0.718	0.34
0.7893	0.6422	5.9889	6.1122	0.541	0.187	0.225	0.200	0.275	0.176	0.218	0.193	0.258	0.183	0.219	0.195	0.267	0.175	0.214	0.191	0.262
0.6181	0.4993	6.6179	7.0558	2.9	0.250	0.200	0.562	0.350	0.235	0.189	0.539	0.327	0.245	0.194	0.555	0.342	0.237	0.191	0.532	0.331
0.8932	0.7385	6.7564	6.8083	0.0633	0.125	0.175	0.812	0.225	0.118	0.169	0.786	0.213	0.121	0.171	0.792	0.219	0.121	0.167	0.768	0.21
0.7889	0.6067	7.4789	7.6605	0.541	0.625	0.150	0.875	0.325	0.595	0.143	0.83	0.311	0.612	0.146	0.853	0.317	0.612	0.142	0.854	0.314
0.584	0.483	7.6496	7.3818	2.9	0.250	0.300	0.500	0.350	0.249	0.288	0.485	0.338	0.243	0.292	0.489	0.341	0.236	0.281	0.474	0.331
0.8739	0.7226	5.0186	5.0486	0.0633	0.500	0.225	0.750	0.275	0.479	0.217	0.718	0.262	0.484	0.216	0.726	0.266	0.479	0.212	0.711	0.258
Average percentage of error									4.46	3.62	3.54	5.26	2.51	2.47	2.43	2.36	4.73	5.1	4.94	4.76
Total percentage of error									**4.22**				**2.44**				**4.89**			

Table 7.2: Comparison of the results obtained from MANFIS, Hybrid BPNN-RBFNN model, Hybrid fuzzy model and experimental analysis for the rotor.

Relative 1st frequency at x-axis direction 'rnfx'	Relative 2nd frequency at y-axis direction 'rnfy'	Relative 1st amplitude at x-axis direction 'rax'	Relative 2nd amplitude at y-axis direction 'ray'	Viscosity of fluid 'v'	Experimental relative				MANFIS relative				Hybrid BPNN-RBFNN relative				Hybrid Fuzzy relative			
					1st crack location 'rfcl'	1st crack depth 'rfcd'	2nd crack location 'rscl'	2nd crack depth 'rscd'	1st crack location 'rfcl'	1st crack depth 'rfcd'	2nd crack location 'rscl'	2nd crack depth 'rscd'	1st crack location 'rfcl'	1st crack depth 'rfcd'	2nd crack location 'rscl'	2nd crack depth 'rscd'	1st crack location 'rfcl'	1st crack depth 'rfcd'	2nd crack location 'rscl'	2nd crack depth 'rscd'
					rfcl	rfcd	rscl	rscd	rfcl	rfcd	rscl	rscd	rfcl	rfcd	rscl	rscd	rfcl	rfcd	rscl	rscd
0.8735	0.7305	5.773	5.8122	0.0633	0.187	0.175	0.125	0.300	0.179	0.165	0.128	0.289	0.179	0.165	0.121	0.288	0.178	0.166	0.119	0.291
0.7804	0.6002	6.3111	6.4533	0.541	0.312	0.162	0.687	0.275	0.296	0.155	0.645	0.259	0.299	0.158	0.658	0.266	0.295	0.154	0.644	0.262
0.5777	0.4778	7.1679	6.6364	2.9	0.375	0.125	0.625	0.175	0.359	0.129	0.605	0.165	0.365	0.118	0.599	0.164	0.364	0.118	0.594	0.165
0.8936	0.7843	5.6307	5.6839	0.0633	0.437	0.250	0.750	0.350	0.419	0.237	0.71	0.326	0.426	0.238	0.725	0.334	0.421	0.235	0.719	0.341
0.7893	0.6422	5.9889	6.1122	0.541	0.187	0.225	0.200	0.275	0.176	0.218	0.193	0.258	0.179	0.213	0.189	0.267	0.175	0.213	0.192	0.265
0.6181	0.4993	6.6179	7.0558	2.9	0.250	0.200	0.562	0.350	0.235	0.189	0.539	0.327	0.235	0.184	0.536	0.335	0.234	0.192	0.533	0.331
0.8932	0.7385	6.7564	6.8083	0.0633	0.125	0.175	0.812	0.225	0.118	0.169	0.786	0.213	0.118	0.164	0.761	0.215	0.122	0.165	0.765	0.213
0.7889	0.6067	7.4789	7.6605	0.541	0.625	0.150	0.875	0.325	0.595	0.143	0.83	0.311	0.598	0.145	0.831	0.315	0.613	0.143	0.853	0.311
0.584	0.483	7.6496	7.3818	2.9	0.250	0.300	0.500	0.350	0.249	0.288	0.485	0.338	0.235	0.274	0.479	0.341	0.237	0.282	0.473	0.331
0.8739	0.7226	5.0186	5.0486	0.0633	0.500	0.225	0.750	0.275	0.479	0.217	0.718	0.262	0.469	0.217	0.712	0.266	0.478	0.213	0.712	0.252
Average percentage of error					4.46	3.62	3.54	5.26	4.6	5.37	4.56	3.86	4.36	5.27	4.8	4.85				
Total percentage of error					**4.22**				**4.60**				**4.82**							

7.4 Summary

The results derived from MANFIS technique for multiple crack identification in the rotor partially submerged in the viscous fluid medium have been summarized below. In the present analysis a technique based on the values of natural frequencies and amplitudes of the rotor system has been proposed for recognition of the crack location and their severities in a rotor using MANFIS model. MANFIS model has one input layer, four hidden layer and one output layer. Two relative natural frequencies, two relative amplitude and viscosity of fluid are used as inputs to the fuzzy segment of the MANFIS model. The output of the developed model is relative crack depth and relative crack location. The result derived from the developed hybrid BPNN-RBFNN, hybrid fuzzy model, FEA, theoretical analysis and MANFIS model have been compared with experimental test results to authenticate the effectiveness of proposed fuzzy models. The total percentage of error of the obtained result of the hybrid BPNN-RBFNN model is 4.60%, for the hybrid fuzzy model is 4.82% for the FEA model is 2.44%, and for the Theoretical analysis is 4.89%.The results found to be good in agreement. Based on above study, it is found that MANFIS model gives better results as comparison to hybrid BPNN-RBFNN, hybrid fuzzy model, FEA, theoretical analysis. Therefore, the developed MANFIS controller can be efficiently used as fault diagnosis tools in dynamically analysis of rotor. The MANFIS model gives more precise result as compared to hybrid BPNN-RBFNN and hybrid fuzzy model. It is found that total percentage of error for MANFIS model is 4.22 %.

Chapter 8

Analysis of Hybrid Fuzzy-Rule Base Technique for Multiple Crack Identification in Rotor

Different fault diagnostics techniques are required to observe the health of various machine components and structural elements for acquiring the un-interrupted service. The detection of crack before failure of the rotor system not only prevents loss of economy but also saves the human life. Various non-destructive techniques have been applied by researchers to locate the damage but they are costly and time consuming. The vibration based method along with intelligent techniques can be used to effectively identify the damage. The rule base system has been done by engineers and researchers from various fields of science and technology for developing intelligent systems for identification of multiple crack. The rule base technique has potential to solve various engineering problems based on concepts of sets of rules.

8.1 Introduction

The current chapter introduces the hybrid fuzzy-rule base technique. Rule base technique stated the knowledge of the environment in the form of rules. Rules are one of the leading type of information exemplification formalisms used in expert systems. The rule comprises the set of conditions (antecedents) and set of conclusions (consequents).The rule base, inference engine and working memory are the typical main component of the rule-base system. The working memory has the information regarding the specific instant of the problem being solved. The rule base controller has been used the set of rules which signify the solving knowledge of problem for a particular domain. The working memory used to derive a new statistics and inference engine uses the rule base. Basically rule-base controller is a tabel look-up technique which is representing the dynamic complex system. In rule base system, each rule is a command of motion control for a particular permutation

of all desired inputs. Entirely rule-based systems need a crack detection approach to resolve conflicts among two or more relevant rules. The accurate rule should be capable to detect the crack locations and depths in rotor in the sense of preset performance circumstance. For the better safety and performance of rotor, the rule-base technique requirements to be revised to overcome variations in crack locations and depths in rotor.

8.2 Analysis of Rule-Base Technique for Identification of Multiple Crack in Rotor

8.2.1 Designing of Rule-Base Controller for Finding the Multiple Crack in Rotor

In current work, the rule base technique are used for the identification of multiple crack in cantilever rotor partially submerged in the viscous fluid medium. In this investigation, there are five inputs and four outputs.

The inputs of the rule-base model are as follows;

(1) rnfx = Relative natural frequency in x-axis direction

(2) rnfy = Relative natural frequency in y-axis direction

(3) rax = Relative amplitude in x-axis direction

(4) ray = Relative amplitude in y-axis direction

(5) ν = Viscosity of fluid

The output parameters are as follows;

(1) rfcl = Relative first crack location (2) rfcd = Relative first crack depth

(2) rscl = Relative second crack location (4) rscd = Relative second crack depth

First, the set of rule are taken from the result obtained from the experimental analysis, FEA and theoretical analysis. Each rule is consisting of five inputs (i.e. rnfx, rnfy, rax, ray and ν) and four outputs (i.e. rfcl, rfcd, rscl and rscd). Some of the rules are mentioned below.

Rule 1:

IF (89.35<first relative natural frequency<89.37) and (74.83<second relative natural frequency<74.86) and (663.06<first relative amplitude<663.07) and (658.38< second relative amplitude<658.39) and (0.06<viscosity of fluid<0.07) **THEN**
(first relative crack location=100) and (first relative crack depth=6) and(second relative crack location=475) and (second relative crack depth=5.5)

Rule 2:

IF (87.67<first relative natural frequency<87.68) and (79.61<second relative natural frequency<79.62) and (666.53<first relative amplitude<666.54) and (652.54<second relative amplitude<652.55) and (0.06<viscosity of fluid<0.07) **THEN**
(first relative crack location=500) and (first relative crack depth=5) and (second relative crack location=750) and (second relative crack depth=5)

Rule 3:

IF (82.44<first relative natural frequency<82.45) and (70.12<second relative natural frequency<70.13) and (612.42<first relative amplitude<612.43) and (601.6<second relative amplitude<601.7) and (0.06<viscosity of fluid<0.07) **THEN**
(first relative crack location=150) and (first relative crack depth=3.5)and (second relative crack location=400) and (second relative crack depth=5.25)

Rule 4:

IF (77.88<first relative natural frequency<77.89) and (64.66<second relative natural frequency<64.67) and (767.88<first relative amplitude<767.89) and (756.04<second relative amplitude<756.05) and (0.541<viscosity of fluid<0.542) **THEN**
(first relative crack location=250) and (first relative crack depth=4.25) and (second relative crack location=500) and (second relative crack depth=7)

Rule 5:

IF (74.24<first relative natural frequency<74.25) and (63.88<second relative natural frequency<63.89) and (746.4<first relative amplitude<746.5) and (736.4<second relative amplitude<736.5) and (0.541<viscosity of fluid<0.542) **THEN**
(first relative crack location=200) and (first relative crack depth=4)and (second relative crack location=575) and (second relative crack depth=5)

Rule 6:

IF (73.68<first relative natural frequency<73.69) and (64.71<second relative natural frequency<64.72) and (758.6<first relative amplitude<758.7) and (747.8<second relative amplitude<747.8) and (0.541<viscosity offluid<0.542) **THEN**
(first relative crack location=475) and (first relative crack depth=4.75)and (second relative crack location=700) and (second relative crack depth=5.5)

Rule 7:

IF (57.63<first relative natural frequency<57.64) and (47.66<second relative natural frequency<47.67) and (671.33<first relative amplitude<671.34) and (563.73<second relative amplitude<563.74) and (2.8<viscosity of fluid<2.9) **THEN**
(first relative crack location=350) and (first relative crack depth=4.5)and (second relative crack location=750) and (second relative crack depth=5.75)

Rule 8:

IF (56.18<first relative natural frequency<56.19) and (46.26<second relative natural frequency<46.27) and (661.33<first relative amplitude<661.34) and (559.46<second relative amplitude<559.47) and (2.8<viscosity of fluid<2.9) **THEN**
(first relative crack location=150) and (first relative crack depth=3.25)and (second relative crack location=450) and (second relative crack depth=5.75)

Rule 9:

IF (53.08<first relative natural frequency<53.09) and (43.47<second relative natural frequency<43.48) and (637.72<first relative amplitude<638.72) and (535.77<second relative amplitude<535.78) and (2.8<viscosity of fluid<2.9) **THEN**
(first relative crack location=250) and (first relative crack depth=3) and (second relative crack location=575) and (second relative crack depth=4.5)

Rule 10:

IF (52.98<first relative natural frequency<52.99) and (42.86<second relative natural frequency<42.87) and (629.51<first relative amplitude<629.52) and (525.08<second relative amplitude<525.09) and (2.8<viscosity of fluid<2.9) **THEN**
(first relative crack location=200) and (first relative cracdepth=3.75)and (second relative crack location=400) and (second relative crack depth=3.5)

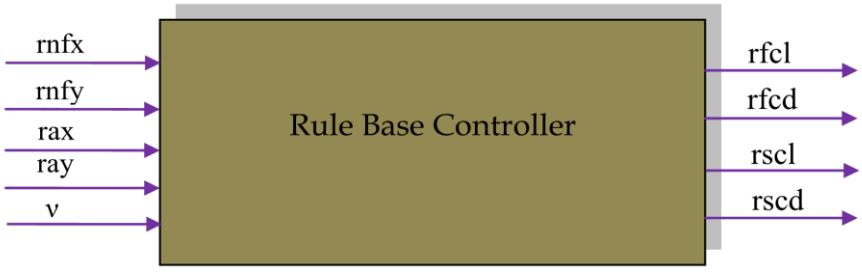

Figure 8.1: Rule base controller for identification of multiple cracks.

In this section, the rule-based technique has been implemented for identification of multiple crack in cantilever rotor partially immersed in the viscous fluid medium. Figure 8.1 shows the resulting architecture of fuzzy rule base technique. The rule base controller

has been designed with five inputs i.e. rnfx, rnfy, rax, ray, ν and four output parameters i.e. rfcl, rfcd, rscl, rscd.

8.3 Analysis of Hybrid Fuzzy-Rule Base Technique for Finding the Multiple Crack in Rotor

This section discusses about the mechanism of hybrid fuzzy-rule based technique for identification of multiple crack in cantilever rotor partially immersed in the viscous fluid medium. A novel hybrid fuzzy –rule base technique has been designed to identifying the locations and depths of multiple crack in cantilever rotor.

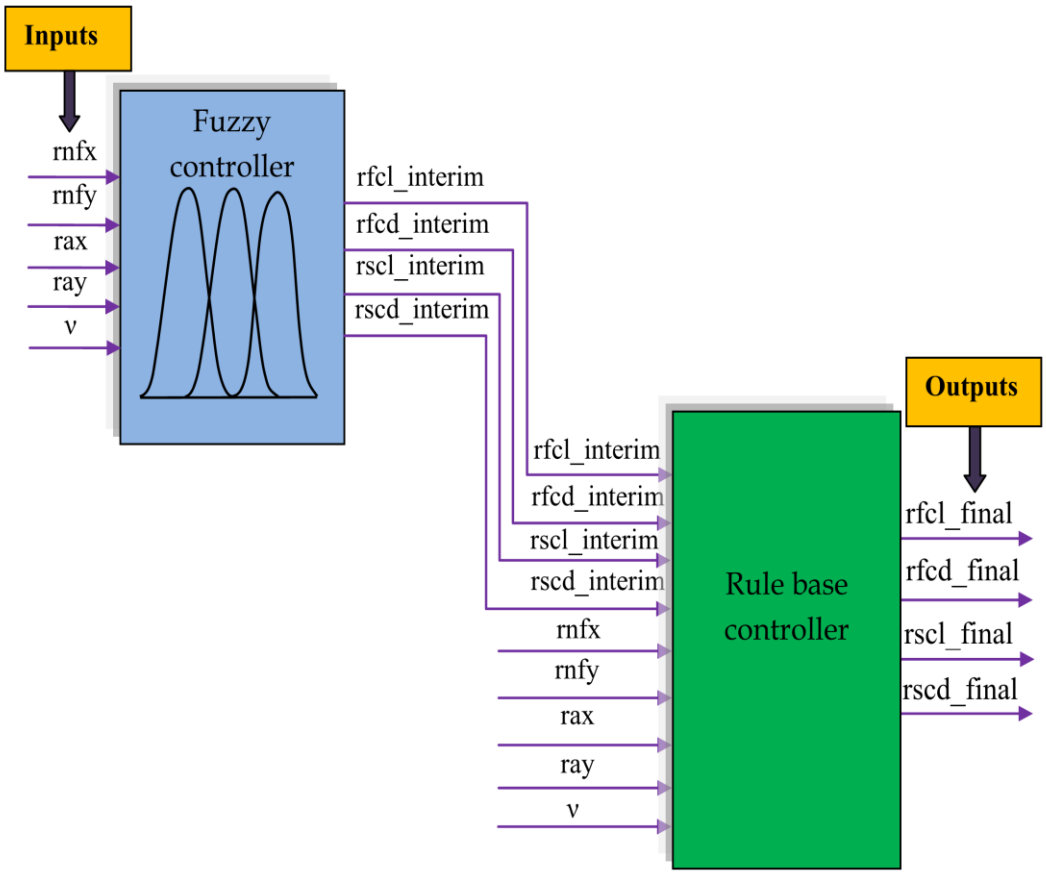

Figure 8.2: Hybrid fuzzy-rule base technique for identification of multiple crack.

Hybrid fuzzy-rule base controller has been designed with combination of fuzzy-base controller and rule base controller. The extracted vibration behavior from theoretical, finite element and experimental analysis are employed to train the hybrid fuzzy-rule base model. Two relative natural frequency, two relative amplitude and viscosity of fluid are used as an input to a fuzzy controller and rfcl_interim, rfcd_interim, rscl_interim, rscd_interim are the outputs from the fuzzy base controller. The output from the fuzzy

controller along with two relative natural frequency, two relative amplitude and viscosity of fluid are fed to the rule base controller. Finally, rfcl_final, rfcd_final, rscl_final, rscd_final are the output parameters from the hybrid fuzzy-rule base technique. The fuzzy controller used here is a taken from Chapter-4. From the previous chapter it is concluded that gaussian membership function is the best among other membership function. Therefore gaussian membership function is used in the fuzzy controller. A comparison of results obtained from theoretical, finite element, gaussian fuzzy, MANFIS, hybrid fuzzy rule base model and experimental analysis have been presented in Table 8.1 and Table 8.2 and the results are found to be in close agreement. The proposed hybrid fuzzy-rule base technique can be used as a robust technique to identify multiple crack in cantilever rotor partially submerged in the viscous medium. The detail architecture of the hybrid fuzzy-rule base controller model has been shown in Figure 8.2.

8.4 Results and Discussion

The current section of this chapter analyses the results obtained from the developed rule base technique and hybrid fuzzy-rule base technique employed for identifying the multiple crack in cantilever rotor partially submerged in the viscous medium. The extracted results from theoretical, finite element and experimental analysis are used to train the rule base model and hybrid fuzzy-rule base model. The rule base model has been designed with inputs i.e. two relative natural frequencies, two relative amplitudes, viscosity of fluid and outputs i.e. first and second relative crack locations and crack depths. Figure 8.1 illustrates the architecture of rule base technique.The proposed hybrid fuzzy- rule base system comprises with two layers. The first layer is the fuzzy base controller, where as the second layer is rule-base controller. The gaussian membership based fuzzy segment of the hybrid fuzzy-rule base model has been developed using the set of fuzzy rules, fuzzy linguistic terms, two relative natural frequencies, two relative amplitudes, viscosity of fluid and the interim output i.e. the rfcl_interim, rfcd_interim, rscl_interim, rscd_interim.The interim outputs from the fuzzy base model along with two relative natural frequencies, two relative amplitudes, viscosity of fluid are fed to the rule base model. Finally, the output parameters i.e. rfcl_final, rfcd_final, rscl_final, rscd_final are obtained. Figure 8.2 illustrates the architecture of hybrid fuzzy-rule base technique.The depiction of the fuzzy linguistic terms for the input and output parameters are shown in Table 5.1. and 5.2 represents twenty numbers of the fuzzy rules out of the several hundred fuzzy rules used

for designing the fuzzy membership functions. A comparison of results obtained from theoretical, finite element, hybrid fuzzy-rule base model and experimental analysis have been presented in Table 8.1. The comparision of obtained results from the rule-base technique, hybrid fuzzy-rule base controller, MANFIS and experimental analysis have been illustrated in Table 8.2.

Table 8.1: Comparison of the results obtained from rule-base technique, Hybrid fuzzy-rule-base , MANFIS and experimental analysis for the rotor.

Relative 1st frequency at x-axis direction 'mfx'	Relative 2nd frequency at y-axis direction 'mfy'	Relative 1st amplitude at x-axis direction 'rax'	Relative 2nd amplitude at y-axis direction 'ray'	Viscosity of fluid 'v'	Experimental relative 1st crack location 'rfcl'				Rule-Base relative 1st crack location 'rfcl'				Hybrid Fuzzy-Rule Base relative 1st crack location 'rfcl'				MANFIS relative 1st crack location 'rfcl'			
					rfcl	rfcd	rscl	rscd	rfcl	rfcd	rscl	rscd	rfcl	rfcd	rscl	rscd	rfcl	rfcd	rscl	rscd
0.8735	0.7305	5.773	5.8122	0.0633	0.187	0.175	0.125	0.300	0.181	0.169	0.122	0.291	0.183	0.172	0.123	0.296	0.179	0.165	0.128	0.289
0.7804	0.6002	6.3111	6.4533	0.541	0.312	0.162	0.687	0.275	0.302	0.161	0.679	0.264	0.305	0.158	0.672	0.267	0.296	0.155	0.645	0.259
0.5777	0.4778	7.1679	6.6364	2.9	0.375	0.125	0.625	0.175	0.363	0.121	0.599	0.172	0.367	0.122	0.605	0.169	0.359	0.129	0.605	0.165
0.8936	0.7843	5.6307	5.6839	0.0633	0.437	0.250	0.750	0.350	0.432	0.238	0.741	0.338	0.427	0.244	0.733	0.341	0.419	0.237	0.71	0.326
0.7893	0.6422	5.9889	6.1122	0.541	0.187	0.225	0.200	0.275	0.183	0.215	0.195	0.262	0.181	0.221	0.193	0.287	0.176	0.218	0.193	0.258
0.6181	0.4993	6.6179	7.0558	2.9	0.250	0.200	0.562	0.350	0.237	0.195	0.538	0.335	0.237	0.197	0.556	0.341	0.235	0.189	0.539	0.327
0.8932	0.7385	6.7564	6.8083	0.0633	0.125	0.175	0.812	0.225	0.121	0.164	0.786	0.213	0.122	0.171	0.794	0.231	0.118	0.169	0.786	0.213
0.7889	0.6067	7.4789	7.6605	0.541	0.625	0.150	0.875	0.325	0.606	0.145	0.839	0.314	0.613	0.146	0.856	0.317	0.595	0.143	0.83	0.311
0.584	0.483	7.6496	7.3818	2.9	0.250	0.300	0.500	0.350	0.237	0.294	0.489	0.338	0.236	0.291	0.494	0.342	0.249	0.288	0.485	0.338
0.8739	0.7226	5.0186	5.0486	0.0633	0.500	0.225	0.750	0.275	0.479	0.217	0.727	0.268	0.491	0.225	0.728	0.269	0.479	0.217	0.718	0.262
Average percentage of error					3.37	3.41	2.82	3.58	2.89	2.02	2.23	1.27	4.46	3.62	3.54	5.26				
Total percentage of error					**3.3**				**2.1**				**4.22**							

Table 8.2: Comparison of the results obtained from Hybrid fuzzy-rule base , FEA, theoretical and experimental analysis for the rotor.

Relative 1st frequency at x-axis direction 'mfx'	Relative 2nd frequency at y-axis direction 'mfy'	Relative 1st amplitude at x-axis direction 'rax'	Relative 2nd amplitude at y-axis direction 'ray'	Viscosity of fluid 'v'	Experimental relative				Hybrid fuzzy-rule base relative				FEA relative				Theoretical relative			
					1st crack location 'rfcl'				1st crack location 'rfcl'				1st crack location 'rfcl'				1st crack location 'rfcl'			
					1st crack depth 'rfcd'				1st crack depth 'rfcd'				1st crack depth 'rfcd'				1st crack depth 'rfcd'			
					2nd crack location 'rscl'				2nd crack location 'rscl'				2nd crack location 'rscl'				2nd crack location 'rscl'			
					2nd crack depth 'rscd'				2nd crack depth 'rscd'				2nd crack depth 'rscd'				2nd crack depth 'rscd'			
					rfcl	rfcd	rscl	rscd	rfcl	rfcd	rscl	rscd	rfcl	rfcd	rscl	rscd	rfcl	rfcd	rscl	rscd
0.8735	0.7305	5.773	5.8122	0.0633	0.187	0.175	0.125	0.300	0.183	0.172	0.123	0.296	0.181	0.172	0.122	0.294	0.179	0.165	0.118	0.292
0.7804	0.6002	6.3111	6.4533	0.541	0.312	0.162	0.687	0.275	0.305	0.158	0.672	0.267	0.302	0.158	0.671	0.271	0.296	0.155	0.643	0.261
0.5777	0.4778	7.1679	6.6364	2.9	0.375	0.125	0.625	0.175	0.367	0.122	0.605	0.169	0.367	0.123	0.605	0.172	0.356	0.119	0.593	0.166
0.8936	0.7843	5.6307	5.6839	0.0633	0.437	0.250	0.750	0.350	0.427	0.244	0.733	0.341	0.432	0.246	0.733	0.342	0.41	0.238	0.718	0.34
0.7893	0.6422	5.9889	6.1122	0.541	0.187	0.225	0.200	0.275	0.181	0.221	0.193	0.287	0.183	0.219	0.195	0.267	0.175	0.214	0.191	0.262
0.6181	0.4993	6.6179	7.0558	2.9	0.250	0.200	0.562	0.350	0.237	0.197	0.556	0.341	0.245	0.194	0.555	0.342	0.237	0.191	0.532	0.331
0.8932	0.7385	6.7564	6.8083	0.0633	0.125	0.175	0.812	0.225	0.122	0.171	0.794	0.231	0.121	0.171	0.792	0.219	0.121	0.167	0.768	0.21
0.7889	0.6067	7.4789	7.6605	0.541	0.625	0.150	0.875	0.325	0.613	0.146	0.856	0.317	0.612	0.146	0.853	0.317	0.612	0.142	0.854	0.314
0.584	0.483	7.6496	7.3818	2.9	0.250	0.300	0.500	0.350	0.236	0.291	0.494	0.342	0.243	0.292	0.489	0.341	0.236	0.281	0.474	0.331
0.8739	0.7226	5.0186	5.0486	0.0633	0.500	0.225	0.750	0.275	0.491	0.225	0.728	0.269	0.484	0.216	0.726	0.266	0.479	0.212	0.711	0.258
Average percentage of error					2.89	2.02	2.23	1.27	2.51	2.47	2.43	2.36	4.73	5.1	4.94	4.76				
Total percentage of error					**2.1**				**2.44**				**4.89**							

8.5 Summary

This chapter has described rule-based and hybrid fuzzy-rule based techniques for identifying the multiple crack in cantilever rotor partially submerged inside the viscous medium. The following summary can be drawn by analyzing the results in terms of crack locations and crack depths derived from rule-base controller and hybrid fuzzy rule base controller. The rule base technique has a set of rules obtained through rule induction and enhanced with manually derived heuristics. In this chapter, an intelligent hybrid fuzzy-rule based controller have been presented. The vibration characteristics and property of viscous fluid derived from theoretical, finite element and experimental analysis for various crack depths and crack locations for cantilever rotor partially submerged in the viscous medium.These data is fed as inputs to the hybrid fuzzy-rule base model and outputs are first and second relative crack depth and location. The gaussian fuzzy model gives most efficient results. It is suggested that the gaussian fuzzy-base controller is used in the hybrid fuzzy-rule base controller. The feasibility of rule-base controller and hybrid fuzzy-rule base model has been verified by experimental examination. It is observed that percentage of error is least in the rule-based controller when compared with experimental results.The error 3.3 % for the cantilever rotor. The hybrid fuzzy-rule base controller produces best results for first and second crack locations and cracks depth in comparison to other artificial intelligence model.The error is found to be 2.1 % for the cantilever rotor when diagnosis is done using rule-base technique.

Chapter 9

Analysis & Description of Experimental Investigation

The experimental investigation has been carried out to evaluate the vibration behavior (natural frequencies and amplitude) of non-cracked and cracked cantilever rotor partially submerged in the viscous fluid medium for the different combination of crack depths and crack locations. The dynamic response evaluated from experimental test has been compared with that of theoretical, numerical and various AI techniques data as discussed in previous chapters. This chapter addresses the organized experimental investigation procedure and discusses vibration behavior measuring devices for evaluating the vibration response of cantilever rotor.

9.1 Detail Specification of Apparatuses used in the Experimental Analysis

Experiments have been accomplished using the developed experimental setup (Figure 9.1) for measuring the dynamic response (natural frequency and amplitude of vibration) of the mild steel cantilever rotor attached disc at the free end (length and radius are 0.8m, 0.01m respectively).The experiments are conducted for cantilever rotor partially submerged in the viscous medium. Cracked mild steel rotor specimens have been taken for experimental analysis with different crack locations and depths. Three different viscous fluids are used as a viscous medium. The cantilever rotor is connected to the power motor which is supported by the ball bearing. The cracked, and non-cracked cantilever rotor has been displaced from its original position while rotating with the help of power motor. The amplitude of the rotor has been recorded by ultrasonic sensors which are connected to Arduino micro-controller with the help of jumper wire. The ultrasonic sensors are used for recognizing the displacement of the rotating rotor from the original position. The sensing displacement data of ultrasonic sensor are displaced in the computer system with the help of Arduino microcontroller. The rotating speed of rotor is controlled by the variac.The

accessories used in the experimental analysis have been shown in Table 9.1with their specifications in detail.

Table 9.1: Detail description and specifications of the apparatus used in the experiments

Sl. No.	Name of the Instrument	Description of Instruments
1	Power motor	Type AC/DC, FHP Motor
		125 Watt, 220V,
		Speed: 6000RPM
2	Micro-controller	Arduino UNO ATmega 328 ,32KB
		Operating Voltage 5V, SRAM 2KB
		Analog Input Pins 6
		Input voltage 6-20V
		Digital Input Pins 14
3	Communication	USB connection Serial Port
4	Bread board	Small Size Bread Board.
5	3 Ultrasonic Sensors	Range of distance measure: 0.01m to 4m
6	Power supply	50Hz ,230 to 240v AC
7	Variac	Input : 230v, 50 to 60 Hz,
		Output: 0 to 270 v
		Maximum Load 8 Amp.
8	Vessel	Dia. of vessel= 260mm, Height=400mm
9	Display device	Computer system
10	Test specimen	Double cracked mild steel rotor
		Radius of Rotor (R_1) is 0.01m
		Length of Rotor(Ls) = 0.8m
11	Techo meter	Laser photo /contact tachometer
		Detacting 5 digits, 10 mm (0.4") LCD.
		Measuring range 0.5 to 20000 RPM
		± (0.05% + 1 digit), RPM only.

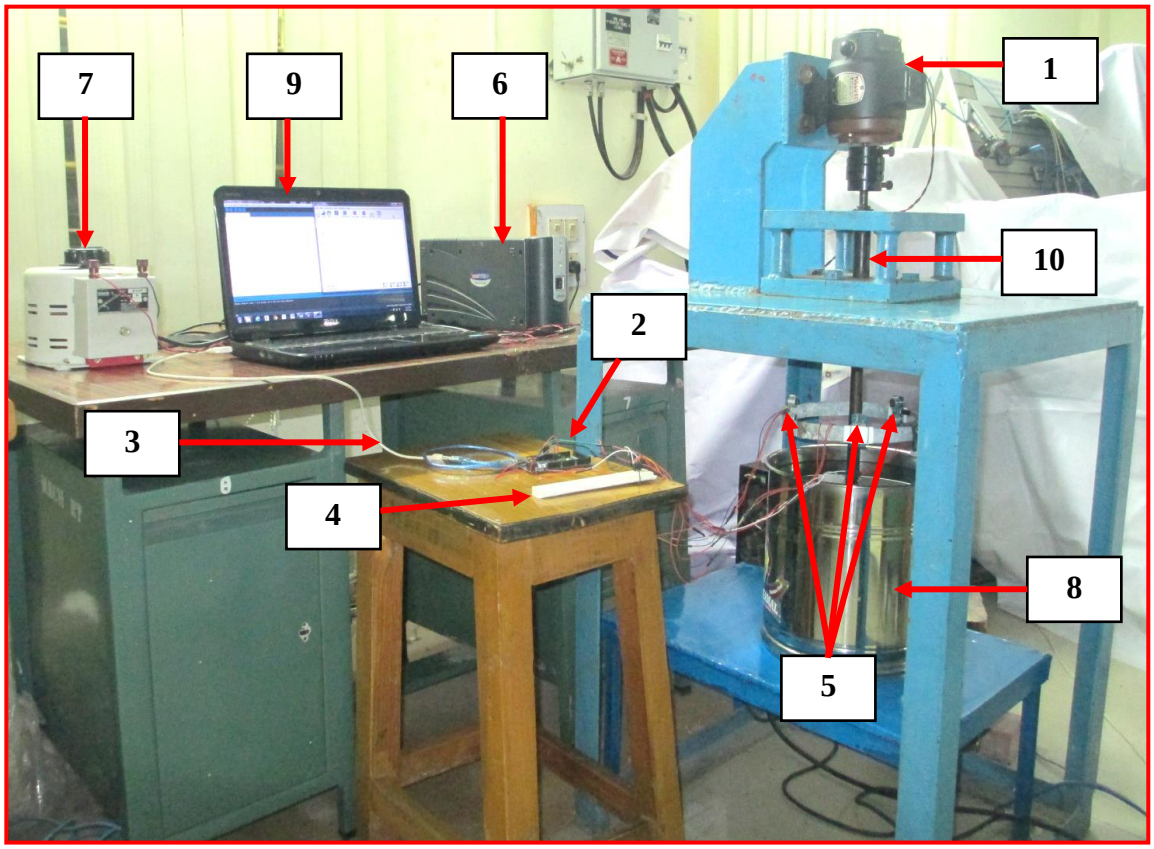

Figure 9.1 : View of the experimental setup.

1.Power Motor, 2.Aurdino Micro-controller, 3.USB Connection Serial Port, 4.Bread Board, 5.3Ultrasonic Sensors, 6.Power Supply, 7.Variac, 8.Fluid Filled Container, 9.Dispaly Device, 10. Cantilever Rotor

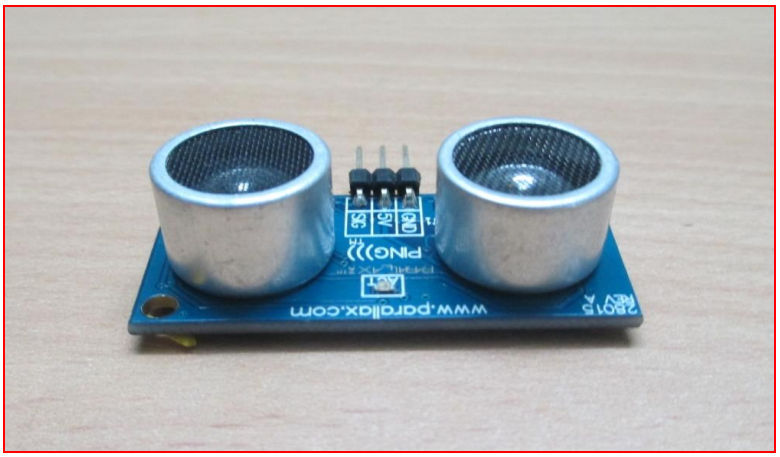

Figure 9.1(a): Ultrasonic sensor

Figure 9.1(b): Aurdino micro-controller

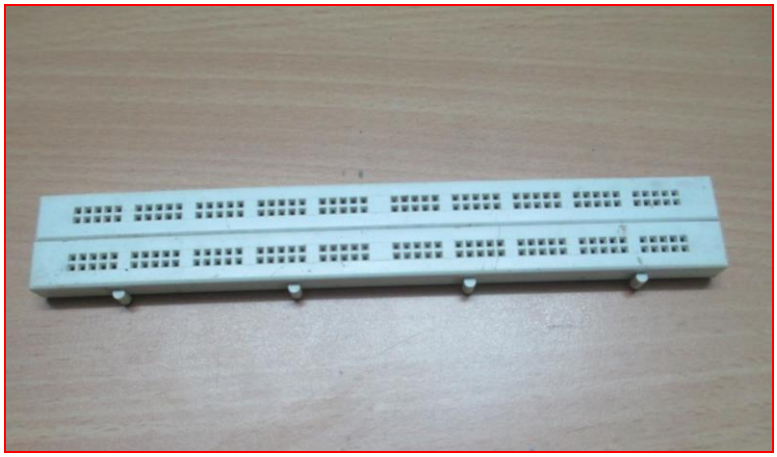

Figure 9.1(c): Bread board

Figure 9.1(d): Variac

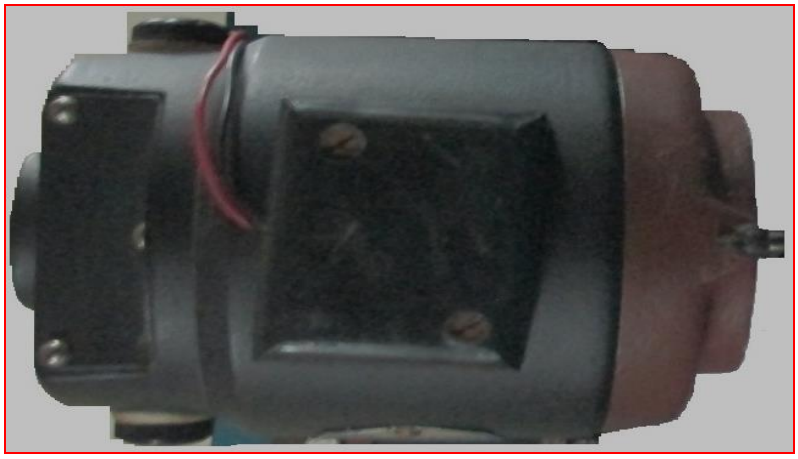

Figure 9.1(e): Power motor

Figure 9.1(f) : Tachometer

Figure 9.1(g): Display device

9.2 Experimental Procedure for the Analysis of Rotor System

The experimental investigation has been performed on the non-cracked and cracked rotating cantilever rotor partially submerged in the viscous fluid medium to verify the robustness of the results derived from theoretical, numerical and various artificial intelligence techniques.

The experimental setup comprises of a multiple cracked rotor with additional mass, power motor, variac, arduino micro-controller, breadboard, USB connection serial port ,three ultrasonic sensors and fluid filled vessel as shown in Figure 9.1.The cracks at various locations and different depths are introduced in the specimen with the help of wire cut EDM for mild steel rotor. The inside diameter and length of fluid container are 260mm and 400mm respectively. The additional mass (i.e. disc) attached at the free end tip of the rotor. The rotating speed of the cantilever rotor is controlled by the variac. One end of the variac is connected to the power motor and other end is connected to power supply. The shaft of the motor is coupled with the cantilever rotor by the universal joint. The rotor is supported by ball bearing. It is assumed that the operated loads are acted radially on the bearing and there are no thrust loads of significant magnitudes. There are also other assumptions taken into account for the ball bearing [213] and are given below.

1. The rolling surfaces are free of defects and perfectly smooth.
2. The rolling balls are equi-pitched around the rotor.
3. The complete ball bearing assembly is rigid excluding for the point of contact between the raceways and the rolling bodies.
4. The rolling balls of the bearing assembly are massless. This eliminates independent radial degrees of freedom.
5. The outer race of the ball bearing is firmly attached to a rigid housing while the inner race is sustaining the heavy elastic rotor.

The kinematic viscosities of the fluids are taken at the temperature 25^0C.When the rotor rotates inside the fluid medium, the temperature of the fluid increases little due to shearing action. Due to altered temperature, there are very slight changes in the kinematic viscosity of the fluid. So the effect of temperature on the viscosity of the fluid is neglected. In the present analysis, first mode is taken into account. As it is the major contributor of amplitude as compared to other modes of vibration. In the current analysis, other modes of

vibration (apart from the 1st mode) and shearing inertia effect are not considered. Three ultrasonic sensors are arranged at the 8cm circumferential radius of the rotor, which is connected to the Arduino micro-controller with the help of wire. Sensors data are displayed on the screen of computer system. Experimental results for amplitude of transverse vibration at particular location along the length of the rotor are recorded by positioning the three ultrasonic sensors at the corresponding resonant frequencies.Each sensor has separate deflection data for the rotor. For accuracy, reading has been taken for three times at the same speed. Each set has 900 samples measured by sensors within 15 minutes (i.e. sampling time 1sec/sample).The pictorial view of various apparatuses used in the experimental test are shown in Figures 9.2(a) to 9.2(g).

9.3 Results and Discussion

The present section describes the analysis of results obtained from the experimental investigation. The non-cracked and cracked rotor with various crack locations and different crack depths partially submerged in the viscous fluid medium have been examined in the experiment at set up to get the vibration signatures. This is used to verify the robustness of results obtained from the various techniques discussed in the previous chapters. Comparison of results derived from the theoretical analysis for multiple crack cantilever rotor with orientation of cracks (β_1=0.125, β_2=0.175, β_3=0.225 and β_4=0.275), crack location (α_1=0.313, α_2=0.563) and viscosity of fluid (ν_1= 0.0633, ν_2= 0.541, ν_3= 2.9) are shown in Chapter 3 and they are plotted with result of experiment examination in the Figures 3.2 to 3.9 and 3.11 to 3.18 for the mild steel cantilever rotor. The results derived from the theoretical and experimental observation are presented in tabular form with relative amplitude and relative crack location and crack depth in the Tables 3.3 to 3.8 for the cantilever rotor. Agreement between the results is observed. Theoretical results for cantilever cracked rotor are found to be within 5% error when compared with the experimental results. The results for both transverse direction (i.e. 44 and 55-axis direction) relative natural frequency and relative amplitude are obtained from finite element analysis for multiple crack rotor with several depths of cracks (β_1=0.125, β_2=0.175, β_3=0.225 and β_4=0.275), crack locations (α_1=0.313, α_2=0.563) and viscosity of fluids (ν_1= 0.0633, ν_2= 0.541, ν_3= 2.9 stokes) in Chapter 4. The results are plotted with corresponding relative amplitudes derived from theoretical and experimental investigation for cracked cantilever rotor and has been illustrated in Figures 4.3 to 4.13. The results for

first relative crack depth and crack position and second relative crack location and crack depth are derived from theoretical, numerical and experimental examination corresponding to relative natural frequencies and amplitude in both transverse direction. The results are presented in Tables 4.3 to 4.13 for cantilever rotor. The finite element analysis results for cantilever cracked rotor are found within 2.5% error when compared with the experimental results. In Chapter 5, the results derived from Mamdani gaussian fuzzy, Sugeno gaussian fuzzy, hybrid gaussian fuzzy model and experimental test have been compared in Table 5.7 for cantilever rotor. Tables 5.3 to 5.6 present the comparison of results obtained from Mamdani and Sugeno fuzzy model along with three membership function (Triangular, Gaussian and Trapezoidal) for cantilever rotor. The total percentage of error of results for Mamdani Triangular fuzzy model is 7.32%, for Mamdani gaussian fuzzy model is 5.25%, for Mamdani Trapezoidal fuzzy model is 6.77% for the cantilever rotor. Similarly, total percentage of error of results for Sugeno Triangular fuzzy model is 6.98%, for Sugeno gaussian fuzzy model is 5.01 %, for Sugeno Trapezoidal fuzzy model is 6.12%. The total percentage of error of results for hybrid gaussian fuzzy model is 4.82%. Chapter 6 presents discussion about BPNN, RBFNN and hybrid BPNN-RBFNN neural network model. The results derived from BPNN, RBFNN and hybrid BPNN-RBFNN model are compared with experimental analysis results and have been presented in Table 6.4 for cantilever rotor. The percentage of total error for BPNN is 5.16% ,for RBFNN is 4.98% and hybrid BPNN-RBFNN model is 4.60% for cantilever rotor. The comparison of results derived from MANFIS systems have been displayed in Tables 7.1, and 7.2 for cantilever rotor. The total percentage of error for MANFIS is 4.22% for cantilever rotor. The comparison of results obtained from rule base technique have been presented in Tables 8.1 and 8.2. The total percentage of error for rule-base controller and hybrid fuzzy-rule base controller is 3.3% and 2.1% respectively. Close proximity is found between the compared results. After the study of results, it is observed that Sugeno gaussian fuzzy, RBFNN, hybrid fuzzy,MANFIS, rule-base technique and hybrid fuzzy-rule base system provides the least error in the result when compared with results obtained from experimental analysis.

Chapter 10

Results and Discussion

10.1 Introduction

This chapter introduces the systematic analysis of performance of various techniques used for identification of multiple crack in cantilever rotor partially submerged in the viscous fluid cited in the above chapters. The dynamic responses of cracked rotor have been used for development of fault diagnosis tool. Several techniques are discussed in the current dissertation for assessment of multiple crack in cantilever rotor. These techniques are: theoretical method (Chapter 3), Finite element method (Chapter 4), fuzzy logic system (Chapter 5), and artificial neural network (Chapter 6), MANFIS (Chapter 7), hybrid fuzzy-rule base technique (Chapter 8) and experimental investigation (Chapter 9).

10.2 Analysis of Results

Ten techniques have been employed in current research for development of crack identification tool of cantilever rotor partially immersed in the viscous fluid as discussed in introduction (Chapter 1). This dissertation comprises two introductory chapters (Chapter 1- Introduction and Chapter 2 - Literature review) besides eight chapters. This section addressed the analysis of results derived from various methods cited in different chapters. The introduction section (Chapter 1) of the thesis addressed aims and objective along with the motivation factors to carry out current research. The outline of the dissertation is also discussed in last section of Chapter 1. The literature review (Chapter 2) part addresses the various methodologies that have been presented by researchers and engineers for prediction of cracks in structures (i.e. rotor, beam, plate) and machine components. Finally, this section discusses the results obtained from the investigations. The vibration response has been obtained by theoretical analysis of rotating non-cracked and cracked fixed-fixed supported rotor and cantilever rotor partially submerged in the viscous medium cited in Chapter 3. The whirling position of cantilever rotor with attached disc at the free end has been illustrated in Figure 3.1. The results obtained from the theoretical analysis are depends upon viscosity and density, length of rotor, radius of fluid

filled container, mass of disc and damping coefficient. Figures 3.2, 3.3, 3.7, 3.8, 3.20 and 3.21 represent the effect of viscosity and density of fluid on the vibration response of non-cracked rotor. It is observed that as the viscosity and density of the external fluid increases, the amplitude as well as critical speed decreases. Comparing the results presented in Figures 3.2-3.3, 3.7-3.8 and 3.20-3.21, it is found that the amplitude of vibration for the longer rotor is smaller than that of the smaller rotor. This is a peculiar phenomenon which is caused because of higher values of the virtual mass coefficient and damping coefficient in case of longer rotor. Figures 3.4 and 3.22 show the effect of gap ratio (i.e. fluid container radius increases) on the vibration response of non-cracked rotor. It is observed that the amplitude of rotor increases with the increase in container radius. Figures 3.5, 3.9 and 3.23 show the virtual mass effect on the amplitude of non-cracked rotor. It is noticed that as the virtual mass effect increases the amplitude of vibration decreases and it also decreases the resonance frequency for the rotor. Figures 3.6 and 3.24 illustrate the damping coefficient on the vibration response of rotor. It is observed that the damping has reduced only the amplitude of vibration rather then shifting the resonance frequency for the rotor. Figures 3.12, 3.13, 3.26 and 3.27 show the effect of multiple crack depths on the vibration response of the rotor in the both transverse direction (i.e.44-direction and 55-direction). It is observed that due to increase in multiple crack depths, the critical speed as well as amplitude of vibration decreases. The comparison between 44-direction and 55-direction amplitude of vibration has been presented in the Figures 3.14 and 3.28. It is found that the obtained amplitude of vibration in 44-direction is greater then the obtained amplitude of vibration in 55-direction of crack in rotor. It is found that there is significant error in the amplitude and natural frequency due to the presence of a crack. Figures 3.16 and 3.29 illustrate the effect of virtual mass on the vibration response of the cracked rotor. A comparison and authentication of the results obtained from theoretical analysis are plotted with results from experimental analysis and have been plotted in Figures 3.31 to 3.41. Figures 3.11(a), 3.11(b) and 3.11(c) describe the full view of the cantilever rotor with crack element, Cross-section of crack element and coupling forces on the crack element for the theoretical analysis of cracked rotor respectively. Full view of fixed-fixed rotor and schematic of multiple cracked fixed-fixed rotor submerged in the viscous fluid have been illustrated in the Figures 3.19 and 3.25 respectively. Schematic block diagram of experimental setup for the multi-cracked cantilever rotor partially submerged in the viscous medium has been presented in the Figure 3.30. A comparison and authentication of the results obtained from the theoretical analysis and experimental

analysis have been plotted in Figures 3.31 to 3.41. The result obtained from theoretical and experimental observation have been presented in Tables 3.3 to 3.8 for cantilever rotor. The results derived from the theoretical analysis compared with the experimental results for effect of change in viscosity of fluid on the vibration response of non-cracked cantilever rotor and has been presented in Table 3.4.The result derived from the theoretical analysis compared with the experimental results for effect of virtual mass on vibration behavior of non-cracked and cracked cantilever rotor have been presented in Tables 3.4 and 3.5 respectively. Tables 3.6 and 3.7 have presented the comparison of derived theoretical and experimental result for the effect of change in radius of fluid filled container on non-cracked and cracked cantilever rotor. A comparison between theoretical and experimental results for the effect of multiple crack depths in crack locations in both transverse directions (i.e. 44-direction and 55-direction) of cantilever rotor partially submerged in the viscous fluid medium and has been presented in Table 3.8. As can be seen, the results obtained using the theoretically shows agreement with the experimental results.The total percentage of error of finite element analysis is 5% for cantilever rotor.The finite element based simulation software package ANSYS has been used to extract vibrational features of cantilever rotor (in Chapter 4). It is noticed that presence of damage in the form of crack in the cantilever rotor can vary the vibration responses. The various steps involved in the ANSYS to solve the problem have been discussed. The results obtained from the finite element method have been authenticated by results of experimental analysis for the cantilever rotor partially submerged in the viscous medium. The SOLID187 element is used for the solid mild steel cantilever rotor. The geometry of the SOLID187 element is presented in Figure 4.1. The FLUID30 3-D acoustic fluid element is used for the viscous fluid. The geometry of FLUID30 3-D acoustic fluid is presented in the Figure 4.2. The properties of the mild steel rotor and fluid medium are presented in Tables 4.1 and 4.2.The results obtained from the finite element analysis are plotted with results derived from theoretical and experimental analyses for non-cracked and cracked cantilever rotor partially submerged in the viscous medium and have been presented in Figures 4.3 to 4.13. The results for 44-direction with altered relative crack depths and relative crack locations obtained from finite element analysis have been plotted with results derived from the theoretical and experimental analysis for cracked cantilever rotor and are shown in Figures 4.8 to 4.10. The results for 55-direction with altered relative crack depths and relative crack locations obtained from finite element analysis have been plotted with results derived from the theoretical and experimental analysis for

cracked cantilever rotor and are shown in Figures 4.11 to 4.13.The comparison of obtained FEA result with the theoretical and experimental result for effect of change in viscosity of fluid on the non-cracked cantilever rotor has been presented in Table 4.3. The comparison of FEA result with theoretical and experimental result for virtual mass effect on the non-cracked and cracked cantilever rotor partially submerged in the viscous medium and have been represented in Tables 4.4 and 4.5 respectively. The comparison of FEA result with theoretical and experimental results for effect of change in radius of fluid filled container on the vibration response of non-cracked and cracked cantilever rotor has been illustrated in Tables 4.6 and 4.7 respectively. The comparison of FEA result with theoretical and experimental results for the effect of different relative crack depths and crack locations on the vibration response of the cantilever rotor partially submerged in the viscous medium in both transverse direction (i.e. 44-direction and 55-direction) have been presented in the Table 4.8. It is observed that results have good agreement with each other. The total percentage of error of results from finite element analysis and experimental results is 3% for cantilever rotor. The analysis of results derived from the developed fuzzy model for identification of multiple crack in cantilever rotor has been depicted in Chapter 5. The fuzzy logic system has been developed with simple but effective architecture for five input variables (relative first natural frequencies, relative second natural frequency, relative first amplitude, relative second amplitude and viscosity of fluid) and four output variables (relative first and second crack locations and crack depths). Three types of membership functions (Triangular, Gaussian and Trapezoidal) are employed in the development of the Mamdani and Takagi-Sugeno fuzzy system and are presented in Figures 5.1(a), 5.1(b) and 5.1(c) respectively. The various phase involved in the fuzzy logic system has been shown in Figure 5.2. The complete structure of the Mamdani fuzzy system including three different type of membership functions with the linguistic variable has been illustrated in Figures 5.4 to 5.6.The defuzzification of inputs using various membership functions (Triangular, Gaussian and Trapezoidal) have been performed with the help of activated rules 5 and 18 of Table 5.2 and are presented in Figures 5.7 to 5.9. Figure 5.11 represents the structure of the hybrid fuzzy model. The results derived from various Mamdani and Takagi-Sugeno fuzzy models (Triangular, Gaussian and Trapezoidal) and experimental test have been compared in Tables 5.3 and 5.5 respectively for cantilever rotor. Table 5.4 represents the comparison of results obtained from theoretical, finite element analysis, Mamdani Fuzzy gaussian model and experimental analysis for cantilever rotor. The comparison of results obtained from

theoretical, finite element analysis, Takagi-Sugeno fuzzy gaussian model and experimental analysis have been represented in Table 5.6.The comparison of results obtained from the Mamdani gaussian fuzzy, Takagi-Sugeno gaussian fuzzy and hybrid gaussian fuzzy system have been presented in Table 5.7. The total percentage of error of results for the Mamdani triangular fuzzy model is 7.32%, for Mamdani gaussian fuzzy model is 5.25%, for the Mamdani Trapezoidal fuzzy model is 6.77% for the cantilever rotor. Similarly, the total percentage of error of results for the Sugeno Triangular fuzzy model is 6.98%, for Sugeno gaussian fuzzy model is 5.01 %, for the Sugeno Trapezoidal fuzzy model is 6.12% for cantilever rotor. The total percentage of error of results for hybrid gaussian fuzzy model is 4.82% for cantilever rotor. Chapter 6 depicts the discussion on the analysis of results derived from various neural models such as BPNN and RBFNN. Figure 6.1 presents the model of neuron of artificial neural network. Figure 6.2 illustrates the nine-layered Feed forward back propagation neural network techniques used for identification of first and second crack locations, and crack depths and are presented in Figure 6.3. First relative natural frequency, second relative natural frequency, first relative amplitude, second relative amplitude and viscosity of fluid have been used as input variables to input layer of Feed forward back propagation neural network model. These input variables process through seven hidden layers then output layer gives first and second relative crack depths and relative crack locations. The RBFNN is a feed forward, supervised learning type of neural network. In present work, RBFNN is employed for localization and quantification of cracks, present in the cantilever rotor partially submerged in the viscous medium. Similar to BPNN model, RBFNN consists of one input layer and output layer. But RBFNN has only one hidden layer. Moreover, output layer gives relative crack locations and crack depths. Figure 6.5 denotes architecture of radial basis function neural network for identification of multiple crack. The results obtained from neural network techniques (BPNN and RBFNN) and the experimental test are compared and close agreement between each other is observed. The results derived from BPNN model compared with theoretical, finite element and experimental analysis results are presented in Tables 6.1. The results derived from RBFNN model compared with theoretical, finite element and experimental analysis results are presented in Tables 6.2. The total percentage of error for BPNN is 5.16%, for RBFNN is 4.98% and for hybrid BPNN-RBFNN is 4.60% for the cantilever rotor. The results obtained from BPNN, RBFNN, Mamdani fuzzy gaussian model and experimental analysis has been compared in Table 6.3 for cantilever rotor. The results obtained from BPNN, RBFNN, hybrid BPNN-

RBFNN and experimental analysis has been compared in Table 6.4. It is observed that the hybrid BPNN-RBFNN model gives better results as compared to BPNN, RBFNN and the Mamdani fuzzy gaussian model for the cantilever rotor. Chapter 7 describes the analysis of results obtained from the Multiple Adaptive neuro fuzzy system (MANFIS). The fuzzy system with bell-shaped membership function is integrated with MANFIS models for designing the smart crack identification mechanism for cantilever rotor. Figure 7.1 presents the model of bell shaped membership function and Figures 7.2(a) and 7.2(b) represent the MANFIS controller and Adaptive neuro fuzzy inference system (ANFIS) for crack identification in cantilever rotor respectively. First relative natural frequencies, second relative natural frequencies, first relative amplitude second relative amplitude and viscosity of fluid are used as inputs to the fuzzy segment of the MANFIS model. The output of the MANFIS model is first and second relative crack locations and crack depths. MANFIS can predict the crack depth and its location using the vibration response (i.e. natural frequency and amplitude) of the rotating cantilever rotor partially submerged in the viscous medium. The comparison of results derived from MANFIS, RBFNN, Sugeno fuzzy gaussian model and experimental analysis have been presented in the Table 7.1. The comparison of results derived from MANFIS, FEA, theoretical and experimental analysis have been presented in the Table 7.2. The total percentage of error is 4.22% for MANFIS model for multiple crack identification in the rotor. It is observed that the MANFIS can predict the crack locations and their intensities and are very close to the results compared to results from FEA, RBFNN, Sugeno fuzzy gaussian and experimental analysis.The analysis of results obtained from the developed hybrid fuzzy-rule base model for identification of multiple crack in cantilever rotor partially submerged in the viscous medium and has been depicted in Chapter 8. The total percentage of error for rule-base controller and hybrid fuzzy-rule base controller is 3.3% and 2.1% respectively. The hybrid fuzzy-rule base controller has given least error as compared to other artificial intelligence techniques.The experimental investigation is performed to verify the robustness of the results derived from the theoretical analysis, finite element analysis, fuzzy logic system, neural network techniques, MANFIS and hybrid fuzzy-rule base technique and is discussed in Chapter 9. The schematic and snapshot view of the experimental set up with all required instruments and test specimen are shown in Figures 3.12 and 9.1.The developed experimental setup comprises of the following apparatuses: 1-Cracked cantilever rotor, 2-Disk, 3-Fluid filled container, 4-Arduino Micro-controller, 5-Vraiac, 6-

Power motor, 8-there ultrasonic sensors.The systematic experimental procedure is described in the section 9.3 of Chapter 9.

10.3 Summary

After the comprehensive investigation of the current chapter it is observed that the hybrid fuzzy model provides better results as compared to the results derived from standalone AI techniques. Among all proposed hybrid models, hybrid fuzzy-rule base technique gives far better results. The total percentage of error for hybrid fuzzy-rule base model with experimental results is 2.1%.

Chapter 11

Conclusions and Scope for Future Research

11.1 Introduction

In the current investigation, localization and quantification of crack locations and depths present in the cantilever rotor partially submerged in the viscous fluid using vibration response have been addressed. The effects of multiple transverse cracks on cantilever rotor are analyzed using the intelligent fault diagnosis system. The dynamic responses of cantilever rotor have been determined using theoretical, finite element and experimental analysis. The influence of cracks on the dynamic behavior of the rotor is found to be very sensitive in regards to crack location, crack depth in the viscous medium. The dynamic response has been adopted to design inverse intelligent crack identification tools such as fuzzy logic system, neural network, multiple adaptive neuro fuzzy-interference system (MANFIS) and hybrid fuzzy-rule base technique for assessment of relative crack locations and relative crack depths.

11.2 Conclusions

The conclusions are drawn on the basis of results derived from various methods as discussed in the above chapters and are as follows;

- The theoretical, finite element and experimental analyses for cantilever rotor containing multiple transverse crack partially submerged in the viscous fluid have been derived to evaluate the natural frequencies and amplitude of the system.
- The rheological properties (i.e.viscosity and density) of viscous fluid have great influence on the dynamic response of the spinning rotor. From the theoretical analysis, it is observed that the resonant frequency of the rotor is decreased with the increasing viscosity and density of the viscous fluid. Also, the critical speed of the rotor reduces due to increasing in virtual mass and the amplitude of vibration decreases due to increasing in damping coefficient factor.

- It is observed from the analysis that increasing the radius of the container (i.e. gap ratio), increases the amplitude of vibration, which is due to decreases in damping factor and virtual mass effect. The increment in the damping factor, decreases the amplitude of vibration.
- The positions of the cracks affect significantly the changes in the natural frequencies of vibrations in the case of constant relative depth of the cracks. When there is increase in the distance of the crack location from fixed end of cantilever rotor the natural frequencies tend to increase.
- The critical speed reduces due to the presence of multiple transverse crack in the rotor. The stiffness of the cracked rotor along the crack (55-Direction) is lower than the stiffness in perpendicular to the crack (44-Direction) and both transverse directional stiffness of cracked rotor are lower than the stiffness of non-cracked rotor. The critical speed measured along the crack (55-Direction) is inferior than that measured in the direction of perpendicular to the crack (44-Direction) and again both are lower then the non-cracked rotor.
- The experimental test on cracked cantilever rotor with different crack orientations has been performed to verify the authentication of the dynamic response obtained from theoretical and finite element methods for cantilever rotor (shown in Figures 4.8 to 4.13). The results are in close agreement. The percentage of error is found within 5% between theoretical and experimental results.
- The dynamic response (i.e. relative natural frequencies and amplitude) corresponding to different crack locations and its size have been used as a platform to develop the fuzzy logic system for multiple crack identification of cantilever rotor system partially submerged in the viscous fluid.
- The triangular, gaussian and trapezoidal membership functions have been employed to design and develop the Mamdani fuzzy and Takagi-Sugeno fuzzy logic system with five input and four output parameters. From the analysis of results, it is reported that fuzzy system can be efficiently used for identification of crack locations and depths.
- Both fuzzy models (i.e. Mamdani fuzzy and Takagi-Sugeno fuzzy) with gaussian membership function provide better results as compared to Triangular and Trapezoidal fuzzy models. It is reported by the analysis of results from the fuzzy models. Hence, a fuzzy model with gaussian membership function is found most suitable for identification of crack present in the rotor system.

- The hybrid fuzzy model with gaussian membership function has been designed to predict the crack present in the cantilever rotor system. From the analysis of results, it is concluded that the hybrid fuzzy model with gaussian membership function provides better results as compared to Mamdani fuzzy and Takagi-Sugeno fuzzy models. The hybrid Fuzzy model with gaussian membership function can be used as potential crack identification tools.
- The artificial neural network techniques such as BPNN,RBFNN and hybrid BPNN-RBFNN method have been used as crack identification tool with five input and four output parameters in current research. The training data for developed neural models have been derived from theoretical, finite element and experimental investigations. The results predicted by neural network techniques in terms of relative crack locations and its size have good agreement with the experimental results. The results predicted by proposed hybrid BPNN-RBFNN model provides the least error from experimental results. The percentage of error is found 4.6% between hybrid BPNN-RBFNN model and experimental results.The hybrid BPNN-RBFNN model can be used more efficiently than BPNN and RBFNN models for the identification of crack in the rotor.
- Multiple adaptive neuro fuzzy inference system (MANFIS) has been employed to develop a crack identification tool in rotor system. From the investigation of results predicted from MANFIS technique, it is observed that the MANFIS technique can find the crack parameters with greater accuracy as compared to Fuzzy logic model and neural network model and the MANFIS results are in close proximity with the experimental analysis results.The total percentage of error is found 4.22% between theoretical and experimental results. Hence, the developed crack identification technique is proficient to identify crack in the faulty rotor system.
- The rule base and hybrid fuzzy-rule base technique has been designed with five input and four output parameters. By analyzing the results from rule base technique, it is noticed that the hybrid fuzzy-rule base technique results are more accurate in comparison to fuzzy logic, neural network and MANFIS techniques. The total percentage of error is found 2.1% between hybrid fuzzy-rule base technique and experimental results.
- The results predicted from proposed AI techniques have been compared with the results obtained from the theoretical, numerical and experimental analysis. The results predicted from hybrid fuzzy-rule base model provides more accurate results as compared to other AI techniques discussed in above chapters. It is concluded that

hybrid fuzzy-rule base technique can be used as an efficient crack identification tool in the engineering system.

- The developed artificial intelligent fault diagnosis system can be used for identification of cracks present in cantilever type long rotating shaft used in drilling jigs, high speed centrifuges, high-speed turbine rotor, mechanical systems, marine structures, various engineering systems etc. This theory can also be used for fault detection of the rotor rotating in the viscous medium for conditioning monitoring.

11.3 Future Scope of Research

- Bearing characteristics for rotor system play an important role on its dynamics behaviour, which can be incorporated in the theory for higher accuracy.
- The application of AI techniques may be extended to estimation of damage present in the dynamic engineering system.
- The hybridization of AI techniques can be used as an effiecient, accurate and robust fault detection technique for identification of damage present in various vibrating dynamic systems such as turbine shafts, helicopter rotors etc.

Appendix-A

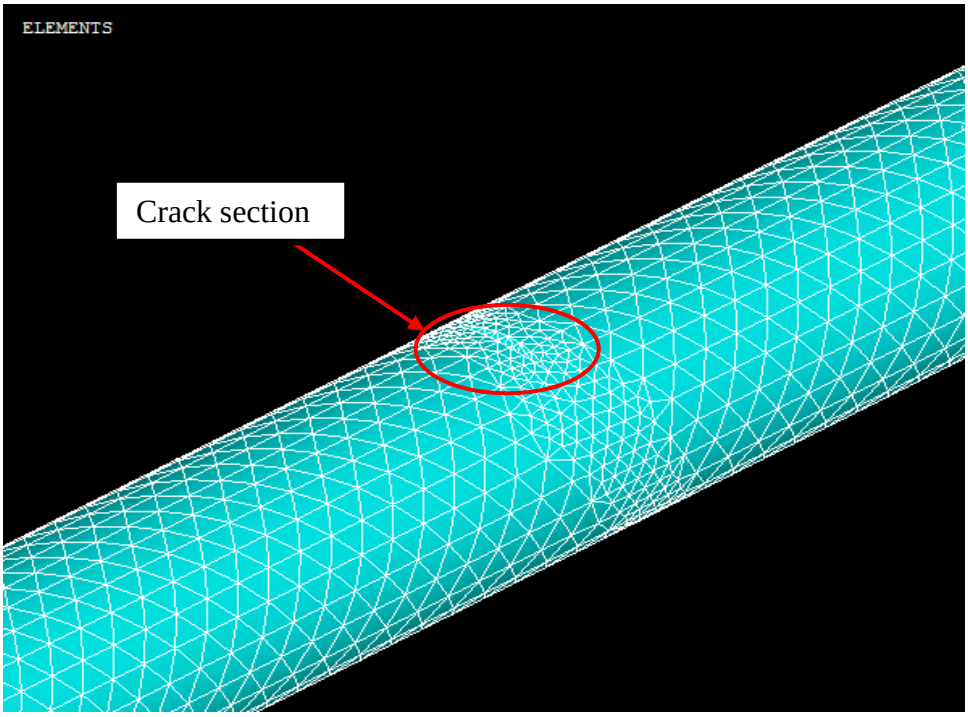

Figure A1: FEA model of crack rotor

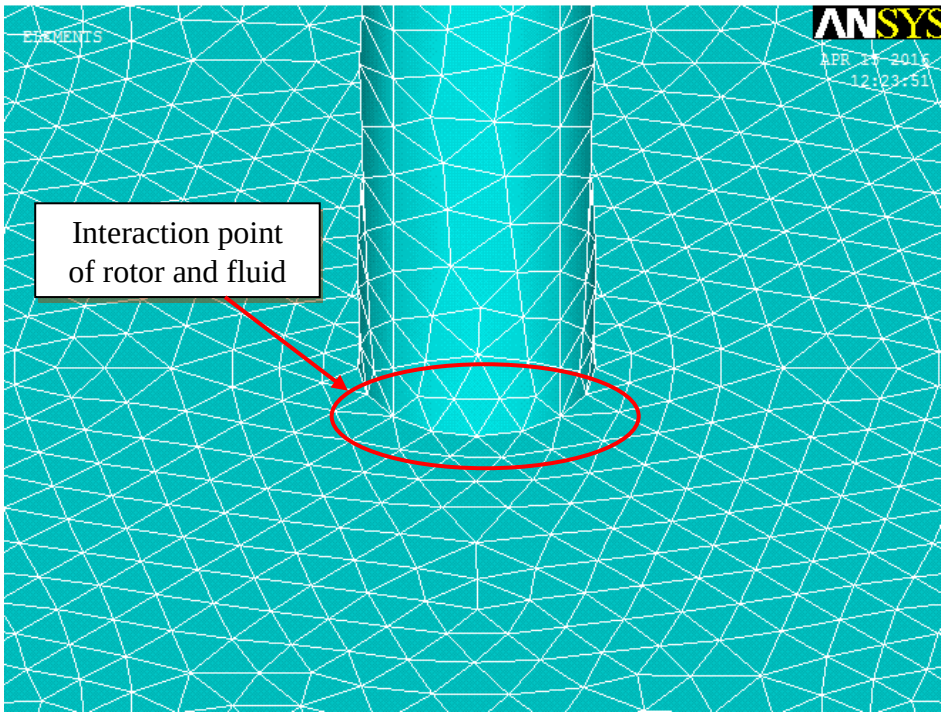

Figure A2: FEA model of rotor immersed in the fluid medium

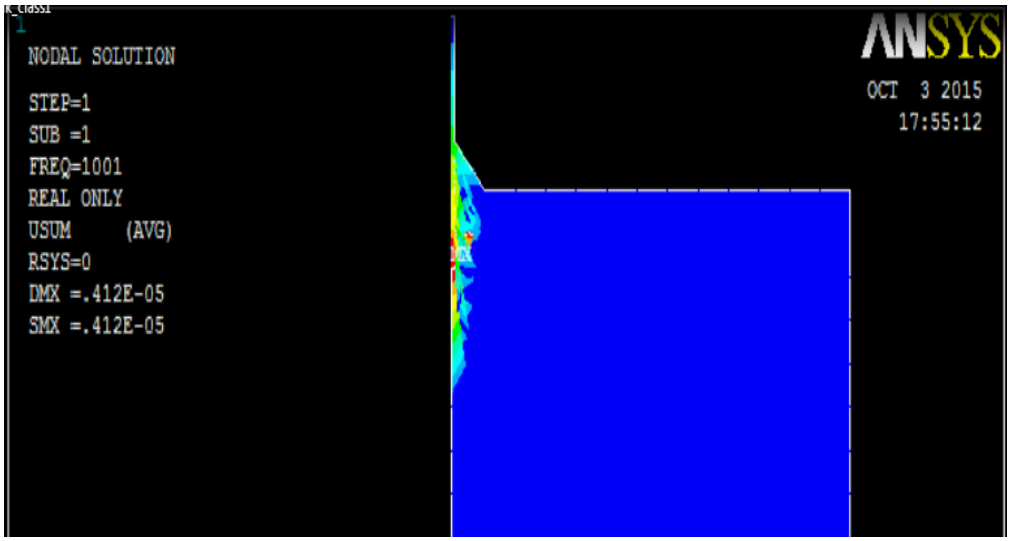

Figure A3: FEA solution of Rotor with fluid medium in axisymmetric position.

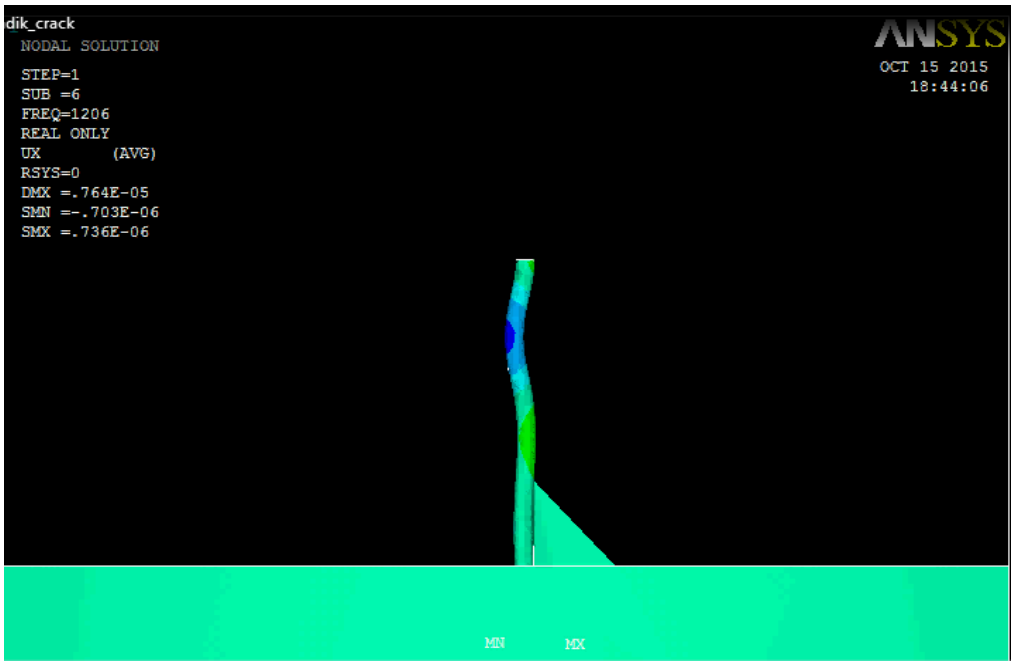

Figure A4: FEA solution of rotor with fluid medium.

Bibliography

[1] A. D. Dimarogonas, "Vibration of cracked structures: A state of the art review," *Engineering fracture mechanics*, vol. 55,no. 5, pp. 831-857, 1996.

[2] S. W. Doebling, C. R. Farrar, M. B. Prime and D. W. Shevitz, "Damage identification and health monitoring of structural and mechanical systems from changes in their vibration characteristics: A literature review (No. LA--13070-MS)," Los Alamos National Laboratory,NM (United State) 1996.

[3] J. T. Katsikadelis and G. C.Tsiatas, "Non-linear dynamic analysis of beams with variable stiffness," *Journal of Sound and Vibration*, vol. 270, no. 4, pp. 847-863, 2004.

[4] M. Gams, M. Saje, S. Srpčič and I. Planinc, "Finite element dynamic analysis of geometrically exact planar beams," *Computer and Structures*, vol.85, no. 17, pp.1409-1419, 2007.

[5] J. Chung and H. H. Yoo, "Dynamic analysis of a rotating cantilever beam by using the finite element method," *Journal of Sound and Vibration*, vol. 249, no.1, pp. 147-164, 2002.

[6] G. P. Cai, J. Z. Hong and S. X. Yang, "Dynamic analysis of a flexible hub-beam system with tip mass," *Mechanics Research Communications*, vol.32, no.2, pp.173-190, 2005.

[7] T. P. Chang and Y. N. Liu, "Dynamic Finite element analysis of a nonlinear beam subjected to a moving load," *International Journal of Solid Structures*, vol. 33, no. 12, pp. 1673-1688, 1996.

[8] Q. S. Li, L. F. Yang, Y. L. Zhao and G. Q. Li, "Dynamic analysis of non-uniform beams and plates by finite elements with generalized degrees of freedom," *International Journal of Mechanical Sciences*, vol. 45, no. 5, pp. 813–830, 2003.

[9] P. Fedeliński, "Boundary element method in dynamic analysis of structures with cracks," *Engineering Analysis with Boundary Elements*, vol. 28, no. 9, pp. 1135-1147, 2004.

[10] S. Orhan, "Analysis of free and forced vibration of a cracked cantilever beam," *NDT&E International*, vol. 40, no. 6, pp. 443-450, 2007.

[11] S. M. Ghoneam, "Dynamic analysis of open cracked laminated composite beams," *Composite Structures*, vol. 32, no. 1, pp. 3-11, 1995.

[12] H.Y. Lin, "Dynamic analysis of a multi-span uniform beam carrying a number of various concentrated elements," *Journal of Sound and Vibration*, vol. 309, no. 1, pp. 262–275, 2008.

[13] H. P. Lin and J. D.Wu, "Dynamic Analysis of Planar Closed-frame Structure," *Journal of Sound and Vibration*, vol. 282, no. 1, pp. 249-264, 2005.

[14] R. Fotouhi, "Dynamic analysis of very flexible beams," *Journal of Sound and Vibration*, vol. 305, no. 3, pp. 521-533, 2007.

[15] J. R. Banerjee, "Free vibration of beams carrying spring-mass systems," *Computers and Structures*, vol. 104, no. 105, pp. 21–26, 2012.

[16] J. Xiang, Y. Zhong, X. Chen and Z. He, "Crack detection in a shaft by combination of wavelet-based elements and genetic algorithm," *International Journal of Solids and Structures*, vol. 45, no. 17, pp. 4782-4795, 2008.

[17] F. M. El-Saeidy, "Finite element dynamics analysis of a rotating shaft with or without nonlinear boundary conditions subjected to a moving load," *Nonlinear Dynamics*, vol. 21, no. 4, pp. 377-408, 2000.

[18] Y. M. Fu, Y. F. Zheng and Z. K. Hou, "Analysis of non-linear dynamic stability for a rotating shaft-disk with a transverse crack," *Journal of Sound and Vibration*, vol. 257, no. 4, pp. 713-731, 2002.

[19] A. S. Sekhar and P. B. Prasad, "Dynamic analysis of a rotor system considering a slant crack in the shaft," *Journal of Sound and Vibration*, vol. 208, no. 3, pp. 346-363, 1997.

[20] O. S. Jun, "Dynamic behavior analysis of cracked rotor based on harmonic motion," *Mechanical Systems and Signal Processing*, vol. 30, pp.186-203, 2012.

[21] Q. Han and F. Chu, "Dynamic instability and steady-state response of an elliptical cracked shaft," *Archive of Applied Mechanics*, vol. 82, no. 5, pp.709-722, 2012.

[22] M. D. Rajab and A. Al-Sabeeh, "Vibrational characteristics of cracked shafts," *Journal of Sound and Vibration*, vol.147, no. 3, pp. 465-473, 1991.
[23] T. C. Tsai and Y. Z. Wang, "Vibration analysis and diagnosis of a cracked shaft," *Journal of Sound and Vibration*, vol. 192, no. 3, pp. 596-519, 1996.
[24] S. K. Singh and R. Tiwari, "Identification of a multi-crack in a shaft system using transverse frequency response functions," *Mechanism and Machine Theory*, vol. 45, no. 12, pp. 1813-1827, 2010.
[25] C. A. Papadopoulos and A. D. Dimarogonas, "Coupled longitudinal and bending vibrations of a rotating shaft with an open crack," *Journal of Sound and Vibration*, vol. 117, no. l, pp. 81-93, 1987.
[26] M. S. Nerantzaki and J. T. Katsikadelis, "Nonlinear dynamic analysis of circular plates with varying thickness," *Archive of Applied Mechanics*, vol. 77, no. 6, pp. 381–391, 2007.
[27] S. H. Hashemi, S. Farhadi and S. Carra, "Free vibration analysis of rotating thick plates,"*Journal of Sound and Vibration*. Vol. 323, no. 1, pp. 366–384, 2009.
[28] X. Si, W. Lu and F. Chu, "Dynamic analysis of rectangular plates with a single side crack and in contact with water on one side based on the Rayleigh-Ritz method," *Journal of Fluids and Structures*, vol. 34, pp. 90-104, 2012.
[29] M. H. Hsu, "Vibration analysis of edge-cracked beam on elastic foundation with axial loading using the differential quadrature method," *Computer Methods in Applied Mechanics and Engineering*, vol. 194, no. 1, pp. 1-17, 2005.
[30] O. S. Jun, H. J. Eun, Y. Y. Earmme and C. W. Lee, "Modeling and vibration analysis of a simple rotor with a breathing crack," *Journal of Sound and Vibration*, vol. 155, no. 2, pp. 273-290, 1992.
[31] A. K. Darpe, K. Gupta and A. Chawla, "Dynamics of a two-crack rotor," *Journal of Sound and Vibration*, vol. 259, no. 3, pp. 649-675, 2003.
[32] I. Takahashi, "Vibration and stability of a cracked shaft simultaneously subjected to a follower force with an axial force," *International Journal of Solid Structures*, vol. 35, no. 23, pp. 3071-3080, 1998.
[33] J. Buśkiewicz, "A dynamic analysis of a coupled beam/slider system," *Applied Mathematical Modelling*, vol. 32, no. 10, pp. 1941–1955, 2008.
[34] H. Nahvi and M. Jabbari, "Crack detection in beams using experimental modal data and finite element model," *International Journal of Mechanical Sciences*, vol. 47, no. 10, pp. 1477-1497, 2005.
[35] H. Y. Hwang and C. Kim, "Damage detection in structures using a few frequency responses measurements," *Journal of Sound and Vibration*, vol. 270, no. 1, pp. 1–14, 2004.
[36] B. Binici, "Vibration of beams with multiple open cracks subjected to axial force," *Journal of Sound and Vibration*, vol. 287, no. 1, pp. 277–295, 2005.
[37] E. Çam, S. Orhan and M., Lüy, "An analysis of cracked beam structure using impact echo method," *NDT&E International*, vol. 38, no. 5, pp. 368–373, 2005.
[38] O. S. Jun and M. S. Gadala, "Dynamic behavior analysis of cracked rotor," *Journal of Sound and Vibration*, vol. 309, no. 1, pp. 210-245, 2008.
[39] A. Prokić and D. Lukić, "Dynamic analysis of thin-walled closed-section beams," *Journal of Sound and Vibration*, vol. 302, no. 4, pp. 962–980, 2007.
[40] P. N. Saavedra and L. A. Cuitino, "Crack detection and vibration behavior of cracked beam," *Computers and Structures*, vol. 79, no. 16, pp. 1451-1459, 2001.
[41] L. W. Chen and H. K. Chen, "Stability analyses of a cracked shaft subjected to the end load," *Journal of Sound and Vibration*, vol.188, no. 4, pp. 497-513, 1995.
[42] G. L. Qian, S. N. Gu and J. S. Jiang, "The dynamic behavior and crack detection of a beam with a crack," *Journal of Sound and Vibration*, vol.138, no. 2, pp. 233-243, 1990.
[43] J. J. Sinou and A. W. Lees, "The influence of cracks in rotating shaft," *Journal of Sound and Vibration*, vol. 285, no. 4, pp. 1015–1037, 2005.
[44] C. Song, F. Tin-Loi and W. Gao, "Transient dynamic analysis of interface in anisotropic biomaterials by the scaled boundary finite-element method," *International Journal of Solids and Structures*, vol. 47, pp. 978-989, 2010.

[45] M. R. Arruda and L. M. S. Castro, "Structural dynamic analysis using hybrid and mixed finite element models," *Finite Elements in Analysis and Design*, vol. 57, pp. 43-54, 2012.

[46] B. K. Eshmatov, "Dynamic stability of viscoelastic plates under increasing compressing loads," *Journal of Applied Mechanics and Technical Physics*, vol. 47, no. 2, pp. 289-297, 2006.

[47] L. Cheng and M. Hatam, "Vibrational analysis of point-coupled structures," *Thin-Walled Structures*, vol. 36, no. 3, pp. 197-212, 2000.

[48] D. P. Patil and S. K. Maiti, Detection of multiple cracks using frequency measurements," *Engineering Fracture Mechanics*, vol. 70, no. 12, pp.1553-1572, 2003.

[49] S. Ebersbach and Z. Peng, "Expert system development for vibration analysis in machine condition monitoring," *Expert systems with applications*, vol. 34, no. 1, pp. 291-299, 2008.

[50] M. N. Cerri, M. Dilena and G. C. Ruta, "Vibration and damage detection in undamaged and cracked circular arches: experimental and analytical results," *Journal of sound and vibration*, vol. 314, no. 1, pp. 83-94, 2008.

[51] J. Humar, A. Bagchi and H. Xu, "Performance of vibration-based techniques for the identification of structural damage," *Structural Health Monitoring*, vol. 5, no. 3, pp. 215-241, 2006.

[52] Y. He, J. Ye, X. Chen and Z. He, "Discussion on calculation of the local flexibility due to the crack in a pipe," *Mechanical systems and signal processing*, vol. 23, no. 3, pp. 804-810, 2009.

[53] J. Zou, J. Chen, J. C. Niu and Z. M. Geng, "Discussion on the local flexibility due to the crack in a cracked rotor system," *Journal of Sound and Vibration*, vol. 262, no. 2, pp. 365-369, 2003.

[54] T. H. Patel and A. K. Darpe, "Influence of crack breathing model on nonlinear dynamics of a cracked rotor," *Journal of Sound and Vibration*, vol. 311, no. 3, pp. 953-972, 2008.

[55] N. Bachschmid, P. Pennacchi and E. Tanzi, "Some remarks on breathing mechanism, on non-linear effects and on slant and helicoidal cracks," *Mechanical Systems and Signal Processing*, vol. 22, no. 4, pp. 879-904, 2008.

[56] J. T. Sawicki, M. I. Friswell, Z. Kulesza, A. Wroblewski and J. D. Lekki," Detecting cracked rotors using auxiliary harmonic excitation," *Journal of Sound and Vibration*, vol. *330*, no. 7, pp.1365-1381, 2011.

[57] L. Xiao-feng, X. Ping-yong, S. Tie-lin and Y. Shu-zi, "Nonlinear analysis of cracked rotor with whirling," *Applied Mathematics and Mechanics*, vol. 23, no. 6, pp.721-731, 2002.

[58] C. Zhu, D. A. Robb and D. J. Ewins, "The dynamics of a cracked rotor with an active magnetic bearing," *Journal of Sound and Vibration*, vol. 265, no. 3, pp. 469–487, 2003.

[59] A. P. Bovsunovskii, On determination of the natural frequency of transverse and longitudinal vibrations of cracked beam: part 1: analytical approach," *Strength of Materials*, vol. 31, no. 2, pp. 130-137, 1999.

[60] P. C. Müller, J. Bajkowski and D. Söffker, "Chaotic motions and fault detection in a cracked rotor," *Nonlinear Dynamics*, vol. 5, no. 2, pp. 233-254, 1994.

[61] T. Zhou, Z. Sun, J. Xu and W. Han, "Experimental analysis of cracked rotor," *Journal of Dynamic Systems, Measurement and Control*, vol.127, no. 3, pp. 313-320, 2005.

[62] Y. Ishida and T. Inoue, "Detection of a rotor crack using harmonic excitation and nonlinear vibration analysis," *Journal of Vibration and Acoustics*, vol. 128, no. 6, pp. 741-749, 2006.

[63] W. Qin, G. Chen and X. Ren, "Grazing bifurcation in the response of cracked jeffcott rotor," *Nonlinear Dynamics*, vol. 35, no. 2, pp. 147-157, 2004.

[64] J. K. Sinha, "Higher order spectra for crack and misalignment identification in the shaft of a rotating machine," *Structural Health Monitoring*, vol. 6, no. 4, pp. 325-334, 2007.

[65] T. R. Babu, S. Srikanth and A. S. Sekhar, "Hilbert–Huang transform for detection and monitoring of crack in a transient rotor," *Mechanical Systems and Signal Processing*, vol. 22, no. 4, pp. 905-914, 2008.

[66] D. Guo and Z. K. Peng, "Vibration analysis of a cracked rotor using Hilbert–Huang transform," *Mechanical Systems and Signal Processing*, vol. 21, no. 8, pp. 3030-3041, 2007.

[67] Q. Han, J. Zhao and F. Chu, "Dynamic analysis of a geared rotor system considering a slant crack on the shaft," *Journal of Sound and Vibration*, vol. 331, no. 26, pp. 5803-5823, 2012.

[68] H. M. Khanlo, M. Ghayour and S. Ziaei-Rad, "The effects of lateral-torsional coupling on the nonlinear dynamic behavior of a rotating continuous flexible shaft-disk system with rub-impact," *Communications in Nonlinear Science and Numerical Simulation*, vol. 18, no. 6, pp. 1524-1538, 2013.

[69] C. Guo, M. A. AL-Shudeifat, J. Yan, L.A. Bergman, D. M. McFarland and E. A. Butcher, "Stability analysis for transverse breathing cracks in rotor systems," *European Journal of Mechanics A/Solids*, vol. 42, pp. 27-34, 2013.

[70] N. M. Auciello and G. Nole, "Vibrations of a cantilever tapered beam with varying section properties and carrying a mass at the free end," *Journal of Sound and Vibration*, vol. 214, no. 1, pp. 105-119, 1998.

[71] S. Caddemi, I. Caliò and M. Marletta, "The non-linear dynamic response of the Euler-Bernoulli beam with an arbitrary number of switching cracks," *International Journal of Non-Linear Mechanics*, vol. 45, no. 7, pp. 714-726, 2010.

[72] A. Presas, D. Valentin, E. Egusquiza and C. Valero, "Influence of the rotation on the natural frequencies of a submerged-confined disk in water," *Journal of Sound and Vibration*, vol. 337, pp. 161-180, 2015.

[73] A. K. Darpe, K. Gupta and A. Chawla, "Dynamics of a bowed rotor with a transverse surface crack," *Journal of Sound and Vibration*, vol. 296, no. 4, pp. 888-907, 2006.

[74] S. K. Georgantzinos and N. K. Anifantis, "An insight into the breathing mechanism of a crack in a rotating shaft," *Journal of Sound and Vibration*, vol. 318, no. 1, pp. 279-295, 2008.

[75] N. Bachschmid and E. Tanzi, "Deflections and strains in cracked shafts due to rotating loads: A numerical and experimental analysis international," *Journal of Rotating Machinery*, vol. 10, no. 4, pp. 283–291, 2003.

[76] A. S. Sekhar, Vibration characteristics of a cracked rotor with two open cracks," *Journal of Sound and Vibration*, vol. 223, no. 4, pp. 497-512, 1999.

[77] A. C. Chasalevris and C. A. Papadopoulos, "Identification of multiple cracks in beams under bending," *Mechanical Systems and Signal Processing*, vol. 20, no.7, pp.1631-1673, 2006.

[78] A. Nandi, Reduction of finite element equations for a rotor model on non-isotropic spring support in a rotating frame," *Finite Elements in Analysis and Design*, vol. 40, no. 9, pp. 935-952, 2004.

[79] A. A. Mohamed, R. Neilson, P. MacConnell, N. C. Renton and W. Deans, "Monitoring of fatigue crack stages in a high carbon steel rotating shaft using vibration," *Procedia Engineering*, vol. 10, pp. 130-135, 2011.

[80] P. R. Baviskar and V. B. Tungikar, "Analysis of crack in shaft of blower using finite element analysis and experimental technique," *International Journal of Research and Reviews in Applied Sciences*, vol. 8, no. 1, pp. 30-36, 2011.

[81] A. Hossain, L. Humphrey and A. Mian, "Prediction of the dynamic response of a mini cantilever beam partially submerged in viscous media using finite element method," *Finite Elements in Analysis and Design*, vol. 48, no. 1, pp.1339-1345, 2012.

[82] S. K. Georgantzinos and N. K. Anifantis, "An insight into the breathing mechanism of a crack in a rotating shaft," *Journal of Sound and Vibration*, vol. 318, no. 1, pp. 279-295, 2008.

[83] Y. Kerboua, A. A. Lakis, M. Thomas and L. Marcouiller, "Vibration analysis of rectangular plates coupled with fluid," *Applied Mathematical Modelling*, vol. 32, no. 12, pp. 2570-2586, 2008.

[84] A. K. Darpe, "A novel way to detect transverse surface crack in a rotating shaft," *Journal of Sound and Vibration*, vol. 305, no. 1, pp.151-171, 2007.

[85] A. K. Darpe, "Coupled vibrations of a rotor with slant crack," *Journal of Sound and Vibration*, vol. 305, no. 1, pp.172-193, 2007.

[86] A. K. Darpe," Dynamics of a jeffcott rotor with slant crack," *Journal of Sound and Vibration*, vol. 303, pp. 1–28, 2007.

[87] M. Silani, S. Ziaei-Rad and H. Talebi, "Vibration analysis of rotating systems with open and breathing cracks," *Applied Mathematical Modelling*, vol. 37, no. 24, pp. 9907-9921, 2013.

[88] Z. Kulesza, "Dynamic behavior of cracked rotor subjected to multisine excitation," *Journal of Sound and Vibration*, vol. 333, no. 5, pp. 1369-137, 2014.

[89] A. S. Sekhar and P. B. Prasad, "Dynamic analysis of a rotor system considering a slant crack in the shaft," *Journal of Sound and Vibration*, vol. 208, no. 3, pp. 346-363, 1997.

[90] K. V. Nguyen and H. T. Tran, "Multi-cracks detection of a beam-like structure based on the on-vehicle vibration signal and wavelet analysis," *Journal of Sound and Vibration*, vol. *329*, no. 21, pp. 4455-4465, 2010.

[91] Z. Ren, S. Zhou, E. Chunhui, M. Gong, B. Li and B. Wen, "Crack fault diagnosis of rotor systems using wavelet transforms," *Computers & Electrical Engineering*, vol. 45, pp. 33-41, 2015.

[92] B. Yang, C. S. Suh and A. K. Chan, "Characterization and detection of crack-induced rotary instability," *Journal of Vibration and Acoustics*, vol. 124, no. 1, pp. 40-48, 2002.

[93] J. Xiang, X. Chen, Q. Mo and Z. He, "Identification of crack in a rotor system based on wavelet finite element method," *Finite Elements in Analysis and Design*, vol. 43, no.14, pp. 1068-1081, 2007.

[94] Z. Jibing, G. Hangshan and G. Yinchao, "Application to wavelet transform to bifurcation and chaos study," *Applied mathematics and mechanics*,vol. 19, no. 6, pp. 593-599, 1998.

[95] J. Ma, J. Xue, S. Yang and Z. He, "A study of the construction and application of a Daubechies wavelet-based beam element," *Finite Elements in Analysis and Design*, vol. 39, no. 10, pp. 965-975, 2003.

[96] B. Li, X. F. Chen, J. X. Ma and Z. J. He, "Detection of crack location and size in structures using wavelet finite element methods," *Journal of Sound and Vibration*, vol. 285, no. 4, 767-782, 2005.

[97] J. Gomez-Mancilla, J. J. Sinou, V. R. Nosov, F. Thouverez and A. Zambrano, "The influence of crack-imbalance orientation and orbital evolution for an extended cracked jeffcott rotor," *Comptes Rendus Mecaniques*, vol. 332, no. 12, pp. 955-962, 2004.

[98] R. Gasch, "Dynamic behavior of the laval rotor with a transverse crack," *Mechanical Systems and Signal Processing*, vol. 22, no. 4, pp. 790-804, 2008.

[99] R. Sino, T. N. Baranger, E. Chatelet and G. Jacquet, "Dynamic analysis of a rotating composite shaft," *Composites Science and Technology*, vol. 68, no. 2, pp. 337-345, 2008.

[100] J. Wang, D. Qin and T. C. Lim, "Dynamic analysis of horizontal axis wind turbine by thin-walled beam theory," *Journal of Sound and Vibration*, vol. 329, no. 17, pp. 3565-3586, 2010.

[101] T. Szolc, P. Tauzowski, R. Stocki and J. Knabel, "Damage identification in vibrating rotor-shaft systems by efficient sampling approach," *Mechanical Systems and Signal Processing*, vol. 23, no. 5, pp.1615-1633, 2009.

[102] M. J. Gómez, C. Castejón and J. C. García-Prada, "Crack detection in rotating shafts based on 3 × energy: Analytical and experimental analyses," *Mechanism and Machine Theory*, vol. 96, pp. 94-106, 2016.

[103] N. G. Shulzhenko and G. B. Ovcharova, "Effect of break of the elastic axis of a rotor with transverse crack on its vibrational characteristics," *Strength of Materials*, vol. 29, no. 4, pp. 382-385, 1997.

[104] H. B. Dong, X. F. Chen, B. Li, K. Y. Qi and Z. J. He, "Rotor crack detection based on high-precision modal parameter identification method and wavelet finite element model," *Mechanical Systems and Signal Processing*, vol. 23, no. 3, pp. 869-883, 2009.

[105] C. M. Stoisser and S. Audebert, A comprehensive theoretical, numerical and experimental approach for crack detection in power plant rotating machinery," *Mechanical Systems and Signal Processing*, vol. 22, no. 4, pp. 818-844, 2008.

[106] F. Mueller, A. Scholz and C. Berger, Comparison of different approaches for estimation of creep crack initiation," *Engineering Failure Analysis*, vol. 14, no. 8, pp.1574-1585, 2007.

[107] C. Chen, L. Dai and Y. Fu, Nonlinear response and dynamic stability of a cracked rotor," *Communications in Nonlinear Science and Numerical Simulation*, vol. 12, no. 6, pp. 1023-1037, 2007.

[108] P. Pennacchi and A. Vania, "Diagnostics of a crack in a load coupling of a gas turbine using the machine model and the analysis of the shaft vibrations," *Mechanical Systems and Signal Processing*, vol. 22, no. 5, pp. 1157-1178, 2008.

[109] M. Shahgholi, S. E. Khadem and S. Bab, "Free vibration analysis of a nonlinear slender rotating shaft with simply support conditions," *Mechanism and Machine Theory*, vol. 82, pp.128-140, 2014.

[110] C. N. Phan, M. Aureli and M. Porfiri, "Finite amplitude vibrations of cantilevers of rectangular cross sections in viscous fluids," *Journal of Fluids and Structures*, vol. 40, pp. 52-69, 2013.

[111] O. Curadelli, D. Ambrosini, A. Mirasso and M. Amani, "Resonant frequencies in an elevated spherical container partially filled with water: FEM and measurement," *Journal of Fluids and Structures*, vol. 26, no. 1, pp. 148-159, 2010.

[112] M. Chouksey, J. K. Dutt and S. V. Modak, "Modal analysis of rotor-shaft system under the influence of rotor-shaft material damping and fluid film forces," *Mechanism and Machine Theory*, vol. 48, pp. 81-93, 2012.

[113] C. C. Liang, C. C. Liao, Y. S. Tai and W. H. Lai, "The free vibration analysis of submerged cantilever plates," *Ocean Engineering*, vol. 28, no. 9, pp.1225-1245, 2001.

[114] A. Uściłowska and J. A. Kołodziej, "Free vibration of immersed column carrying a tip mass," *Journal of Sound and Vibration*, vol. 216, no. 1, pp. 147-157, 1998.

[115] M. R. Arruda and L. M. S. Castro, "Structural dynamic analysis using hybrid and mixed finite element models. *Finite Elements in Analysis and Design*, 57: 43-54, 2012.

[116] S. K. Singh and R. Tiwari, "Detection and localisation of multiple cracks in a shaft system:An experimental investigation. *Measurement*, vol. 53, pp. 182-193, 2014.

[117] L. Rubio, B. Muñoz-Abella and G. Loaiza, "Static behaviour of a shaft with an elliptical crack," *Mechanical Systems and Signal Processing*, vol. 25, no. 5, pp.1674-1686, 2011.

[118] A. Vaziri and H. Nayeb-Hashemi, "The effect of crack surface interaction on the stress intensity factor in mode III crack growth in round shafts," *Engineering Fracture Mechanics*, vol. 72, no. 4, pp. 617-629, 2005.

[119] A. A. Gubran and J. K. Sinha, "Shaft instantaneous angular speed for blade vibration in rotating machine," *Mechanical Systems and Signal Processing*, vol. 44, no. 1, pp. 47–59, 2014.

[120] B. Eftekharnejad, A. Addali, and D. Mba, "Shaft crack diagnostics in a gearbox," *Applied Acoustics*, vol. 73, no. 8, pp. 723-733, 2012.

[121] R. T. Liong and C. Proppe, "Application of the cohesive zone model for the evaluation of stiffness losses in a rotor with a transverse breathing crack," *Journal of Sound and Vibration*, vol. 332, no. 8, pp. 2098-2110, 2013.

[122] O. M. Abuzeid and M. H. Dado, "Fractal model to predict the crack roughness effect on the local bending compliance of circular shafts," *International Journal of Mechanical Sciences*, vol. 46, no. 5, pp. 695-702, 2004.

[123] L. Cheng, N. Li, X. F. Chen and Z. J. He, "The influence of crack breathing and imbalance orientation angle on the characteristics of the critical speed of a cracked rotor," *Journal of Sound and Vibration*, vol. 330, no. 9, pp. 2031-2048, 2011.

[124] Y. Yadykin, V. Tenetov and D. Levin," The added mass of a flexible plate oscillating in a fluid, *Journal of Fluids and Structures*, vol. 17, no. 1, pp.115-123, 2003.

[125] Y. Fu and W. G. Price, Interactions between a partially or totally immersed vibrating cantilever plate and the surrounding fluid," *Journal of Sound and Vibration*, vol. 118, no. 3, pp. 495-513, 1987.

[126] K. Wada, N. Hayano and H. Oka, "Application of the fuzzy control method for level control of a hopper," *Advance Power Technol*, vol. 2, no. 3, pp. 163-172, 1991.

[127] R. Ganguli, A fuzzy logic system for ground based structural health monitoring of a helicopter rotor using modal data, *Journal of Intelligent Material Systems and Structures*, vol. 12, no. 6, pp. 397-407, 2001.

[128] L. J. De Miguel and L. F. Blázquez, "Fuzzy logic-based decision-making for fault diagnosis in a DC motor," *Engineering Applications of Artificial Intelligence*, vol. 18, no. 4, pp. 423-450, 2005.

[129] C. W. Chen, "Stability conditions of fuzzy systems and its application to structural and mechanical systems," *Advances in Engineering Software*, vol. 37, no. 9, pp. 624-629, 2006.

[130] T. Boutros and M. Liang, "Mechanical fault detection using fuzzy index fusion," *International Journal of Machine Tools and Manufacture*, vol. 47, no. 11, pp.1702-1714, 2007.

[131] L. Zhang, Z. Wang and S. Zhao, "Short-term fault prediction of mechanical rotating parts on the basis of fuzzy-grey optimising method," *Mechanical Systems and Signal Processing*, vol. 21, no. 2, pp. 856-865, 2007.

[132] Y. M. Kim, C. K. Kim, and G. H. Hong, "Fuzzy set based crack diagnosis system for reinforced concrete structures, "*Computers and Structures*, vol. 85, no. 23, pp.1828-1844, 2007.

[133] P. Angelov, E. Lughofer and X. Zhou, "Evolving fuzzy classifiers using different model architectures," *Fuzzy Sets and Systems*, vol. 159, no. 23, pp. 3160-3182, 2008.

[134] M. Chandrashekhar and R. Ganguli, "Damage assessment of structures with uncertainty by using mode shape curvatures and fuzzy logic," *Journal of Sound and Vibration*, vol.326, no. 3, pp. 939-957, 2009.

[135] N. Saravanan, S. Cholairajan and K. I. Ramachandran, "Vibration-based fault diagnosis of spur bevel gear box using fuzzy technique," *Expert Systems with Applications*, vol. 36, no. 2, pp.3119-3135, 2009.

[136] Q. Wu and R. Law, "Complex system fault diagnosis based on a fuzzy robust wavelet support vector classifier and an adaptive gaussian particle swarm optimization," *Information Sciences*, vol. 180, no. 23, pp. 4514-4528, 2010.

[137] D. R. Parhi and S. Choudhury, "Smart crack detection of a cracked cantilever beam using fuzzy logic technology with hybrid membership functions," *Journal of Engineering and Technology Research*, vol. 3, no. 8, pp. 270-278, 2011.

[138] H. H. Choi and J. W. Jung, "Takagi–Sugeno fuzzy speed controller design for a permanent magnet synchronous motor," *Mechatronics*, vol. 21, no. 8, pp.1317-1328, 2011.

[139] R. P. Hasanzadeh, S. H. H. Sadeghi, M. Ravan, A. R. Moghaddamjoo and R. Moini, "A fuzzy alignment approach to sizing surface cracks by the ac field measurement technique," *NDT&E International*, vol. 44, no.1, pp. 75-83, 2011.

[140] V. Sugumaran and K. I. Ramachandran, "Fault diagnosis of roller bearing using fuzzy classifier and histogram features with focus on automatic rule learning," *Expert Systems with Applications*, vol. 38, no. 5, pp. 4901-4907, 2011.

[141] D. K. Mohanta, P. K. Sadhu and R. Chakrabarti, "Fuzzy Markov model for determination of fuzzy state probabilities of generating units including the effect of maintenance scheduling," *IEEE Transactions on Power Systems*, vol. 20, no. 4, pp. 2117-2124, 2005.

[142] D. R. Parhi, "Navigation of mobile robots using a fuzzy logic controller," *Journal of Intelligent and Robotic Systems*, vol. 42, no. 3, pp. 253-273, 2005.

[143] S. W. Liu, J. H. Huang, J. C. Sung and C. C. Lee, "Detection of cracks using neural networks and computational mechanics," *Computer Methods in Applied Mechanics and Engineering*, vol. 191, no. 25, pp. 2831-2845, 2002.

[144] X. Fang, H. Luo and J. Tang, "Structural damage detection using neural network with learning rate improvement," *Computers and Structures*, vol. 83, no. 25, pp. 2150-2161, 2005.

[145] M. Mehrjoo, N. Khaji, H. Moharrami and A. Bahreininejad, "Damage detection of truss bridge joints using artificial neural networks," *Expert Systems with Applications*, vol. 35, no. 3, pp. 1122-1131, 2008.

[146] J. D. Wu and C. H. Liu, "Investigation of engine fault diagnosis using discrete wavelet transform and neural network," *Expert Systems with Applications*, vol. 35, no. 3, pp.1200-1213, 2008.

[147] F. Just-Agosto, D. Serrano, B. Shafiq and A. Cecchini, "Neural network based non-destructive evaluation of sandwich composites," *Composites Part B: Engineering*, vol. 39, no. 1, pp. 217-225, 2008.

[148] J. D. Wu and J. J. Chan, "Faulted gear identification of a rotating machinery based on wavelet transform and artificial neural network," *Expert Systems with Applications*, vol. 36, no. 5, pp. 8862-8875, 2009.

[149] V. N. Ghate and S. V. Dudul, "Optimal MLP neural network classifier for fault detection of three phase induction motor," *Expert Systems with Applications*, vol. 37, no. 4, pp. 3468-348, 2010.

[150] B. Fan, Z. Du, X. Jin, X. Yang and Y. Guo, "A hybrid FDD strategy for local system of AHU based on artificial neural network and wavelet analysis," *Building and Environment*, vol. 45, no. 12, pp. 2698-2708, 2010.

[151] C. C. Wang, Y. Kang, P. C. Shen, Y. P. Chang and Y. L. Chung, "Applications of fault diagnosis in rotating machinery by using time series analysis with neural network," *Expert Systems with Applications*, vol. 37, no. 2, pp.1696-1702, 2010.

[152] N. Saravanan, V. K. Siddabattuni and K. I. Ramachandran, "Fault diagnosis of spur bevel gear box using artificial neural network (ann) and proximal support vector machine (PSVM). *Applied Soft Computing*, vol. 10, no. 1, pp. 344-360, 2010.

[153] G. Paviglianiti, F. Pierri, F. Caccavale and M. Mattei, "Robust fault detection and isolation for proprioceptive sensors of robot manipulators," *Mechatronics*, vol. 20, no. 1, pp.162-170, 2010.

[154] M. Schlechtingen and I. F. Santos, "Comparative analysis of neural network and regression based condition monitoring approaches for wind turbine fault detection," *Mechanical Systems and Signal Processing*, vol. 25, no. 5, pp.1849-1875, 2011.

[155] I. Eski, S. Erkaya, S. Savas and S. Yildirim, "Fault detection on robot manipulators using artificial neural networks," *Robotics and Computer-Integrated Manufacturing*, vol. 27, no. 1, pp.115-123, 2011.

[156] D. Thatoi and P. K. Jena, "Inverse analysis of crack in fixed-fixed structure by neural network with the aid of modal analysis," *Advances in Artificial Neural Systems*, 2013.

[157] A. J. Oberholster and P. S. Heyns, "On-line fan blade damage detection using neural networks," *Mechanical Systems and Signal Processing*, vol. 20, no. 1, pp.78-93, 2006.

[158] M. Rakideh, M. Dardel and M. H. Pashaei, "Crack detection of timoshenko beams using vibration behavior and neural network," *International Journal of Engineering-Transactions C: Aspects*, vol. 26, no. 12, pp.1433-1444, 2013.

[159] C. Y. Kao and S. L Hung, "Detection of structural damage via free vibration responses generated by approximating artificial neural networks," *Computers & Structures*, vol. 81, no. 28, pp. 2631-2644, 2003.

[160] A. Quteishat and C. P. Lim, "A modified fuzzy min-max neural network with rule extraction and its application to fault detection and classification," *Applied Soft Computing*, vol. 8, no. 2, pp. 985-995. 2008.

[161] A. Hajnayeb, A. Ghasemloonia, S. E. Khadem and M. H. Moradi, "Application and comparison of an ann-based feature selection method and the genetic algorithm in gearbox fault diagnosis," *Expert Systems with Applications*, vol. 38, no. 8, pp. 10205-10209, 2011.

[162] B. Samanta, "Gear fault detection using artificial neural networks and support vector machines with genetic algorithms," *Mechanical Systems and Signal Processing*, vol. 18, no. 3, pp. 625-644, 2004.

[163] S. Haykin, "Neural Networks: A Comprehensive Foundation," Pearson Education, 2006.

[164] B. Samanta, K. R. Al-Balushi and S. A. Al-Araimi, "Artificial neural networks and support vector machines with genetic algorithm for bearing fault detection," *Engineering Applications of Artificial Intelligence*, vol. 16, no. 7, pp. 657-665, 2003.

[165] W. Q. Wang, M. F. Golnaraghi and F. Ismail, "Prognosis of machine health condition using neuro-fuzzy systems," *Mechanical Systems and Signal Processing*, vol.18, no. 4, 813-831, 2004.

[166] H. C. Kuo and H. K. Chang, "A new symbiotic evolution-based fuzzy-neural approach to fault diagnosis of marine propulsion systems," *Engineering Applications of Artificial Intelligence*, vol.17, no. 8, pp. 919-930, 2004.

[167] Z. Ye, A. Sadeghian and B. Wu, "Mechanical fault diagnostics for induction motor with variable speed drives using adaptive neuro-fuzzy inference system," *Electric Power Systems Research*, vol. 76, no. 9, pp.742-752, 2006.

[168] E. Zio and G. Gola, "A neuro-fuzzy technique for fault diagnosis and its application to rotating machinery," *Reliability Engineering & System Safety*, vol. 94, no. 1, pp.78-88, 2009.

[169] B. S. Yang, M. S. Oh and A. C. C. Tan, "Fault diagnosis of induction motor based on decision trees and adaptive neuro-fuzzy inference," *Expert Systems with Applications*, vol. 36, no. 2, pp. 1840-1849, 2009.

[170] R. Eslamloueyan, "Designing a hierarchical neural network based on fuzzy clustering for fault diagnosis of the Tennessee-eastman process," *Applied Soft Computing*, vol.11, no. 1, pp.1407-1415, 2011.

[171] K. Salahshoor, M. S. Khoshro and M. Kordestani, "Fault detection and diagnosis of an industrial steam turbine using a distributed configuration of adaptive neuro-fuzzy inference systems," *Simulation Modelling Practice and Theory*, vol. 19, no. 5, pp. 1280-1293, 2011.

[172] M. Sadeghian and A. Fatehi, "Identification, prediction and detection of the process fault in a cement rotary kiln by locally linear neuro-fuzzy technique," *Journal of Process Control*, vol. 21, no. 2, pp. 302-308, 2011.

[173] P. Beena and R. Ganguli, "Structural damage detection using fuzzy cognitive maps and hebbian learning," *Applied Soft Computing*, vol. 11, no. 1, pp. 1014-1020, 2011.

[174] F. Zhu, Z. Deng and J. Zhang, "An integrated approach for structural damage identification using wavelet neuro-fuzzy model," *Expert Systems with Applications*, vol. 40, no.18, pp. 7415-7427, 2013.

[175] B. Chen, P. C. Matthews and P. J. Tavner, "Wind turbine pitch faults prognosis using a-priori knowledge-based ANFIS," *Expert Systems with Applications*, vol. 40, no. 17, pp. 6863-6876, 2013.

[176] I. O. Bachi, N. Abdulrazzaq and Z. He, "Neuro fuzzy model for predicting the dynamic characteristics of beams. *Acta. Mechanica Solida Sinica*, vol. 27, no. 1, pp. 85-96, 2014.

[177] E. T. Al-Shammari, M. Amirmojahedi, S. Shamshirband, D. Petković, N. T. Pavlović and H. Bonakdari, "Estimation of wind turbine wake effect by adaptive neuro-fuzzy approach," *Flow Measurement and Instrumentation*, vol. 45, pp.1-6, 2015.

[178] D. Petković, M. Issa, N. D. Pavlović and L. Zentner, "Potential of adaptive neuro-fuzzy inference system for contact positions detection of sensing structure," *Measurement*, vol.61, pp. 234-242, 2015.

[179] L. Zhang, G. Xiong, H. Liu, H. Zou and W. Guo, "Bearing fault diagnosis using multi-scale entropy and adaptive neuro-fuzzy inference," *Expert Systems with Applications*, vol. 37, no. 8, pp. 6077-6085, 2010.

[180] M. A. Boyacioglu and D. Avci, "An adaptive network-based fuzzy inference system (ANFIS) for the prediction of stock market return: the case of the istanbul stock exchange," *Expert Systems with Applications*, vol. 37, no. 12, pp. 7908-7912, 2010.

[181] J. Zhang, W. Dai, M. Fan, H. Chung, Z. Wei and D. Bi, "An investigation into the use of delay coordinate embedding technique with MIMO ANFIS for nonlinear prediction of chaotic signals," *Springer-Verlag Berlin Heidelberg*, pp. 677- 688, 2005.

[182] J. Hinojosa and G. Doménech-Asensi, "Space-mapped neuro-fuzzy optimization for microwave device modelling," *Microwave And Optical Technology Letters*, vol. 49, no. 6, pp. 1328-1334, 2007.

[183] Y. Lei, Z. He, Y. Zi and Q. Hu, "Fault diagnosis of rotating machinery based on multiple ANFIS combination with gas," *Mechanical Systems and Signal Processing*, vol. 21, no. 5, pp. 2280-2294, 2007.

[184] G. D. Asensi, J. Hinojosa, R. Ruiz and J. A. D. Madrid, "Accurate and reusable macromodeling technique using a fuzzy-logic approach," *Circuits and Systems, ISCAS* 2008, *IEEE International Symposium*, pp. 508-511, 2008.

[185] A. F. Güneri, T. Ertay and A. YüCel, "An approach based on ANFIS input selection and modeling for supplier selection problem," *Expert Systems with Applications*, vol. 38, no. 12, pp. 14907-14917, 2011.

[186] A. K. Dash and D. R. Parhi, "Development of a vibration based crack diagnostic application using the MANFIS technique," *International Journal of Acoustics and Vibration*, vol. 17, no. 2, pp. 90-99, 2012.

[187] A. Ghaffari, A. Khodayari, F. Alimardani and H. Sadati, "MANFIS based modeling and prediction of the driver-vehicle unit behavior in overtaking scenarios," *International Journal of Automotive Engineering*, vol. 3, no. 2, pp. 394-411, 2013.

[188] R. A. Saeed, A. N. Galybin and V. Popov, "3D fluid-structure modelling and vibration analysis for fault diagnosis of francis turbine using multiple ANN and multiple ANFIS," *Mechanical Systems and Signal Processing*, vol. 34, no. 1, pp. 259-276, 2013.

[189] N. D. Linh and H.V. Long, "A lossless DEM compression for fast retrieval method using fuzzy clustering and MANFIS neural network," *Engineering Applications of Artificial Intelligence*, vol. 29, pp. 33-42, 2014.

[190] M. Subhi Al-batah, N. A. Mat Isa, M. F. Klaib and M. A. Al-Betar, "Multiple adaptive neuro-fuzzy inference system with automatic features extraction algorithm for cervical cancer recognition," *Computational and Mathematical Methods in Medicine*, 2014. doi.org/10.1155/2014/181245.

[191] S. Takagi and Y. Okawa, "Rule-based control of a mobile robot for the push- a- box operation," *IEEE/RSJ International Workshop on Intelligent Robots and Systems*, pp.1338-1343, 1991.

[192] H. Gaeta, D. Friedman, W. Ritter and G. Hunt, "Age-related changes in neural trace generation of rule-based auditory features," *Neurobiology of Aging*, vol. 23, no. 3, pp. 443-455, 2002.

[193] M. A. F. De Souza and M. A. G. V. Ferreira, "Designing reusable rule-based architectures with design patterns," *Expert Systems with Applications*, vol. 23, no. 4, pp. 395-403, 2002.

[194] J. Dietrich, A. Kozlenkov, M. Schroeder and G. Wagner, "Rule-based agents for the semantic web," *Electronic Commerce Research and Applications*, vol. 2, no. 4, pp. 323-338, 2003.

[195] E. Tunstel, A. Howard and H. Seraji, "Rule-based reasoning and neural network perception for safe off-road robot mobility," Expert Systems, vol. 19, no. 4, pp. 191-200, 2002.

[196] B. S. McIntosh, R. I., Muetzelfeldt, C. J. Legg, S. Mazzoleni and P. Csontos, "Reasoning with Direction and Rate of Change in Vegetation State Transition Modeling," *Environmental Modelling & Software*, vol. 18, no. 10, pp. 915-927, 2003.

[197] J. J. Pfeiffer Jr, "A rule-based visual language for small mobile robots," *IEEE Symposium on Visual Languages*, pp. 164-165, 1997.

[198] J. J. Pfeiffer Jr, "Case study: Developing a rule-based language for mobile robots," *IEEE Symposium Visual Languages*, pp. 204-209, 1998.

[199] J. J. Pfeiffer Jr, "Altaira: A rule-based visual language for small mobile robots," *Journal of Visual Languages and Computing*, vol. 9, no. 2, pp. 127-150, 1998.

[200] J. Fei and C. Isik, "Adapting to environmental variations in a rule-based mobile robot controller," *IEEE International Conference on Systems, Man and Cybernetics*, vol. 1, pp. 332-333, 1989.

[201] B. J. Gilmore and D. A. Streit, "A rule-based algorithm to predict the dynamic behavior of mechanical part orienting operations," *IEEE International Conference Robotics and Automation*, vol. 2, pp. 1251-1259, 1988.

[202] S. Bonner and R. B. Kelley, "A representation scheme for rapid 3d collision detection," *IEEE International Symposium Intelligent Control*, pp. 320-325, 1988.

[203] S. Bonner and R. B. Kelley, "Planning 3-D collision-free paths," *IEEE International Symposium Intelligent Control*, pp. 550-555, 1989.

[204] S. Bonner and R. B. Kelley, "A novel representation for planning 3-d collision-free paths," *IEEE Transactions on Systems, Man and Cybernetics*, vol. 20, no. 6, pp. 1337-1351, 1990.

[205] H. Tada, P.C. Paris and G. R. Irwin, "The stress analysis of cracks handbook 2nd ed. St. Louis, MO: Paris production incorporated and del research corporation," 1985.

[206] W.T. Thomson, "Theory of vibration with application,Third edition, Prentics Hall," 1988.

[207] T. Takagi and M. Sugeno, "Fuzzy identification of system and its application to modelling and control," *IEEE Transactions on systems, Man and Cybernetics*,vol. 15, no. 1, pp. 116-132,1985.

[208] P. Melin and O. Castillo, "A new method for adaptive model-based control of non-linear dynamic plants using a neuro-fuzzy-fractal approach," *Soft Computing*, vol. 5, no. 2, pp. 171-177, 2001.

[209] J. A. Leonard, M. A. Kramer and L. H. Ungar, "Using radial basis functions to approximate a function and its error bounds," *IEEE Transactions on Neural Networks/ A Publication of the IEEE Neural Networks Council*, vol. *3*, no. 4, pp. 624-627,1991.

[210] S. Weiss and C. Kulikowski, "Computer systems that learn,"1991.

[211] E. H. Mamdani and S. Assilian, "An experiment in linguistic synthesis with fuzzy logic controller," *International Journal of Man-machine Studies*, vol. 7, no. 1, pp. 1-13,1975.

[212] L. A. Zadeh, "Fuzzy sets," *Information and control*, vol. 8, no. 3, pp. 338-353, 1965.

[213] M. Matsubara, H. Rahnejat and R. Gohar, "Computational modelling of precision spindles supported by ball bearings," *International Journal of Machine Tools and Manufacture*, vol. 28, no. 4, pp. 429-442,1988.

Dissemination

Journal Articles

1. Dayal R. Parhi and **Adik R. Yadao**, Analysis of Dynamic Behavior of Multi-cracked Cantilever Rotor in Viscous Medium. *Proceeding of the Institution of Mechanical Engineers: Part K Journal of Multi-body*, 12/2015, DOI:10.1177/146441931561803**.**
2. **Adik R. Yadao** and Dayal R.Parhi, The Influence of Crack in Cantilever Rotor System with Viscous Medium. *International Journal of Dynamics and Control,* DOI.10.1007/s40435-014-0141-2, 2014**.**
3. Dayal R. Parhi, **Adik R. Yadao** and Ranjan K. Behera, A review on the dynamic analysis of cracked rotor by different method. *International Journal of Artificial Intelligence and Computational Research*, 6(1): 1-8, 2014.
4. **Adik R. Yadao** and Dayal R. Parhi, Dynamic Analysis of Fixed-Fixed Type Cracked Rotor in Viscous Medium. *Journal of Vibration Engineering & Technologies* (Accepted).
5. D. R. Parhi and **Adik R. Yadao**, Review of dynamic analysis of structure by different method. *International Journal of Artificial Intelligence and Computation Researc*h, 4(2): 87-94, 2012.
6. D. R. Parhi, **Adik Yadao** and Irshad A khan, "Vibration Analysis of Spinning Cantilever Shaft with a Disc in Viscous Fluid", *International Journal of Artificial Intelligence and Computational Research*, 6(1), 17-24, 2014.

Book Chapters

1. **Adik R. Yadao** and D. R. Parhi, Experimental and Numerical Analysis of Cracked Shaft in Viscous Medium a Finite Region. *Book Chapter of Advances in structural engineering,*1601-1609, 2015.

Conference Presentations

1. **Adik Yadao**, Irshad A. Khan and D. R. Parhi, Vibration Characteristics of Rotating Simply Supported Shaft in Viscous Fluid. In proceeding of *International Conference on Industrial Engineering, Science and Applications*, 58-63,2014.
2. **Adik Yadao**, Irshad A. Khan and D. R.Parhi, Modal Analysis of a Multiple Cracked Cantilever Bar. *International Conference on Advances in Engineering and Technology, IOSR Journal of Mechanical and civil Engineering*, 6: 12-15, 2013.
3. **Adik R.Yadao**, Ravi P. Singh and Dayal R. Parhi, Influence of Parameters of Cracked Rotor System on its Vibration Characteristics in Viscous Medium at Finite

Region. *International Mechanical Engineering Congress*: *International Journal of Applied Mechanics and Materials*, 592(594):2061-2065, 2014.

4. **Adik Yadao** and D.R.Parhi, Theoretical and Experimental Verification of Vibration Characteristics of Cracked Rotor System in Viscous Medium. In Proceeding of *5th International & 26th All India Manufacturing Technology, Design and Research Conference*, pages 46(1-6), 2014.
5. **Adik Yadao** and D. R. Parhi, Experimental and Numerical Analysis of Cracked Shaft in Viscous Medium a Finite Region. *Structural Engineering Convention,2015.*

Communicated Articles

1. **Adik R. Yadao** and Dayal R. Parhi, Effect of Variable Fluid Properties on the Vibration Response of Cantilever Rotor. *Journal of Low Frequency Noise, Vibration and Active Control*, Manuscript ID. **LF_2015-65**.

2. Dayal R. Parhi and **Adik R. Yadao**, Dyanamic Analysis of Multi-Cracked Rotor in Viscous Medium using Artificial Neural Network. *Proceedings of the Institution of Mechanical Engineers, Part L: Journal of Materials: Design and Applications*, Manuscript ID**. JMDA-16-0144**.

Vitae

Mr. **Adik Ramdayal Yadao** was born in August 1982 at Darbhanga district of Bihar. He has completed his class X from Zilha Parishad High School, Tumsar (Maharastra) in 1999 and Diploma in Mechanical Engineering from Maharastra State Board of Technical Education,Mumbai, Maharastra. He completed his Bachelor of Engineering in Mechanical Engineering from Goverment College of Engineering, Chandarapur, Nagpur University in 2006 and his Master of Engineering in Mechanical Engineering (specialization in Computer aided Design and Computer aided Manufacturing) from University college of Engineering, Osmania University, Hydrabad (A.P.) in 2011. After the completion of his Post-Graduation he has joined Ph.D. program at Department of Mechanical Engineering, National Institute of Technology, Rourkela in July 2012 and submitted the Ph.D. thesis in June 2016. His research interest includes Mechanical vibration, Rotor Dynamics and Fluid Structure Interaction.